AWARD NUMBER: W81XWH-13-1-0352

TITLE: Microenvironment-Programmed Metastatic Prostate Cancer Stem Cells (mPCSCs)

PRINCIPAL INVESTIGATOR: Dean G. Tang, M.D., Ph.D.

CONTRACTING ORGANIZATION: The University of Texas MD Anderson Cancer Center
Houston, TX 78957

REPORT DATE: October 2015

TYPE OF REPORT: Annual Report

PREPARED FOR: U.S. Army Medical Research and Materiel Command
Fort Detrick, Maryland 21702-5012

REPORT DOCUMENTATION PAGE

Form Approved
OMB No. 0704-0188

1. REPORT DATE	2. REPORT TYPE	3. DATES COVERED
October 2015	Annual	13 Sep 2014 - 12 Sep 2015

4. TITLE AND SUBTITLE

Microenvironment-Programmed Metastatic Prostate Cancer Stem Cells (mPCSCs)

5a. CONTRACT NUMBER

5b. GRANT NUMBER
W81XWH-13-1-0352

5c. PROGRAM ELEMENT NUMBER

6. AUTHOR(S)
Dean G. Tang

E-Mail:

5d. PROJECT NUMBER

5e. TASK NUMBER

5f. WORK UNIT NUMBER

7. PERFORMING ORGANIZATION NAME(S) AND ADDRESS(ES)

The University of Texas MD
Anderson Cancer Center
Smithville, Texas 78957

8. PERFORMING ORGANIZATION REPORT NUMBER

9. SPONSORING / MONITORING AGENCY NAME(S) AND ADDRESS(ES)

U.S. Army Medical Research and Materiel Command
Fort Detrick, Maryland 21702-5012

10. SPONSOR/MONITOR'S ACRONYM(S)

11. SPONSOR/MONITOR'S REPORT NUMBER(S)

12. DISTRIBUTION / AVAILABILITY STATEMENT

Approved for Public Release; Distribution Unlimited

13. SUPPLEMENTARY NOTES

14. ABSTRACT

Prostate cancer (PCa) metastasis represents the worst outcome that eventually kills the patient. Although many PCa cell-intrinsic molecules and end-organ factors have been implicated in the metastatic dissemination of PCa cells, the role of primary tumor microenvironment and the nature of the metastatic PCa cells remain poorly defined. By establishing a reliable and quantifiable experimental PCa metastasis model in NOD/SCID mice, we have found that PCa cells implanted orthotopically (i.e., in the prostate) metastasize much more extensively and widely than those implanted ectopically (i.e., subcutaneously or s.c). Microarray-based gene expression profiling reveals that the orthotopically implanted human PCa cells upregulate several classes of genes that have been intimately implicated in metastasis. These and many other preliminary observations allow us to HYPOTHESIZE that PCa cells reciprocally interact with the host cells to establish a proinflammatory microenvironment highly conducive to PCa metastasis and that metastatic PCa cells are endowed with CSC properties. By the end of the second year, we have largely accomplished what's initially proposed in Aims 1 and 2 with relevant manuscripts are under preparation now. The final year will be dedicated to Aim 3, whose is focus is on elucidating the signaling mechanisms that promote PCa cell metastasis

15. SUBJECT TERMS
Prostate cancer; metastasis; microenvironment; stem cells; cancer stem cells; orthotopic implantation; ectopic implantation; metastatic prostate cancer stem cells

16. SECURITY CLASSIFICATION OF:			17. LIMITATION OF ABSTRACT	18. NUMBER OF PAGES	19a. NAME OF RESPONSIBLE PERSON
a. REPORT	b. ABSTRACT	c. THIS PAGE			USAMRMC
U	U	U	UU	112	19b. TELEPHONE NUMBER *(include area code)*

Standard Form 298 (Rev. 8-98)
Prescribed by ANSI Std. Z39.18

Table of Contents

Page

Department of Defense PCRP IDEA Award
PROGRESS REPORT (Sept 13, 2014 to Sept 12, 2015)

W81XWH-13-1-0352, "Microenvironment-Programmed Metastatic Prostate Cancer Stem Cells (mPCSCs)"

PI: Dean Tang

1. INTRODUCTION: The main goal of this project is to help elucidate the cellular and molecular mechanisms underlying prostate cancer (PCa) metastasis. Specifically, we test the overarching hypothesis that *prostatic microenvironment facilitates PCa metastasis by promoting the phenotypic as well as functional manifestations of metastatic prostate cancer stem cells (mPCSCs)*. In the application, we proposed three Specific Aims:
1) To perform functional studies on the genes upregulated in the DP human prostate tumors;
2) To test the hypothesis that the DP human PCa cells overexpressing CSC markers possess mPCSC properties; and
3) To test the hypothesis that HOXB9 represents a 'master' regulator of mPCSCs and PCa metastasis.

2. KEYWORDS: Prostate cancer; metastasis; microenvironment; stem cells; cancer stem cells; orthotopic implantation; ectopic implantation; metastatic prostate cancer stem cells

3. ACCOMPLISHMENTS:

Major Goals of the Project (SOW):

Specific Aim 1: To perform further functional studies on the genes upregulated in the DP human prostate tumors (months 1 – 24).
The main goal of this Aim is to perform systematic knockdown experiments in several PCa models on the following 12 genes, CXCR4, PROM1 (CD133), NOS2A, TACSTD2 (TROP2), LRIG1, ABCG2, CD24, WNT4, ID3, NKX3.1, SMAD1, and HOXB9, and to determine the impact of their knockdown on the metastatic potential of human PCa cells in the mouse DP.
A). Test 3 independent shRNA lentiviral vectors for each gene (i.e., a total of 36 knockdown vectors together with 3 control shRNA lentivectors targeting non-coding scramble, GFP, and luciferase) and determine their knockdown efficiency by performing qPCR and Western blotting analysis.
B). Employ the most efficient vector for each gene (i.e., 12 in total plus control vectors) for in vivo tumor/metastasis experiments first by working on PC3 and xenograft-purified LAPC9 cells.

Specific Aim 2: To test the hypothesis that the DP human PCa cells overexpressing CSC markers possess mPCSC properties (months 12-30)
The main goal of this Aim is to determine whether PCa cells overexpressing CSC surface markers actually possess mPCSC properties, i.e., enhanced metastatic potential.
A*). To determine the metastatic potential of single marker-sorted PCa cells*. (12-24 months).
B*). To determine the metastatic potential of combinatorial marker purified PCa cells.* (20-30 months).

Specific Aim 3: To test the hypothesis that HOXB9 represents a 'master' regulator of mPCSCs and PCa metastasis (months 15-36).

***A**). To correlate HOXB9 with PCa progression in patient tumors*. (15-24 months)

***B**). To directly determine the functions and mechanisms of HOXB9 in mPCSCs and PCa metastasis*. (20-36 months). We estimate to use ~250 male NOD/SCID mice for these functional studies.

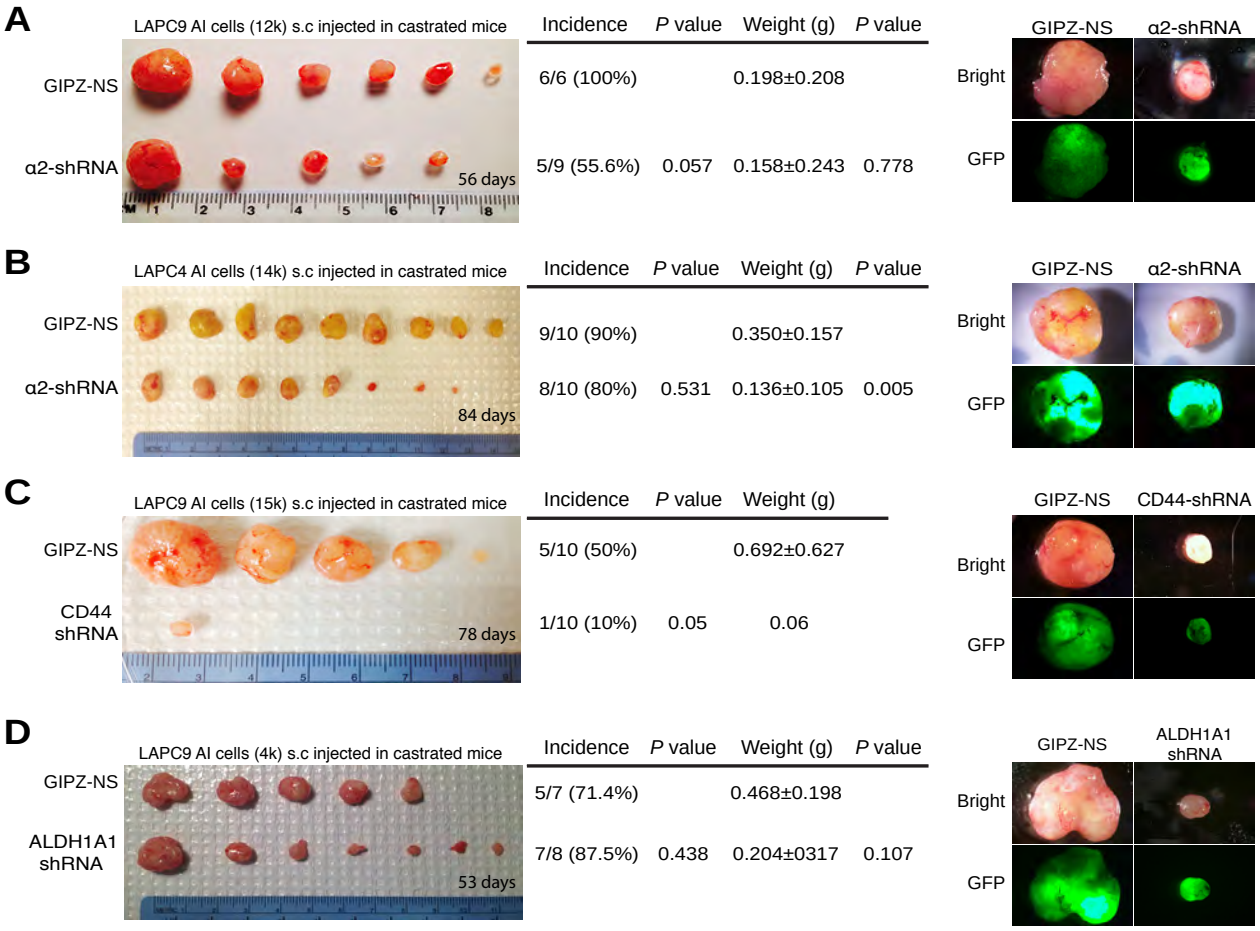

Figure 1. Functional importance of CSC markers in aggressive AI PCa regeneration.
(A-B) *Integrin α2 knockdown reduces tumor initiation in LAPC9 AI (androgen-independent; A) tumors and lowers tumor burden in LAPC4 AI (B) tumors. Bulk LAPC9 (A) and LAPC4 (B) AI cells were infected with the control or α2 shRNA-encoding lentiviral vectors for ~72 h at an MOI of 10-20, and s.c injected in castrated NOD/SCID male mice. Tumor incidence, weight and P values were indicated. Shown on the right were representative phase and GFP images of the endpoint tumors.* ***(C)*** D44 knockdown inhibits LAPC9 tumor regeneration in castrated male hosts. ***(D)*** ALDH1A1 knockdown partially inhibits the growth of LAPC9 AI tumors.

What was accomplished under these goals:

A. *Accomplishment of all goals in Aim 1*.

Human PCa cells (e.g., PC3, LAPC4, LAPC9, LNCaP) implanted in the DP (dorsal prostate) of male NOD/SCID mice upregulate several dozens of invasion/metastasis and stem cells/cancer stem cell (CSC) associated genes including the 12 genes proposed in Aim 1 as well as CD44, integrin a2 and b1, ALDH1A1 and ALDH7A1, BCL-2, and MYC, among many others (see original proposal). Whether these upregulated genes play a causal role in the metastasis of PCa cells remains largely unknown. We first carried out pilot experiments by knocking down CSC markers CD44, a2, and ALDH1A1 (1-9) in very aggressive androgen-independent (AI) PCa cells and assessed the impact of the deficiency of these genes on tumor regeneration in fully castrated NOD/SCID mice. As shown in Figure 1 (previous page), knocking down 3 genes all inhibited the incidence and/or the growth of LAPC9 or LAPC4 cells, suggesting that these 3 phenotypic markers are causally required for tumorigenic properties of AI PCa cells.

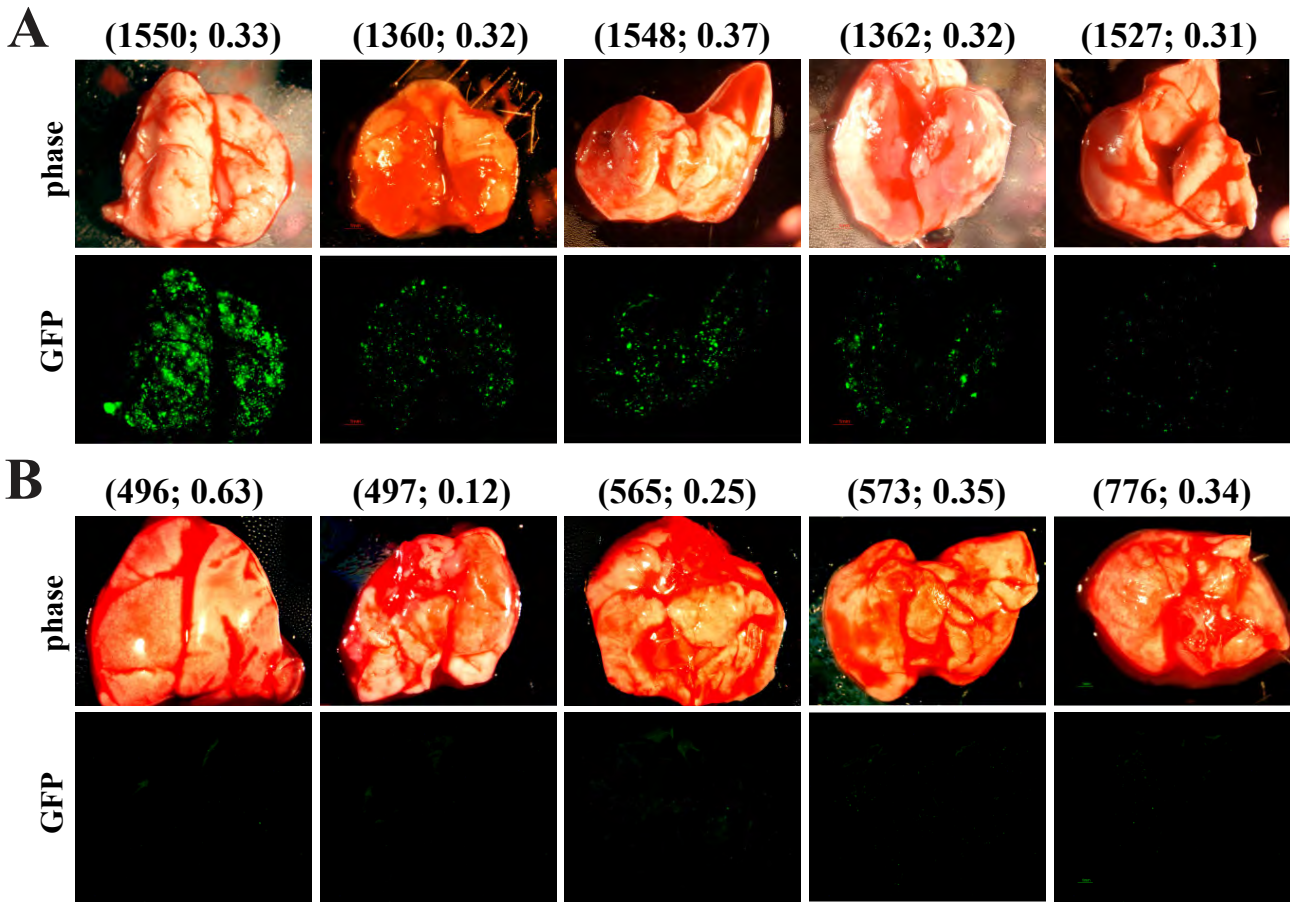

Figure 2. CD44 knockdown inhibits PC3 cell lung metastasis.
PC3 cells were infected with either non-silencing (NS) pGIPz control (A) or pGIPz-CD44shRNA (B) lentiviral vectors, both of which were GFP-tagged and used at MOIs of ~20. The CD44 knockdown effect of the CD44shRNA vector was confirmed by Western blotting (not shown). 24 h after infection, 500,000 live cells of each type were implanted, in 50% Matrigel, in the DP of male NOD/SCID mice (n=8 for each group). Animals were terminated at 40 d after implantation. Tumors were harvested and weighed. Lungs and several other organs including kidney, renal lymph nodes, spleen, pancreas, liver, and brain were also harvested to image and quantify GFP+ pulmonary metastases under a fluorescence dissecting microscope. Tumor weights showed no difference between the two groups (0.33 ± 0.12 g for NS and 0.34 ± 0.19 g for CD44shRNA, respectively; mean ± S.D). However, the CD44-shRNA animals (B) showed much less lung metastasis than in NS-shRNA animals (A). Shown are 5 representative lungs for each group (animal number and tumor weight indicated on top).

CD44 is an extremely interesting molecule. Systematic studies from our lab have established that the CD44$^+$ PCa cell population (i.e., the cells that express high levels of CD44 on the surface) in multiple xenograft models as well as primary patient tumors is enriched in clonogenic and tumorigenic cells that fulfill CSC definitions (1,3,4,6,7,9). Importantly, we have previously demonstrated that the CD44$^+$ PCa cells also manifest high metastatic potential (3,6,9). Here, as a 'positive' control for our proposed knockdown experiments in the 12 genes (i.e., *CXCR4, PROM1 (CD133), NOS2A, TACSTD2 (TROP2), LRIG1, ABCG2, CD24, WNT4, ID3, NKX3.1, SMAD1, and HOXB9*), we first knocked down CD44 in two tumor systems implanted in the DP of NOD/SCID mice, i.e., PC3 (Figure 2) and LAPC4 (Figure 3). In both cases, *CD44* knockdown greatly inhibited GFP-labeled PCa cell metastasis to the lung (Figure 2 & 3) and also some other organs such as the LN and liver (not shown).

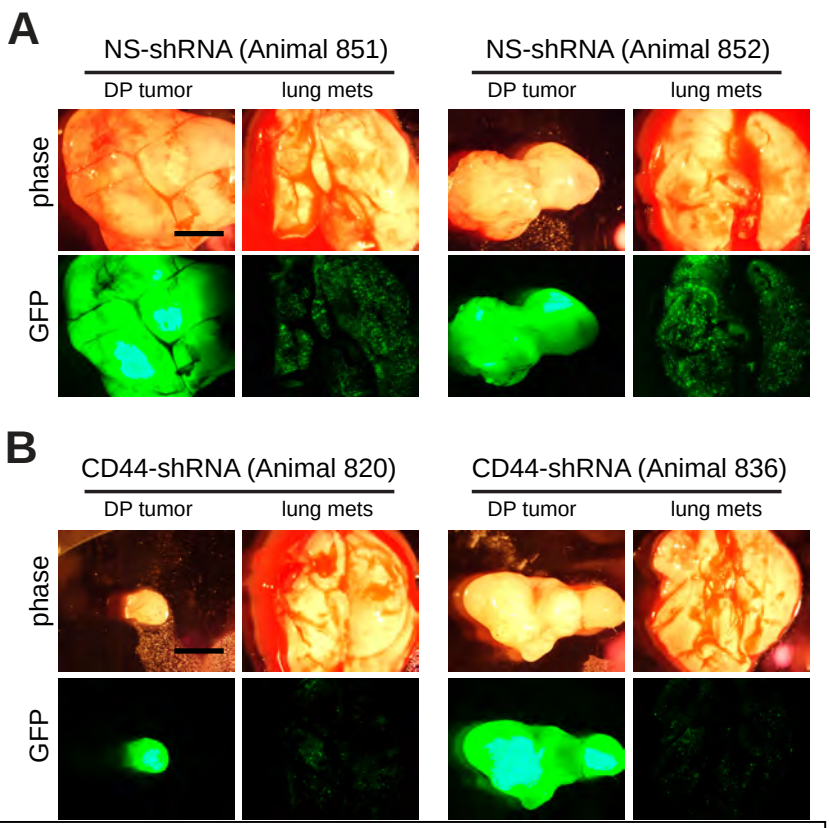

Figure 3. CD44 knockdown inhibits LAPC4 lung metastasis. *Purified LAPC4 cells infected with either non-silencing (NS) pGIPz control lentiviral vector or pGIPz-CD44shRNA (see Supplementary Fig. 1d) were implanted in the DP of male NOD-SCID mice (euthanized at 76 d). Shown are the images of DP tumors and the lungs from two representative animals in each group (n = 7). The CD44-shRNA animals (B) had both smaller DP tumors and less lung metastasis (GFP+ foci) than in NS-shRNA animals (A). Scale bar, 100 µm.*

Using the CD44 knockdown as the positive control, we spent ~1.5 years to systematically study the roles of the above-mentioned 12 'representative' genes, which were initially uncovered in our microarray analysis of differentially expressed genes in subcutaneous and DP prostate tumors and which we hypothesized might play a causal role in facilitating the microenvironment-reprogrammed PCa metastasis. As we have always done in the past with knocking down of >3 dozens of genes (e.g., 1,3,4,6,7,9,10), we chose 3 pGIPz lentiviral vectors targeting 3 different regions of each molecule and first infected PC3 cells at different dilutions to determine the knockdown efficiency. We subsequently picked the most efficient knockdown vector for each gene and infected PC3 (Figure 4A) and LAPC9 (Figure 4B) cells at an MOI (multiplicity of infection) of 10-20, determined by Western blotting analysis of the knockdown effects at which >80% of the target proteins were shut down (data not shown). 72 h after infection, we implanted PC3 (200,000 cells each) or LAPC9 (500,000 cells each) cells into the DP of the castrated NOD/SCID mice (n=12-16 mice per gene group depending on the availability of male mice at the time of experiments). Generally, within ~1.5-2 months animals began to manifest signs of morbidity (slow movement, hunching postures, reduced appetite, rough hair coat, etc) caused by metastasis when we would terminate all animals in the same group. After tumor-bearing animals were sacrificed, 7 end organs (lung, kidney, pancreas, liver, spleen, brain, and bone marrow) were harvested and examined for metastatic GFP$^+$ human PCa cells (see Figure 2 in the original application).

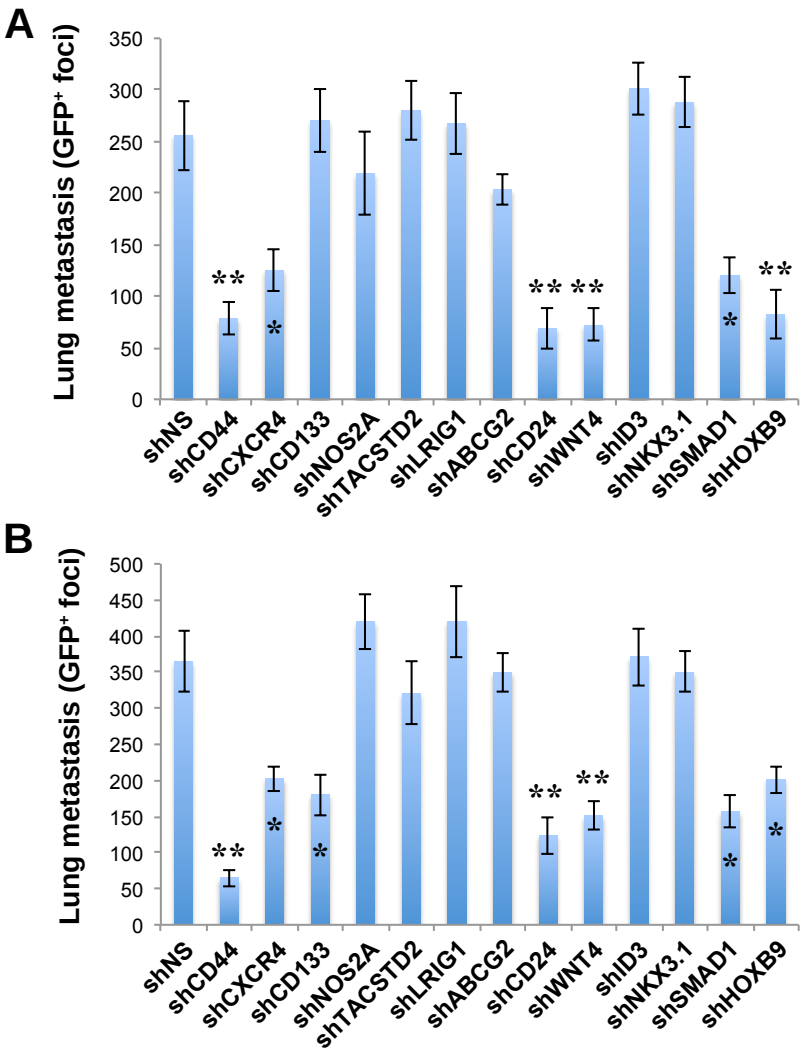

Figure 4. Systematic dissection of the roles of 12 genes uncovered in experimental PCa metastasis models in mediating metastasis.
This figure summarizes the work in the past ~1.5 years (Aim 1).
*PC3 (**A**) and LAPC9 (**B**) cells were purified from the respective xenograft tumors and infected with the pGIPz lentiviral vectors targeting the indicated molecules (NS, non-silencing control) at an MOI of 10-20 (based on experiments determining the knockdown efficiency). 72 h later, cells were harvested and implanted (PC3, 200,000 cells/injection; LAPC9, 500,000 cells/injection) into the DP of the castrated male NOD/SCID mice (n=12-16 mice/gene). Animals were terminated generally at ~40-60 days after cell implantation when they began to manifest signs of morbidity. At termination, lungs were harvested and imaged under a fluorescence dissection microscope and GFP+ lung metastatic foci were enumerated (6). Shown are the mean±S.D. Note both consistent and discordant results in the two metastasis models. *P<0.05; **P<0.01 (Student's t-test).*

In such spontaneous PCa metastasis models, dissemination to the lung represents the most prominent and also the most quantifiable organ (3,6; Figure 2 & 3). Consequently, we focused on our analysis on the lung metastasis. As summarized in Figure 4A, CD44 knockdown dramatically reduced PC3 cell lung metastasis. Surprisingly, most of the 12 genes (i.e., 7), when knocked down, did not manifest significant inhibitory effects on the metastasis of PC3 cells to the lung (Figure 4A) and other organs (data not shown). However, knocking down CD24, CXCR4, WNT4, SMAD1, and HOXB9, significantly inhibited PC3 cell lung metastasis (Figure 4A) and LN (not shown). Analysis of the overall metastatic rate in all organs combined (see Figure 2g in grant application) showed very similar functional patterns with CD24, CXCR4, WNT4, SMAD1, and HOXB9 knockdown exhibiting partial metastasis-suppressive effects (data not shown).

Interestingly, similar comprehensive knockdown experiments in the LAPC9 system revealed similar though not identical results (Figure 4B). Similar to in PC3 cells, knocking down CD24, CXCR4, WNT4, SMAD1, and HOXB9, to different degrees, inhibited LAPC9 lung metastasis. Different from in PC3 cells, CD133 knockdown also significantly inhibited LAPC9 lung metastasis (Figure 4B).

These results, taken together, suggest that: **1)** surprisingly, <50% of the genes uncovered to be upregulated in the metastasis-prone DP tumors (compared to s.c tumors) and we tested seem to be functionally critical in mediating metastasis, at the single gene levels; **2)** the majority of the genes interrogated, when individually knocked down, did not manifest

significant impact on PCa cell metastasis, suggesting that either individually they are not critically important or powerful enough in modulating PCa metastasis or that they only contribute to PCa metastasis subtly such that combined functions of many of these genes are required; **3)** nevertheless, the results in both models point to the crucial involvement of 5 genes, i.e., CD24, CXCR4, WNT4, SMAD4, and HOXB9 in regulating PCa metastasis thus implicating them as potential anti-metastasis therapeutic targets. These results are consistent with recently emerged evidence implicating CD24 and CXCR4 molecules and the WNT and TGFb signaling pathways in regulating the metastatic process in PCa and other cancers (e.g., 11-14); and **4)** as expected, there likely exist model-dependent effects of individual genes in controlling PCa metastasis, as exemplified by the differential effects of knocking down CD133 in PC3 vs. LAPC9 cells.

B. *Accomplishment of part of the goals in Aim 2*.

As alluded above, the metastasis-prone DP tumors were found to overexpress CD44, SPP1 (also called osteopontin or OPN), CD133, LRIG1, and CD24. By far, we have knocked down all these 5 genes and assessed their impact on PCa metastasis: knocking down CD44 (3,6,9; Figure 2-4), SPP1 (Figure 4d-e in the original application), and CD24 (Figure 4A-B) all greatly inhibited metastasis of PC3, LAPC9, and some other PCa cells whereas knocking down CD133 inhibited metastasis only in some PCa models (Figure 4A-B). In contrast, knocking down LRIG1 did not affect metastasis (Figure 4).

In the Aim 2 of the grant proposal, we advocated a 'reciprocal' hypothesis, i.e., that PCa cells preferentially expressing (some of) these CSC markers may possess high metastatic potential in comparison to the marker low-expressing counterparts, i.e., mPCSCs. To test this hypothesis, we purified out $CD44^{+/hi}$ ($CD44^{+}$) vs. $CD44^{-/lo}$ ($CD44^{-}$) PC3 cells (as positive control) from the DP tumors and injected them back into the DP of new animals. As shown in Figure 5A, 100 $CD44^{+}$ PC3 cells recovered from the DP tumors showed prominent lung metastasis whereas 1,000 $CD44^{-}$ PC3 cells from the DP tumors showed little lung metastasis. Similarly, the DP PC3 tumors

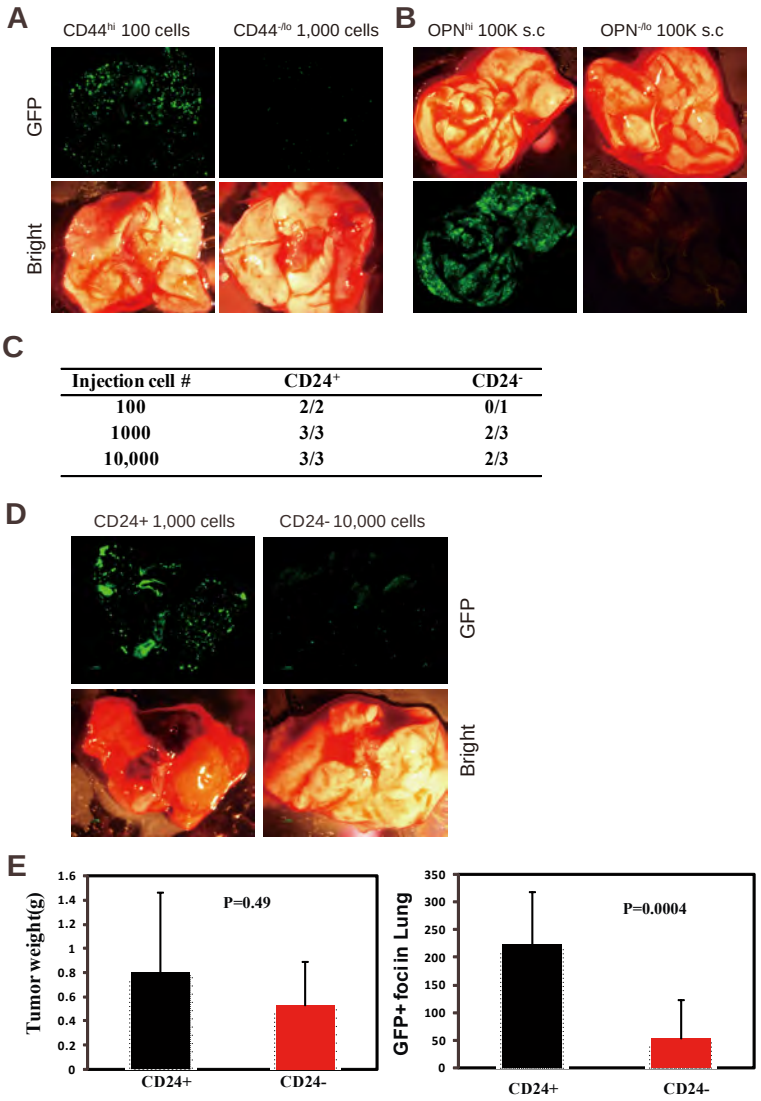

Figure 5. CSC marker-expressing PC3 cells in the DP tumors show preferential metastatic capacities.
A. *$CD44^{+}$ (i.e., $CD44^{hi}$) PC3 cells in the DP tumors show much higher metastatic propensity than the $CD44^{-/lo}$ PC3 cells when re-implanted in the DP.* ***B***. *OPN^{+} PC3 cells purified from the DP tumors exhibit higher metastatic capacity than the OPN^{-} PC3 cells when re-implanted in the subcutis.* ***C-E***. *$CD24^{+}$ PC3 cells purified from the DP tumors manifest higher tumor-initiating and metastatic abilities than the $CD24^{-}$ cells when re-implanted in the DP. See Text for more discussions.*

overexpressed OPN based on the microarray analysis. We purified out OPN^{hi} and $OPN^{-/lo}$ PC3 cells from the 'reporter' DP tumors and implanted them subcutaneously. Remarkably, the OPN^{hi} PC3 cells initiated prominent lung metastasis even in the subcutaneum, an anatomical site where little metastasis normally occurs; in contrast, $OPN^{-/lo}$ PC3 cells hardly showed any lung metastasis (Figure 5B). Finally, we performed a series of experiments in $CD24^{+/-}$ PC3 cells purified from the DP tumors (Figure 5C-E). The $CD24^{+}$ PC3 cells showed 100% tumor-initiating capacity with as few as 100 cells being able to regenerate tumors in the DP; in contrast, the $CD24^{-}$ PC3 cells exhibited only ~57% tumor-regenerating capability ($P<0.01$; c2 test). Importantly, tumors established from $CD24^{+}$ and $CD24^{-}$ PC3 cells were of similar sizes; however, the $CD24^{+}$ PC3 cells showed much more extensive lung metastases than 10x more $CD24^{-}$ cells implanted in the DP (Figure 5D-E). These observations provide strong evidence that the mouse prostatic microenvironment promotes the manifestation of mPCSC subpopulations that overexpress CSC markers and possess high metastatic potential.

C. *Accomplishment of part of the goals in Aim 3*.

The goal of Aim 3 is to test the hypothesis that HOXB9 represents a 'master' regulator of mPCSCs and PCa metastasis via regulating the TGFb/SMADs signaling which in turn controls CSC molecules such as SPP1, MMP9, CD44, and CD24 (see Figure 5e in the original proposal). This hypothesis was put forth based on the following observations: 1) HOXB9 was one of the genes upregulated in the metastasis-prone DP tumors (compared to non-metastatic s.c tumors); 2) TGFb1, and, in particular, TGFb2, are both upregulated in the DP tumors; 3) knocking down TGFb2 and SMAD1 both inhibits PCa metastasis (Figure 4; data not shown); 4) knocking down CD44, SPP1, MMP9, and CD24 all partially inhibits PCa cell metastasis; and 5) finally, $CD44^{+}$, $CD24^{+}$ and OPN^{+} PCa cells all manifest higher metastatic potential than the corresponding marker-negative PCa cell populations.

So, might HOXB9 be a master regulator of the entire metastatic cascade in PCa cells. Interestingly, up to now, Pubmed search on "HOXB9 AND prostate cancer metastasis" still just turns up on reference (15), suggesting that either HOXB9 represents an extremely novel PCa metastasis regulator or HOXB9 might not be critically important regulator of PCa metastasis. Our knockdown experiments in two PCa metastasis models both revealed positive roles of HOXB9 in PCa metastasis (Figure 4). To address the potential involvement of HOXB9 in functionally regulating

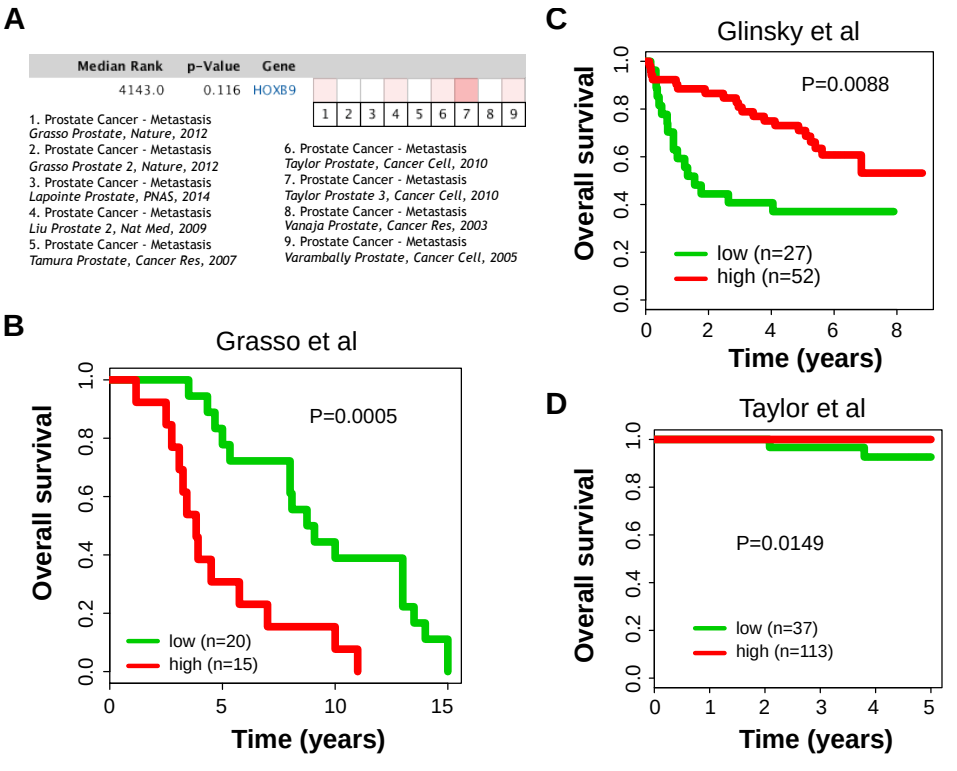

Figure 6. Linking HOXB9 mRNA expression to patient data and patient survival. ***A****. Slight upregulation of HOXB9 mRNA levels in 9 Oncomine data sets that contain metastasis cases.* ***B-C****. High levels of HOXB9 mRNA levels are associated with poor patient survival in one data set (B) and better patient survival in two other data sets (C-D).*

PCa development, progression, and metastasis, we performed exhaustive bioinformatics based correlation studies on *HOXB9* mRNAs with various patient parameters. **FIRST**, we analyzed TCGA PRAD (Prostate Adenocarcinoma) data set, in which there are 52 normal prostate tissue samples and 498 tumor samples including 432 untreated tumors (45 Gleason 6, 241 Gleason 7, 50 Gleason 8, and 96 Gleason 9) and 66 treated (hormone therapy and/or chemotherapy). The *HOXB9* mRNA levels are significantly reduced when comparing normal vs. either untreated or treated tumors or vs. tumors of different Gleason grades (data not shown). **SECOND**, we systematically interrogated all eligible Oncomine datasets that contain metastasis cases (9) and in all 9 datasets we only found a relatively weak upregulation of *HOXB9* mRNA levels in metastatic samples compared with primary tumors (Figure 6A). **FINALLY**, we performed detailed Kaplan-Meier survival analysis, which revealed discordant results: in one data set high *HOXB9* mRNA levels correlated with poor patient survival (Figure 6B; thus suggesting a pro-metastasis function) whereas in two other data sets high *HOXB9* mRNA levels correlated with better overall patient survival (Figure 6C-D; implicating an anti-metastasis role).

References:

1. Patrawala, L. *et al*. Side population is enriched in tumorigenic, stem-like cancer cells, whereas ABCG2^{+} and ABCG2^{-} cancer cells are similarly tumorigenic. *Cancer Res* **65**, 6207-6219 (2005).
2. Collins, A.T. *et al*. Prospective identification of tumorigenic prostate cancer stem cells. *Cancer Res* **65**, 10946-10951 (2005).
3. Patrawala, L. *et al.* Highly purified CD44^{+} prostate cancer cells from xenograft human tumors are enriched in tumorigenic and metastatic progenitor cells. *Oncogene* **25**, 1696-1708 (2006).
4. Patrawala, L., Calhoun-Davis, T., Schneider-Broussard, R. & Tang, D.G. Hierarchical organization of prostate cancer cells in xenograft tumors: the CD44^{+}a2b1^{+} cell population is enriched in tumor-initiating cells. *Cancer Res* **67**, 6796-6805 (2007).
5. Rajasekhar, V.K., Studer, L., Gerald, W., Socci, N.D., & Scher, H.I. Tumour-initiating stem-like cells in human prostate cancer exhibit increased NF-κB signalling. *Nat Commun* **2**, 162 (2011).
6. Liu, C. *et al.* The microRNA miR-34a inhibits prostate cancer stem cells and metastasis by directly repressing CD44. *Nat Med* **17**, 211-215 (2011).
7. Qin, J. *et al*. The PSA$^{-/lo}$ prostate cancer cell population harbors self-renewing long-term tumor-propagating cells that resist castration. *Cell Stem Cell* **10**, 556-569 (2012).
8. Rybak, A.P., Bristow, R.G., & Kapoor, A. Prostate cancer stem cells: deciphering the origins and pathways involved in prostate tumorigenesis and aggression. *Oncotarget* **6**, 1900-1919 (2015).
9. Liu, X. et al. Systematic dissection of phenotypic, functional, and tumorigenic heterogeneity of human prostate cancer cells. *Oncotaget* **6**, 23959-23986 (2015).
10. Liu, C. *et al.* Distinct microRNA expression profiles in prostate cancer stem/progenitor cells and tumor-suppressive functions of let-7. *Cancer Res* **72**, 3393-3404 (2012).
11. Wang, L. *et al*. Intracellular CD24 disrupts the ARF-NPM interaction and enables mutational and viral oncogene-mediated p53 inactivation. *Nat Commun*. **6**, 5909 (2015).
12. Wong D, Kandagatla P, Korz W, Chinni SR. Targeting CXCR4 with CTCE-9908 inhibits prostate tumor metastasis. *BMC Urol.* **14**, 12 (2014).
13. Miyamoto DT *et al*. RNA-Seq of single prostate CTCs implicates noncanonical Wnt signaling in antiandrogen resistance. *Science* **349**, 1351-1356 (2015).
14. Fournier, P.G. *et al*. The TGF-β Signaling Regulator PMEPA1 Suppresses Prostate Cancer Metastases to Bone. *Cancer Cell* **27**, 809-821 (2015).

15. De Pinieux, G., *et al.* Clinical and experimental progression of a new model of human prostate cancer and therapeutic approach. *Am J Pathol* **159**, 753-764 (2001).

What opportunities for training and professional development has the project provided?
Nothing to Report

How were the results disseminated to communities of interest?
Nothing to Report

What do you plan to do during the next reporting period to accomplish the goals?
Aim 1: We have finished Aim 1 and are in the process of summarizing the data (together with other results) for a manuscript.

Aim 2: We should be able to finish testing several combinatorial marker profiles as potential better mPCSC markers in the third year of the grant.

Aim 3: In the final year of the grant, we shall focus on the proposed HOXB9 pathway in dictating human PCa metastasis. Results so far obtained are not completely congruent with our initial hypothesis – although prospective knockdown experiments in two PCa metastasis models (PC3 and LAPC9) both revealed a pro-metastasis function for HOXB9 (Figure 4), its mRNA levels are actually reduced in primary tumors in comparison with the normal tissues (not shown), only slightly increased in Oncomine metastasis cases (Figure 6A), and are discordantly associated with patient survival (Figure 6B-D). These observations suggest that HOXB9 might be a tumor-dependent regulator of PCa metastasis and not a 'universal' controller of the complicated process of metastasis. We'll largely stick to the original plan and offer interpretations of our data according to these new developments.

4. IMPACT:

a. **What was the impact on the development of the principal discipline(s) of the project?**
For the first time, we have generated convincing data that when human PCa cells are implanted subcutaneously in immunodeficient NOD/SCID mice, they readily regenerate tumors but rarely metastasize. In contrast, orthotopically implanted human PCa cells generate less tumors but extensively metastasize. This message should greatly impact how future studies on human PCa metastasis should be modeled and executed.

b. **What was the impact on other disciplines?**
The findings here should also have bearing on similar metastasis studies of other solid tumors such as breast and colon cancers.

c. **What was the impact on technology transfer?**
Nothing to Report

d. **What was the impact on society beyond science and technology?**
Nothing to Report

5. CHANGES/PROBLEMS:
Nothing to Report

6. PRODUCTS:
The current project **intersects** with several other projects in the lab, all of which have a **common** goal, i.e., to dissect PCa cell heterogeneity and to elucidate the role of different subpopulations of PCa stem/progenitor cells in tumor initiation, maintenance, progression, drug resistance, and metastasis. The following published manuscripts have **cited** the partial support of the DOD grant although only reference 2 is **directly** related to what is proposed in the DOD grant.

1. Rycaj K, Tang DG. Cell-of-Origin of Cancer versus Cancer Stem Cells: Assays and Interpretations. Cancer Res. 2015 Oct 1;75(19):4003-11. doi: 10.1158/0008-5472.CAN-15-0798. Epub 2015 Aug 19.

2. Liu X, Chen X, Rycaj K, Chao HP, Deng Q, Jeter C, Liu C, Honorio S, Li H, Davis T, Suraneni M, Laffin B, Qin J, Li Q, Yang T, Whitney P, Shen J, Huang J, Tang DG. Systematic dissection of phenotypic, functional, and tumorigenic heterogeneity of human prostate cancer cells. Oncotarget 2015 Sep 15;6(27):23959-86.

3. Gong S, Li Q, Jeter CR, Fan Q, Tang DG, Liu B. Regulation of NANOG in cancer cells. Mol Carcinog. 2015 Sep;54(9):679-87. doi: 10.1002/mc.22340. Epub 2015 May 27.

4. Deng Q, Tang DG. Androgen receptor and prostate cancer stem cells: Biological mechanisms and clinical implications. Endocr Relat Cancer. 2015 Aug 18. 22(6):T209-20. pii: ERC-15-0217.

5. Li Q, Rycaj K, Chen X, Tang DG. Cancer stem cells and cell size: A causal link? Semin Cancer Biol. 2015 Aug 1. 35:191-9. pii: S1044-579X(15)00061-9. doi:

6. Jeter CR, Yang T, Wang J, Chao HP, Tang DG. NANOG in Cancer Stem Cells and Tumor Development: An Update and Outstanding Questions. Stem Cells. 2015 Aug;33(8):2381-90. doi: 10.1002/stem.2007. Epub 2015 May 13.

7. PARTICIPANTS & OTHER COLLABORATING ORGANIZATIONS

Name:	Xin Chen
Project Role:	Post doc
Researcher Identifier (e.g. ORCID ID):	N/A
Nearest person month worked:	12
Contribution to Project:	Dr. Chen performed most metastasis related and gene knockdown assays.
Funding Support:	This DOD grant

Name:	Hseuh-Ping (Eva) Chao
Project Role:	Graduate Student
Researcher Identifier (e.g. ORCID ID):	N/A
Nearest person month worked:	6
Contribution to Project:	Eva was involved in bioinformatically analyzing differentially expressed genes
Funding Support:	This DOD grant

Has there been a change in the active other support of the PD/PI(s) or senior/key personnel since the last reporting period?
Nothing to Report

What other organizations were involved as partners?
Nothing to Report

8. SPECIAL REPORTING REQUIREMENTS:
N/A

APPENDICES:

Published OnlineFirst August 19, 2015; DOI: 10.1158/0008-5472.CAN-15-0798

Review

Cancer Research

Cell-of-Origin of Cancer versus Cancer Stem Cells: Assays and Interpretations

Kiera Rycaj[1] and Dean G. Tang[1,2]

Abstract

A tumor originates from a normal cell that has undergone tumorigenic transformation as a result of genetic mutations. This transformed cell is the cell-of-origin for the tumor. In contrast, an established clinical tumor is sustained by subpopulations of self-renewing cancer cells operationally called cancer stem cells (CSC) that can generate, intraclonally, both tumorigenic and nontumorigenic cells. Identifying and characterizing tumor cell-of-origin and CSCs should help elucidate tumor cell heterogeneity, which, in turn, should help understand tumor cell responses to clinical treatments, drug resistance, tumor relapse, and metastatic spread. Both tumor transplantation and lineage-tracing assays have been helpful in characterizing these cancer cell populations, although each system has its strengths and caveats. In this article, we briefly review and summarize advantages and limitations of both assays in support of a combinatorial approach to accurately define the roles of both cancer-initiating and cancer-propagating cells. As an aside, we also wish to clarify the definitions of cancer cell-of-origin and CSCs, which are often interchangeably used by mistake. *Cancer Res; 75(19); 4003–11. ©2015 AACR.*

Introduction

Epithelial cancers are complex and exhibit intertumoral and intratumoral heterogeneity. Identifying specific cell types that initiate and sustain tumorigenesis is key to addressing tumor cell heterogeneity and other outstanding tumor biology questions. Cancer-initiating cell, or the cell-of-origin of cancer, is the normal cell that receives the first cancer-causing mutations. In other words, the cancer-initiating cell founds a future clinical tumor. Cancer stem cells (CSC), on the other hand, are the cells that maintain tumor propagation (1–3). Aptly referred to as cancer-propagating cells, CSCs are defined by two attributes, self-renewal and multipotency. The phenotypes between cancer-initiating cells and cancer-propagating cells may differ and dynamically change and, in most cases, the relationship between the two is not well understood. Two assays have been helpful in characterizing these two cell types: transplantation assays and lineage-tracing assays (Fig. 1). The serial tumor transplantation assay is the current "gold standard" for identifying CSCs because it can assess both self-renewal and multipotency. Transplantation assays can also be used to determine the cell-of-origin of cancers. Lineage tracing is the current gold standard for defining the cell-of-origin of transformation in mouse models. Lineage tracing is also being used to provide insight into the proliferative potential and fate of stem cells during tumor formation as evidenced by recent progress in identifying CSCs in solid tumors.

The Transplantation Assay

In the transplantation assay, tumor cell populations are fractionated and xenografted into immunocompromised mice. When identifying CSCs, cancer cell subpopulations are sorted using FACS based on relatively specific or presumed CSC markers followed by limiting dilution assay (LDA) and serial tumor transplantations to determine the CSC frequency and multilineage potential of a given marker phenotype (Fig. 1A, a). Populations of CSC marker–positive cells that give rise to serially transplantable tumors that histologically recapitulate the cellular heterogeneity of the parental tumors can therefore be classified as CSCs, whereas populations of CSC marker–negative cells with no or limited tumor-propagating activity can be excluded from the CSC candidates (Fig. 1A, a). These assays have demonstrated the existence of CSCs in human cancers, including acute myeloid leukemia (AML), chronic myeloid leukemia (CML), breast cancer, glioblastoma, colorectal cancer, and others (1–3).

Historically, in the early 1950s, it was shown that a small fraction of cells in murine tumors could withstand freeze-thawing as indicated by proliferation *in vitro*, providing early evidence for functional heterogeneity in sarcoma cell subpopulations (4). Subsequent quantitative transplantation assays determined that 1 of 27 viable cells was capable of giving rise to a tumor when cells from a murine sarcoma tumor, S37, were xenotransplanted into 4- to 6-week-old albino mice (5). Direct proof for the existence of leukemic stem cells (LSC) was provided in the mid-1990s (reviewed in ref. 3), and in the 2000s, evidence for CSCs was extended to human solid tumors. It was first shown that in human breast cancer, as few as 100 cells bearing the $CD44^{+}CD24^{-/low}Lin^{-}$ cell surface marker profile could regenerate serially transplantable tumors in mice (6). Shortly thereafter, xenotransplantation assays evinced CSCs in human brain tumors, with the $CD133^{+}$ tumor cell fraction

[1]Department of Epigenetics and Molecular Carcinogenesis, The University of Texas MD Anderson Cancer Center, Smithville, Texas. [2]Cancer Stem Cell Institute, Research Center for Translational Medicine, East Hospital, Tongji University School of Medicine, Shanghai, China.

Corresponding Author: Dean G. Tang, Department of Epigenetics and Molecular Carcinogenesis, The University of Texas MD Anderson Cancer Center, Science Park, 1808 Park Road 1C, Smithville, TX 78957. Phone: 512-237-9575; Fax: 512-237-2475; E-mail: dtang@mdanderson.org

doi: 10.1158/0008-5472.CAN-15-0798

Published OnlineFirst August 19, 2015; DOI: 10.1158/0008-5472.CAN-15-0798

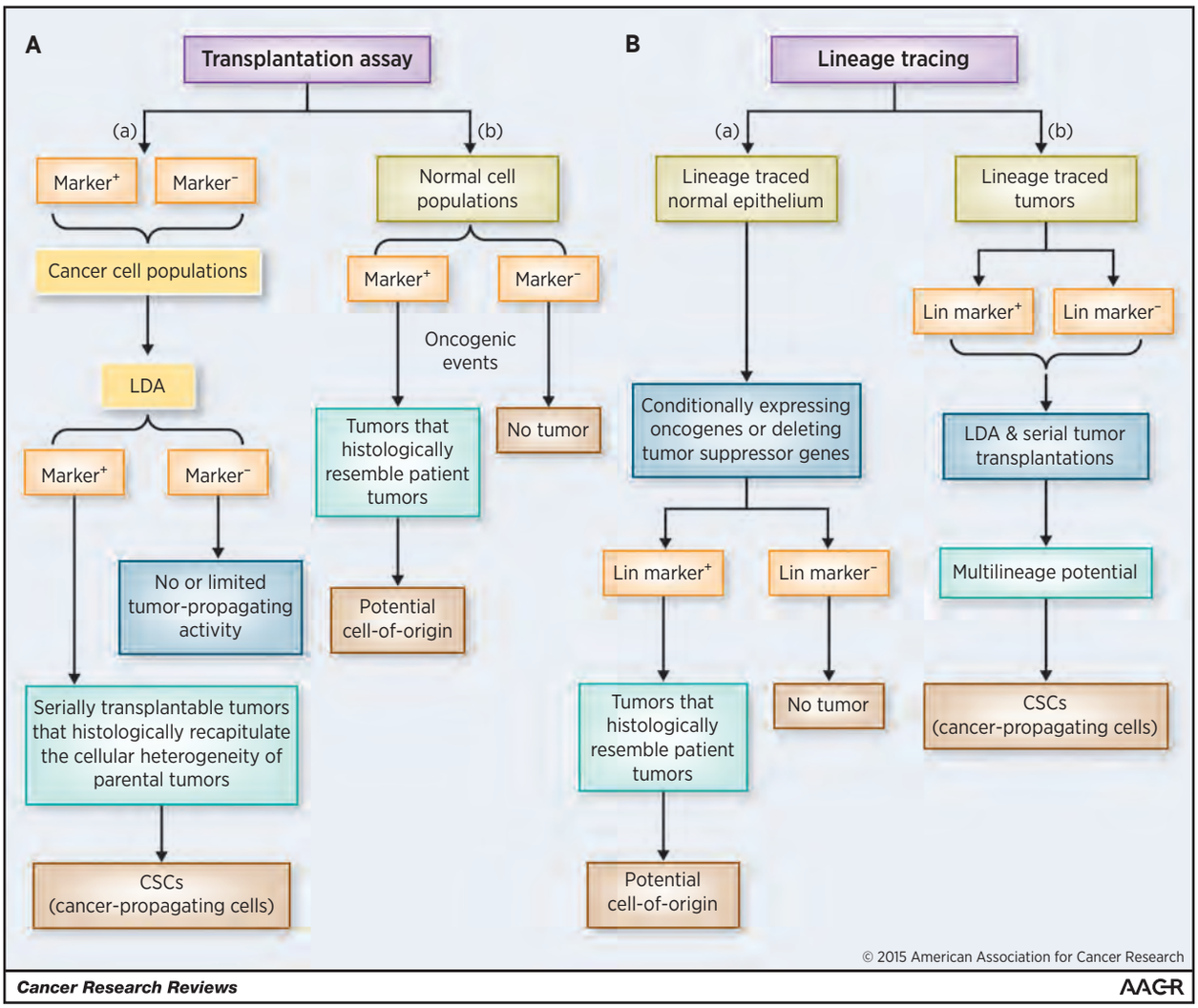

Figure 1.
A comparison of transplantation and lineage-tracing assays. A, tumor transplantation assay. LDA can be used in combination with serial transplantations to assess CSC abundance and properties in a candidate marker–positive tumor cell population (a). The transplantation assay can also be used to determine cell-of-origin in cancers (b). B, lineage-tracing assay. This is most commonly used to determine the potential cell-of-origin for a cancer. In a specific normal cell population, transformation events can be introduced via activation of oncogenes or inactivation of tumor suppressor genes. Labeled tumors can then be traced back to a specific cell-of-origin (a). Lineage tracing can also be used to determine and/or authenticate the CSC properties of the marked cell population in the established, traced tumor (b).

containing cells capable of tumor regeneration in nonobese diabetic/severe combined immunodeficiency (NOD/SCID) mouse brains (7).

The key elements in properly using the xenotransplantation assay to identify and characterize CSCs in human tumors are to perform rigorous LDA and serial tumor transplantations (Fig. 1A, a). In the LDA, CSC frequency is measured by transplanting increasingly diluted single-cell preparations. After tumor regeneration is evaluated for each cell dose, the frequency of cancer cells present in a given cell population that can regenerate a xenograft tumor can be approximated. For this reason, CSCs are also frequently called tumor-initiating cells, which is actually not very accurate and should rather be termed tumor-regenerating cells. In subsequent serial transplantations, true CSCs or CSC-enriched population should be able to perpetuate the xenograft tumors for multiple generations, thus attesting that these particular cells have an inherently unlimited life span when propagated *in vivo* (Fig. 1A, a). Important, LDA combined with serial tumor transplantations helps assess one of the most important biologic traits of CSCs, that is, self-renewal *in vivo*. As an example, in a recent study, prostate-specific antigen (PSA)-positive (PSA^{+}) and $PSA^{-/lo}$ human prostate cancer cells were separated and used in serial tumor transplantations (8). The study revealed that the $PSA^{-/lo}$ population could regenerate and propagate xenograft tumors virtually indefinitely, whereas the PSA^{+} prostate cancer cell population could only propagate xenograft tumors for about three generations (8). This study illustrates that the serial tumor transplantation assay has the

Published OnlineFirst August 19, 2015; DOI: 10.1158/0008-5472.CAN-15-0798

ability to compare isogenic subpopulations under identical experimental conditions to determine differences in tumor regeneration and long-term tumor-propagating capacities. Similar serial transplantation studies have demonstrated that human breast (6) and colon (9) CSCs can initiate serially transplantable tumors and thus can self-renew in immunodeficient mice.

Transplantation assays can be used to probe the potential cell-of-origin of cancer as well (Fig. 1A, b). In this scenario, normal cell subpopulations are sorted via FACS based on specific markers followed by introduction of oncogenic events (overexpressing oncogenes and/or knocking out tumor suppressor genes) and subsequent survey of differential tumor formation in xenotransplantation assays. When a marker-positive population gives rise to tumors that histologically resemble parental or patient tumors, cells within this population can then be considered as a potential cell-of-origin for that specific type of cancer (Fig. 1A, b). One example comes from a recent study that demonstrates that the basal epithelial cells from primary benign human prostate tissue, upon tumorigenic transformation, can initiate prostate cancer in immunodeficient mice (10). The authors developed a system whereby naïve adult human prostate epithelium is directly transformed with genetic alterations commonly found in human prostate cancer. When primary human prostate basal and luminal cells transduced with lentivirus carrying red fluorescent protein were combined with murine urogenital sinus mesenchyme cells in Matrigel and injected subcutaneously into NOD/SCID/IL-2Rγ^{null} (NSG) mice, outgrowths were observed only from basal cells (10). Important, when the lentivirus cocktail included both activated (myristoylated) AKT and ERG, basal cell but not luminal cell–derived lesions fulfilled the histologic criteria for the diagnosis of high-grade precursor lesion (10). With the addition of AR (androgen receptor) to the mix, adenocarcinomas developed from transformed basal cells but not luminal cells (10). This study (10) thus indicates that the human basal prostate epithelial cells can function as a potential cell-of-origin for prostate cancer. Using similar transplantation assays, Taylor and colleagues also demonstrated that basal epithelial cells could act as cells-of-origin for prostate cancer (11). One word of caution when using transplantation assays to study cancer cell-of-origin is that a positive outcome only indicates that a specific cell population *CAN* function as the target of tumorigenic transformation but may not necessarily *BE* the actual cell-of-origin for cancer *in vivo*.

For obvious reasons, human tumor cells can only be xenotransplanted to immunodeficient mice to assess their inherent CSC properties. As a result, a major disadvantage of cell transplantation assays is that dissociated single cells may not behave the same way as they do in their natural tissue microenvironment (i.e., niche), thereby misrepresenting the existence or abundance of CSCs (see below). By teasing apart the intact tissue to resolve subpopulations, we inevitably change the cells' metabolism, their apparent role in the tissue hierarchy, and potentially their developmental trajectory. Therefore, it may not be certain whether transplantation assays demonstrate selection of phenotypically plastic cells that survive and proliferate in the new environment or whether they are actually assaying the implicit CSC traits. In addition, solid tumor cells exist in complex microenvironments that are not readily modeled by transplantation because xenotransplants differ in architecture and stroma compared with their native environment. Another caveat associated with xenotransplantations lies in the lack of an immunocompetent microenvironment such that many have argued that the transplantation-based CSC assays may not assess the intrinsic properties of stem cells but may instead be assessing the ability of transplanted human cancer cells in evading immune surveillance. However, this may be a circular argument—it is precisely because CSCs lack the expression of differentiation markers such as MHC molecules that they can better escape host immune–mediated attack, take root, and initiate and propagate human tumors in mice (12).

Understandably, the outcome of xenotransplantation experiments can be influenced by many variables, including the level of malignancy (or differentiation) of donor human tumors and the level of immunodeficiency of recipient mice (2). For instance, the frequency of human melanoma CSCs was found to be as high as 15% to 25% when assayed in NSG mice compared with 1 in 10^5 cells in NOD/SCID mice (13). The high frequency of melanoma CSCs in NSG mice has been interpreted by many as evidence for lack of tumorigenic hierarchy in melanoma. However, in that study (13), most melanoma samples used were very advanced high-grade tumors and it is well-known that advanced, undifferentiated human cancers are highly enriched in CSCs (1–3, 8). Indeed, when early stages of melanoma specimens were later used in CSC studies, it was found that $CD271^+$ melanoma cells identify rare melanoma CSCs (14). Along the same line, in a syngeneic transplantation study of pre-B/B lymphoma cells from Eμ-myc transgenic mice, a very high frequency of the tumor-initiating cells was observed (15), which again was construed by many as evidence to refute the CSC concept. However, the Eμ-myc lymphoma cells are known to be extremely aggressive, resembling undifferentiated human tumors in which CSCs are greatly enriched. Recent lineage-tracing studies in mouse models of tumors have also provided direct evidence for CSCs (see below).

The Lineage-Tracing Assay

The lineage-tracing assay is mostly commonly used to determine the potential cell-of-origin of tumors (Fig. 1B, a), although it can also be used to study CSCs (Fig. 1B, b). In the lineage-tracing assay, use of different cell-specific promoters allows distinct cell subpopulations to be labeled, allowing tracking of a single cell–derived clone in animals (see below). The ability to resolve individual cell fate is the greatest advantage of this assay. To determine cell-of-origin, normal (epithelial) cells are genetically labeled followed by introduction of activating and inactivating mutations in various oncogenes and tumor suppressors in the same cell type. The fully transformed cell that forms a tumor can then be traced and identified as the cellular source of the tumor (Fig. 1B, c). On the other hand, in the established, traced tumors, single marked tumor cells can be purified out and used in the LDA and serial tumor transplantations to determine whether the lineage-traced tumor cells have true CSC properties, that is, self-renewing and long-term tumor-propagating activity (Fig. 1B, d). This latter tracing strategy can also be adapted to dissect tumor cell heterogeneity in cultured cancer cells and human xenograft tumors. For example, a PSA promoter was used to drive reporters (GFP and RFP) in a lentiviral vector, which was used to infect cultured as well as xenograft prostate cancer cells and to separate the $PSA^{-/lo}$ and PSA^+ prostate cancer cells (8). When traced *in vitro* and *in vivo*, the $PSA^{-/lo}$ prostate cancer cells were found

Published OnlineFirst August 19, 2015; DOI: 10.1158/0008-5472.CAN-15-0798

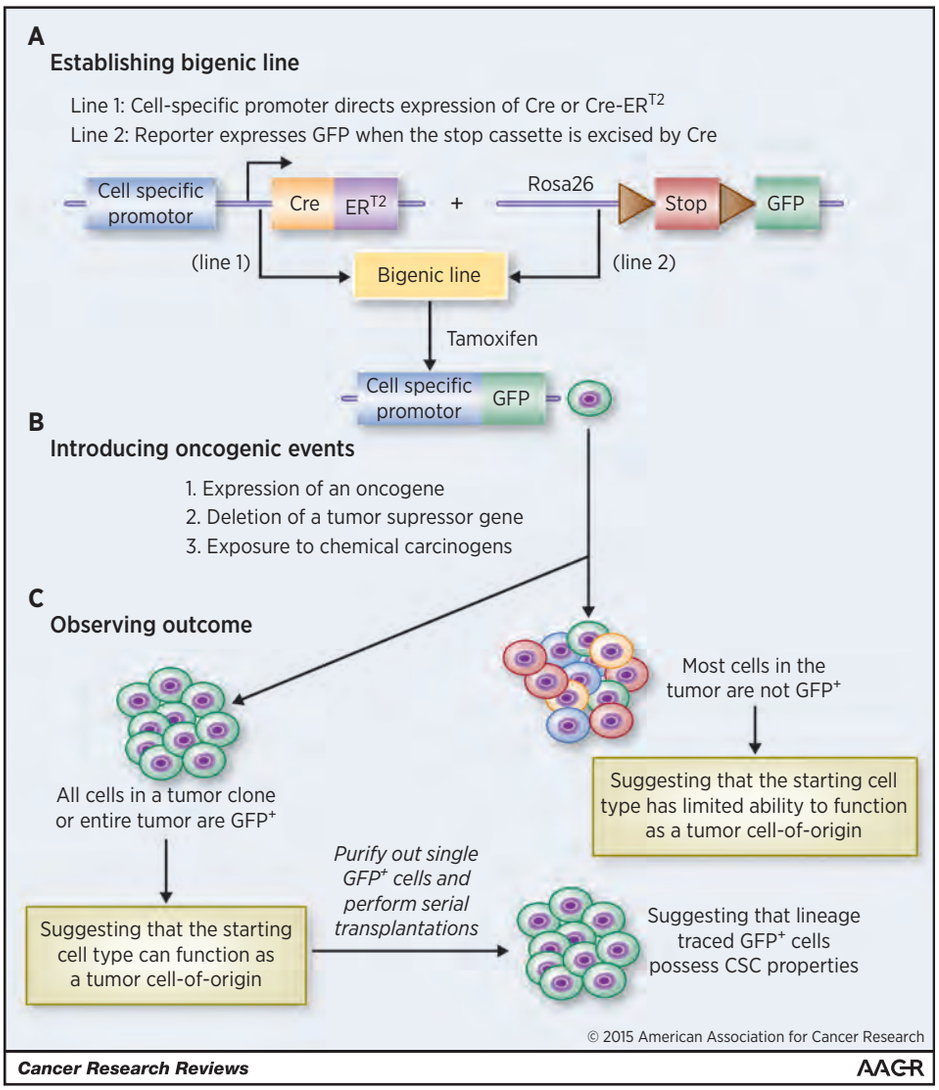

Figure 2.
Schematic for a lineage-tracing study. Three main steps are outlined. See text for detailed descriptions.

to be able to undergo asymmetric cell division generating PSA$^+$ cells under time lapse microscopy as well as in serially transplanted tumors (8). Similarly, a Wnt reporter was used to trace colorectal CSCs and to demonstrate that the secreted soluble molecules from the neighboring myofibroblasts activate the Wnt signaling in these CSCs (16).

Figure 2 depicts a basic scheme for performing a lineage-tracing study. The first step is to establish a bigenic mouse line by crossing an inducible Cre line, which expresses the Cre recombinase, with a "generic" reporter line to achieve cell-specific labeling (Fig. 2A). For the inducible Cre transgenic (Tg) line, a cell-type–specific gene promoter is used to drive the expression of modified, tamoxifen-inducible Cre (CreER or CreER^{T2}). The gene promoters can be stem cell–specific (e.g., *p63*, *Lrig1*, *Lgr5*, *Sox9*, *Nkx3.1*, etc.) or the ones active in differentiated lineages (e.g., *K8* and *K18*). Promoter can be endogenous, in which CreER or CreERT2 expression cassette is knocked into the endogenous promoter locus. Alternatively, an exogenous promoter can be used to drive Cre expression in a conventional Tg line. An example is the use of human *PSA* gene promoter to drive Cre expression in a Tg model to show that regenerated prostatic epithelial cells upon castration—androgen supplementation—were derived from the pre-existent luminal cells (17). In the second mouse line, a reporter (either fluorogenic such as GFP and RFP or colorigenic such as β-galactosidase) is flanked by a *loxP-STOP-loxP* sequence (Fig. 2A). In the bigenic mice, tamoxifen activates Cre expression via excising *loxP-STOP-loxP*, which in turn activates the reporter in cells that express the promoter activity (Fig. 2A). Doxycycline-inducible TetO-Cre system or orthotopic adenoviral delivery of lineage-specific Cre recombinases (AdCre) can also be used to express Cre in specific cell types.

To study tumor development, the second step is to introduce oncogenic events, which can be either genetic or chemical, to the specifically labeled cell types (Fig. 2B). For genetic approaches, this is accomplished by crossing the above bigenic line with the third Tg line that overexpresses certain oncogenes (*Myc*, *Ras*, *Tcf*, etc), or has some tumor suppressors (e.g., *Pten*, *Rb*, *p53*) deleted. For chemical carcinogenesis, the bigenic animals are challenged by chemical carcinogens (e.g., DMBA)

Published OnlineFirst August 19, 2015; DOI: 10.1158/0008-5472.CAN-15-0798

known to cause cancer in the specific tissues/cells. The molecular basis of chemical carcinogenesis is still genetic—for instance, DMBA mainly causes mutations in K-*ras*. In the final step of lineage tracing (Fig. 2C), tumor development is observed by monitoring the expression pattern of the trace label. For instance, if all cells in a tumor clone or the entire tumor is label (e.g., GFP)-positive, it suggests that the specific cell type marked by GFP *CAN* function as a cancer cell-of-origin in that specific context. These GFP^+ tumor cells can be purified out in serial tumor transplantations to further demonstrate their CSC or tumor-propagating activities (Fig. 2C). On the other hand, if the majority of tumor cells are GFP^-, it would suggest that the initially traced cell type does not function as the cell-of-origin for the tumor development (Fig. 2C).

Recently, three lineage-tracing studies (18–20) provided support for the CSC model across three different types of solid tumors—skin, intestinal, and brain (Fig. 3). In one study (18), lineage tracing was used to pinpoint a putative endogenous glioma stem cell population that plays a pivotal role in tumor maintenance and recurrence after chemotherapy (Fig. 3A). A nestin-ΔTK-IRES-GFP transgene labeled quiescent subventricular zone (SVZ) adult neural stem cells and the labeled GFP^+ cells could be ablated by ganciclovir (GCV) through the action of the truncated thymidine kinase (TK; Fig. 3A, a). When this Tg line was crossed with glioma-prone mouse line called Mut7 (induced by concerted deletion of three tumor suppressors, i.e., *Nf1*, *p53*, and *Pten* in GFAP-expressing cellular compartment), a subset of endogenous glioma tumor cells was also labeled by GFP and these GFP^+ cells could also be ablated by GCV (Fig. 3A, b). Interestingly, most GFP^+ glioma cells were $Sox2^+$ and not dividing (i.e., $Ki67^-$) whereas most $Ki67^+$ glioma cells were GFP^- (Fig. 3A, b). Temozolomide, a drug used to treat patients with glioma, eliminated most $GFP^-/Ki67^+$ tumor cells leaving behind a significant fraction of $GFP^+/Ki67^-$ quiescent mouse glioma cells, which mediated recurrent tumor formation (Fig. 3A, b). Remarkably, ablation of the GFP^+ cells with chronic GCV administration significantly retarded tumor growth, leading to extended animal survival, and combined temozolomide and ganciclovir treatment impeded tumor development (Fig. 3A, c; ref. 13). GCV administration also reduced tumor growth in secondary tumor transplants (Fig. 3A, d). This lineage-tracing study demonstrates that a relatively quiescent subset of endogenous glioma cells, with properties similar to those proposed for CSCs, is responsible for sustaining long-term tumor growth.

In the second study (19), use of a multicolor Cre reporter R26R-Confetti and the β-naphtoflavone–inducible Ah-Cre mouse strain demonstrated that the crypt stem cell marker Lgr5 also marked a subpopulation of adenoma cells induced by loss of *Apc* (Fig. 3B, a). When R26R-Confetti was crossed into the Lgr5 knock-in Cre-expressing mouse strain, tamoxifen injection allowed single $Lgr5^+$ stem cells to randomly adopt one of the four fluorescent colors encoded in the R26R-Confetti allele. The formation of adenomas was derived from individual *Apc*-mutant stem cells. In addition, the location of the labeled $Lgr5^+$ cells was near the base of the wedge-shaped adenoma segments, concurrent with the crypt stem cell niche (Fig. 3B, a). Transcriptional profiles and clonogenic potential of Lgr5-GFP^{hi} cells suggested that this population constituted multipotent stem cells. The fate of $Lgr5^+$ adenoma cells in individual clones was back-traced *in vivo*, and it was concluded that the cells were derived from a single adenoma stem cell (Fig. 3B, b).

The third lineage-tracing study used a classical chemical 2-stage carcinogenesis model (20), in which skin papillomas were initiated by the carcinogen DMBA and then propagated by tumor promoter TPA (Fig. 3C, a). The bigenic line, K14CreER/Rosa-YFP, was created by crossing K14-driven CreER line with the Rosa26-YFP reporter line (Fig. 3C, a). In the presence of tamoxifen, all K14-expressing basal keratinocytes would be labeled as YFP^+. Upon DMBA/TPA treatment and tamoxifen application, cells within the papillomas were labeled and the YFP^+ tumor cells were capable of generating all cell types that comprised the tumor (Fig. 3C, a). Interestingly, the majority of labeled tumor cells in benign papillomas had limited proliferative potential, whereas a particular fraction had the capacity to persist long term (20). Specifically, the more persistent population displayed stem cell–like characteristics and cycled twice per day, whereas a slower cycling transient population gave rise to terminally differentiated tumor cells. Data from 3-dimensional (3D) reconstruction using confocal analyses of clones indicated that papillomas were sustained by a cellular hierarchy in which a minor population of tumor cells with stem cell–like properties gave rise to a more transient progenitor cell pool (Fig. 3C, c).

Lineage tracing has now been used to identify probable cells-of-origin for many mouse models of cancers, including intestinal, prostate and basal cell carcinomas, brain and breast tumors, as well as pancreatic ductal adenocarcinoma. In prostate cancer, for example, the lineage-tracing assay was used to identify a rare luminal epithelial population, termed CARNs (castration-resistant Nkx3.1-expressing cells) with stem cell properties during prostate regeneration in mice (21). These cells were marked using a genetically engineered mouse line in which an inducible Cre^{ERT2} recombinase was put under the control of the endogenous promoter for *Nkx3.1*, a prostate tumor suppressor. After Cre activation by tamoxifen treatment in castrated *Nkx3.1CreERT2*$^{/+}$; *R26R-YFP*$^{/+}$ male mice, YFP expression was observed in luminal epithelial cells, corresponding to lineage-marked CARNs. All CARNs in the regressed prostate were strictly luminal and growth-quiescent. However, after regeneration upon testosterone treatment, the percentage of lineage-marked cells increased 9-fold, indicating their proliferative potential, and, important, basal cells appeared, indicating that CARNs contained bipotential progenitors. Subsequent single-cell transplantation of lineage-marked CARNs further indicated the multipotency of these cells. The authors further demonstrated that by crossing the compound reporter mice with *Pten* mutant mice, the CARNs could function as cells-of-origin for prostate cancer (21). The same group later showed that basal cells, upon loss of *Pten*, gave rise to tumors with luminal phenotypes, but they noted that these basal cells displayed substantial phenotypic plasticity when removed from their endogenous tissue microenvironment (22). Hence, the authors stressed that transplantation-based assays have a tendency to overestimate the frequency of putative stem cells and that genetic lineage tracing *in vivo* should be preferably used for identification of potential tumor cell-of-origin (22).

Another group genetically marked mouse prostate basal cells and luminal cells in adult mice using K14-CreER and K8-$CreER^{T2}$, respectively, to further interrogate the cellular origin of prostate cancer (23). It was found that prostate basal cells only generated basal cells, whereas luminal cells only generated luminal cells, suggesting that adult prostate epithelial lineages are maintained

Published OnlineFirst August 19, 2015; DOI: 10.1158/0008-5472.CAN-15-0798

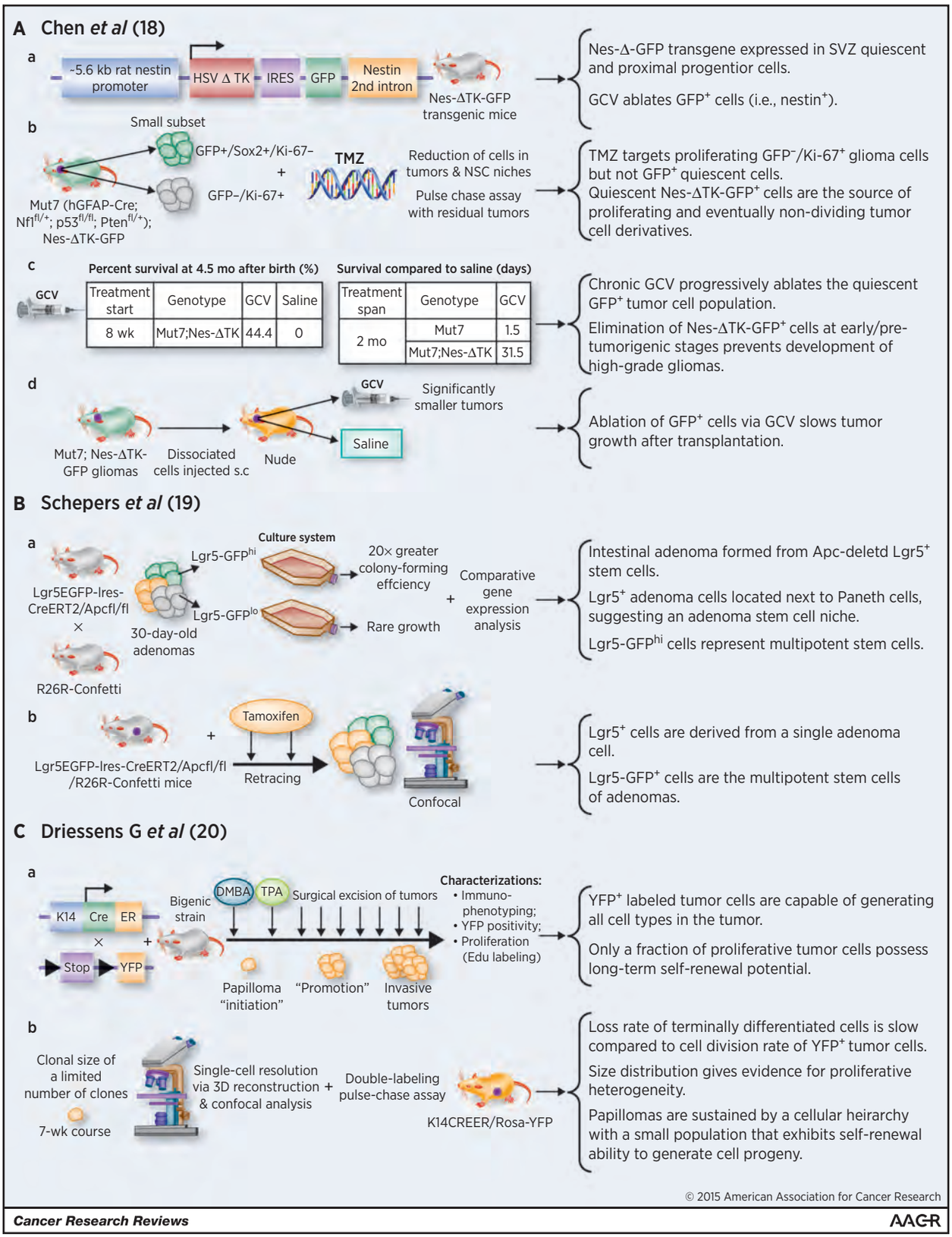

Figure 3.
Summary of three recent lineage-tracing studies providing support for the CSC model. Details for each study are discussed in the text. The lineage-tracing tumor models are presented on the left and main outcomes and conclusions summarized on the right.

Published OnlineFirst August 19, 2015; DOI: 10.1158/0008-5472.CAN-15-0798

by unipotent progenitors or self-duplication of epithelial cells. *Pten* was then knocked out in both cell types, and interestingly, prostatic intraepithelial neoplasia, a precursor lesion to prostate cancer, appeared in both mice but only after a long latency in the K14-CreER mice, suggesting that basal cells had to convert into luminal cells in the context of tumor development by *Pten* deletion. This study demonstrates that both prostate basal and luminal cells can serve as the cellular origin for prostate cancer.

As in all other techniques, there are caveats and problems associated with lineage tracing. First of all, lineage tracing can only be conducted in mice and there are fundamental differences between human and rodent organs and cells. Take prostate again, mouse prostate has four distinct lobes that do not exist in the human counterpart. Mouse prostate does not even express PSA, the most "important" molecule in defining the prostate as a male glandular organ and in defining fully differentiated luminal epithelial cells. Also, somatic mouse cells possess high telomerase activity and express significantly longer telomeres than the human cells, suggesting that mouse cells in most lineages may never undergo true terminal differentiation. These latter molecular features underlie the reasons why rodent cells are highly susceptible to spontaneous immortalization as well as experimental tumorigenic transformation. Consequently, results with mouse studies should never be directly equated to human systems and always be put in appropriate context.

Second, the labeling efficiency in lineage-tracing studies is highly variable depending on the Cre- or reporter-driving promoters and generally low and the results may oftentimes be subject to alternative interpretations. When endogenous promoters are used, the promoter activity in less differentiated cells may not be strong enough to turn on the transgene, leading to low efficiency and spurious interpretations. In the example presented in Fig. 4, when CreER is driven by the endogenous k5 promoter, lineage-tracing studies in adult mice may lead to the conclusion that k5-expressing (basal) cells can only regenerate more k5-positive basal cells. However, in multipotent progenitor cells that have the ability to differentiate into not just k5 cells but also luminal or even neuroendocrine cells because they have just started expressing k5 mRNA and the k5 promoter activity in these progenitor cells is too weak to activate the Cre, these cells will not be labeled (Fig. 4). In other words, only more differentiated cells that have already undergone lineage specification will be tagged by the reporter (Fig. 4), leading to inaccurate or even erroneous conclusions. Along this line, when exogenous or heterologous promoters are used in lineage tracing, they will randomly integrate into the genome, resulting in patterns of expression different from the endogenous gene. Furthermore, such promoters are likely regulated by quite different mechanisms than the endogenous promoters. In some cases, promoters exhibit some expression in tissues outside of those predicted, due to regulatory elements or read-through transcripts at the site of insertion.

Third, when lineage tracing is combined with mouse tumor models to elucidate cell-of-origin, there exists another problem. Most human epithelial cancers develop through decades of clonal evolution and accumulation of genetic mutations and epigenetic alterations. However, in mouse models of human cancer, the promoter is instantly turned on, leading to all-at-once genetic defects in an entire population of cells, a phenomenon fundamentally unlike the sequential acquisition of mutations found in most human cancers. Ideally, a cancer model should recapitulate the natural history of the disease by introducing a low frequency of sporadic mutations at a defined time.

Finally, the remaining construct and its insertional effects must be optimized. In most inducible lines, in which there is a single element to control Cre, the system frequently becomes

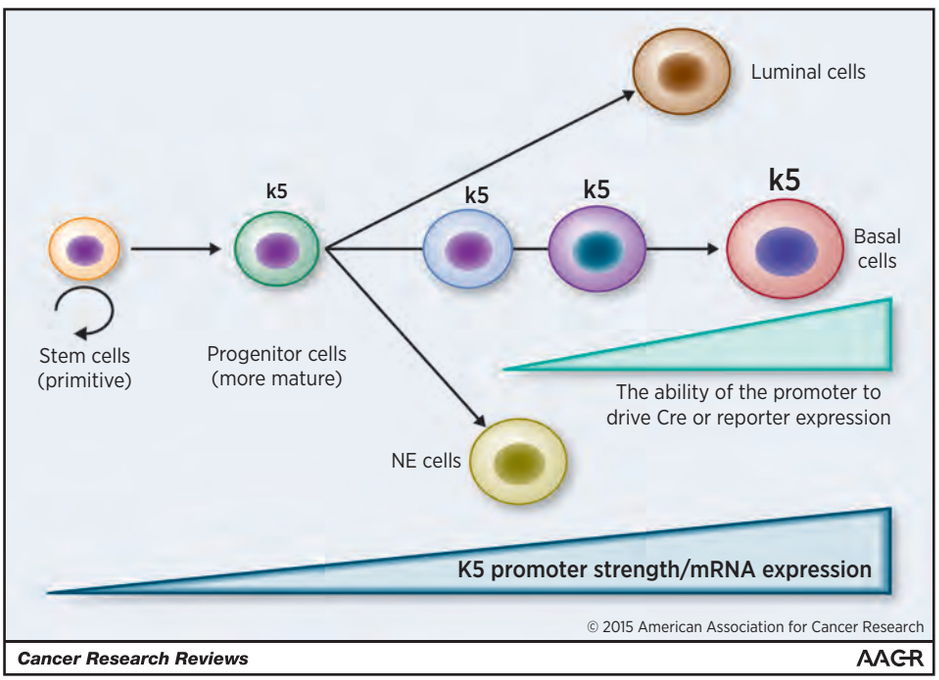

Figure 4.
Potential problems associated with lineage tracing. In this example, primitive stem cells with self-renewing activity do not express k5, whereas more mature progenitor cells start expressing low levels of k5 mRNA but the promoter activity is not strong enough to drive Cre or reporter gene expression. Hence, the promoter strength in less differentiated cells may not be strong enough to reach the labeling threshold, thereby failing to label the true primitive stem cells that possess the ability to undergo multilineage differentiation. NE, neuroendocrine.

Published OnlineFirst August 19, 2015; DOI: 10.1158/0008-5472.CAN-15-0798

leaky, having minor but detectable Cre activity in the absence of the inducer, resulting in spontaneous background recombination. In some cases, an alternative transgenic line, Ah*cre*ER^{T}, can be used to eliminate background recombination via controlling Cre activity transcriptionally both by Ah promoter and by tamoxifen binding (24). In addition, transgene insertion of Cre recombinase under the control of a specific promoter may alter the function of the endogenous locus via activation or silencing. Incomplete incorporation of regulatory elements into the driver construct or alternatively unexpected excision can also occur (25). *Lox*P-flanked target genes can differ dramatically with respect to their sensitivity to Cre-mediated recombination (26). Finally, Cre activity can be modified by strain genetic background and variable maternal/paternal germline expression can occur, highlighting the need for animal model optimization.

Concluding Remarks and Perspectives

The preceding discussions highlight the varying conclusions that may reflect differences and limitations in each assay used. A combinatorial approach of the two assays has the potential to lead to a better understanding of the cellular origins of cancer and CSCs and the development of more effective cancer therapies. A major consideration in performing both CSC and tumor cells-of-origin studies is the emergence of CSCs via cellular dedifferentiation (reviewed in detail in ref. 2). Several recent studies have demonstrated that non-CSCs can acquire CSC-like activity under certain conditions (27–30). For instance, many aggressive CSCs within individual tumors can be newly derived from their non-CSC counterparts, and this dedifferentiation may occur continually during the development of the tumor. In melanoma, differentiated cancer cells can dedifferentiate into cells resembling embryonic stem cells that organize into vessel-like structures (30). In breast cancer, CSCs exist in distinct mesenchymal-like and epithelial-like states (27). Remarkably, these two populations of CSCs manifest different locations in the tumors and functional activities: while mesenchymal-like CSCs ($CD24^{-}CD44^{+}$) are mainly localized at the invasive tumor front and are largely quiescent, the epithelial-like CSCs ($ALDH^{+}$) are located more centrally and are highly proliferative (30). Understanding the plasticity of CSCs and identifying the subpopulations of non-CSCs that are poised to convert to CSCs (2) should greatly facilitate the efforts in dissecting tumor cell heterogeneity and developing CSC-specific therapeutics. It has become clear that to eradicate cancer and prevent relapse, both CSCs and their less tumorigenic progeny must be targeted.

Disclosure of Potential Conflicts of Interest

No potential conflicts of interest were disclosed.

Acknowledgments

The authors thank colleagues in the Tang laboratory for helpful discussions and advice and Joi Holcomb for graphical assistance. They apologize to authors whose work could not be cited because of space constraint.

Grant Support

Work in the authors' laboratory was supported, in part, by grants from NIH (R01-CA155693), Department of Defense (W81XWH-13-1-0352 and W81XWH-14-1-0575), CPRIT (RP120380), and MDACC Center for Cancer Epigenetics (all to DGT). K. Rycaj was supported in part by an NIH postdoctoral fellowship.

Received March 22, 2015; revised May 18, 2015; accepted May 18, 2015; published OnlineFirst August 19, 2015.

References

1. Visvader JE. Cells of origin in cancer. Nature 2011;469:314–22.
2. Tang DG. Understanding cancer stem cell heterogeneity and plasticity. Cell Res 2012;22:457–72.
3. Kreso A, Dick JE. Evolution of the cancer stem cell model. Cell Stem Cell 2014;14:275–91.
4. Passey RD, Dmochowski L, Lasnitzki I, Millard A. Cultivation *in vitro* of frozen and desiccated mouse tumour tissues. Br Med J 1950;2:1134–6.
5. Hewitt HB. Studies of the quantitative transplantation of mouse sarcoma. Br J Cancer 1953;7:367–83.
6. Al-Hajj M, Wicha MS, Benito-Hernandez A, Morrison SJ, Clarke MF. Prospective identification of tumorigenic breast cancer cells. Proc Natl Acad Sci USA 2003;100:3983–8.
7. Singh SK, Hawkins C, Clarke ID, Squire JA, Bayani J, Hide T, et al. Identification of human brain tumour initiating cells. Nature 2004;432:396–401.
8. Qin J, Liu X, Laffin B, Chen X, Choy G, Jeter CR, et al. The PSA(-/lo) prostate cancer cell population harbors self-renewing long-term tumor-propagating cells that resist castration. Cell Stem Cell 2012;10:556–69.
9. O'Brien CA, Pollett A, Gallinger S, Dick JE. A human colon cancer cell capable of initiating tumor growth in immunodeficient mice. Nature 2007;445:106–10.
10. Goldstein AS, Huang J, Guo C, Garraway IP, Witte ON. Identification of a cell of origin for human prostate cancer. Science 2010;329:568–71.
11. Taylor RA, Toivanen R, Frydenberg M, Pedersen J, Harewood L, Australian Prostate Cancer B, et al. Human epithelial basal cells are cells of origin of prostate cancer, independent of CD133 status. Stem Cells 2012;30:1087–96.
12. Domingo-Domenech J, Vidal SJ, Rodriguez-Bravo V, Castillo-Martin M, Quinn SA, Rodriguez-Barrueco R, et al. Suppression of acquired docetaxel resistance in prostate cancer through depletion of notch- and hedgehog-dependent tumor-initiating cells. Cancer Cell 2012;22:373–88.
13. Quintana E, Shackleton M, Sabel MS, Fullen DR, Johnson TM, Morrison SJ. Efficient tumour formation by single human melanoma cells. Nature 2008;456:593–8.
14. Boiko AD, Razorenova OV, van de Rijn M, Swetter SM, Johnson DL, et al. Human melanoma-initiating cells express neural crest nerve growth factor receptor CD271. Nature 2010;466:133–7.
15. Kelly PN, Dakic A, Adams JM, Nutt SL, Strasser A. Tumor growth need not be driven by rare cancer stem cells. Science 2007;317:337.
16. Vermeulen L, De Sousa E, Melo F, van der Heijden M, Cameron K, de Jong JH, Borovski T, et al. Wnt activity defines colon cancer stem cells and is regulated by the microenvironment. Nat Cell Biol 2010;12:468–76.
17. Liu J, Pascal LE, Isharwal S, Metzger D, Ramos Garcia R, Pilch J, et al. Regenerated luminal epithelial cells are derived from preexisting luminal epithelial cells in adult mouse prostate. Mol Endocrinol 2011;25:1849–57.
18. Chen J, Li Y, Yu TS, McKay RM, Burns DK, Kernie SG, et al. A restricted cell population propagates glioblastoma growth after chemotherapy. Nature 2012;488:522–6.
19. Schepers AG, Snippert HJ, Stange DE, van den Born M, van Es JH, van de Wetering M, et al. Lineage tracing reveals Lgr5+ stem cell activity in mouse intestinal adenomas. Science 2012;337:730–5.
20. Driessens G, Beck B, Caauwe A, Simons BD, Blanpain C. Defining the mode of tumour growth by clonal analysis. Nature 2012;488:527–30.
21. Wang X, Kruithof-de Julio M, Economides KD, Walker D, Yu H, Halili MV, et al. A luminal epithelial stem cell that is a cell of origin for prostate cancer. Nature 2009;461:495–500.
22. Wang ZA, Mitrofanova A, Bergren SK, Abate-Shen C, Cardiff RD, Califano A, et al. Lineage analysis of basal epithelial cells reveals their unexpected

Published OnlineFirst August 19, 2015; DOI: 10.1158/0008-5472.CAN-15-0798

plasticity and supports a cell-of-origin model for prostate cancer heterogeneity. Nat Cell Biol 2013;15:274–83.
23. Choi N, Zhang B, Zhang L, Ittmann M, Xin L. Adult murine prostate basal and luminal cells are self-sustained lineages that can both serve as targets for prostate cancer initiation. Cancer Cell 2012;21: 253–65.
24. Kemp R, Ireland H, Clayton E, Houghton C, Howard L, Winton DJ. Elimination of background recombination: somatic induction of Cre by combined transcriptional regulation and hormone binding affinity. Nucleic Acids Res 2004;32:e92.
25. Heffner CS, Herbert Pratt C, Babiuk RP, Sharma Y, Rockwood SF, Donahue LR, et al. Supporting conditional mouse mutagenesis with a comprehensive cre characterization resource. Nat Commun 2012; 3:1218.
26. Schmidt-Supprian M, Rajewsky K. Vagaries of conditional gene targeting. Nat Immunol 2007;8:665–8.
27. Liu S, Cong Y, Wang D, Sun Y, Deng L, Liu Y, et al. Breast cancer stem cells transition between epithelial and mesenchymal states reflective of their normal counterparts. Stem Cell Reports 2013;2:78–91.
28. Gupta PB, Fillmore CM, Jiang G, Shapira SD, Tao K, Kuperwasser C, et al. Stochastic state transitions give rise to phenotypic equilibrium in populations of cancer cells. Cell 2011;146:633–44.
29. Roesch A, Fukunaga-Kalabis M, Schmidt EC, Zabierowski SE, Brafford PA, Vultur A, et al. A temporarily distinct subpopulation of slow-cycling melanoma cells is required for continuous tumor growth. Cell 2010; 141:583–94.
30. Hendrix MJ, Seftor EA, Hess AR, Seftor RE. Molecular plasticity of human melanoma cells. Oncogene 2003;22:3070–5.

Cancer Research
The Journal of Cancer Research (1916–1930) | The American Journal of Cancer (1931–1940)

AACR American Association for Cancer Research

Cell-of-Origin of Cancer versus Cancer Stem Cells: Assays and Interpretations

Kiera Rycaj and Dean G. Tang

Cancer Res 2015;75:4003-4011. Published OnlineFirst August 19, 2015.

Systematic dissection of phenotypic, functional, and tumorigenic heterogeneity of human prostate cancer cells

Xin Liu[1,*], Xin Chen[1,*], Kiera Rycaj[1,*], Hsueh-Ping Chao[1,3], Qu Deng[1,3], Collene Jeter[1], Can Liu[1], Sofia Honorio[1], Hangwen Li[1], Tammy Davis[1], Mahipal Suraneni[1], Brian Laffin[1], Jichao Qin[1], Qiuhui Li[1], Tao Yang[2], Pamela Whitney[1], Jianjun Shen[1], Jiaoti Huang[4], Dean G. Tang[1,2,3,5]

[1]Department of Epigenetics and Molecular Carcinogenesis, University of Texas MD Anderson Cancer Center, Science Park, Smithville, TX 78957, USA

[2]Cancer Stem Cell Institute, Research Center for Translational Medicine, East Hospital, Tongji University School of Medicine, Shanghai 200120, China

[3]Program in Molecular Carcinogenesis, University of Texas Graduate School of Biomedical Sciences (GSBS), Houston, TX 77030, USA

[4]Department of Pathology and Laboratory Medicine, David Geffen School of Medicine, UCLA, Los Angeles, CA 90095, USA

[5]Centers for Cancer Epigenetics, Stem Cell and Developmental Biology, RNA Interference and Non-Coding RNAs, and Molecular Carcinogenesis, University of Texas MD Anderson Cancer Center, Houston, TX 77030, USA

[*]These authors have contributed equally to this work

Correspondence to:
Dean G. Tang, **e-mail:** dtang@mdanderson.org

Keywords: *prostate cancer*, *cancer stem cells*, *stem cells*, *differentiation*, *heterogeneity*

Received: *April 15, 2015* ***Accepted:*** *June 12, 2015* ***Published:*** *June 24, 2015*

ABSTRACT

Human cancers are heterogeneous containing stem-like cancer cells operationally defined as cancer stem cells (CSCs) that possess great tumor-initiating and long-term tumor-propagating properties. In this study, we systematically dissect the phenotypic, functional and tumorigenic heterogeneity in human prostate cancer (PCa) using xenograft models and >70 patient tumor samples. In the first part, we further investigate the PSA$^{-/lo}$ PCa cell population, which we have recently shown to harbor self-renewing long-term tumor-propagating cells and present several novel findings. We show that discordant AR and PSA expression in both untreated and castration-resistant PCa (CRPC) results in AR^{+}PSA^{+}, AR^{+}PSA^{-}, AR^{-}PSA^{-}, and AR^{-}PSA^{+} subtypes of PCa cells that manifest differential sensitivities to therapeutics. We further demonstrate that castration leads to a great enrichment of PSA$^{-/lo}$ PCa cells in both xenograft tumors and CRPC samples and systemic androgen levels dynamically regulate the relative abundance of PSA^{+} versus PSA$^{-/lo}$ PCa cells that impacts the kinetics of tumor growth. We also present evidence that the PSA$^{-/lo}$ PCa cells possess distinct epigenetic profiles. As the PSA$^{-/lo}$ PCa cell population is heterogeneous, in the second part, we employ two PSA^{-} (Du145 and PC3) and two PSA^{+} (LAPC9 and LAPC4) PCa models as well as patient tumor cells to further dissect the clonogenic and tumorigenic subsets. We report that different PCa models possess distinct tumorigenic subpopulations that both commonly and uniquely express important signaling pathways that could represent therapeutic targets. Our results have important implications in understanding PCa cell heterogeneity, response to clinical therapeutics, and cellular mechanisms underlying CRPC.

INTRODUCTION

Cellular heterogeneity represents an omnipresent feature in human tumors, which contain cells with diverse morphology, cytogenetic markers, growth kinetics, immunological characteristics, metastatic ability, and sensitivity to therapeutics [1]. Clonal evolution, driven by genetic instability of tumor cells, and phenotypic maturation and diversification, driven by cancer stem cells (CSCs), operate hand-in-hand to generate tumor cell

heterogeneity [2]. Specifically, clonal evolution creates genetic diversity and drives clonal competition between multiple subclones in the tumor whereas CSC-directed differentiation and maturation generates phenotypic diversity within individual subclones [2].

One of the key biological properties of CSCs is the 'stemness', which confers on a subpopulation of cancer cells two fundamental traits of normal stem cells, i.e., self-renewal and differentiation ability. Like normal stem cells, whose self-renewal and multi-lineage differentiation (i.e., pluripotency) are regulated by an intricate network of transcription factors, CSC stemness is also bestowed by critical signaling pathways (e.g., Notch, HH, and Wnt) and transcription factors and epigenetic regulators such as Nanog, Bmi-1, and Polycomb proteins [3–5]. It has now become clear that intra-clonally, genetic mutations, epigenetic changes and tumor microenvironment converge on regulating the CSC stemness to generate the phenotypic diversity and functional heterogeneity of tumor cells [2].

Many different experimental strategies and approaches have been adopted and developed to purify and enrich CSC populations. These include cell surface marker-based flow sorting, marker-independent strategies such as holoclone, clonogenic sphere formation and label-retaining assays, functional assays such as Side Population (SP; which measures the drug-effluxing ability in CSCs) and Aldefluor assay (which measures the aldehyde dehydrogenase [ALDH] mediated detoxification capability), and *in vitro* and *in vivo* lineage tracing assays [1]. To study the stemness properties, a 'gold-standard' functional assay is to xenotransplant candidate human CSC populations in immunodeficient mice at decreasing cell doses, an assay often called limiting dilution (tumor) assay or LDA [1]. The LDA measures tumor-regenerating or tumor-initiating capacity, which, when combined with serial tumor transplantations, would measure the self-renewal ability of the candidate CSCs [1].

Prostate cancer (PCa) is extremely heterogeneous but the cellular basis for PCa cell heterogeneity remains largely unknown. Understanding PCa cell heterogeneity is of clear clinical importance as it likely underlies differential PCa cell response to androgen-deprivation therapy (ADT) and other therapeutics such as docetaxel and helps explain PCa recurrence and metastasis. Work from our lab in the past 10 years has generated important clues to understanding the cellular heterogeneity of PCa. We have demonstrated that PCa cell SP and holoclones, as well as $CD44^+$ and $CD44^+\alpha2\beta1^+$ subpopulations in some PCa models are enriched in prostate CSCs (PCSCs) with high tumorigenic and metastatic potential [6–12]. Using a PSA promoter (PSAP) driven EGFP lentiviral tracing reporter, we have recently provided evidence that the undifferentiated ($PSA^{-/lo}$) PCa cell population harbors long-term tumor-propagating PCSCs that preferentially express stem cell-associated genes and can self-renew to generate PSA^+ PCa cells by asymmetric cell division [13]. Of clinical significance, $PSA^{-/lo}$ PCa cells can initiate robust tumor regeneration in fully castrated hosts, survive androgen deprivation, and mediate tumor recurrence [13]. Many other groups have also reported PCSC subpopulations [14–24].

One of the issues in PCSC studies is that different research groups often use divergent PCa models and different phenotypic markers or experimental approaches to enrich for putative PCSCs, making direct comparison of the results difficult. The main goals of our current study are to systematically dissect the PCa cell heterogeneity via assessing a spectrum of PCa cell line and xenograft models as well as primary tumor cells and samples, to address the relationship between and among different PCSC subpopulations, and dissect the relationship between PCSCs and AR, PSA, and castration resistance. The results presented here greatly advance our understanding of PCa cell heterogeneity and help to illuminate cellular mechanisms of PCa therapy resistance.

RESULTS

PCa cell heterogeneity: Inverse correlation between tumor *PSA* mRNA levels with clinical parameters and discordant *AR* and *PSA* mRNA expression in PCa samples

We started our studies by systematically analyzing 27 'eligible' *Oncomine* data sets of PCa cDNA microarrays (Supplementary Table 1) and by correlating tumor *PSA* mRNA levels versus Gleason grade, hormone-refractory and metastatic status, and patient survival. The results revealed several interesting points. FIRST, an inverse correlation was observed between tumor *PSA* mRNA and tumor grade in all data sets with information on *PSA* mRNA and Gleason grade of the tumors and with sufficient number of cases (Figure 1A–1C; 13). Reduced *PSA* mRNA was also noted in high-grade (i.e., Gleason 8–10) tumors in the data sets of Best 2, Holzbeierlein, and Wallace (not shown). SECOND, reduced *PSA* levels were observed in hormone-refractory PCa in data sets of Best 2 (Figure 1D), and of Tamura and Tomlins (not shown). THIRD, we observed reduced tumor *PSA* mRNA in PCa metastases in all 11 data sets that contained ≥ 5 metastatic samples (Figure 1E–1H). Interestingly, although the draining lymph node (LN) only occasionally showed reduced *PSA* mRNA (e.g., in the Chandran data set; Figure 1H), distant metastases, e.g., those to the adrenal gland, bone, and liver, generally exhibited consistent reduction in *PSA* mRNA (Figure 1H). Distant metastases also tended to express lower *PSA* mRNA than the benign/normal (B/N) tissues (Figure 1H). FINALLY, overall patient survival correlated with high intra-tumoral PSA mRNA levels in the data sets of Nakagawa [13], Setlur, Grasso, and Taylor (Figure 1I).

Strikingly, we frequently observed a discordant relationship between *PSA* and *AR* in individual primary (Figure 1A–1C), hormone-refractory (Figure 1D) and metastatic (Figure 1E–1F) samples. *PSA* mRNA was decreased across all data sets (Figure 1A–1F; data not

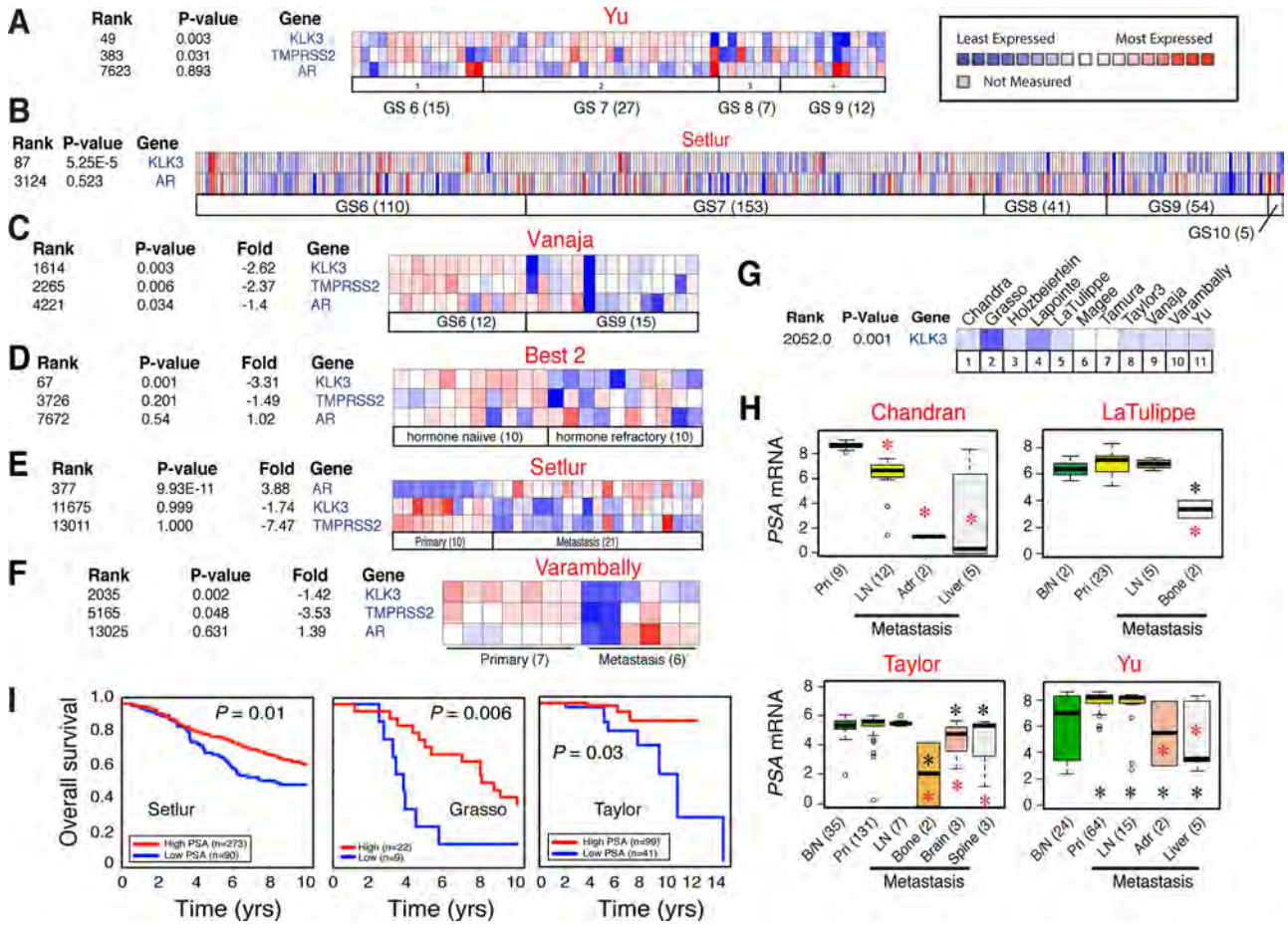

Figure 1: Inverse correlation between tumor *PSA* mRNA levels and clinical parameters. A–C. Heat map presentation of the mRNA levels of *PSA*, *AR*, and/or *TMPRSS2* in relation to tumor grade (GS, Gleason score) in three representative *Oncomine* data sets (indicated above; see Supplementary Table 1 for information). Note that in individual samples, the *AR* and *PSA* expression patterns are frequently discordant. The legend on the right applies to all heat maps. **D–F.** Heat map showing discordant *AR* and *PSA* expression and reduced *PSA* mRNA levels in CRPC (D) and/or in metastases (E–F). **G.** Reduced *PSA* mRNA levels in PCa metastases across all 11 eligible data sets. **H.** Examples of reduced *PSA* mRNA levels in PCa metastasis. B/N, benign/normal; pri, primary tumor; LN, lymph node; Adr., adrenal gland. Red asterisk, $P < 0.05$ in comparison with primary tumors; black asterisk, $P < 0.05$ compared to B/N samples. **I.** Overall patient survival positively correlates with high *PSA* mRNA levels in 3 data sets.

shown) except the Setlur data set in which *PSA* reduction was not statistically significant although the decreasing trend was clear (Figure 1E). Another AR target, *TMPRSS2*, was also reduced in most data sets analyzed (Figure 1A, 1C–1F; 13). In contrast, the *AR* mRNA levels were not correlated with tumor grade, hormone refractoriness, or metastasis (Figure 1A–1F; 13; data not shown). In one data set (Vanaja), the *AR* mRNA levels were actually decreased in Gleason 9 tumors compared to Gleason 6 tumors (Figure 1C).

PCa cell subtypes in untreated patient tumors, enrichment of PSA$^{-/lo}$ PCa cells in CRPC and castration-resistant xenograft tumors, and differential drug responses in PCa cell subtypes

Discordant mRNA expression patterns between *AR* and *PSA* suggest 4 subpopulations of PCa cells, i.e., AR$^+$PSA$^+$, AR$^-$PSA$^+$, AR$^+$PSA$^-$, and AR$^-$PSA$^+$ cells. Immunofluorescence (IF) analysis of AR and PSA proteins in 11 untreated primary patient tumors (HPCa; Supplementary Table 2) directly supports this premise as the 4 subpopulations of PCa cells could be identified in all samples, although, as expected, the AR$^+$PSA$^+$ PCa cells represented the major subpopulation (Figure 2A–2B; Supplementary Figure 1 and 2). In these analyses, AR showed typical nuclear staining with a spectrum of intensities (negative, weak, intermediate, and strong) whereas PSA generally showed cytoplasmic staining (Figure 2A; Supplementary Figure 1 and 2). Occasionally, nuclear PSA (Supplementary Figure 1C; Supplementary Figure 2B) and secreted PSA in the lumen of the prostatic glands (Supplementary Figure 2C) were observed.

Next, we analyzed AR and PSA protein expression in 23 CRPC samples including 20 samples (CRPC1–20) in a tissue microarray (TMA) and 3 regular CRPC (CRPC21–23) samples (Figure 2C; Supplementary Figure

3A–3B). AR expression showed wide variability in these CRPC samples. For example, CRPC5 and CRPC12 showed apparently increased AR expression and AR^+ PCa cells compared to untreated PCa but many CRPC samples (e.g., CRPC9, 16, and 20–23) significantly lacked AR^+ PCa cells (Figure 2C; Supplementary Figure 3, Ab, B). Furthermore, in all AR^+ CRPC samples, AR^- PCa cells could be readily identified, e.g., in CRPC8 (Figure 2C) and CRPC2 and 7 (Supplementary Figure 3B). In sharp contrast to the AR expression patterns, the majority of the 23 CRPC samples mostly lacked appreciable PSA expression or PSA^+ PCa cells (Figure 2C; Supplementary Figure 3A–3B). Only one sample (CRPC12) was found to have somewhat concordant AR and PSA expression and only CRPC19 (the patient was treated with Lupron for ~2 weeks) expressed high intratumoral PSA (Supplementary Figure 3A). The IHC studies in this cohort of 23 CRPC samples indicate that *$PSA^{-/lo}$* PCa cells (which can be AR^+ or AR^-) are enriched in patient CRPC samples.

Subsequently, we investigated the relative abundance of the 4 subtypes of PCa cells in 3 AD (androgen-dependent) and AI (androgen-independent) PCa xenograft models, LNCaP, LAPC4 and LAPC9 (13). In all 3 models, the AI tumors were highly enriched in $PSA^{-/lo}$ PCa cells (Figure 2D–2E; Supplementary Figure 3C–3D; data not shown). In LNCaP AD tumors, ~80% of the cells were AR^+PSA^+ and the other 3 subtypes of cells represented the minority (Figure 2D–2E; Supplementary Figure 3C). In contrast, the LNCaP AI tumors showed greatly reduced AR^+PSA^+ cells and dramatically increased $PSA^{-/lo}$ ($AR^+PSA^{-/lo}$ and $AR^-PSA^{-/lo}$) cells (Figure 2D–2E; Supplementary Figure 3C). Similarly, $PSA^{-/lo}$ PCa cells were significantly increased in LAPC4 (Supplementary Figure 3D) and LAPC9 (not shown) AI tumors. Interestingly, in LAPC4 AI tumors, most AR localized to the cytoplasm (Supplementary Figure 3D).

To explore potential differences between subtypes of PCa cells in response to therapeutics, we performed a preliminary study in three types of LNCaP cells (Figure 2F), i.e., AR^+PSA^+ wild-type LNCaP, AR^+PSA^- LNCaP-abl [25], and AR^-PSA^- LNCaP-CDSS and LNCaP-MDV cells, the two castration-resistant LNCaP sublines we recently established (Rycaj et al., manuscript submitted). We treated these 3 LNCaP cell types with two antiandrogens, i.e., bicalutamide and MDV3100 (MDV; Enzalutamide), two chemotherapeutic drugs (etoposide and docetaxel), and two molecularly targeted drugs, i.e., ABT-199, which selectively inhibits Bcl-2 [26, 27], and AEW541, an inhibitor of IGF-1R [28], which is important for the $PSA^{-/lo}$ PCa cells [13]. In this relatively short (72 h) cytotoxicity assay, the three LNCaP cells manifested differential responses to the 6 drugs (Figure 2G). The AR^+PSA^+ wild-type LNCaP cells displayed responses to all 6 drugs except Bicalutamide whereas AR^+PSA^- LNCaP-abl cells behaved overall similarly to wild-type LNCaP cells and showed only resistance to 10 μM ABT-199 (Figure 2G). In contrast, the AR^-PSA^- LNCaP-CDSS and LNCaP-MDV cells manifested prominent resistance to both etoposide and docetaxel as well as to MDV and ABT-199 (Figure 2G). Interestingly, LNCaP-abl cells showed higher sensitivity to 10 μM AEW541 than both wild-type LNCaP and LNCaP-CDSS and LNCaP-MDV cells (Figure 2G). This pilot experiment establishes the proof-of-principle that subtypes of PCa cells with distinct AR and PSA expression profiles may respond differently to anticancer therapeutics.

$PSA^{-/lo}$ PCa cells: Heterogeneity in AR expression, quiescence, and resistance to antiandrogens and other therapeutics

The converging findings from the above studies are that: 1) the $PSA^{-/lo}$ PCa cells pre-exist in untreated HPCa; 2) $PSA^{-/lo}$ PCa cells become enriched in patient CRPC and AI xenograft models; and 3) $PSA^{-/lo}$ PCa cells respond to antiandrogens and several other therapeutics differently than the PSA^+ PCa cells. We recently employed a series of lentiviral GFP/RFP reporters to separate $PSA^{-/lo}$ from PSA^+ PCa cells to compare their molecular, cell biological, and tumorigenic properties [13]. Herein, we continue to use this system to further explore the cellular and molecular distinctions between these cell subsets, investigate their differential responses to therapeutics *in vitro* and to systemic androgen levels *in vivo*, and interrogate the relationship between the $PSA^{-/lo}$ PCa cells vs. several other PCSC populations.

Infection of LNCaP cells with the PSAP-GFP lentivector at an MOI of 20 led to 100% infection and GFP positivity faithfully reported the endogenous PSA expression [13]. Consistent with earlier results [13], all PSA^+ (i.e., GFP^+) LNCaP cells were nuclear AR^+ whereas only ~30% $PSA^{-/lo}$ (i.e., $GFP^{-/lo}$) LNCaP cells had strong nuclear AR (Supplementary Figure 4A). Similar results were obtained in LAPC9 and LAPC4 xenografts [13; data not shown]. These observations suggest that the $PSA^{-/lo}$ PCa cell population is heterogeneous with respect to AR expression, consistent with the above IHC-based immunophenotypic analysis of AR and PSA expression in both untreated HPCa and CRPC samples.

We have previously demonstrated [13] that under time-lapse videomicroscopy, single PSA^+ PCa cells exclusively undergo symmetrical cell divisions (SCD) whereas $PSA^{-/lo}$ PCa cells undergo both SCD and asymmetrical cell division (ACD). Here we employed time lapse-based single-cell tracking to determine cell-cycle transit times in two populations of LNCaP cells (Figure 3A–3E). As observed previously [13], the PSA^+ (i.e., GFP^+) LNCaP cells underwent rapid and exclusive SCD to generate more PSA^+ cells (Figure 3A; Figure 3D, top). In contrast, many $PSA^{-/lo}$ (i.e., GFP^-) LNCaP cells underwent ACD during the first cell division (Figure 3B; Figure 3D, middle). Very occasionally, we observed rare $PSA^{-/lo}$

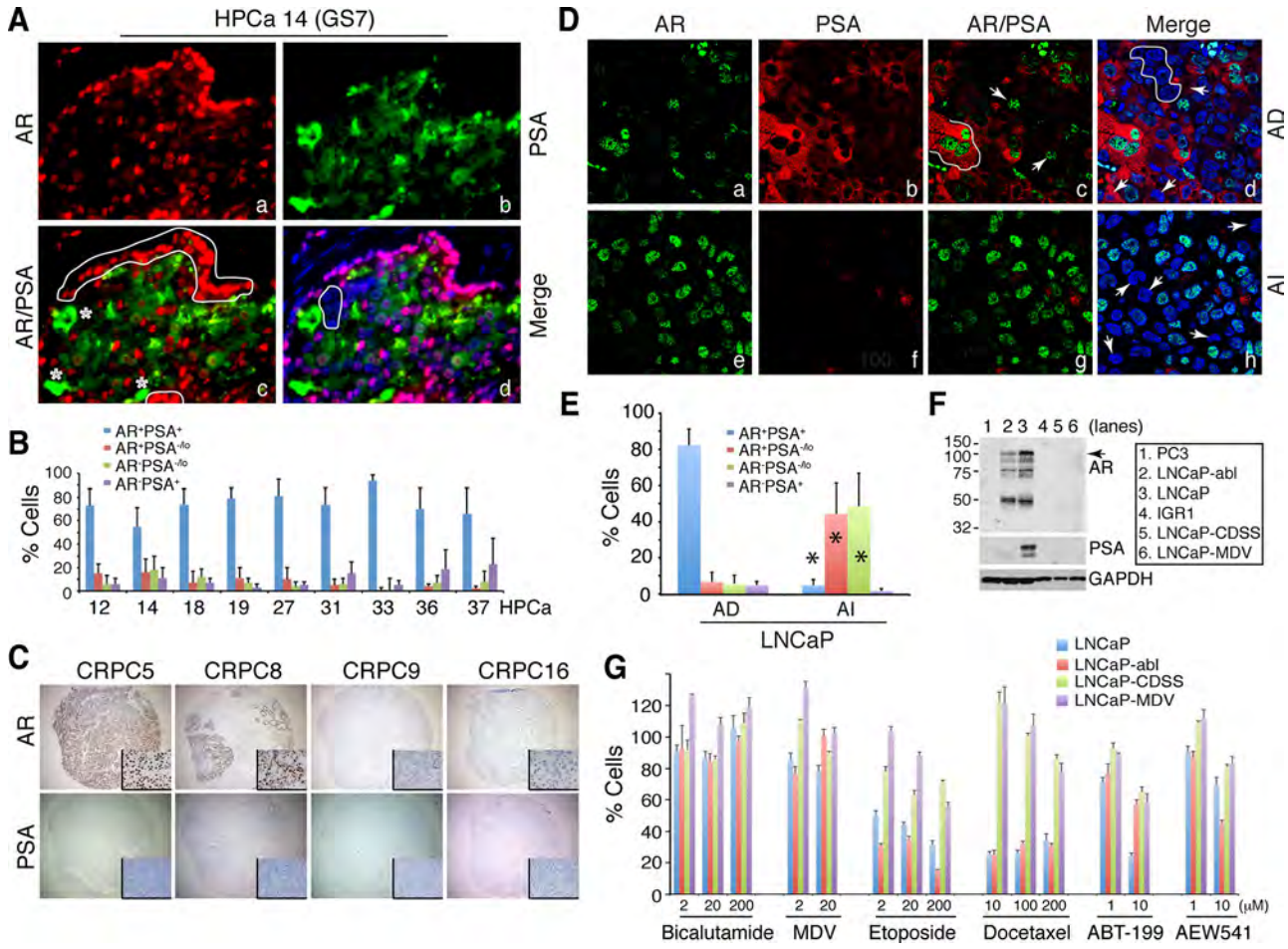

Figure 2: Discordant PSA and AR protein expression in PCa, 4 subtypes of PCa cells, enrichment of PSA$^{-/lo}$ PCa cells in CRPC, and differential drug responses in subtypes of PCa cells. A–B. Representative immunofluorescence images (×400) illustrating discordant PSA and AR protein expression in HPCa 14 (A) and quantification of 4 subpopulations of PCa cells in the 9 HPCa samples (B). In A, AR^{+}PSA^{+} PCa cells are marked by red nuclei and green cytosplasm, AR^{+}PSA$^{-/lo}$ cells by red alone (panel c, white circled areas), AR^{-}PSA^{+} cells by green alone (panel c, asterisks), and AR^{-}PSA$^{-/lo}$ cells by being negative (or low) for both red and green staining (panel d, white circled area). **C.** IHC analysis of AR and PSA in the TMA samples. Shown are 4 CRPC samples illustrating homogeneous loss of PSA in all 4 samples and heterogeneous expression of AR (insets: 400×). **D.** Double immunofluorescence staining of AR and PSA in AD vs. AI LNCaP xenograft tumors. In panel c, the white line demarcates 3 AR^{+}PSA^{+} cells and the arrows point to 2 AR^{+}PSA$^{-/lo}$ cells. In panel d, the white circle demarcates several AR^{-}PSA$^{-/lo}$ cells and the arrows point to 3 AR^{-}PSA^{+} cells. In panel h, the arrows illustrate several AR^{-}PSA$^{-/lo}$ cells. Shown are representative confocal images (original magnification; ×400). **E.** Quantification of the 4 subtypes of PCa cells in AD and AI LNCaP xenograft tumors. A total of 809 and 907 cells were counted from several AD and AI tumors, respectively. *$P < 0.001$ in AI compared in AD tumors. **F.** Western blotting analysis of AR and PSA. PC3 and IGR1 cells, which are known to be negative for both proteins, were used as controls. Note that the wild-type LNCaP cells (lane 3) were AR^{+}PSA^{+} whereas LNCaP-abl cells AR^{+}PSA^{-} (lane 2). LNCaP-CDSS and LNCaP-MDV cells were both AR^{-}PSA^{-} (lanes 5–6). The arrow indicates the ~114 kD full-length AR and lower bands might represent AR splice variants (top panel). **G.** Drug responses in subtypes of LNCaP cells. LNCaP (AR^{+}PSA^{+}), LNCaP-abl (AR^{+}PSA^{-}), and LNCaP-CDSS and LNCaP-MDV (AR^{-}PSA^{-}) cells were treated with the drugs at the indicated concentrations for 72 h. Relative cell numbers were determined by Alamar Blue assays (see Methods). For Bicalutamide, at 2 and 20 μM, only LNCaP-MDV cells showed partial resistance ($P < 0.05$). At 200 μM, Bicalutamide even slightly promoted wild-type LNCaP cell growth probably due to its well-known agonist effects. For MDV3100, at 2 μM, LNCaP-CDSS and LNCaP-MDV but not LNCaP-abl cells showed partial resistance ($P < 0.05$). At 200 μM of MDV, all 3 LNCaP sublines showed partial resistance ($P < 0.05$) in comparison to wild-type cells. Note prominent resistance in LNCaP-CDSS and LNCaP-MDV cells to etoposide and docetaxel ($P < 0.001$ for all comparisons between these two cell types vs. either wild-type or LNCaP-abl cells). All LNCaP cell types responded similarly to 1 μM ABT-199 but the 3 LNCaP sublines (LNCaP-abl, -CDSS, and –MDV) showed common resistance to 20 μM ABT-199 ($P < 0.01$). LNCaP-CDSS and LNCaP-MDV but not LNCaP-abl cells showed partial resistance to 1 μM of AEW541 ($P < 0.05$) and this resistance phenotype dissipated at 10 μM AEW541, at which LNCaP-abl cells showed higher sensitivity than wild-type cells ($P < 0.05$).

cells that underwent SCD during the first cell division followed by complex division modes during subsequent divisions (Figure 3C; Figure 3D, bottom). Strikingly, the PSA^{+} daughter cells derived from ACD in most cases underwent rapid SCD whereas the PSA$^{-/lo}$ mother cells rarely divided again (Figure 3B), suggesting that the PSA$^{-/lo}$

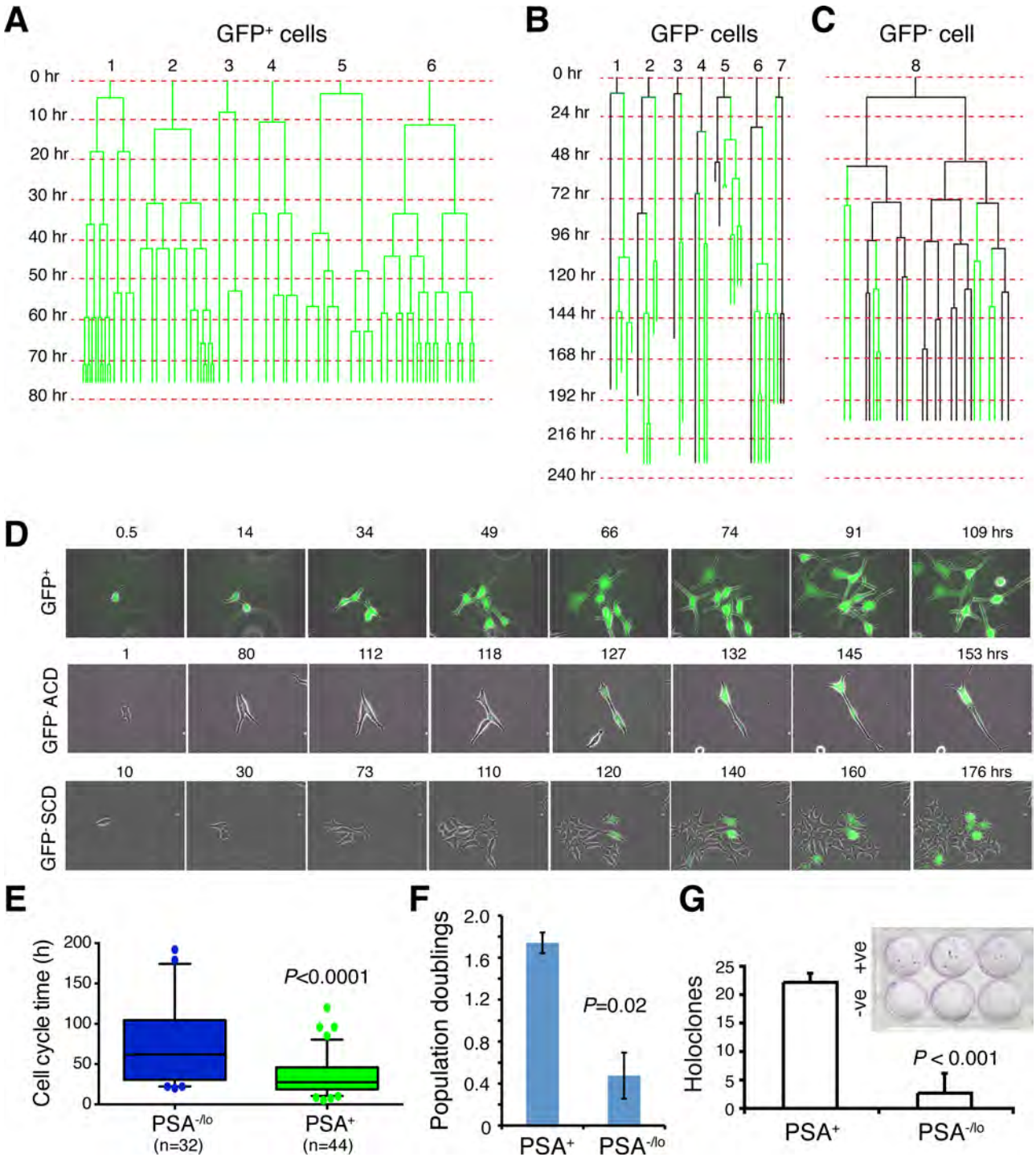

Figure 3: PSA$^{-/lo}$ LNCaP cells are more quiescent than PSA^{+} cells. A–C. Cell division mode and cell-cycle transit times in LNCaP cells in regular serum-containing culture medium as determined by time-lapse videomicroscopy. Shown in A are six representative GFP^{+} LNCaP cells that underwent symmetrical cell divisions. Shown in B are seven representative GFP^{-} LNCaP cells that underwent asymmetric cell divisions. Shown in C is one GFP^{-} LNCaP cell that underwent complex cell divisions (see Text). Time scale is shown on the left for each cell recorded. **D.** Time-lapse images showing one GFP^{+} LNCaP cell undergoing symmetrical cell divisions in the first round and all subsequent rounds (top panels), one GFP^{-} cell undergoing ACD during the first cell division (middle panels), and one GFP^{-} cell undergoing symmetrical cell division during the first cell division followed by complex division modes in the progeny (bottom panels). **E.** Graphical presentation of cell-cycle transition times in PSA$^{-/lo}$ vs. PSA^{+} LNCaP cells based on the time-lapse tracking of the 2 cell types. **F.** PSA^{+} and PSA$^{-/lo}$ LNCaP cells were FACS-purified and plated in quadruplicate in 96-well plate (1,500 cells/well) and cultured in regular serum-containing medium. Live cells were enumerated 3 days after plating and presented are the population doublings. **G.** PSA^{+} (+ve) and PSA$^{-/lo}$ (–ve) LNCaP cells were plated at clonal density (100 cells/well in triplicate) and cultured in RPMI-5% FBS plus 10 nM R1881 for 2 weeks. At the end, holoclones were enumerated. Shown are the bar graphs (mean ± S.D) pooled from three repeat experiments and a representative Giemsa-stained image (inset).

cells overall divided more slowly than the isogenic PSA$^+$ cells. Indeed, quantification of time-lapse images indicated that the PSA$^{-/lo}$ LNCaP cells had longer average cell-cycle transit times than PSA$^+$ cells (Figure 3E). Consistent with the single cell analysis, PSA$^{-/lo}$ LNCaP cells demonstrated lower cumulative population doublings (Figure 3F) and holoclone [10] forming efficiency (Figure 3G) in regular medium containing serum (which contained small amount of steroid hormones) than the corresponding PSA$^+$ cells. In another holoclone assay, in which we sorted single PSA$^+$ and PSA$^{-/lo}$ LNCaP cells into 96-well plates and cultured them in serum-containing medium. 18 days later, 19 holoclones developed in 36 single PSA$^+$ LNCaP cells (i.e., cloning efficiency = 53%) whereas 24 clones developed in 83 single PSA$^{-/lo}$ cells (cloning efficiency = 29%). Taken together, these results suggest that the PSA$^{-/lo}$ PCa cells, in the presence of androgen, are more quiescent than PSA$^+$ PCa cells.

Are there any differences between PSA$^{-/lo}$ and PSA$^+$ PCa cells in the absence of androgen or in the presence of stresses? In our earlier studies [13], we performed cDNA microarray analyses comparing gene expression profiles in PSA$^{-/lo}$ and PSA$^+$ LNCaP as well as xenograft LAPC9 cells. A total of 570 probesets representing 337 genes (see Methods) were commonly upregulated (1.5 fold; $P < 0.05$) in PSA$^{-/lo}$ cells in both cell types (Supplementary Figure 4B). Remarkably, when we performed Gene Ontology (GO) analysis on the 337 genes using DAVID, the top 10 GO terms were all related, in some ways, to cellular responses to stress and wound healing (Supplementary Figure 4C). Preferential enrichment of anti-stress and regeneration genes coupled with their quiescent nature would render the PSA$^{-/lo}$ PCa cells resistant to stresses and therapeutics. Several experiments confirmed this prediction. First, when acutely purified PSA$^+$ and PSA$^{-/lo}$ LNCaP cells were cultured in androgen-deficient conditions, i.e., in medium containing charcoal dextran-stripped serum (CDSS), the PSA$^{-/lo}$ cells underwent significant expansion (Figure 4A), sharply contrasting with the scarce growth observed in androgen-proficient conditions (Figure 3F). As a matter of fact, only the PSA$^{-/lo}$ LNCaP cells showed significant survival and expansion during continued culture of up to 1 month (Figure 4B). Importantly, the suppressive effects of CDSS on PSA$^+$ LNCaP cells could be dose-dependently relieved by exogenous R1881 (Figure 4C). In another set of experiments, we treated the two purified populations of LNCaP cells side-by-side with CDSS plus bicalutamide (20 μM), etoposide (1 μM), paclitaxel (20 nM), or H2O2 (1 μM) for 4 days and then analyzed for apoptosis. As shown in Figure 4D, the PSA$^{-/lo}$ LNCaP cells were more resistant to all these treatments. Finally, we performed yet another set of side-by-side experiments with the two purified populations using the MTT assays to measure the cells that survived treatments. As shown in Figure 4E, PSA$^{-/lo}$ cells survived better than PSA$^+$ LNCaP cells in response to both Taxol and H2O2. Since we employed two purified populations of LNCaP cells to directly compare their apoptotic sensitivities (Figure 4), the results excluded the possibility that treatments caused de-differentiation in turning PSA$^+$ LNCaP cells to PSA$^{-/lo}$ cells during the treatment period (i.e., 4 days). In support, we observed that all live PSA$^+$ LNCaP cells 48 h after treatments remained GFP$^+$ (not shown).

Systemic androgen levels regulate the relative abundance of PSA$^+$ and PSA$^{-/lo}$ PCa cells in tumors

We next explored how systemic androgen levels dynamically affect the relative abundance of PSA$^{-/lo}$ vs. PSA$^+$ cells in the tumors (Figure 5). LAPC9 tumors continuously maintained in male mice (i.e., the 'AD' tumors) contained 20.9% ± 10.3% ($n = 10$) PSA$^{-/lo}$ cells with the majority being PSA$^+$ cells (Figure 5A, and 5C). When bulk LAPC9 cells from these AD tumors were transferred to androgen-deficient hosts (i.e., either castrate male or female mice) for ~2 months, PSA$^+$ cells declined significantly whereas PSA$^{-/lo}$ cells increased to ~50% (Figure 5A, and 5C). When LAPC9 tumors were maintained in androgen-deficient hosts for ~2 years (i.e., the 'AI' tumors), PSA$^{-/lo}$ cells increased to 89.3% ± 9.8% ($n = 12$) (Figure 5B). When unsorted LAPC9 cells from such AI tumors were put back in intact male mice, PSA$^+$ LAPC9 cells in the tumors again increased (Figure 5B). These results are remarkably similar to what we observed earlier in AD/AI LNCaP and LAPC4 systems and suggest that systemic androgen levels dynamically regulate the abundance of PSA$^+$ vs. PSA$^{-/lo}$ cells in prostate tumors.

When unsorted LAPC9 cells from the AD tumors, in which 70–90% cells were PSA$^+$, were implanted in different hosts, they initiated much larger tumors in male mice than in castrated male or female mice (Figure 5D). In contrast, when bulk LAPC9 cells from the AI tumors, in which ~90% cells were PSA$^{-/lo}$, were implanted in different hosts, they initiated larger tumors in androgen-deficient hosts (Figure 5E). These results indicate that the relative abundance of PSA$^+$ versus PSA$^{-/lo}$ cells greatly influences tumor growth rate in hosts with different levels of androgen.

Evidence that PSA$^{-/lo}$ PCa cells possess distinct epigenetic profiles: Analysis of bivalent chromatin domains in several genes

The above observations that systemic androgen levels regulate the relative abundance of the two populations of PCa cells *in vivo* implicate epigenetic mechanisms. Previous microarray analyses showed that the PSA$^{-/lo}$ PCa (LAPC9, LNCaP, as well as HPCa) cells overexpressed several dozens of stem cell-associated genes [13]. Of importance, the PSA$^{-/lo}$ LNCaP cells, compared to PSA$^+$ cells, also overexpressed some (e.g., EED, HDAC4, PHF8) whereas under-expressed other (e.g., DNMT3B, PHF19) chromatin modifiers/ epigenetic regulators [13]. Embryonic stem cells (ESCs) are

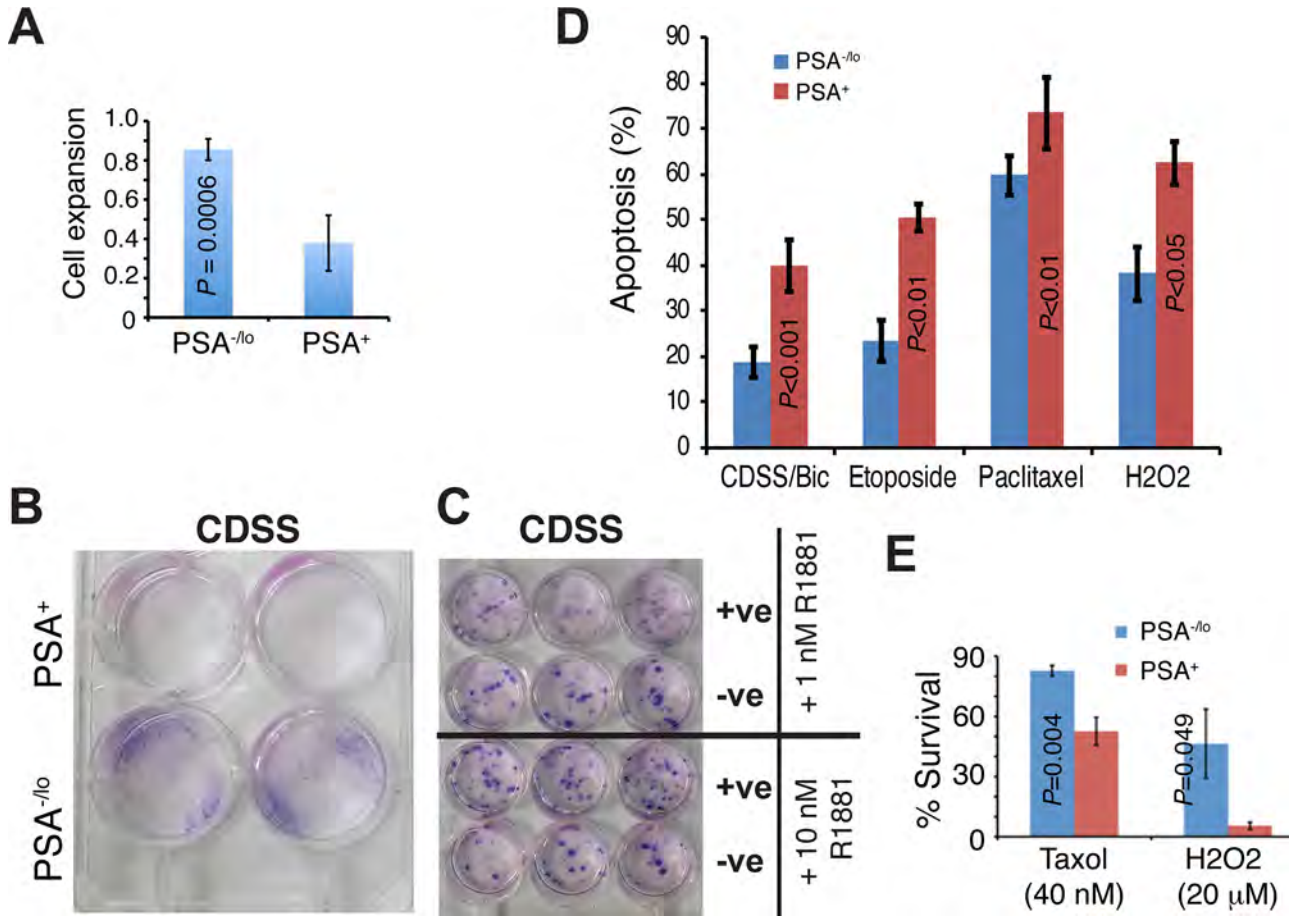

Figure 4: Differential apoptotic responses of PSA$^{-/lo}$ and PSA^{+} LNCaP cells to therapeutics. A. PSA^{+} and PSA$^{-/lo}$ LNCaP cells were plated (1,500/well) in quadruplicate in RPMI containing either 7% regular FBS or 7% charcoal dextran stripped serum (CDSS). 11 days later, live cells were measured by MTT assays. The results are presented as the cell growth (expansion) of each population in CDSS medium RELATIVE to the corresponding FBS medium (which is 1). **B.** PSA^{+} and PSA$^{-/lo}$ LNCaP cells (10,000/well) were cultured in RPMI containing 7% CDSS for 1 month and plates were stained by Giemsa. **C.** PSA^{+} and PSA$^{-/lo}$ LNCaP cells (10,000/well) were cultured in RPMI-7% CDSS plus either 1 nM or 10 nM R1881 for 25 days and plates were stained by Giemsa. Note that R1881 dose-dependently 'overcame' the CDSS effect and promoted the clonal expansion of PSA^{+} LNCaP cells. **D.** Apoptosis assessed by the Vybrant apoptosis assays. Unsorted bulk LNCaP cells infected with PSAP-GFP lentiviral reporter were plated at 120 k cells/well in 6-well plates. Cells were treated for 4 days with either DMSO, 2% CDSS plus 20 μM Bicalutamide (CDSS/Bic), 20 nM Paclitaxel, 1 μM etoposide, or 1 μM H2O2. The % apopotsis represents the mean ± S.D ($n = 3$) and P values determined by Student's t-test. No difference in apoptosis was observed in the two populations in response to vehicle DMSO (not shown). **E.** PSA$^{-/lo}$ LNCaP cells preferentially survive stress treatments. Purified PSA$^{-/lo}$ and PSA^{+} cells were plated (1,000/well) in 96-well plate in regular serum-containing medium containing Taxol (Docetaxel) or H2O2 for 48 h. At the end of treatments, live cells were measured by MTT assays and cell survival normalized to vehicle control DMSO (which is 100%).

enriched in genes associated with bivalent chromatin marks consisting of large regions of the repressive H3 lysine 27 trimethylation (H3K27me3) harboring smaller regions of H3 lysine 4 trimethylation (H3K4me3) [29]. To explore whether PSA$^{-/lo}$ PCa cells may also be epigenetically different from the differentiated isogenic PSA^{+} cells, we performed ChIP and re-ChIP (also called ChIP and sequential ChIP) analysis using the Bernstein protocol [30]. We purified PSA$^{-/lo}$ and PSA^{+} LNCaP and LAPC9 cells and analyzed 8 genes whose promoters have been associated with the bivalent marks in ESCs [29] including FGF5, NKX3.1, BCL2, CDH2 (i.e., N-cadherin), CD61 (i.e., integrin β3), AR, ASCL1, and PPP2R4. We first performed regular ChIP assays using rabbit polyclonal antibodies to pan-histone 3 (panH3), H3K4me3, or H3K27me3 in purified PSA^{+}/PSA$^{-/lo}$ LNCaP (Figure 6A) or LAPC9 (Figure 6B) cells. We then performed sequential ChIP on the first ChIP products using a mAb to H3K27me3.

The results revealed that in LNCaP cells, 4 genes, i.e., *NKX3.1, FGF5, BCL2,* and *CDH2* showed bivalent binding patterns preferentially in the PSA$^{-/lo}$ cell population (Figure 6C). In contrast, the other 4 genes (i.e., CD61, ASCL1, AR, and PPP2R4) showed overall similar re-ChIP profiles, which did not differ significantly between PSA$^{-/lo}$ vs. PSA^{+} cells (Figure 6C; data not shown). In LAPC9 cells, 4 genes, i.e., *FGF5, BCL2, CDH2* and *CD61* showed bivalent binding patterns preferentially in PSA$^{-/lo}$ cells (Figure 6D) whereas *NKX3.1* showed similarly low levels of bivalency in both populations. The other 3 genes (ASCL1,

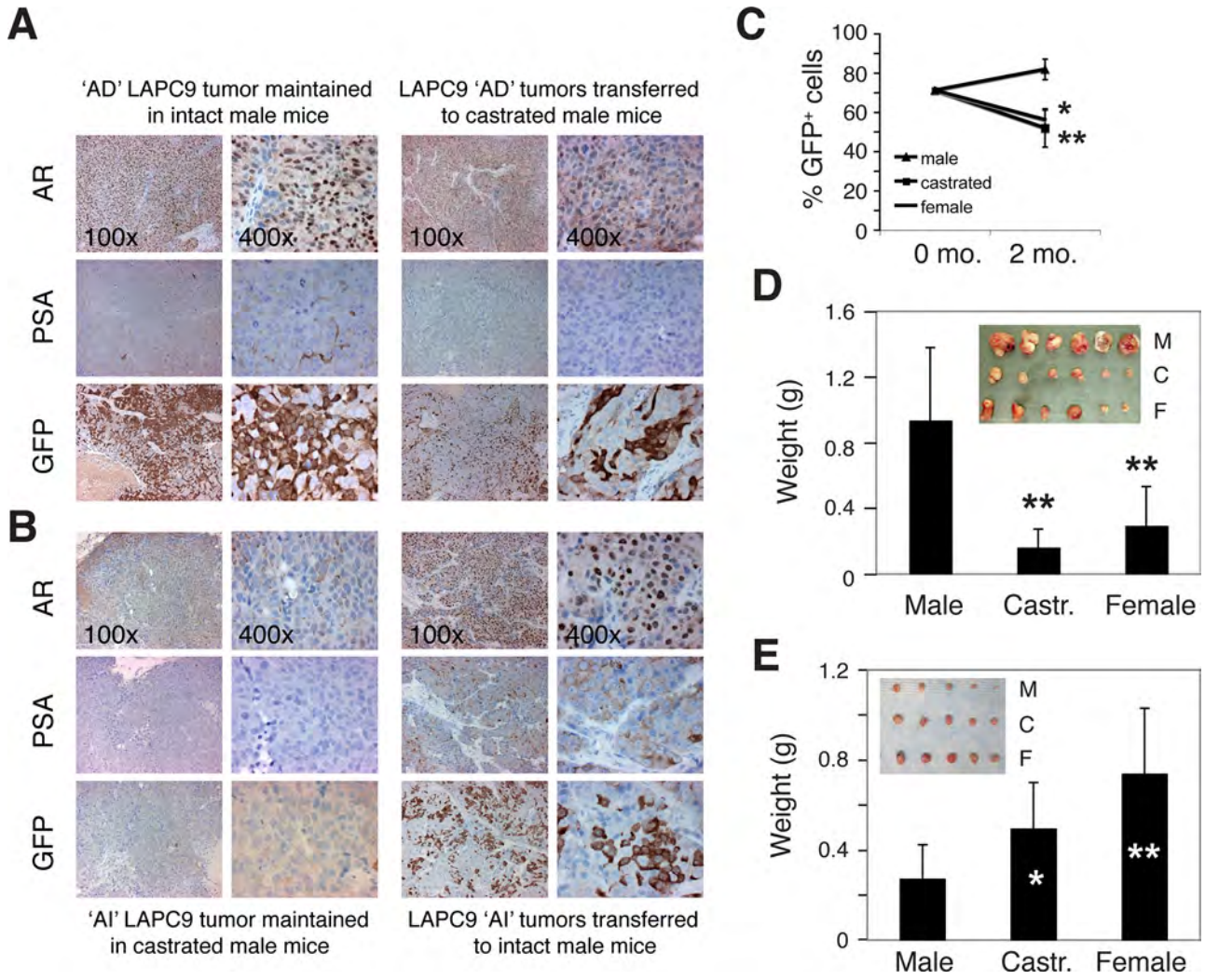

Figure 5: Systemic androgen levels regulate the relative abundance of PSA$^+$ and PSA$^{-/lo}$ cells in the tumors. A–B. Systemic androgen regulates the abundance of PSA$^+$ PCa cells in LAPC9 tumors. (A) The majority of PCa cells in LAPC9 reporter tumors maintained in intact male NOD-SCID mice expressed nuclear AR, PSA, and GFP (the left panel; note less sensitive PSA staining than corresponding GFP staining). When LAPC9 tumors in male mice were transferred to castrated mice, AR became excluded from nucleus (which was expected due to lack of the ligand), PSA staining was reduced, and % GFP$^+$ cells significantly decreased (right panels). (B) Tumor cells in the LAPC9 reporter tumors maintained in castrated male mice showed dramatically reduced numbers of AR$^+$ and PSA$^+$, and GFP$^+$ cells (the left panel; note that in these tumors GFP sequence could be readily detected by PCR analysis of genomic DNA; not shown); however, when the LAPC9 tumors in castrated mice were transferred back to intact male mice, many tumor cells again displayed nuclear AR as well as PSA/GFP positivity (right panels). **C.** LAPC9 tumor cells were purified from a maintenance reporter tumor maintained in intact male NOD/SCID mice). The bulk tumor cells contained ~72% GFP$^+$ LAPC9 cells as assessed by FACS (i.e., at 0 month). Then 100,000 unsorted LAPC9 cells were injected subcutaneously, in 50% Matrigel, in intact male mice, castrated male mice (castrated ~2 weeks earlier), or female mice ($n = 4$ for each), respectively. Two months after tumor cell implantation, tumors were harvested and the % of GFP$^+$ cells in each tumor was determined by FACS. *$P < 0.05$ and **$P < 0.01$, when compared to the tumors in male mice. **D–E.** Bulk LAPC9 cells purified from maintenance tumors in male (D) or castrated (E) mice were injected (200, 000 cells/injection) s.c in three different types of hosts (M, male; C, castrated; F, female). Tumor weights (mean ± S.D) were presented. *$P < 0.05$; **$P < 0.01$. Insets: tumor images.

AR, and PPP2R4) did not show significant differences in bivalent patterns between PSA$^{-/lo}$ vs. PSA$^+$ LAPC9 cells (data not shown). It is interesting that LNCaP and LAPC9 cells showed similar bivalent chromatin marks on 3 gene promoters (i.e., FGF5, BCL2, and CDH2) but differed in NKX3.1 and CD61. Also of interest, LNCaP cDNA microarray analysis revealed higher levels of *NKX3.1* and *FGF5* mRNAs in PSA$^{-/lo}$ cells [13] and correspondingly, our ChIP assays showed high H3K4me3 association with the *NKX3.1* and *FGF5* gene promoters also in PSA$^{-/lo}$ cells (Figure 6C), supporting the preferential activation of these two genes in PSA$^{-/lo}$ LNCaP cells. These preliminary ChIP/re-ChIP results provide evidence that the PSA$^{-/lo}$ and PSA$^+$ PCa cells may possess different epigenetic profiles.

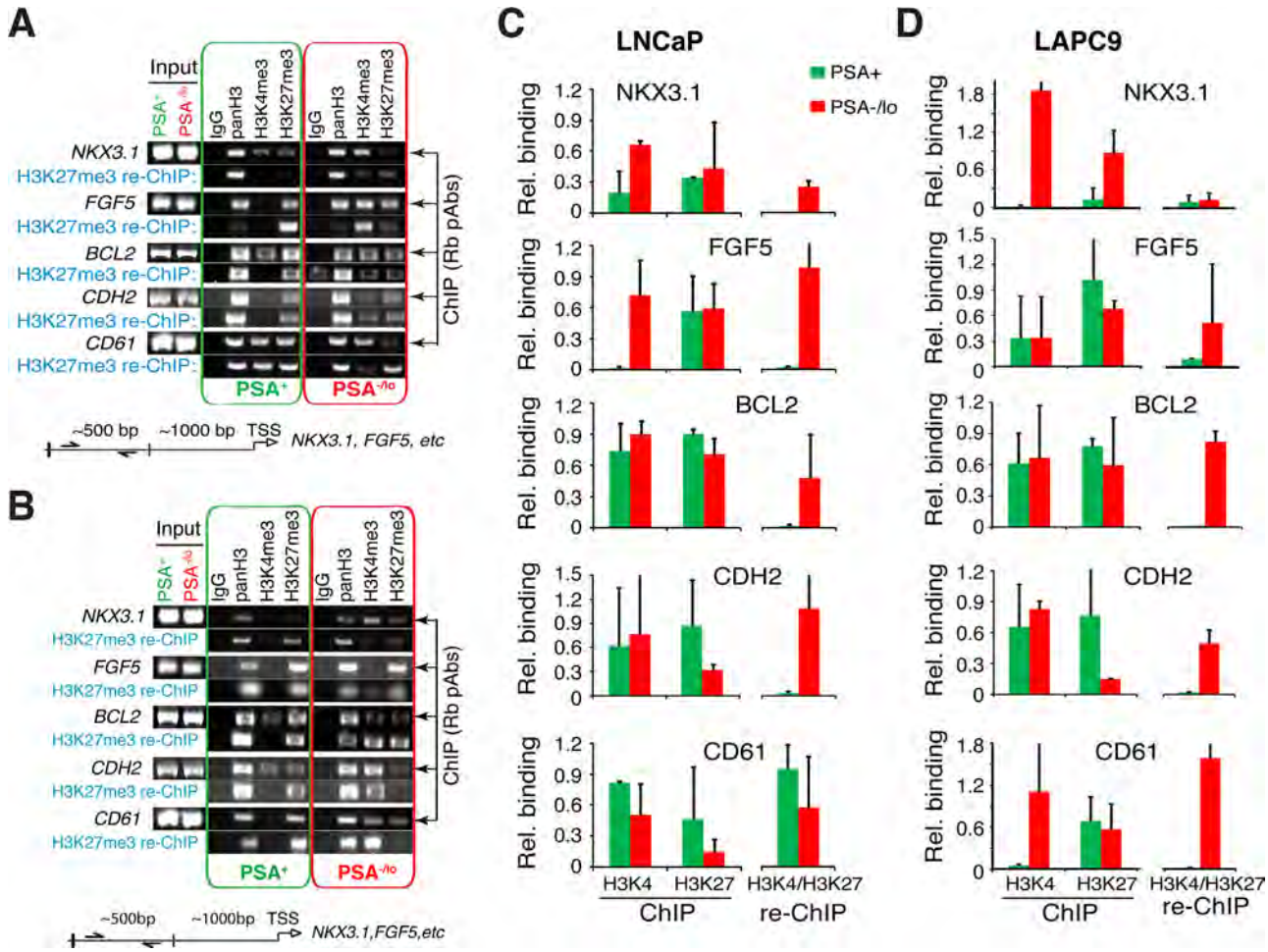

Figure 6: PSA$^{-/lo}$ PCa cells show preferential gene promoter association with bivalent chromatin marks. ChIP/re-ChIP experiments were performed in purified PSA$^{-/lo}$ and PSA^{+} LNCaP **(A** and **C).** and LAPC9 **(B** and **D).** cells. ChIP was performed with individual rabbit polyclonal antibodies (Rb pAbs) and re-ChIP was performed with a monoclonal anti-H3K27me3 antibody. Shown are representative gel images (A and B) and quantification (C and D; $n = 3$) normalized to panH3. The re-ChIP bar graphs (C and D; right) represent bivalent marks.

Relationship between PSA$^{-/lo}$ PCa cells and other tumorigenic PCa cell subsets

In our previous studies, cDNA microarray analysis revealed that the PSA$^{-/lo}$ LAPC9 cells expressed higher mRNA levels of several CSC markers including *CD44*, integrin *α2β1*, and *ALDH1A1* in comparison to PSA^{+} LAPC9 cells [13]. Indeed, using PSA^{+}/PSA$^{-/lo}$ LAPC9 cells freshly purified from xenograft reporter tumors [13], we observed lower levels of *PSA* and *AR* mRNAs (Supplementary Figure 5A) but higher levels of *CD44* mRNA (Supplementary Figure 5B) in PSA$^{-/lo}$ cells. Tumors initially derived from PSA$^{-/lo}$ LAPC9 cells, even after 3 passages in intact male mice, still expressed high levels of α2β1, CD44, and ALDH1A1 proteins compared to similarly passaged tumors initially derived from the PSA^{+} cells (Supplementary Figure 5C). These results suggest an opposite relationship between PSA expression and the three phenotypic PCSC markers. Indeed, double IF staining in benign prostate tissues showed basal expression of CD44, ALDH1A1, and α2β1 but luminal expression of PSA (Supplementary Figure 5D–5E). Similar experiments in HPCa samples also revealed mutually exclusive expression patterns between PSA versus the three PCSC markers (Figure 7A). Differential quantification demonstrated that α2β1^{+} (Figure 7B) and ALDH1A1^{+} (Figure 7C) cells were mainly PSA$^{-/lo}$. Strikingly, when we performed the opposite experiments by purifying out CD44^{+}/CD44^{-} primary tumor cells from 12 untreated tumor samples (Supplementary Table 2) and analyzing *AR* and *PSA* mRNAs in the two populations, we found that the *PSA* mRNA was preferentially expressed in CD44^{-} HPCa cells in 10 samples whereas *AR* mRNA expression pattern was more complex with preferential enrichment in CD44^{-} HPCa cells in only 6 samples (Figure 7D). In 4 samples, *AR* mRNA was actually higher in CD44^{+} HPCa cells (Figure 7D).

Comprehensive dissection of tumorigenic subsets in PCa culture and xenograft models

The above studies in primary human PCa (HPCa) samples (Figure 7; Supplementary Figure 5) suggest a concordant relationship between PSA$^{-/lo}$ cells and

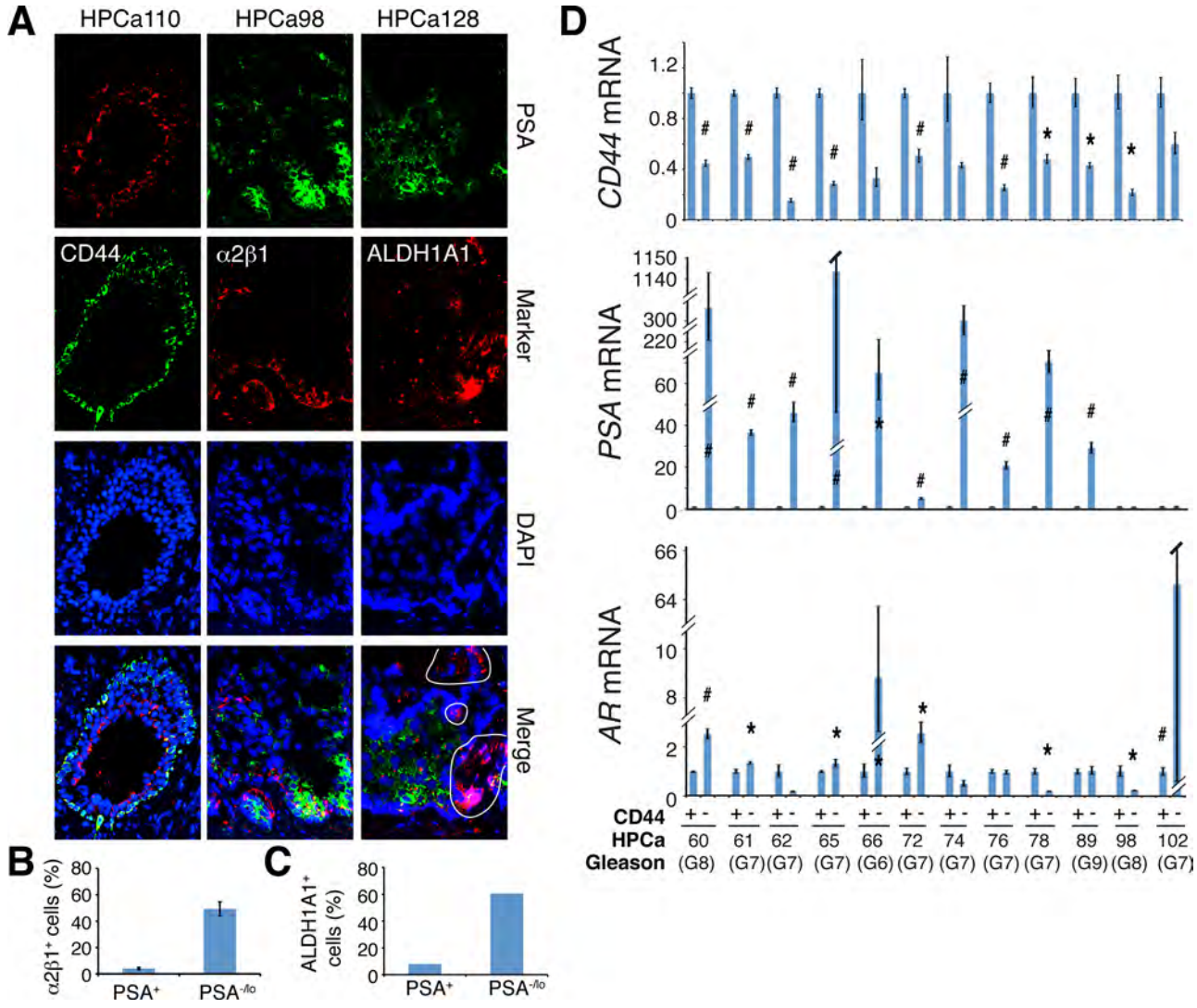

Figure 7: Relationship of PSA$^{-/lo}$ PCa cells and other PCSC marker-expressing subpopulations in HPCa. A. Representative IF images (×400) illustrating reciprocal expression patterns of ALDH1A1, α2β1, and CD44 versus PSA in the 3 HPCa samples (indicated on top). Note the mutually exclusive staining patterns of PSA versus ALDH1A1 (right; circled areas were ALDH1A1$^+$ but PSA$^-$), α2β1 (middle), or CD44 (left). **B–C.** Quantification of marker-positive cells in PSA$^{-/lo}$ vs. PSA$^+$ HPCa cells. The results for α2β1 were data pooled from counting > 500 cells each in HPCa96, HPCa98, and HPCa110 (B). The PSA$^{-/lo}$ cells contained significantly more α2β1$^+$ cells (mean ± S.D; $P < 0.0001$). The bar graph for ALDH1A1 was obtained from counting ALDH1A1-postive cells in ~1,000 each of PSA$^+$ and PSA$^{-/lo}$ cells in HPCa128. **D.** qPCR analysis of *CD44*, *AR*, and *PSA* mRNAs in CD44$^+$ and CD44$^-$ HPCa cells freshly purified from untreated primary prostate tumors. The results are expressed as relative levels in CD44$^+$ HPCa cells to those in the matched CD44$^-$ HPCa cells. *$P < 0.05$; #$P < 0.01$.

PCa cells expressing CSC markers CD44, α2β1, and ALDH1A1. Unfortunately, primary HPCa cells, and even primary HPCa pieces, are well-known to be very difficult to regenerate tumors in immunocompromised mice [11, 31]. Therefore, to further dissect the PCa cell heterogeneity, in this part of the project, we employed both surface markers (CD44, α2β1, and, for comparison, ABCG2) and functional (i.e., SP and Aldefluor) assays to dissect the tumorigenicity of PCa cell subpopulations in three PSA$^-$ (Du145, PPC-1 and PC3; all three models do not express AR and PSA and contain only PSA$^-$ cells) and three PSA$^+$ (LNCaP, LAPC4 and LAPC9; all 3 models contain PSA$^+$ and PSA$^{-/lo}$ cells) PCa models. It should be noted that although we have previously reported tumor-initiating cells in some of these models [6–12], those studies were conducted in by different investigators and at different time points. Herein, we aim to conduct side-by-side, in-depth dissection of PCa cell heterogeneity in the same models. We performed a spectrum of functional assays *in vitro* and (serial) tumor transplantations by implanting 1 to 5 × 10^5 cells in NOD/SCID mice followed by determining and comparing the tumor-initiating

frequency (TIF) of matched PCa cell subpopulations. As we describe below, the results revealed distinct phenotypic profiles of tumor-initiating cells in individual PCa models.

In vitro studies in the 4 PCa cell lines (LNCaP, Du145, PPC-1 and PC3) showed (Supplementary Figure 6; Supplementary Table 3) that they all expressed the luminal cell marker cytokeratin 18 (CK18) but only LNCaP cells expressed the differentiation markers AR and PSA. In contrast, the basal/stem cell markers CD44, α2β1, and CK5 were not detected in LNCaP cells but observed in a fraction of Du145 cells and expressed in the majority of PC3 and PPC-1 cells. We also measured telomerase activity in these cells, which mirrored the expression pattern of basal/stem cell markers (Supplementary Table 3). Interestingly, the clonogenic, tumorigenic, and metastatic capacity of the 4 PCa cells positively correlated with their telomerase activity and the abundance of basal/stem cell markers.

Subsequently, we performed limiting-dilution tumor-regeneration assays (LDA) in Du145 and PC3 cells, two surrogate PSA^- PCa models, using both marker-based and functional assays (Table 1; Figure 8A–8E; Supplementary Figure 7–8). Among the 3 single surface marker (ABCG2, CD44, and α2β1) profiles, the $ABCG2^+$ Du145 cell population (from either cultures or xenografts) manifested significantly higher tumor-regenerating activity than the $ABCG2^-$ population (Table 1). Consistent with our earlier results (7), the $CD44^+$ Du145 cells were >30 fold more tumorigenic than the $CD44^-$ counterparts (Table 1). The integrin $\alpha2\beta1^+$ Du145 cells were also much more tumorigenic than the $\alpha2\beta1^-$ Du145 cells (Table 1; Supplementary Figure 7). Interestingly, when we sorted out Du145 cells double positive for CD44 and α2β1, there was only ~2 fold difference in TIF between $CD44^+\alpha2\beta1^+$ vs. $CD44^-\alpha2\beta1^-$ populations, which was not statistically significant (Table 1; see below). In the two functional (i.e., SP and Aldefluor) assays performed, Du145 cells did not show a detectable SP (not shown), as we previously reported [6]. In contrast, ~20% Du145 cells had high Aldefluor activity (i.e., $ALDH^+$; Figure 8A; Supplementary Figure 8A). The $ALDH^+$ Du145 cells demonstrated relatively higher clonogenic capacity (Supplementary Figure 8B) and significantly higher tumorigenicity (Supplementary Figure 8C; Table 1) than $ALDH^-$ cells. In secondary (2°) tumor transplantation experiments (Figure 8B), the $ALDH^+$ Du145 cells purified from the first generation (1°) tumors were greatly enriched in tumor-regenerating activity giving rise to a striking TIF of 1/1 (Figure 8C; Table 1), suggesting that nearly every single $ALDH^+$ cell was tumorigenic. $ALDH^+$ Du145 cells self-renewed *in vivo* as both the 1° (Supplementary Figure 8D) and 2° (not shown) tumors, like the parental cultures, harbored only a fraction of $ALDH^+$ cells with the majority being $ALDH^-$.

PC3 cells, unlike Du145, were nearly all positive for CD44 and α2β1 (Supplementary Figure 6A; Supplementary Table 3). Therefore, these two surface markers would not be able to stratify tumorigenic vs. non-tumorigenic subsets. On the other hand, ~40% PC3 cells were $ALDH^+$ (Figure 8A; Supplementary Figure 8A) and purified $ALDH^+$ PC3 cells showed much higher clonal (Figure 8D), sphere-formation (Figure 8E), and tumor-regeneration (Table 1) capacities than the corresponding $ALDH^-$ PC3 cells.

Next, we studied LAPC9 and LAPC4, two xenograft models that contain both AR^+/AR^- and PSA^+/PSA^- cells [13]. Unlike what we observed in Du145 cells, $ABCG2^+$ and $ABCG2^-$ LAPC9 cells did not show any difference in tumorigenic capacities (Table 2). The $\alpha2\beta1^+$ and $\alpha2\beta1^-$ LAPC9 cells, whether implanted subcutaneously or in the DP, also did not manifest any difference in tumor-regenerating activity (Table 2). $CD44^+$ LAPC9 cells, however, when implanted subcutaneously or orthotopically in the dorsal prostate (DP), exhibited ~6- and 19-fold, respectively, higher tumor-initiating potential than corresponding $CD44^-$ LAPC9 cells (Table 2). The higher tumor-initiating capacity of $CD44^+$ LAPC9 cells was corroborated in an independent orthotopic LDA experiment (Supplementary Figure 9A). Importantly, the *in vivo* self-renewal ability of the $CD44^+$ LAPC9 cells was revealed in 2° transplantation experiments (Supplementary Figure 9B). Remarkably, however, the $CD44^+\alpha2\beta1^+$ LAPC9 cells, unlike $CD44^+\alpha2\beta1^+$ Du145 cells, demonstrated > 900 fold enrichment in tumor-initiating capacity compared to the double-negative cells (Table 2). In fact, we even observed tumor development with a single $CD44^+\alpha2\beta1^+$ LAPC9 cell (Table 2; see discussion below). In the two functional assays we performed, the LAPC9 SP cells, as we observed earlier [6], constituted ~0.05–1% of the total (not shown) and possessed much higher tumor-initiating capacity than the non-SP cells (Table 2; Supplementary Figure 9C). Like the $CD44^+$ and $CD44^+\alpha2\beta1^+$ cells, the LAPC9 SP cells self-renewed *in vivo* and a single LAPC9 SP cell was able to establish a 2° tumor (Supplementary Figure 9C and 9D). The $ALDH^+$ LAPC9 cells in regular AD tumors constituted ~10% of the total (Figure 8A; Supplementary Figure 8A) and displayed higher sphere-forming (Supplementary Figure 8E) and tumor-regenerating (Table 2) activities than the corresponding $ALDH^-$ cells. Interestingly, the $ALDH^+$ LAPC9 cells purified from AI tumors, which were enriched in $ALDH^+$ cells (not shown), also manifested higher sphere-forming capacity than $ALDH^-$ cells (Figure 8F).

When we purified out $CD44^+/CD44^-$ and $\alpha2\beta1^+/\alpha2\beta1^-$ LAPC4 cells from the xenografts and performed similar LDA tumor experiments, surprisingly, the marker-positive and marker-negative subpopulations appeared similarly tumorigenic (Table 2). LAPC4 cells did not have a detectable SP (data not shown) but had ~35% $ALDH^+$ cells (Figure 8A; Supplementary Figure 8A). The $ALDH^+$ LAPC4 cells again

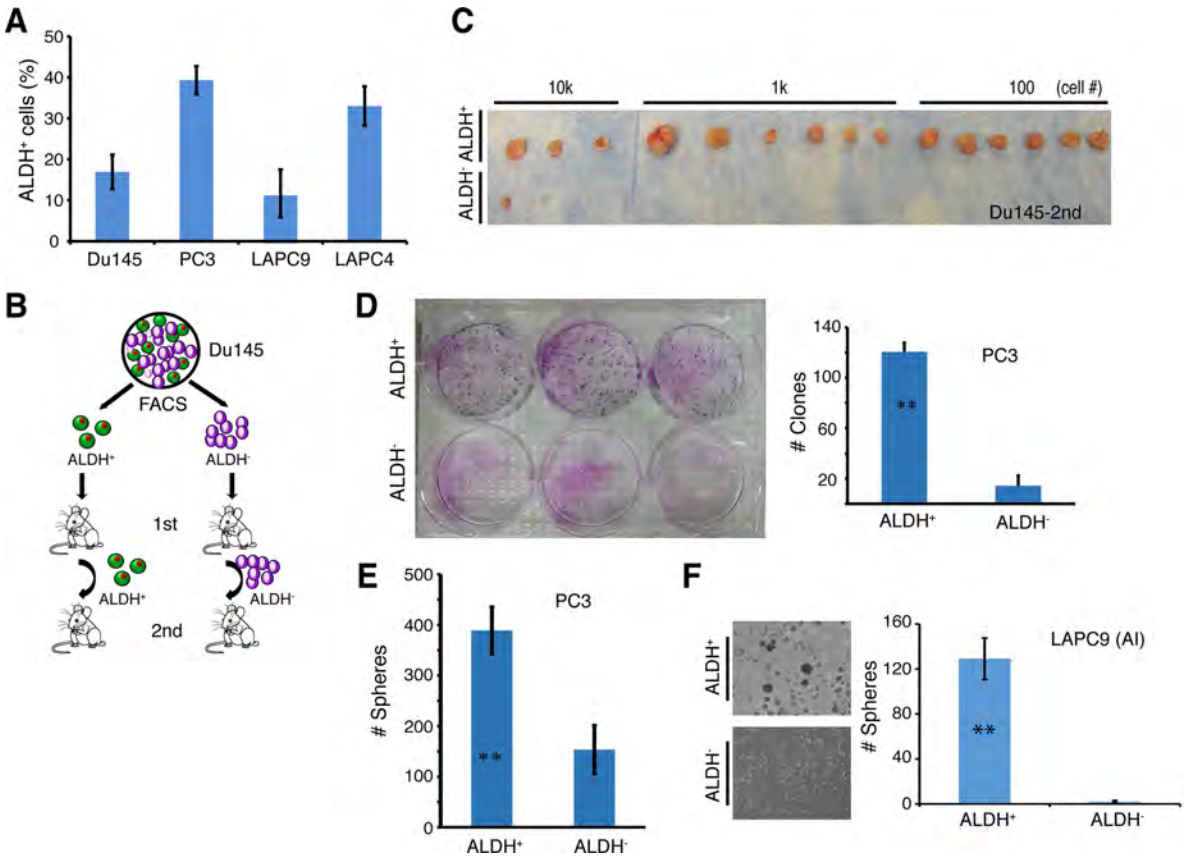

Figure 8: The ALDH⁺ PCa cell subpopulations are enriched in self-renewing tumor-initiating cells. A. The percentage of ALDH⁺ cells in four PCa models. ALDH activity was measured by the ALDEFLUOR assay and analyzed by flow cytometry. Tumor cells purified from Du145 and PC3 cultures or LAPC9 and LAPC4 xenografts were incubated in ALDEFLUOR assay buffer containing ALDH substrate and analyzed by FACS. Cells treated with DEAB were used as negative control. Shown is the bar graph derived from at least 3 independent experiments (mean ± SEM). **B.** Experimental scheme for Du145 serial tumor transplantation assays. ALDH⁺ and ALDH⁻ Du145 cells were purified and used for LDA in intact male NOD/SCID mice. The 1° tumors derived from ALDH⁺ and ALDH⁻ were harvested and utilized to purify ALDH⁺ and ALDH⁻ cells, respectively, for 2° transplantation. **C.** ALDH⁺ and ALDH⁻ Du145 cells were sorted from 1° tumors derived from ALDH⁻ and ALDH⁺ cells, respectively, and LDA was performed in NOD/SCID male mice (see also Table 1). Shown were 2° tumor transplantation images at the cell doses indicated. **D.** PC3 cells were sorted by FACS for ALDH⁺ and ALDH⁻ cells, and plated at clonal density (400 cells/well in 6-well dishes) in triplicate. Nine days after plating, holoclones were counted. Shown is the bar graph (mean ± S.D; $n = 3$; $^{**}P < 0.001$) and clone images. **E.** ALDH⁺ and ALDH⁻ PC3 cells were sorted and cultured in anchorage-independent conditions. 10 days later, spheres were counted. Presented are the mean ± S.D ($n = 3$; $^{**}P < 0.01$). **F.** ALDH⁺ and ALDH⁻ cells were purified from a LAPC9 xenograft tumor long-term maintained in castrated male mice (AI) and cultured in ultra-low attachment plates. Shown are the representative sphere images (left) and bar graphs (mean ± S.D; $n = 4$, $^{**}P < 0.001$).

did not exhibit any difference in tumor-regenerating activity compared to the ALDH⁻ cells (Table 2; Supplementary Figure 8F). If anything, the ALDH⁻ LAPC4 cells appeared to be slightly more tumorigenic than the ALDH⁺ cells (Supplementary Figure 8F). However, CD44⁺α2β1⁺ LAPC4 cells displayed (statistically) higher tumor-regenerating activity than the corresponding CD44⁻α2β1⁻ LAPC4 cells (Table 2; Supplementary Figure 10).

Further dissection of phenotypic and functional heterogeneity of PCSC subpopulations

The above exhaustive side-by-side tumor studies in two PSA⁻ and two PSA⁺ tumor systems (summarized in Supplementary Table 4) demonstrate that tumor-initiating Du145 cells can be enriched by all three surface markers (ABCG2, α2β1, and CD44) as well as Aldefluor assay but not SP analysis as this model lacks the SP. Tumorigenic LAPC9 cells can be enriched by CD44⁺, CD44⁺α2β1⁺, and SP and ALDH⁺ phenotypes but not the α2β1⁺ or ABCG2⁺ phenotypes. Tumorigenic PC3 cells may be enriched by the ALDH⁺ phenotype but not ABCG2 whereas *only* the CD44⁺α2β1⁺ phenotype can enrich tumor-initiating cells in the LAPC4 model (Supplementary Table 4). Serial tumor transplantation experiments have established that the Du145 ALDH⁺, and LAPC9 CD44⁺, CD44⁺α2β1⁺, and SP populations all can self-renew *in vivo*, attesting to their true CSC properties. These results, collectively,

Table 1. Tumor-initiating frequecy (TIF) of Du145 and PC3 cells

Phenotype*	Cell dose					TIF (range)[$]	P value[#]
	10^5	10^4	10^3	10^2	10		(fold differ.)
Du145							
ABCG2$^+$ (cells)			2/6	3/8		1/1,100 (1/415-1/2,915)	6.44e-119 (10x)
ABCG2$^-$ (cells)		2/6	1/6	2/6		1/10,897 (1/4060-1/29,246)	
ABCG2$^+$ (xenografts)			1/2	2/6		1/623 (1/165-1/2,347)	1.19e-89 (13x)
ABCG2$^-$ (xenografts)		1/4	2/6	2/6		1/7,891 (1/2,686-1/23,183)	
CD44$^+$			5/8	5/8		1/530 (1/245-1/1,146)	7.6e-210 (33x)
CD44$^-$		3/8	0/6	1/8		1/17,584 (1/6,395-1/48,350)	
$\alpha2\beta1^+$	8/8	7/8	3/8			1/3,744 (1/1,694-1/8,275)	8.47e-09 (31x)
$\alpha2\beta1^-$	2/5	2/8	0/8			1/115,913 (1/40,331-1/333,137)	
CD44$^+\alpha2\beta1^+$		4/8	2/8	1/7	0/8	1/9,152 (1/4,034-1/20,765)	
CD44$^+\alpha2\beta1^-$		1/8	1/7	0/8	0/8	1/41,048 (1/9,936-1/169,575)	
CD44$^-\alpha2\beta1^+$		0/3	1/8	0/8	0/8	1/38,298 (1/4,922-1/298,016)	0.0396
CD44$^-\alpha2\beta1^-$		2/4	0/8	0/8		1/18,963 (1/4,832-1/74,420)	
ALDH$^+$			3/4	1/4		1/615 (1/205-1/1,842)	2.62e-77 (64x)
ALDH$^-$		1/4	0/4	0/4		1/39,188 (1/5,558-1/276,314)	
ALDH$^+$ (2^o)		3/3	6/6	6/6		1/1 (1/1-1/108)	1.07e-141 (6,025x)
ALDH$^-$ (2^o)	3/4 (0.5x10^4)	0/4	0/4			1/6,025 (1/1,995-1/18,195)	
PC3							
ABCG2$^+$		5/5	6/8	2/8		1/615 (1/283-1/1,336)	0.253
ABCG2$^-$		7/8	8/8	5/8		1/1,071 (1/457-1/2,512)	
ALDH$^+$		10/10	4/7	5/8		1/552 (1/245-1/1,245)	0.00869 (4x)
ALDH$^-$		10/11	7/12	2/6		1/2,003 (1/944-1/4,250)	

*Marker-positive and -negative Du145 and PC3 cells were sorted out by FACS from log-phase cultures or, in some cases, from xenografts (indicated), and injected subcutaneously in Matrigel (1:1) in female NOD/SCID mice. Tumors were harvested generally 2-4 months after cell implantations except the experiments with CD44$\alpha2\beta1$, which were terminated at ~5 months after implantation.

[$]TIF was determined using the L-CalcTM software (http://bioinf.wehi.edu.au/software/elda/index.html). The ranges were indicated in the parentheses.

[#]The P values between marker-positive and marker-negative populations were determined by Chi-Square (χ^2) test. Indicated in parenthesis are relative fold enrichment in tumorigencity by comparing TIF in marker-positive and -negative cell populations.

Table 2. Tumor-initiating frequency of LAPC9 and LAPC4 cells

Phenotype*	Cell dose						TIF (range)$	P value#
	10^5	10^4	10^3	10^2	10	1		(fold differ.)
LAPC9								
ABCG2$^+$			5/8	2/8	1/12		1/719 (1/330-1/1,567)	0.458 (1.5x)
ABCG2$^-$		5/5	4/8	2/8			1/1,085 (1/465-1/2,533)	
CD44$^+$		4/4	10/11	10/10	1/4		1/137 (1/60-1/311)	0.00124 (6x)
CD44$^-$		4/4	5/6	0/8			1/752 (1/308-1/1,839)	
CD44$^+$ (DP)		4/9	2/8	0/5			1/12,474 (1/5,350-1/29,082)	1.33e-5 (19x)
CD44$^-$ (DP)	4/5 (5x10^5)	3/5	0/10	0/10	0/5		1/230,530 (1/97,904-1/542,821)	
$\alpha2\beta1^+$		5/6	3/6	0/6			1/3,759 (1/1,528-1/9,244)	0.674 (1.25x)
$\alpha2\beta1^-$	4/6	5/8	6/8	3/6			1/4,694 (1/2,166-1/10,169)	
$\alpha2\beta1^+$ (DP)		1/4	0/4	0/4			1/39,188 (1/5,558-1/276,303)	
$\alpha2\beta1^-$ (DP)	4/4	1/4	0/4	0/4			1/27,813 (1/8,639-1/89,540)	0.766 (1.4x)
CD44$^+\alpha2\beta1^+$		6/6	6/6	2/2	4/12	1/8	1/21 (1/9-1/49)	
CD44$^+\alpha2\beta1^-$		8/8	10/10	7/8	2/8		1/44 (1/20-1/96)	0.207
CD44$^-\alpha2\beta1^+$		6/8	9/10	4/8	1/8		1/2,040 (1/927-1/4,490)	<0.00001
CD44$^-\alpha2\beta1^-$		1/6	2/5	0/8			1/19,791 (1/5,892-1/66,479)	<0.00001(x942)
SP			3/4	2/8			1/554 (1/205-1/1,497)	3.85e-17 (530x)
Non-SP	1/1 (3x10^5)	0/1	0/4				1/216,403 (1/30,607-1/1,530,060)	
ALDH$^+$			7/8	6/8	3/8		1/193 (1/79-1/472)	<0.00001 (91x)
ALDH$^-$	2/2 (0.5x10^5)	2/6	1/8	1/8			1/13,607 (1/5,296-1/34,962)	
LAPC4								
CD44$^+$		3/3	5/6	4/6			1/301 (1/115-1/786)	0.478 (1.4x)
CD44$^-$		7/7	13/14	2/14			1/433 (1/240-1/779)	
$\alpha2\beta1^+$ (DP)		0/2	0/4				N/A	0.349
$\alpha2\beta1^-$ (DP)	5/6	1/4	0/4				1/52,266 (1/20,902-1/130,692)	
CD44$^+\alpha2\beta1^+$			8/8	7/7	1/8		1/35 (1/15-1/80)	0.002 (5.7x)
CD44$^-\alpha2\beta1^-$		8/8	7/8	4/8	4/8		1/200 (1/82-1/487)	
ALDH$^+$		4/8	7/8	1/8			1/4,897 (1/2,285-1/10,495)	
ALDH$^-$		5/8	5/8	5/8			1/3,331 (1/1,503-1/7,373)	0.353

*Marker-positive and -negative LAPC9 or LAPC4 cells were sorted out by FACS from xenograft tumors maintained in intact male NOD/SCID mice and implanted, at different numbers, subcutanesouly (in most cases) or in the dorsal prostate (DP) in Matrigel (1:1) in intact male mice. Tumors were generally harvested in 2-4 months.

[$]TIF was determined using the L-CalcTM software (http://bioinf.wehi.edu.au/software/elda/index.html). The ranges were indicated in the parentheses.

[#]The P values between marker-positive and marker-negative populations were determined by Chi-Square (χ^2) test.

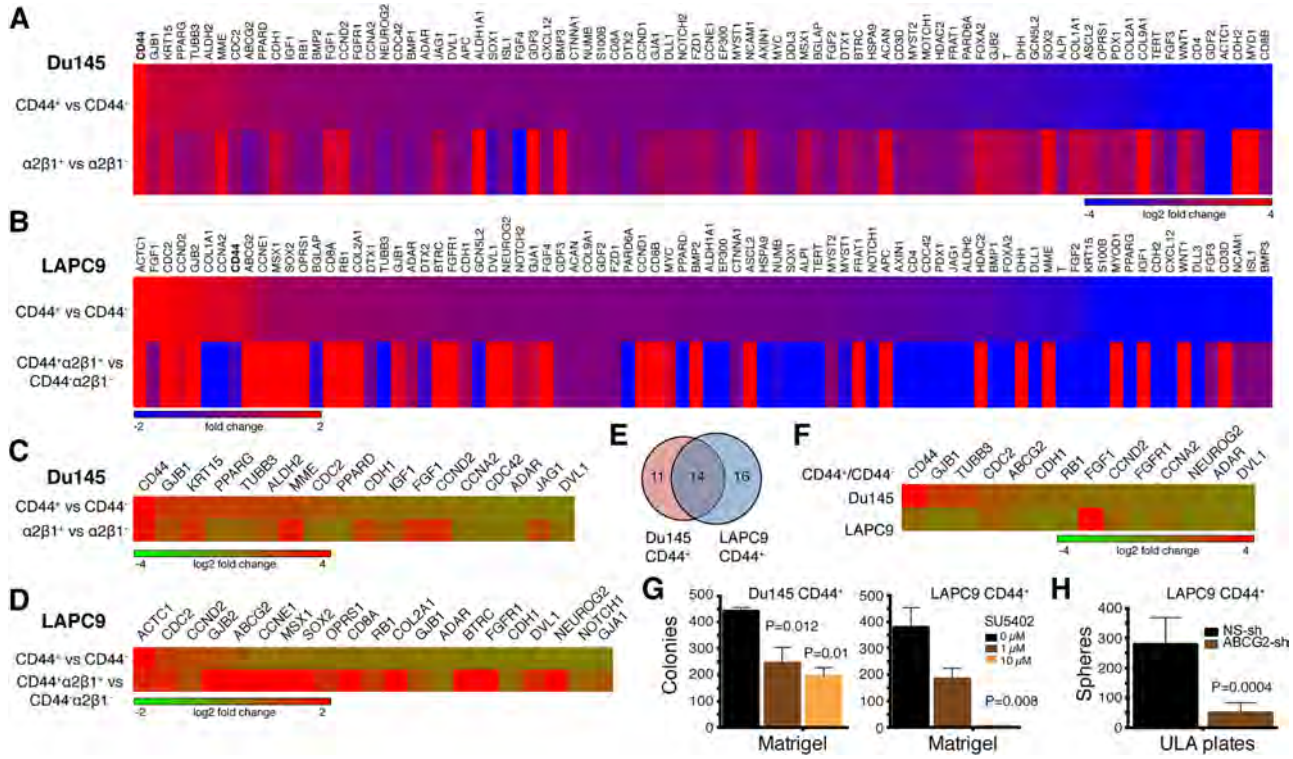

Figure 9: Gene expression profiles and functional studies in PCa cell subpopulations. A–B. Expression of 84 SC-related genes in the indicated marker-positive and corresponding marker-negative Du145 (A) and LAPC9 (B) cells. Relative expression levels were normalized to the average expression levels of 5 internal controls (B2M, HPRT1, RPL13A, GAPDH and ACTB). Scale bars depict fold changes (in log 2 ratio), centered at 0. For both Du145 and LAPC9, genes were presented from the highest to lowest in the $CD44^+$ population. Note that CD44 gene (bold) was the highest expressed gene in Du145 and was among the highest in LAPC9. **C–D.** Heat map of representative genes commonly overexpressed in the two indicated PCa cell populations in Du145 (C) and LAPC9 (D) models. **E–F.** Venn diagram (E) and heat map (F) presenting the genes that were commonly overexpressed in the $CD44^+$ Du145 and LAPC9 cells. **G.** Blocking FGFR signaling compromised clonogenic capacity of $CD44^+$ PCa cells. Freshly purified Du145 and LAPC9 $CD44^+$ cells were plated in Matrigel-coated 12-well plates (3,000 cells/well) and treated with 0 – 10 μM FGFR inhibitor SU5402. Colonies were enumerated 2 weeks after plating. **H.** Knocking down ABCG2 reduced sphere formation in $CD44^+$ LAPC9 cells. Freshly purified $CD44^+$ LAPC9 cells were infected with non-silencing (NS) or ABCG2 shRNAs (MOI 20) and 48 later, plated in 6-well ULA plates (2,000 cells/well). Spheres were counted 2 weeks after plating.

suggest that different PCa models possess distinct profiles of tumorigenic subpopulations.

To investigate the potential relationship between single marker-positive versus double marker-positive PCa cells with respect to their tumor-regenerating activity, we compared $CD44^+\alpha2\beta1^+$ versus $CD44^+$ and $\alpha2\beta1^+$ cells in Du145 and LAPC9 models. Interestingly, the $CD44^+\alpha2\beta1^+$ Du145 cell population was only slightly enriched in tumor-initiating cells and its tumor-initiating capacity was actually lower than in $CD44^+$ Du145 cells (TIF 1/9, 152 vs. TIF 1/530, P = 1.27e-07) (Table 1). Also, the $CD44^+\alpha2\beta1^+$ Du145 cells exhibited only ~2 fold higher tumorigenic potential than $CD44^-\alpha2\beta1^-$ cells (1/9, 152 vs. 1/18, 963, P = 0.343) (Table 1). In sharp contrast to the Du145 model, the $CD44^+\alpha2\beta1^+$ LAPC9 cells were highly tumorigenic in that as few as 1 double-positive cell was able to regenerate a tumor (Table 1) and the regenerated tumor contained only a small % of $CD44^+\alpha2\beta1^+$ LAPC9 cells and could be serially passaged (not shown). Significantly, the $CD44^+\alpha2\beta1^+$ LAPC9 cell population was more tumorigenic than either $CD44^+$ (1/21 vs 1/137; P = 0.0014) or $\alpha2\beta1^+$ (1/21 vs. 1/3, 759; P = 5.12e14) cell population (Table 1). The contrasting results observed in Du145 and LAPC9 models with respect to the tumorigenicity of $CD44^+\alpha2\beta1^+$ cells suggest that the ability of combinatorial marker-sorting strategy to further enrich CSCs over single marker strategies is dependent on the cancer model analyzed.

To further dissect PCSC heterogeneity at the molecular level, we custom-made a RT^2 Profiler™ qPCR Human Stem Cell Superarray that contained 84 stem cell-associated genes (Supplementary Table 5) and analyzed their expression levels in $CD44^+$, $\alpha2\beta1^+$, and/or $CD44^+\alpha2\beta1^+$ Du145 and LAPC9 cell populations (Figure 9A–9F; Supplementary Figure 11A–1B). The results revealed several interesting findings. First, we observed both overexpressed and downregulated genes in marker-positive in comparison to the corresponding marker-negative populations in both models. Second, we observed similarities as well as differences in gene expression both between different subpopulations of cells in the same cell

type and between the same subpopulations of different PCa cell types. For instance, the CD44$^+$ Du145 cells displayed a gene expression pattern that was overall different from that in the α2β1$^+$ Du145 cells (Figure 9A). Gene expression patterns in CD44$^+$ versus CD44$^+$α2β1$^+$ LAPC9 cells were also dissimilar (Figure 9B). Third, the two subpopulations from the same cell type, however, did share some gene expression patterns. For example, the CD44$^+$ and α2β1$^+$ Du145 cells (Figure 9C) and the CD44$^+$ and CD44$^+$α2β1$^+$ LAPC9 cells (Figure 9D) shared many overexpressed genes. Fourth, the CD44$^+$α2β1$^+$ LAPC9 cells, which were among the most tumorigenic and were more tumorigenic than CD44$^+$ LAPC9 cells (Table 2), showed more upregulated genes (Figure 9B and 9D; Supplementary Figure 11A). Among the most highly upregulated genes in CD44$^+$α2β1$^+$ LAPC9 cells were MME (CD10), CCNE1, COL2A1, and those involved in Wnt signaling (FRAT1, BTRC, APC, WNT1), growth factor signaling (FGFR1, IGF1, BMP2, FGF4, NEUROG2), and pluripotency (SOX2) (Supplementary Figure 11A). Many of these molecules are well-known stem cell regulators and have been implicated in PCa etiology and progression [e.g., 32–36].

The qPCR analysis provided clues about potential involvement of certain signaling pathways in commonly regulating several PCSC populations. For example, the CD44$^+$ Du145 and LAPC9 cell populations, both of which were tumorigenic, shared 14 upregulated genes including developmental (FGF1, FGFR1, and DVL1), cell-cycle related (RB1, CDC2, CCND2, and CCNA2), and neuronal (TUBB3 and NEUROG2) genes (Figure 9E–9F). As an example of interrogating the functional significance of the signaling pathways, we treated freshly purified CD44$^+$ Du145 and LAPC9 cells with SU5402, a specific FGFR inhibitor and then performed colony formation assays in Matrigel and sphere formation assays in ultra-low attachment (ULA) plates (6–13). SU5402 dose-dependently compromised colony (Figure 9G) and sphere (Supplementary Figure 11C) forming capabilities of both CD44$^+$ PCa cell populations.

The qPCR results also provided clues about potential relationships between different PCa cell subpopulations. For instance, the CD44$^+$ Du145 cell population was enriched not only in *CD44* mRNA but also mRNAs of *ABCG2* and two ALDH isoforms (*ALDH1A1* and *ALDH2*) and the α2β1$^+$ Du145 cells expressed high levels of *CD44* and *ALDH1A1* mRNAs (Supplementary Figure 11B). These results suggest that in the Du145 model, CD44$^+$, α2β1$^+$, ABCG2$^+$, and ALDH$^+$ cell populations identify overlapping subsets of tumorigenic cells, which is congruent with phenotypic analysis (Supplementary Figure 12A). Similarly, in the LAPC9 model, *ABCG2* mRNA was enriched in both CD44$^+$ and CD44$^+$α2β1$^+$ cell populations (Supplementary Figure 11B), again suggesting that these markers identify overlapping cell populations as corroborated by the flow analysis (Supplementary Figure 12B). Interestingly, the mRNAs of *ALDH1A1* and *ALDH2* were not enriched in the two CD44$^+$ LAPC9 populations (Supplementary Figure 11B) but the ALDH$^+$ cells were nearly completely encompassed in the CD44$^+$ population of LAPC9 cells (Supplementary Figure 12B), suggesting that other ALDH isoform(s) might be involved in mediating the Aldefluor phenotype in the LAPC9 model.

Finally, we employed lentiviral-mediated knockdown to investigate the functions of CD44, integrin α2, and ABCG2 in purified CD44$^+$ Du145 and/or LAPC9 cells. CD44 knockdown did not affect the colony or sphere formation in either model (Supplementary Figure 11D; data not shown). These results are consistent with our earlier studies demonstrating that anti-CD44 antibodies did not interfere with the clonal and clonogenic properties of CD44$^+$ PCa cells [7]. In contrast to CD44, ABCG2 knockdown inhibited clonogenic activities of both LAPC9 (Figure 9H; Supplementary Figure 11E) and Du145 (not shown) CD44$^+$ cells, which is consistent with ABCG2 enrichment and also suggests its functional significance in the two CD44$^+$ PCa cell populations. Interestingly, knocking down integrin α2 also strongly suppressed the clonogenicity of LAPC9 CD44$^+$ cells (Supplementary Figure 11D).

Clonogenic and tumorigenic subpopulations in untreated patient tumors

We showed earlier that untreated primary human PCa (i.e., HPCa) contained CD44$^+$, α2β1$^+$, and ALDH1A1$^+$ cells that were mostly PSA$^{-/lo}$ (Figure 7; Supplementary Figure 5E). Here, we quantitatively analyzed the expression and, importantly, potential functions of PCSC marker-positive HPCa cells, i.e., CD44$^+$, α2β1$^+$, CD44$^+$α2β1$^+$, and ALDH$^+$, as well as CD133 [15] in a large cohort (~50) of HPCa samples (Figure 10; Supplementary Figure 13; Supplementary Table 2). The majority of the HPCa samples we examined (44/46, 96%) contained CD44$^+$ cells, although the percentages varied widely (Figure 10A; Supplementary Table 2). When CD44$^+$ HPCa cells, which were all negative for AR and PSA proteins (Supplementary Figure 13A) as we previously observed [8, 37, 38], were purified out, plated on fibroblast feeders or collagen, and analyzed for their proliferative potential, we observed higher population doublings (PDs) for the CD44$^+$ cell population than CD44$^-$ population in HPCa41 (Figure 10Ba), HPCa43 (Figure 10Bb), HPCa44 (Figure 10Bc), HPCa50 (Supplementary Figure 13C), and HPCa51 (not shown) samples. In fact, most HPCa44 (Figure 10Bc) and HPCa50 (Supplementary Figure 13C) CD44$^-$ cells initially attached but did not proliferate and soon died off whereas the corresponding CD44$^+$ cells expanded exponentially, suggesting that the CD44$^+$ HPCa cells also possess greater survival advantage. On the other hand, as we observed in the xenograft systems, not all patient-derived CD44$^+$ HPCa cells manifested higher proliferative potential than their CD44$^-$ counterparts (e, g., Supplementary Figure 13D).

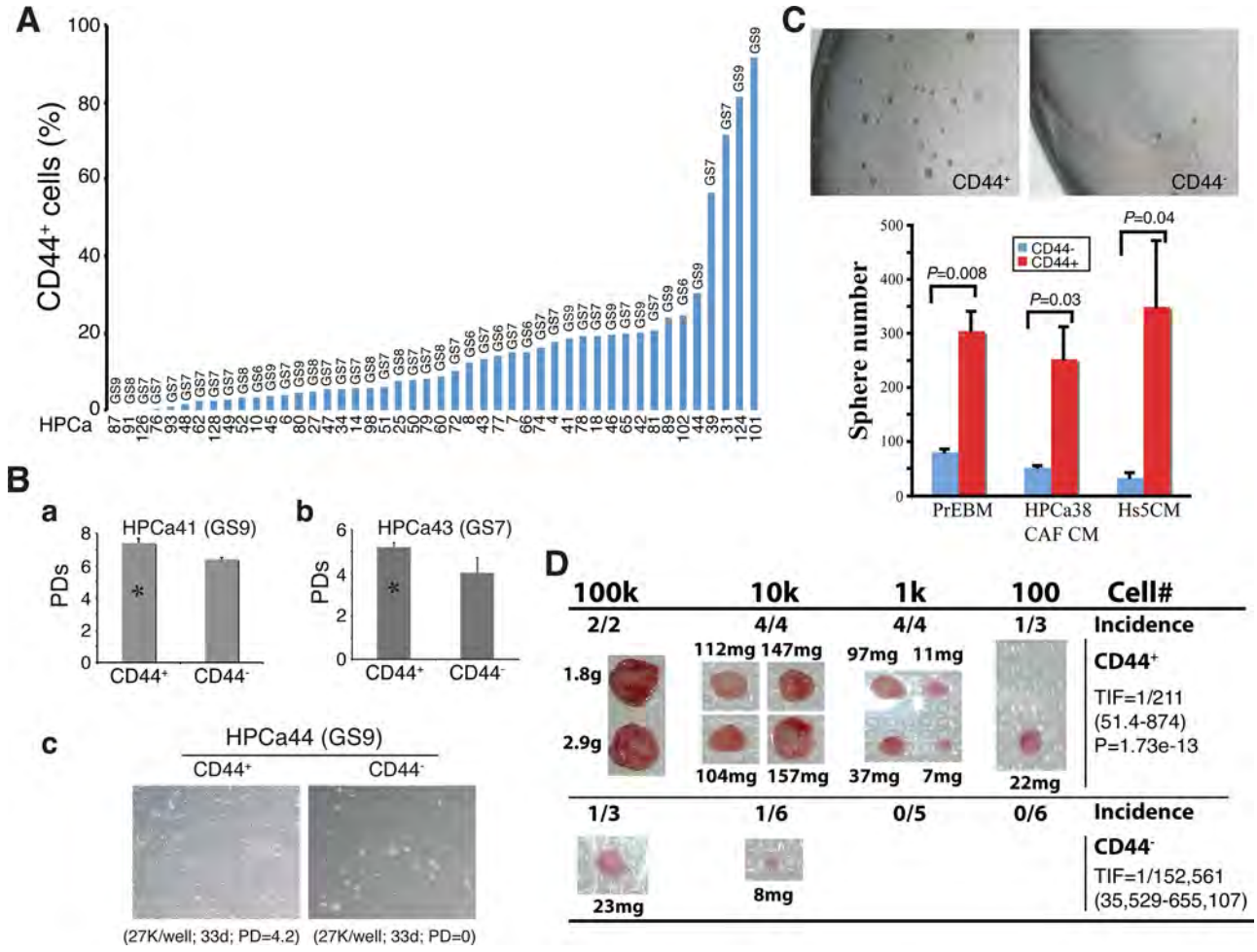

Figure 10: CD44⁺ HPCa cells possess high proliferative, survival, clonogenic, and tumorigenic potential. A. Percentage of CD44⁺ cells in HPCa samples. The combined Gleason score (GS) for each tumor is indicated on top and the patient ID# at the bottom. **B.** CD44⁺ HPCa cells possess higher proliferative and survival advantages than the corresponding CD44⁻ HPCa cells. a. CD44⁺ and CD44⁻ HPCa41 cells were plated in triplicate on Swiss 3T3 feeder layer (1, 000 cells/well) and cell numbers determined 29 days after plating. Shown are the cumulative population doublings (PDs; $*P < 0.05$). b. CD44⁺ and CD44⁻ HPCa43 cells were plated in triplicate on Swiss 3T3 feeder layer (5,000 cells/well) and cell numbers determined 41 days after plating. Shown are the cumulative PDs ($*P < 0.01$). c. Purified CD44⁺ and CD44⁻ HPCa44 cells were plated in triplicate on collagen-coated 6-well dishes. Shown below are the cell numbers plated, time when surviving cells were enumerated, and the cumulative PDs. **C.** CD44⁺ HPCa cells possess high clonogenic potential. CD44⁺/CD44⁻ HPCa51 cells were plated, in triplicate, in Matrigel-coated 12-well plates (10, 000 cells/well). Shown are representative images (40×) of spheres (top) and quantifications of spheres plated in 3 different media (PrEBM, prostate epithelial basal medium; HPCa38 CAF CM, conditioned medium from HPCa38 carcinoma-associated fibroblasts or CAFs; Hs5 CM, conditioned medium from Hs5 immortalized human mesenchymal stem cells) 15 days after plating. **D.** CD44⁺ HPCa cells possess high tumorigenic potential. CD44⁺/CD44⁻ HPCa52 cells were acutely MACS-purified from the patient tumor (GS8) and co-injected, at the indicated cell numbers, with 100k Hs5 cells in 50% Matrigel s.c into irradiated NOD/SCID-γ mice. The 10k and 100k tumors were harvested at ~4 months whereas 100 and 1k tumors were harvested at 7 months after implantation. Shown on the right are the TIF for the two populations and the *P* value for TIF comparison.

We also compared the clonogenic potential of CD44⁺/CD44⁻ HPCa cells by plating them, at clonal density, in Matrigel in several variations of serum-free medium. The results revealed significantly higher sphere-forming ability of the CD44⁺ cells from HPCa50 (not shown) and HPCa51 (Figure 10C) than the respective CD44⁻ HPCa cells. The above clonal and clonogenic assays indicate that primary CD44+ HPCa cells possess certain stem/progenitor cell properties, which was supported by the expression of stem cell marker hTERT (Supplementary Figure 13A; data not shown). Importantly, in a pilot *in vivo* experiment, we purified out CD44⁺/CD44⁻ cells from HPCa52 (GS8) and co-injected them, at increasing cell numbers, with the Hs5 mesenchymal cells [31], subcutaneously in irradiated male NOD/SCID-γ mice supplemented with the exogenous testosterone. As shown in Figure 10D, the CD44⁺ HPCa52 cells demonstrated higher tumor-regenerating capacity than corresponding CD44⁻ cells. This was quite a remarkable finding for the bulk primary HPCa cells are known to be extremely indolent in tumor regeneration [11, 31].

HPCa also expressed other PCSC markers including CD133 [15]. In general, the % of $CD133^+$ HPCa cells was lower than that of $CD44^+$ HPCa cells (Supplementary Figure 13E; Supplementary Table 2). The $CD133^+$ LAPC4 (Supplementary Figure 13F) and HPCa (Supplementary Figure 13G–13H) cells showed higher proliferative and sphere-forming potential than the corresponding $CD133^-$ cells. Interestingly, in a pilot study we observed higher *CD44* and integrin *α2* mRNA levels in $CD133^+$ HPC40 cells than the corresponding $CD133^-$ cells (Supplementary Figure 13I), suggesting a potentially overlapping relationship among the 3 subpopulations in HPCa samples.

Together, these results suggest that untreated primary tumors contain subsets of HPCa cells that express the phenotypic markers of PCSCs and possess enhanced clonal, clonogenic, and even tumorigenic potential.

DISCUSSION

To our knowledge, the present study represents the most comprehensive efforts to dissect the phenotypic, functional, and tumorigenic heterogeneities in human PCa cells using multiple xenograft models and > 70 patient tumor samples. In the first part, we further investigate the $PSA^{-/lo}$ PCa cell population, which we have recently shown to harbor self-renewing long-term tumor-propagating cells [13]. We demonstrate that 1) tumor cell *PSA* mRNA levels inversely correlate with grade, metastasis, and patient survival; 2) discordant AR and PSA expression in both untreated and castration-resistant PCa (CRPC) results in AR^+PSA^+, AR^+PSA^-, AR^-PSA^-, and AR^-PSA^+ subtypes of PCa cells that manifest differential sensitivities to therapeutics; 3) the $PSA^{-/lo}$ PCa cells pre-exist in untreated primary tumors and castration leads to a great enrichment of $PSA^{-/lo}$ PCa cells in both xenograft tumors and CRPC samples; 4) the $PSA^{-/lo}$ PCa cells are quiescent and resistant to castration and other stress treatments; 5) systemic androgen levels dynamically regulate the relative abundance of PSA^+ versus $PSA^{-/lo}$ PCa cells in the tumors that impacts the kinetics of tumor growth; 6) the $PSA^{-/lo}$ PCa cells seem to possess distinct epigenetic profiles; and 7) the $PSA^{-/lo}$ PCa cell population is enriched in several CSC markers including CD44, integrin α2β1, and ALDH1A1.

Heterogeneous and discordant AR and PSA expression in PCa cells has been reported in numerous earlier studies [39–61]; however, our study, for the first time, has proposed and presented the evidence for the 4 subtypes of PCa cells, i.e., AR^+PSA^+, AR^-PSA^+, AR^+PSA^-, and AR^-PSA^+ that pre-exist in untreated HPCa. We have shown preliminary evidence that 3 LNCaP sublines representing 3 subtypes of PCa cells, i.e., AR^+PSA^+ (regular LNCaP), AR^+PSA^- (LNCaP-abl) and AR^-PSA^- (LNCaP-CDSS and LNCaP-MDV) exhibit differential responses to antiandrogens, chemodrugs, and targeted therapeutics. Of clinical significance, the $PSA^{-/lo}$ cell population, which encompasses both $AR^+PSA^{-/lo}$ and $AR^+PSA^{-/lo}$ cells, becomes strikingly enriched in all CRPC samples examined and in castration-resistant xenograft model. These analyses, taken together with evidence of distinct epigenetic profiles of $PSA^{-/lo}$ vs. PSA^+ subsets, suggest that castration selects for undifferentiated $PSA^{-/lo}$ PCa cells.

Our previous work has demonstrated that the $PSA^{-/lo}$ PCa cell population harbors self-renewing long-term tumor-propagating PCSCs that resist castration [13]. The present study follows up on the earlier work by further showing that the $PSA^{-/lo}$ PCa cells are much more quiescent than the PSA^+ cells, based on time-lapse tracking of single cells and clonal analysis. Purified $PSA^{-/lo}$ PCa cells, like the bulk $AR^-PSA^{-/lo}$ LNCaP subline, are also refractory to antiandrogens and other drugs. We further demonstrate that the relative abundance of both $PSA^{-/lo}$ and PSA^+ PCa cells in tumors are regulated dynamically by systemic androgen levels, which in turn impacts tumor regeneration and growth in androgen-proficient versus androgen-deficient conditions. These latter observations implicate differential epigenetic mechanisms in regulating the two populations of PCa cells. In support, targeted ChIP/re-ChIP assays on 8 gene promoters known to be associated with bivalent chromatin domains in ES cells reveal 4 genes possessing bivalent features but preferentially in $PSA^{-/lo}$ PCa cells, consistent with these cells possessing stem cell gene expression profiles and biological characteristics [13]. A genome-wide ChIP-Seq analysis of several histone marks in purified $PSA^{-/lo}$ and PSA^+ PCa cells is under way.

The $PSA^{-/lo}$ PCSC population is heterogeneous [13]. Therefore, in the second part of this project, we carried out exhaustive tumor-regeneration and serial transplantation studies in 2 AR^+/PSA^+ (LAPC9 and LAPC4) and 2 AR^-/PSA^- (PC3 and Du145) PCa models. The results provide indisputable evidence that 1) different PCa models possess distinct profiles of tumorigenic subpopulations; 2), some PCa (e.g., LAPC9 and Du145) may possess several populations of CSCs whereas others (e.g., LAPC4) seem to have a paucity of CSC populations; 3) no single marker profile can track tumor-propagating cells in all models; and 4) the ability of combinatorial marker-sorting strategy to further enrich CSCs over single marker strategies is dependent on the cancer models analyzed (Supplementary Table 2). Therefore, the $CD44^+$ phenotype enriches CSCs in Du145 and LAPC9 but not in LAPC4 models whereas the $ALDH^+$ phenotype enriches tumor-initiating cells in all 4 models except LAPC4. Similarly, the $CD44^+α2β1^+$ phenotype enriches CSCs in LAPC9 and LAPC4 but not in Du145 models. These results provide essential foundation for understanding CSC heterogeneity [1, 2] and also explanations to why different groups, working on individual PCa models, have often reported divergent PCSC phenotypes.

That tumorigenic subpopulations can be enriched by several different markers and functional strategies implies that some tumors contain a CSC pool with heterogeneous tumorigenic subsets that possess distinct tumor-initiating and tumor-propagating properties. In support, the LAPC9

model harbors tumorigenic subpopulations that can be prospectively enriched using $CD44^+$ and $CD44^+\alpha2\beta1^+$ profiles as well as the SP and ALDH assays with the $CD44^+\alpha2\beta1^+$ subpopulation being the most tumorigenic (i.e., ~1 tumor-initiating cell in every 20 cells; Table 2). Detailed phenotypic and molecular profiling in Du145 and LAPC9 models shows that the $CD44^+$, $\alpha2\beta1^+$, $ABCG2^+$, and $ALDH^+$ cell populations identify overlapping subsets of tumor-initiating cells. Functional interrogation demonstrates that integrin α2 and ABCG2 but not CD44 are causally important for the clonal and clonogenic properties of the $CD44^+$ PCa cells. The results with CD44 suggest that the molecule probably regulates PCSC properties in some other ways. Indeed, we have recently shown that CD44 plays a critical role in facilitating the invasive and metastatic behavior of PCSCs [12]. Of significance, the tumorigenic $CD44^+$ cell populations in both Du145 and LAPC9 commonly upregulate 14 genes involved in development (FGF1, FGFR1, and DVL1), cell cycle (RB1, CDC2, CCND2, and CCNA2), and neuronal activity (TUBB3 and NEUROG2), providing potential therapeutic targets for the $CD44^+$ PCa cells. Similar molecular profiling reveals genes preferentially expressed in the most tumorigenic $CD44^+\alpha2\beta1^+$ LAPC9 cells including Wnt (FRAT1, BTRC, APC, WNT1), growth factor (FGFR1, IGF1, BMP2, FGF4, NEUROG2), and pluripotency (SOX2) signaling molecules. As a proof of principle, an FGFR inhibitor potently blocks the clonal and clonogenic activity in $CD44^+$ LAPC9 and Du145 cells.

Our observations in PCa are consistent with the phenotypic heterogeneity and functional diversity of CSCs recently reported in other tumor systems including cancers of the breast, pancreas, and colon as well as acute myeloid leukemia and glioblastoma [1, 2, 25, 62–67]. Our results also support but greatly extend earlier efforts in using CD antigen phenotyping to study PCa cell heterogeneity [68]. Importantly, phenotypic analysis combined with functional studies in ~50 HPCa samples demonstrate that untreated HPCa samples also heterogeneously express CSC markers including CD44, CD133, α2β1, and ALDH and that prospectively purified $CD44^+$ and $CD133^+$ HPCa cells in most (though not all) samples manifest high proliferative, clonal and clonogenic capacities.

Results from the present study reinforce the intrinsic stem cell nature and castration-resistant properties of the $PSA^{-/lo}$ PCa cells. Then what is the relationship between the $PSA^{-/lo}$ PCa cell population and several other populations of PCSCs including $CD44^+$, $\alpha2\beta1^+$ and $ALDH^+$ PCa cells? IF staining combined with molecular profiling indicate that the 3 CSC marker-positive populations of PCa cells are included in the $PSA^{-/lo}$ population (Figure 7; Supplementary Figure 5). The current work, together with our systematic studies published over the past 10 years [6–13] allows us to propose a hypothetical model that unifies most previous PCSC studies (Figure 11). The model posits that untreated prostate tumors contain a spectrum of cancer cells at different stages of differentiation. Undifferentiated ($PSA^{-/lo}$) PCa cells are quiescent and can undergo ACD to generate PSA^+ cells whereas the PSA^+ PCa cells are highly proliferative but only undergo SCD (Figure 11). The $PSA^{-/lo}$ PCa cells possess unlimited whereas PSA^+ PCa cells limited tumor-propagating activity [13]. The $PSA^{-/lo}$ PCa cells are intrinsically more resistant to castration and other therapeutics than PSA^+ cells [this study; 13]. Importantly, the $PSA^{-/lo}$ PCa cell population is heterogeneous harboring and/or overlapping with other tumorigenic subsets including the SP, holoclones, and $ALDH^+$, $CD44^+$, $\alpha2\beta1^+$, and $ABCG2^+$ cells [6–8, 10, 12, 13; this study] (Figure 11) and, likely, other subsets such as $CD133^+$ [15] and TRA-1–$60^+CD151^+CD166^+$ cells [19], which are AR^-PSA^-.

Our model (Figure 11) also provides a framework for understanding PCa cell heterogeneity and potential cell-of-origin to CRPC. Therefore, untreated primary HPCa, like LNCaP, LAPC9, and LAPC4 xenografts, all contain a major population of PSA^+ cells but also a minor $PSA^{-/lo}$ population, in which tumorigenic subsets differ both quantitatively and qualitatively depending on individual HPCa samples and xenograft models. Due to the nearly homogeneous AR expression in PSA^+ PCa cells (Supplementary Figure 4A; 13), primary HPCa and AD xenografts respond well to antiandrogens, leading to prominent reduction in tumor burden. On the other hand, the $PSA^{-/lo}$ PCa cells, being only ~30% AR^+, do not respond well to antiandrogens and will survive ADT leading to the eventual emergence of CRPC. In support, the $PSA^{-/lo}$ PCa cells from multiple PCa models regenerate AI tumors very efficiently in completely androgen-deficient hosts [13]. Significantly, more tumorigenic subsets can be further purified out from the $PSA^{-/lo}$ PCa cell population to establish CRPC [13; Chen *et al*., manuscript submitted]. These observations implicate the $PSA^{-/lo}$ PCa cell population, which pre-exists in primary HPCa, as a cell-of-origin for CRPC due to their preferential survival of castration. This conjecture is fully consistent with classical studies performed decades ago reporting that CRPC might result from selective outgrowth of pre-existent AI clones in primary tumors [69, 70]. In contrast to the untreated HPCa and AD xenografts, the cellular landscape in clinical CRPC and AI xenografts completely changes with the $PSA^{-/lo}$ cells becoming predominant [this study, 13]. The profiles of tumorigenic subsets within the $PSA^{-/lo}$ PCSC pool may also likely to change (Figure 11). Taken together, the current study further highlights the need to develop novel therapeutics that specifically target the $PSA^{-/lo}$ population and other PCSC subsets within, which when used in combination with ADT, should help prevent tumor relapse. Many of our ongoing projects are fulfilling this need.

MATERIALS AND METHODS

Cells and antibodies

PC3, Du145, PPC-1, LNCaP cells were obtained from ATCC (Manassas, VA) whereas 293FT packaging cells were

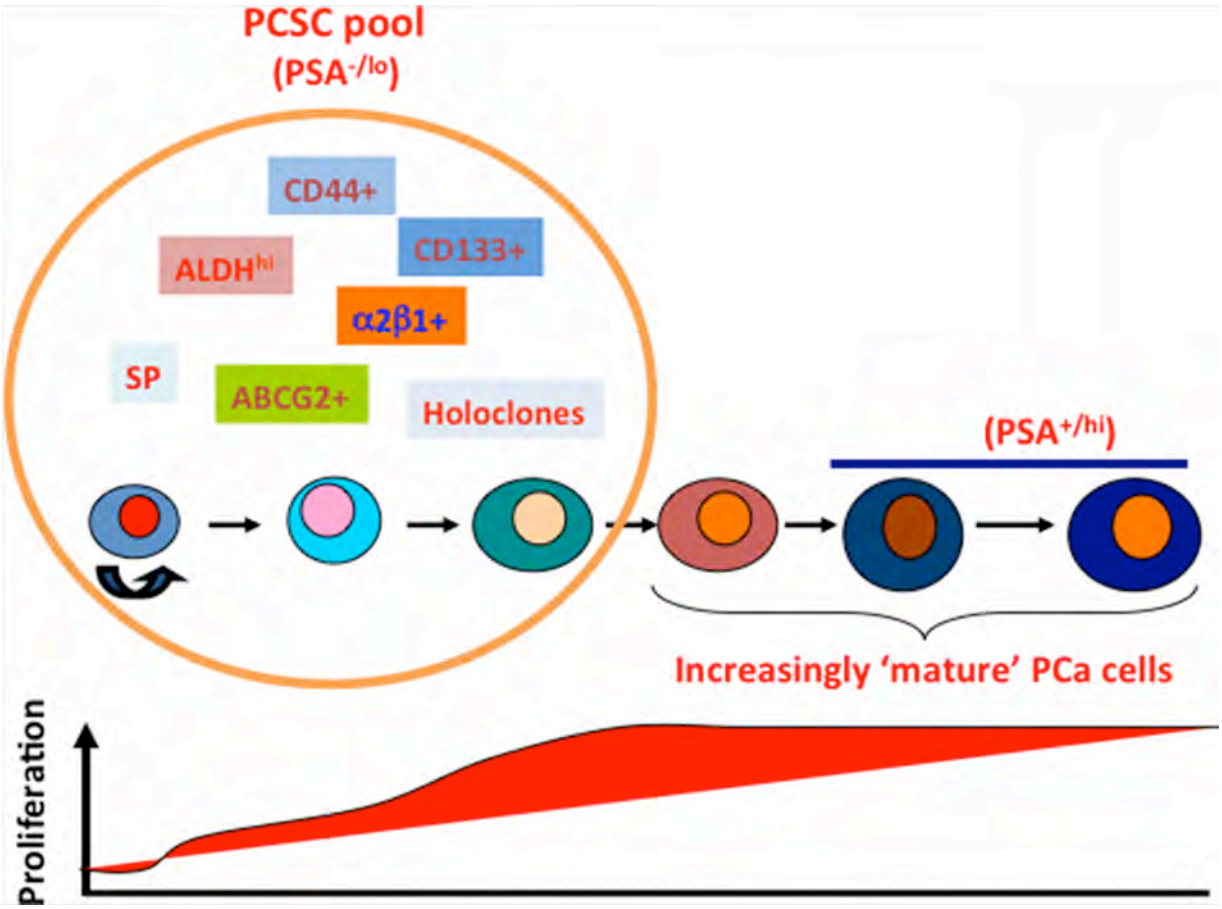

Figure 11: A hypothetical model of tumorigenic heterogeneity of human PCa cells. Untreated (hormone-naïve) PCa contain a spectrum of tumor cells at different stages of differentiation (marked by cells of varying colors and sizes). The PCSC pool in these tumors mainly contains undifferentiated ($PSA^{-/lo}$) PCa cells, which are quiescent (thus low proliferative index; below) and can undergo ACD developing into differentiated cells. The $PSA^{-/lo}$ PCa cells possess long-term tumor-propagating activity. The $PSA^{-/lo}$ PCSC pool is heterogeneous harboring and/or overlapping with other tumorigenic subsets that can be prospectively purified out using the marker profiles indicated. The PCSC pool contains the intrinsically castration-resistant cells. In contrast, fully differentiated (PSA^{+}) PCa cells, despite being highly proliferative (thus high proliferative index, below), only undergo symmetric cell division and possess more limited tumor-propagating capabilities. The $PSA^{-/lo}$ PCSC pool is relatively small and preexists in untreated patient tumors but dramatically enriched in CRPC in which the profiles of tumorigenic subsets may likely be very different from those in the untreated tumors. This model is updated from our earlier model (8). See Text for more discussions.

purchased from Invitrogen (Carlsbad, CA), respectively. All these cells were mycoplasma free, STR-authenticated, and routinely maintained in serum- and antibiotic-containing media as suggested by the providers. Synthetic androgen R1881 and androgen antagonist bicalutamide were purchased from PerkinElmer (cat# NLP005005MG; Waltham, MA) and Toronto Research Chemicals (cat#B382000; Ontario, Canada), respectively. MDV3100 was bought from Selleck Chemicals (car# S1250). All other chemicals were obtained from Sigma unless otherwise specified. Antibodies used in the present study included:

mouse mAb to integrin α2β1 (cat# MAB1998Z, clone BHA2.1; Chemicon, Billerica, MA)
mouse mAb to β-actin (cat# 69100, clone C4; ICN, MP Biomedicals, Solon, OH)
rabbit pAb to ABCG2 (cat# AV43649; Sigma)
mouse mAb to AR (cat# sc-7305, clone 441; Santa Cruz Biotechnology, Santa Cruz, CA)
mouse mAb to Bcl-2 (clone N-19; Santa Cruz Biotech)
mouse mAb to Bcl-2 (cat# 610538; BD Biosciences, San Jose, CA)
mouse mAb to BrdU (cat# B2531, clone BU-33; Sigma, St Louis, MO)
mouse mAb to CD44 (cat# 550932, clone G44–26; BD Biosciences)
mouse mAb to CD44 (cat# sc-7297; Santa Cruz Biotech.)
rabbit pAb to cytokeratin 5 (cat# PRB-160P; BAbCO, Covance, Princeton, NJ)
mouse mAb to cytokeratin 18 (cat# 550511, clone GRE53; BD Biosciences)

mouse mAb to cytokeratin 18 (cat# MAB1600, clone DC-10; Chemicon)
rabbit mAb to GAPDH (cat# sc-25778, clone FL-335; Santa Cruz Biotech)
rabbit pAb to GFP (cat# Ab290; Abcam)
rabbit pAb to Ki-67 (cat# Ab16667; Abcam)
mouse mAb to P63 (cat# sc-8431; clone 4A4; Santa Cruz Biotechnology)
rabbit pAb to PSA (cat# A0562; Dako, Carpinteria, CA)
mouse mAb to PSA (clone A67-B/E13; Santa Cruz Biotechnology)
rabbit pAb to Histone H3 (Cat# 06–755, Millipore)
rabbit pAb to Histone H3K4, trimethyl (cat# 07–473, Millipore)
rabbit pAb to Histone H3K27, trimethyl (cat# 07–449, Millipore)
mouse mAb to Histone H3K27, trimethyl (cat# 61017, Active Motif)
rabbit control IgG, ChIP grade (cat# ab46540, Abcam)
rabbit pAb to hTERT (cat# NB 100–141; Novus)
Alexa Flour 405 conjugated streptavidin (S32351, Invitrogen)
Alexa Flour-conjugated secondary antibodies (Invitrogen)
APC-conjugated goat anti-mouse IgG (550826; BD Biosciences)
Biotin-conjugated pAb to mouse H-2K^{d} (SF1–11; BD Biosciences)
PE-conjugated mAb to H-2K^{d} (clone SF1–1.1; BD Biosciences)
PE conjugated mAb CD44 antibody (550932, BD Bioscience)

Regular immunohistochemical (IHC) staining and double immunofluorescence (IF) staining of AR and PSA in formalin-fixed paraffin-embedded (FFPE) HPCa sample

Basic IHC protocols have been described [12, 13]. Paraffin-embedded sections (4 μm) were deparaffinized and hydrated in xylene followed dehydration in graded alcohols to water. Antigen retrieval was performed in 1.0 mM EDTA Buffer (pH 8.0) for 10 min in a microwave oven followed by a 20-min cool down. Slides were then incubated with various primary antibodies followed by Envision-plus labeled polymer-conjugated horseradish peroxidase and DAB monitoring staining development (Dako). For IHC analysis of PSA^{+} and PSA$^{-/lo}$ cells in FFPE HPCa sections, we first titrated the primary antibody to PSA (A0526, Dako) and found that at 1:5 dilutions, the antibody reliably differentiated the PSA^{+} and PSA$^{-/lo}$ PCa cells. We then utilized this antibody concentration to stain FFPE sections [13]. In general we stained at least 3 consecutive sections from each sample for PSA. Twelve fields were chosen from each slide for counting by two individuals in a blind fashion and PSA^{+} and PSA$^{-/lo}$ PCa cells were averaged.

For PSA and AR double IF staining, HPCa sections (4 μm) were deparaffinized and dehydrated through graded alcohols. Antigen retrieval was performed by soaking slides in pre-warmed target retrieve agent (S1099, Dakocytomation) in boiling water bath (40 min). Slides were incubated with Background Sniper (BS966H, Biocare Medical) at room temperature for 30 min. For primary antibody staining, slides were incubated at 4°C overnight with a mix of mouse monoclonal anti-AR (clone 411, SC-7305, Santa Cruz Technology; 1:50) and rabbit polyclonal anti-PSA (A0526, Carpinteria, CA; 1:5) in PBS containing 0.1% Triton and 5% goat serum. After thorough washing, slides were incubated at RT for 60 min with secondary antibodies (Invitrogen), i.e., Alexa Flour 594-conjugated goat anti-mouse IgG (1:500) and Alexa Flour 488-conjugated goat anti-rabbit IgG (1:500) in PBS plus 0.1% Triton and 5% serum, followed by thorough washing. Then slides were incubated with DAPI (3 μM) diluted in PBS (RT for 5 min). To eliminate autofluorescence, slides were immersed in 70% ethanol for 5 min, incubated in Autofluorescence Eliminator Reagent (2160, Millipore) for 5 min, and were finally passed through 3 changes of 70% ethanol for 1 min each. Upon rinsing in PBS, slides were mounted with 10 μL Gold Antifade Reagent (936590, Prolong). Images were acquired on an Olympus microscope.

Xenograft tumor processing and purification of human PCa cells from xenografts

Basic procedures were detailed elsewhere [11]. Briefly, xenograft tumors were harvested from maintenance tumors and minced into ~1 mm^{3} pieces, which were rinsed once with PBS, digested for 30 min with Accumax (AM105; Innovative Cell Technologies, San Diego, CA) at room temperature, and filtered though 40-μm cell strainer. Dead cells and debris were separated from live cells on a discontinuous Percoll gradient. Lineage-positive mouse cells were depleted using either MACS Lineage Cell Depletion Kit (Miltenyi Biotec) or staining for mouse-specific MHC using PE or Biotin-conjugated monoclonal anti-H-2K^{d} (SF1–11; BD Biosciences).

Primary prostate tumor (HPCa) processing

Our lab has so far worked on >220 HPCa samples and the present study utilized >70 HPCa samples (Supplementary Table 2). All HPCa samples (with the matched normal/benign samples) were obtained with the written informed consent from the patients in accordance with federal and institutional guidelines and with the approved IRB protocols (MDACC LAB04–0498). HPCa processing protocol has been described previously [11–13]. Lineage-positive (i.e., hematopoietic, endothelial, smooth muscle, fibroblast, and other stromal) cells were depleted using the MACS Lin-1 cocktail mix and anti-CD140b-PE (Miltenyi Biotec). Purified HPCa cells

were used in multiple types of experiments and, in some cases, for infection with the PSAP-GFP lentiviral vector. When necessary, HPCa cells were cultured for a short period time in various media, e.g., serum/androgen-free PrEBM supplemented with insulin, EGF, and bovine pituitary extract.

Tumor experiments and serial tumor transplantation in NOD/SCID mice

Subcutaneous (s.c) and orthotopic (i.e., dorsal prostate or DP) tumor transplantations were carried out as previously described [6–8, 11–13]. For serial tumor transplantations in NOD/SCID mice, marker-positive and -negative PCa cells were sorted out by FACS from the first-generation (1°) tumors originally derived from corresponding marker-positive and –negative cells, and implanted s.c or in the DP to generate secondary (2°) tumors. Sequential tumor transplantation was performed using similar strategies. For tumor experiments in castrated mice, male NOD/SCID mice (6–8 weeks) were surgically castrated 1–2 weeks prior to tumor cell injection.

Lentiviral infection of PCa cells

Lentivirus was produced in 293FT packaging cells and titers determined using GFP positivity in HT1080 cells. PCa cells were infected, generally, at a multiplicity of infection (MOI) of 20 and harvested at 48–72 h post-infection. Infected bulk cells or FACS-purified subpopulation of cells were used in various *in vitro* and *in vivo* experiments detailed in each Figure.

Fluorescence-activated cell sorting (FACS)

PCa cells stained for various markers or after PSAP-GFP infection (48–72 h) were dissociated into single-cell suspension and generally 1–10 × 10^6 cells were used for FACS on a BD FACSAria™ Fusion cell sorter. Unstained or uninfected cells were used as negative control for gating. Post-sort analysis was routinely performed to guarantee the purity of each population. HPCa cells freshly purified from primary tumors were first infected with PSAP-GFP and sorted 3–7 days later. To purify marker-positive PCa cells from xenograft tumors, we first incubated PCa cells with FcR blocking agent (Miltenyi Biotec) for 15 min at 4°C and then stained them with various primary antibodies. For double or triple marker populations, we would incubate cells with anti-α2β1 (MAB1998Z; Chemicon) for 30 min on ice followed by staining with APC-conjugated goat anti-mouse IgG (550826; BD Biosciences) for 15 min on ice. Cells were then washed (3x) and stained with PE-conjugated anti-CD44 antibody (550932, BD Bioscience) and biotinylated mouse H2-Kd (553564, BD Pharmingen) for 20 min. After washing, cells were incubated with Alexa Flour 405-conjugated streptavidin for 10 min at 4°C. Cells were incubated in solution containing 1% BSA and 2.5 μg/ml insulin (I-6634, Sigma). PCa cells were suspended in ALDEFLUOR assay buffer containing ALDH substrate (1 μM per 1 × 10^6 cells, the ALDEFLUOR kit; StemCell Technologies, Vancouver, Canada) and incubated for 40 min at 37°C and sorted by FACS. As negative control, we added 50 nmol/l diethylaminobenzaldehyde (DEAB) to the cell suspension.

Clonal and clonogenic sphere-formation assays

Holoclone and sphere-formation assays were conducted as previously described [10, 11] and stringent conditions were employed to ensure that clones, colonies, and spheres were all derived from single cells [12]. Briefly, we performed clonal analysis using purified and/or sorted PCa cells plated at 100 cells/10-cm plate or 100 cells/well in a six-well culture dish. Clones with ≥50 cells were scored ~2 weeks after plating. We performed LAPC9 clonal analysis on mitomycin C (M0530, Sigma) treated Swiss 3T3 cells. The results were expressed as cloning efficiency (%). In some clonal assays, cells were directly sorted into 96-well plates at 1 cell/well and clonal type and size were monitored and scored under a (fluorescence) microscope [10, 11]. For clonogenic sphere-formation assays in xenograft and HPCa cells, cells were plated at 5,000–10,000 cells/well in six-well culture dishes coated with a thin layer of 1% solidified agar or 50% Matrigel or plated in 6-well ultra-low attachment (ULA) plates. Spheres that arose within 1–2 weeks were presented as clonogenicity (%). For serial sphere-formation assays, the first-generation spheres were harvested, disaggregated with 0.025% trypsin/EDTA, triturated with a 27-G needle, filtered through 40-μm mesh, and replated as above. This process was repeated for up to 4–5 generations. We sometimes performed serial clonogenic assays in a different way. Briefly, cells were first resuspended in DMEM/F12 supplemented with B27 (17504–044, Invitrogen) and N2 (17502–048, Invitrogen) and mixed (7:4) thoroughly with methylcellulose (04100, Stem Cell Technology) and plated (600 μl) in 24-well ULA plates at 2, 000 cells/wells. Primary spheres were scored in ~2 weeks. For secondary sphere assays, the first-generation spheres were individually picked up with a transfer pipette under a dissection microscope and dissociated with 0.05% trypsin/EDTA. All the cells derived from individual spheres were mixed with methylcellulose and plated back to one well of a 96-well ULA plate.

Clonogenic assays in $CD44^+$ PCa cells treated with FGFR inhibitor or with gene knockdowns

Du145 and LAPC9 cells were incubated with PE-conjugated anti-CD44 (BD Biosciences; 1:10 dilution) for 1 h at 4°C. Cells were washed and resuspended in sorting buffer, and the $CD44^+$ (top 20%) population was sorted out by FACS (see above). For shRNA (CD44, integrin α2, and ABCG2) infection, 1 × 10^5 sorted cells were plated in a 12-well plate in PrEBM media supplemented with B27,

10 μM EGF, 10 μM FGF, 8 μg polybrene and infected with individual shRNA lentiviral vectors (MOI 20). After 48 h, 2×10^3 cells were plated per well in a 6-well ULA plate in complete PrEBM media and incubated for 2 weeks before scoring. Alternatively, cells were resuspended in a 1:1 ratio of Matrigel:PrEBM media mix and 3×10^3 cells per well were plated around the rim in a 12-well plate. After the Matrigel solidified, 2 ml of complete PrEBM media was added to wells and cells were incubated for 2 weeks before scoring. For treatment with the FGFR inhibitor SU5402, $CD44^+$ cells were plated in both Matrigel and ULA plates immediately after sorting as described above with the indicated SU5402 concentrations.

Immunofluorescence (IF) microscopy

Basic IF procedures have been described [6–8]. To correlate GFP and AR expression in LNCaP cells, GFP^+ and $GFP^{-/lo}$ cells were sorted out by FACS and plated on the glass coverslips overnight. Cells were stained using a monoclonal antibody to AR (clone 441) followed by goat anti-mouse IgG conjugated to Alexa Fluor 594. For Ki-67 staining, cells were sorted out via FACS and plated on the glass coverslips for 8 h. Cells were then incubated with the rabbit mAb to Ki-67 (Abcam; 1:1000) for 60 min at room temperature. Following thorough washing for 3 times with PBS, the coverslips were incubated for 60 min at room temperature with Alexa Fluor 594–conjugated goat anti-rabbit IgG (1:1000). In some experiments, freshly purified CD44+ HPCa cells were plated on collagen-coated glass coverslips and cultured in PrEBM media supplemented with B27, 10 μM EGF, 10 μM FGF, and BPE overnight followed by IF labeling for CD44, α2β1, AR, PSA, and hTERT.

Cell cycle and cell death analyses

To determine the cell-cycle profiles, regular PCa cells or PSAP-GFP infected cells were plated in 3.5-cm culture dish at 30% confluence and harvested at ~60% confluence, fixed in 0.5% PFA for 1 h at 4°C, and then permeabilized in 70% cold ethanol at 4°C for 3 h. Cells were incubated in propidium iodide (PI) working solution (40 μg/ml, P4170; Sigma) at 37°C for 30 min and analyzed by FACS for cell-cycle profiles [11, 13]. To determine differential sensitivities of the $PSA^{-/lo}$ and PSA^+ PCa cell populations to various drug treatments, we performed FACS analysis using the Vybrant Apoptosis Kit (catalog #V23200; Molecular Probes, Invitrogen) according to the manufacturern's instructions. The kit contained biotin-Annexin V, Alexa Fluor 350 (similar spectrum to DAPI) streptavidin, and PI. Briefly, LNCaP cells infected with the PSAP-GFP reporter construct were plated in 10-cm cell culture plates at 500, 000 cells per plate. Cells were treated with DMSO (vehicle control), etoposide (25 μM), paclitaxel (10 nM), CDSS plus bicalutamide (20 μM) or H_2O_2 (10 μM) for various time intervals with fresh drugs added every 1–2 days. Treated cells and controls were analyzed by FACS at 2–5 days after the initiation of treatments. Healthy live cells were identified as Annexin V dim and PI negative; apoptotic cells Annexin V positive and PI low/-; and necrotic cells Annexin V bright and PI bright.

Quantitative RT-PCR (qRT-PCR)

Basic protocols for qRT-PCR have been described [12, 13]. In brief, qRT-PCR was performed using an ABI Prism 7900HT and the TaqMan system (ABI; Applied Biosystems, Foster City, CA; http://www.appliedbiosystems.com). The primers, probes, and assay conditions for other molecules were designed by ABI with the following information: PSA (Hs03063374_m1; assay number), AR (Hs00907244_m1), β-actin (Hs99999903_ml), CD44 (Hs00153304_m1), α2 integrin (Hs00158148_m1), and GAPDH (4326317E).

Time-lapse videomicroscopy and estimate of cell-cycle transit time

Purified GFP^+ and GFP^- LNCaP cells were plated on special glass-bottom dishes, placed on the incubator stage of Nikon Biostation Timelapse system [13], and maintained at 37°C, 5% CO2 and >95% humidity in the RPMI medium supplemented with 7% FBS. Phase and GFP images were collected continuously with a 20X objective lens at a 1-h interval for up to ~1 week. Data analysis was performed using Nikon NIS-Elements software. Several dozens of recorded GFP^+ and GFP^- images were analyzed in detail for cell-cycle transit times using the first cell division as the starting point.

Correlating *PSA* mRNA levels with clinical outcomes of PCa patients in *Oncomine*

A total of 27 *Oncomine* PCa data sets containing *KLK3* mRNA expression data (Supplementary Table 2) were analyzed in detail for correlations with available patient parameters including survival, recurrence, metastasis, Gleason score, serum PSA levels, and LN status. Significance of *PSA* mRNA between conditions was determined by Student's *t*-test, and *P* values less than 0.05 were considered statistically significant. Box plot data presentations and statistical analyses were generated using program R. We also performed survival analysis and generated Kaplan-Meier survival plots using the survival package in R. Briefly, we first input the individual normalized gene expression data from patients with both survival time and survival status from *Oncomine* and ranked the data according to *PSA* mRNA expression. We then assigned the samples with rankings from the first quartile to the third quartile into two groups and compared the *P*-value between these two groups along with different cutoffs. Finally, we set the ultimate cutoff with the smallest *P*-value and plotted a Kaplan-Meier survival curve.

Determination and GO analysis of genes commonly upregulated in both LNCaP and LAPC9 cDNA microarrays

We previously performed cDNA microarrays in $PSA^{-/lo}$ versus PSA^{+} LNCaP and LAPC9 cells [13] and all microarray data have been deposited in the NCBI GEO database (www.ncbi.nlm.nih.gov/geo/query) under the accession number GSE15411 and GSE30114. To determine commonly changed genes, we first selected the genes (by Agilent's Probe ID) either up-regulated or down-regulated using a 1.4FC cutoff from both LAPC9 and LNCaP gene lists (from raw data file) and used these genes for Venn diagram analysis. This analysis identified 3,949 and 3,338 upregulated probe ID's in $PSA^{-/lo}$ LAPC9 and LNCaP cells, respectively, over the corresponding PSA^{+} cells, of which 570 probe ID's were shared (see Supplementary Figure 4B). The probe ID's were then converted into official gene names (symbols) using the ID conversion tool available in DAVID, which identified a total 337 genes commonly upregulated in both LNCaP and LAPC9 $PSA^{-/lo}$ populations. We performed Gene Ontology (GO) analysis of 337 commonly upregulated genes using functional annotation tool in DAVID.

ChIP and re-ChIP assays

To determine if $PSA^{-/lo}$ and PSA^{+} tumor cells differed in chromatin composition and stem-cell associated bivalent domains, ChIP and re-ChIP assays [30] were performed using chromatin from prospectively purified $PSA^{-/lo}$ and PSA^{+} LAPC9 and LNCaP cells. Freshly sorted $PSA^{-/lo}$ and PSA^{+} cells were fixed for 15 min at RT by addition of freshly prepared neutral buffered formalin to their respective media at a final concentration of 0.75%, with gentle rocking. Formalin was quenched by the addition of 2 M glycine to a final concentration of 0.125 M and incubation for 5 min at RT with gentle rocking. Cells were then pelleted and resuspended in 750 µl of ChIP lysis buffer (50 mM HEPES-KOH, 140 mM NaCl, 1 mM EDTA, pH 8.0, 1% Triton X100, 0.1% sodium deoxycholate, and Roche complete protease inhibitor cocktail) for every million cells, and sonicated on ice until the majority of the chromatin had been sheared into 500–1000 bp fragments. 50 µl was removed for use as input, and the remaining chromatin was divided into aliquots for immunoprecipitation (IP) and diluted 10x with dilution buffer (1% Triton X-100, 2 mM EDTA, 150 mM NaCl, 20 mM Tris-HCl, pH 8.0, and Roche protease inhibitor cocktail).

In all immunoprecipitations, 5 µg of primary antibody or control IgG was used for the initial ChIP as well as re-ChIPs performed. Antibodies used in the initial ChIP were ChIP-grade rabbit control IgG, anti-Histone H3, anti-Histone H3K4 (trimethyl), and anti-Histone H3K27 (trimethyl). For the re-ChIP, a mouse monoclonal antibody raised against histone H3K27 (trimethyl) was used. For each ChIP antibody, 60 µl of Invitrogen Dynal beads were washed and blocked in PBS-0.1% BSA. Half of the beads were incubated overnight with the chromatin samples without antibody, as a pre-clearing step to reduce background due to non-specific chromatin interaction with the beads. Beads used for pre-clearing were then discarded. The other half of the beads were incubated with antibodies for ChIP while pre-clearing was ongoing. The following day, IP's were performed by combining pre-cleared chromatin samples with antibody-bead complexes and incubating overnight at 4°C with gentle rocking. The next day, the beads were washed 3 × 5 min. with ChIP wash buffer (0.1% SDS 1% Triton X-100 2 mM EDTA 150 mM NaCl 20 mM Tris-HCl, pH8) and the bound chromatin eluted by incubating the beads with 450 µl of 100 mM sodium bicarbonate, 20 mM DTT for 15 min. at RT. 50 µl of each ChIP was removed for use as input before incubating the IP eluate with the re-ChIP antibody. Re-ChIPs were performed by incubating the eluted chromatin from the first round of ChIP with the H3K27 (trimethyl) mAb/bead mixture overnight at 4°C with gentle rocking. The re-ChIP'ed chromatin was washed 3× for 5 min. in ChIP wash buffer and then eluted by incubation with 450 µl of 100 mM sodium bicarbonate, 1% SDS for 15 min at RT. Prior to use in PCR reactions to detect the immunoprecipitated DNA, all samples and inputs were subjected to cross-link reversal by addition of 5 µl of 20 mg/ml proteinase K and incubation at 60°C overnight. Protein was removed from ChIP samples and inputs by phenol-chloroform extraction and alcohol precipitation, and inputs were resuspended in 100 µl of ddH2O while samples were resuspended in 30 µl ddH2O. PCR was typically performed for 33 cycles with 1 min. for extension and 30 seconds for denaturing and annealing steps with a 5-minute final extension. Promega GoTaq 2X master mix was used for all reactions. ChIP primers were targeted to sequences approximately 1000 bp from the TSS (transcription start site) and were as follows:

AR	Forward: 5′-GGGTGATTTTGCCTTTGAGA-3′ Reverse: 5′-GGCTTTGGAGAAACAAGTGC-3′
ASCL1	Forward: 5′-TTCACCCCAAGTCTTTCCAC -3′ Reverse 5′-ACTAAGGCTGCGCTCTCTTG-3′
BCL2	Forward: 5′-GTCTGGGAATCGATCTGGAA-3′ Reverse: 5′-GCGGAACACTTGATTCTGGT-3′
CD61	Forward: 5′-CACACACACATGCAAACGAG-3′ Reverse: 5′-CACCCTCCCAAACACTAGGA-3′
CDH2	Forward: 5′-GCGGGAGGAATAGGAGAGG-3′ Reverse 5′-ATGTGGAGGTGGAAGTGGAG-3′

FGF5	Forward: 5′-CAATCATCCTCCCCAG AAGA-3′ Reverse: 5′-TTGCATGCTTGGAATG TTTC-3′
NKX3-1	Forward: 5′-ACTCACTGCAGCCTCG ATTT-3′ Reverse: 5′-CCCGTTGCACAGGTAG TTTT-3′
PPP2R4	Forward: 5′-CCTGTCCCCACATGTC TTCT-3′ Reverse: 5′-CCTCTCGCCTTTCACT CTTG-3′

Quantification of relative binding in ChIP assays was performed using NIH ImageJ software (http://stanxterm.aecom.yu.edu/wiki/index.php?page=Using_ImageJ), and each gene promoter was analyzed in 3 independent immunoprecipitations. Arbitrary optical density values obtained through ImageJ were scaled for each ChIP by setting the pan-Histone H3 band to 1.

Statistics

In general, unpaired two-tailed Student's *t*-test was used to compare differences in cell numbers, cell-cycle transit time, cloning and sphere-forming efficiency, tumor weights, and many other parameters. Fisher's Exact Test and χ^2 test were used to compare incidence and latency. Log-Rank test was employed to analyze the survival curves and ANOVA (F-test) was used to compare multiple groups. In all these analyses, a $P < 0.05$ was considered statistically significant.

ACKNOWLEDGMENTS

We thank the Histology Core for assistance in IHC, Drs. D. Cuellar, R. Fagin, and E. Giesler and their Associates for providing HPCa samples, J. Repass for help in qPCR analysis, Drs. B. Bhatia and L. Patrawala for some earlier studies, and the rest of the Tang lab members for insightful discussions. We apologize to the colleagues whose work was not cited due to space constraint.

FUNDING

This project was supported, in part, grants from NIH (NCI R01-CA155693), DOD (W81XWH-13–1-0352 and W81XWH-14–1-0575), CPRIT (RP120380), and MDACC Center for Cancer Epigenetics (all to D.G.T). This study also made use of the Science Park NGS Core, supported by CPRIT Core Facility Support Grant RP120348 (to J.S). C. J was supported in part by CPRIT (RP120394). X. Chen and C. Liu were supported, in part, by DOD postdoc fellowships PC141581 and PC121553, respectively.

CONFLICTS OF INTEREST

The authors claim no conflict of interests.

REFERENCES

1. Tang DG. Understanding cancer stem cell heterogeneity and plasticity. Cell Res. 2012; 22:457–472.
2. Kreso A, Dick JE. Evolution of the cancer stem cell model. Cell Stem Cell. 2014; 14:275–291.
3. Wicha MS. Targeting self-renewal, an Achilles' heel of cancer stem cells. Nat Med. 2014; 20:14–15.
4. Kreso A, van Galen P, Pedley NM, Lima-Fernandes E, Frelin C, Davis T, Cao L, Baiazitov R, Du W, Sydorenko N, Moon YC, Gibson L, Wang Y, et al. Self-renewal as a therapeutic target in human colorectal cancer. Nat Med. 2014; 20:29–36.
5. Jeter CR, Yang T, Wang J, Chao H, Tang DG. Nanog in cancer stem cells and tumor development: An update and outstanding questions. Stem Cells. 2015. In press.
6. Patrawala L, Calhoun T, Schneider-Broussard R, Zhou J, Claypool K, Tang DG. Side population (SP) is enriched in tumorigenic, stem-like cancer cells whereas ABCG2$^+$ and ABCG2$^-$ cancer cells are similarly tumorigenic. Cancer Res. 2005; 65:6207–6219.
7. Patrawala L, Calhoun T, Schneider-Broussard R, Li H, Bhatia B, Tang S, Reilly JG, Chandra D, Zhou J, Claypool K, Coghlan L, Tang DG. Highly purified CD44$^+$ prostate cancer cells from xenograft human tumors are enriched in tumorigenic and metastatic progenitor cells. Oncogene. 2006; 25:1696–1708.
8. Patrawala L, Calhoun-Davis T, Schneider-Broussard R, Tang DG. Hierarchical organization of prostate cancer cells in xenograft tumors: The CD44$^+$α2β1$^+$ cell population is enriched in tumor-initiating cells. Cancer Res. 2007; 67:6796–6805.
9. Tang DG, Patrawala L, Calhoun T, Bhatia B, Choy G, Schneider-Broussard R, Jeter C. Prostate cancer stem/progenitor cells: Identification, characterization, and implications. Mol Carcinogenesis. 2007; 46:1–14.
10. Li HW, Chen X, Calhoun-Davis T, Claypool K, Tang DG. PC3 Human prostate carcinoma cell holoclones contain self-renewing tumor-initiating cells. Cancer Res. 2008; 68:1820–1825.
11. Li HW, Jiang M, Honorio S, Patrawala L, Jeter CR, Calhoun-Davis T, Hayward SW, Tang DG. Methodologies in assaying prostate cancer stem cells. Methods Mol Biol 2009; 569:85–138.
12. Liu C, Kelnar K, Liu B, Chen X, Calhoun-Davis T, Li H, Patrawala L, Yan H, Jeter C, Honorio S, Wiggins JF, Baders AG, Fagin R, et al. The microRNA miR-34a inhibits prostate cancer stem cells and metastasis by directly repressing CD44. Nature Med. 2011; 17:211–215.

13. Qin J, Liu X, Laffin B, Chen X, Choy G, Jeter CR, Calhoun-Davis T, Li H, Palapattu GS, Pang S, Lin K, Huang J, Ivanov I, et al. The PSA$^{-/lo}$ prostate cancer cell population harbors self-renewing long-term tumor-propagating cells that resist castration. Cell Stem Cell. 2012; 10:556–569.

14. Huss WJ, Gray DR, Greenberg NM, Mohler JL, Smith GJ. Breast cancer resistance protein-mediated efflux of androgen in putative benign and malignant prostate stem cells. Cancer Res. 2005; 65:6640–6650.

15. Collins AT, Berry PA, Hyde C, Stower MJ, Maitland NJ. Prospective identification of tumorigenic prostate cancer stem cells. Cancer Res. 2005; 65:10946–10951.

16. Gu G, Yuan J, Wills M, Kasper S. Prostate cancer cells with stem cell characteristics reconstitute the original human tumor *in vivo*. Cancer Res. 2007; 67:4807–4815.

17. Li T, Su Y, Mei Y, Leng Q, Leng B, Liu Z, Stass SA, Jiang F. ALDH1A1 is a marker for malignant prostate stem cells and predictor of prostate cancer patients' outcome. Lab Invest. 2010; 90:234–244.

18. van den Hoogen C, van der Horst G, Cheung H, Buijs JT, Lippitt JM, Guzman-Ramirez N, Hamdy FC, Eaton CL, Thalmann GN, Cecchini MG, Pelger RC, van der Pluijm G. High aldehyde dehydrogenase activity identifies tumor-initiating and metastasis-initiating cells in human prostate cancer. Cancer Res. 2010; 70:5163–5173.

19. Rajasekhar VK, Studer L, Gerald W, Socci ND, Scher HI. Tumour-initiating stem-like cells in human prostate cancer exhibit increased NF-κB signalling. Nat Commun. 2011; 2:162.

20. Mulholland DJ, Kobayashi N, Ruscetti M, Zhi A, Tran LM, Huang J, Gleave M, Wu H. Pten loss and RAS/MAPK activation cooperate to promote EMT and metastasis initiated from prostate cancer stem/progenitor cells. Cancer Res. 2012; 72:1878–1889.

21. Cai H, Memarzadeh S, Stoyanova T, Beharry Z, Kraft AS, Witte ON. Collaboration of Kras and androgen receptor signaling stimulates EZH2 expression and tumor-propagating cells in prostate cancer. Cancer Res. 2012; 72:4672–4681.

22. Domingo-Domenech J, Vidal SJ, Rodriguez-Bravo V, Castillo-Martin M, Quinn SA, Rodriguez-Barrueco R, Bonal DM, Charytonowicz E, Gladoun N, de la Iglesia-Vicente J, Petrylak DP, Benson MC, Silva JM, et al. Suppression of acquired docetaxel resistance in prostate cancer through depletion of notch- and hedgehog-dependent tumor-initiating cells. Cancer Cell. 2012; 22:373–388.

23. Yoshioka T, Otero J, Chen Y, Kim YM, Koutcher JA, Satagopan J, Reuter V, Carver B, de Stanchina E, Enomoto K, Greenberg NM, Scardino PT, Scher HI, et al. β4 Integrin signaling induces expansion of prostate tumor progenitors. J Clin Invest. 2013; 123:682–699.

24. Li X, Liu Y, Chen W, Fang Y, Xu H, Zhu HH, Chu M, Li W, Zhuang G, Gao WQ. TOP2Ahigh is the phenotype of recurrence and metastasis whereas TOP2Aneg cells represent cancer stem cells in prostate cancer. Oncotarget. 2014; 5:9498–513.

25. Culig Z, Hoffman J, Erdel M, Eder IE, Hobisch A, Hittmair A, Bartsch G, Utermann G, Schneider MR, Parczyk K, Klocker H. Switch from antagonist to agonist of the androgen receptor bicalutamide is associated with prostate tumour progression in a new model system. Br J Cancer. 1999; 81:242–51.

26. Souers AJ, Leverson JD, Boghaert ER, Ackler SL, Catron ND, Chen J, Dayton BD, Ding H, Enschede SH, Fairbrother WJ, Huang DC, Hymowitz SG, Jin S, et al. ABT-199, a potent and selective BCL-2 inhibitor, achieves antitumor activity while sparing platelets. Nat Med. 2013; 19:202–208.

27. Vaillant F, Merino D, Lee L, Breslin K, Pal B, Ritchie ME, Smyth GK, Christie M, Phillipson LJ, Burns CJ, Mann GB, Visvader JE, Lindeman GJ. Targeting BCL-2 with the BH3 mimetic ABT-199 in estrogen receptor-positive breast cancer. Cancer Cell. 2013; 4:120–129.

28. Garcia-Echeverria C, Pearson MA, Marti A, Meyer T, Mestan J, Zimmermann J, Gao J, Brueggan J, Capraro HG, Cozens R, Evans DB, Fabbro D, Furet P, et al. *In vivo* antitumor activity of NVP-AEW541-A novel, potent, and selective inhibitor of the IGF-IR kinase. Cancer Cell. 2004; 5:231–239.

29. Sharov AA, Ko MSH. Human ES cell profiling broadens the reach of bivalent domains. Cell Stem Cell. 2007; 1:237–238.

30. Bernstein BE, Mikkelsen TS, Xie X, Kamal M, Huebert DJ, Cuff J, Fry B, Meissner A, Wernig M, Plath K, Jaenisch R, Wagschal A, Feil R, et al. A bivalent chromatin structure marks key developmental genes in embryonic stem cells. Cell. 2006; 125:315–326.

31. Chen X, Liu B, Li Q, Honorio S, Liu X, Liu C, Multani AS, Calhoun-Davis T, Tang DG. Dissociated primary human prostate cancer cells coinjected with the immortalized Hs5 bone marrow stromal cells generate undifferentiated tumors in NOD/SCID-γ mice. PLoS One. 2013; 8:e56903.

32. Ho ME, Quek SI, True LD, Morrissey C, Corey E, Vessella RL, Dumpit R, Nelson PS, Maresh EL, Mah V, Alavi M, Kim SR, Bagryanova L, et al. Prostate cancer cell phenotypes based on AGR2 and CD10 expression. Mod Pathol. 2013; 26:849–859.

33. Dudley AC, Khan ZA, Shih SC, Kang SY, Zwaans BM, Bischoff J, Klagsbrun M. Calcification of multipotent prostate tumor endothelium. Cancer Cell. 2008; 14:201–218.

34. Wang J, Zhu HH, Chu M, Liu Y, Zhang C, Liu G, Yang X, Yang R, Gao WQ. Symmetrical and asymmetrical division analysis provides evidence for a hierarchy of prostate epithelial cell lineages. Nat Commun. 2014; 5:4758.

35. Cojoc M, Peitzsch C, Kurth I, Trautmann F, Kunz-Schughart LA, Telegeev GD, Stakhovsky EA, Walker JR, Simin K, Lyle S, Fuessel S, Erdmann K, Wirth MP, et al. Aldehyde dehydrogenase is regulated by Beta-catenin/TCF and promotes radioresistance in prostate cancer progenitor cells. Cancer Res. 2015; Feb 10;. pii: canres.1924.2014 [Epub ahead of print].

36. Wan X, Corn PG, Yang J, Palanisamy N, Starbuck MW, Efstathiou E, Tapia EM, Zurita AJ, Aparicio A, Ravoori MK, Vazquez ES, Robinson DR, Wu YM, et al. Prostate cancer cell-stromal cell crosstalk via FGFR1 mediates antitumor activity of dovitinib in bone metastases. Sci Transl Med. 2014; 6, 252ra122.

37. Bhatia B, Tang S, Yang P, Doll A, Aumueller G, Newman RA, Tang DG. Cell-autonomous induction of functional tumor suppressor 15-lipoxygenase 2 (15-LOX2) contributes to replicative senescence of human prostate progenitor cells. Oncogene. 2005; 24:3583–3595.

38. Bhatia B, Jiang M, Suraneni M, Patrawala L, Badeaux M, Schneider-Broussard R, Multani AS, Jeter CR, Calhoun-Davis T, Hu L, Hu J, Tsavachidis S, Zhang W, et al. Critical and distinct roles of p16 and telomerase in regulating the proliferative lifespan of normal human prostate epithelial progenitor cells. J Biol Chem 2008; 283:27957–27972.

39. Purnell DM, Heatfield BM, Trump BF. Immunocytochemical evaluation of human prostatic carcinomas for carcino-embryonic antigen, nonspecific cross-reacting antigen, beta-chorionic gonadotrophin, and prostate-specific antigen. Cancer Res. 2984; 44:285–292.

40. Stein BS, Vangore S, Petersen RO. Immunoperoxidase localization of prostatic antigens. Comparison of primary and metastatic sites. Urol. 1984; 24:146–152.

41. Feiner HD, Gonzalez R. Carcinoma of the prostate with atypical immunohistological features. Clinical and histologic correlates. Am J Surg Pathol. 1986; 10:765–770.

42. Abrahamsson PA, Lilja H, Falkmer S, Wadström LB. Immunohistochemical distribution of the three predominant secretory proteins in the parenchyma of hyperplastic and neoplastic prostate glands. Prostate. 1988; 12:39–46.

43. Gallee MP, Visser-de Jong E, van der Korput JA, van der Kwast TH, ten Kate FJ, Schroeder FH, Trapman J. Variation of prostate-specific antigen expression in different tumour growth patterns present in prostatectomy specimens. Urol Res. 1990; 18:181–187.

44. de Winter JA, Trapman J, Brinkmann AO, Boersma WJ, Mulder E, Schroeder FH, Claassen E, van der Kwast TH. Androgen receptor heterogeneity in human prostatic carcinomas visualized by immunohistochemistry. J Pathol. 1990; 160:329–332.

45. Masai M, Sumiya H, Akimoto S, Yantani R, Chang CS, Liao SS, Shimazaki J. Immunohistochemical study of androgen receptor in benign hyperplastic and cancerous human prostates. Prostate. 1990; 17:293–300.

46. van der Kwast TH, Schalken J, Ruizeveld de Winter JA, van Vroonhoven CC, Mulder E, Boersma W, Trapman J. Androgen receptors in endocrine-therapy-resistant human prostate cancer. Int J Cancer. 1991; 48:189–193.

47. Oesterling JE. Prostate specific antigen: a critical assessment of the most useful tumor marker for adenocarcinoma of the prostate. J Urol. 1991; 145:907–923.

48. Sadi MV, Walsh PC, Barrack ER. Immunohistochemical study of androgen receptors in metastatic prostate cancer. Comparison of receptor content and response to hormonal therapy. Cancer. 1991; 67:3057–3064.

49. Chodak GW, Kranc DM, Puy LA, Takeda H, Johnson K, Chang C. Nuclear localization of androgen receptor in heterogeneous samples of normal, hyperplastic and neoplastic human prostate. J Urol. 1992; 147:798–803.

50. Sadi MV, Barrack ER. Image analysis of androgen receptor immunostaining in metastatic prostate cancer. Heterogeneity as a predictor of response to hormonal therapy. Cancer. 1993; 71:2574–2580.

51. Ruizeveld de Winter JA, Janssen PJ, Sleddens HM, Verleun-Mooijman MC, Trapman J, Brinkmann AO, Santerse AB, Schroder FH, van der Kwast TH. Androgen receptor status in localized and locally progressive hormone refractory human prostate cancer. Am J Pathol. 1994; 144:735–746.

52. Aihara M, Lebovitz RM, Wheeler TM, Kinner BM, Ohori M, Scardino PT. Prostate specific antigen and gleason grade: an immunohistochemical study of prostate cancer. J Urol. 1994; 151:1558–1564.

53. Tilley WD, Lim-Tio SS, Horsfall DJ, Aspinall JO, Marshall VR, Skinner JM. Detection of discrete androgen receptor epitopes in prostate cancer by immunostaining: Measurement by color video image analysis. Cancer Res. 1994; 54:4096–4102.

54. Pertschuk LP, Macchia RJ, Feldman JG, Brady KA, Levine M, Kim DS, Eisenberg KB, Rainford E, Prins GS, Greene GL. Immunocytochemical assay for androgen receptors in prostate cancer: a prospective study of 63 cases with long-term follow-up. Ann Surg Oncol. 1994; 1:495–503.

55. Hobisch A, Culig Z, Radmayr C, Bartsch G, Klocker H, Hittmair A. Distant metastases from prostatic carcinoma express androgen receptor protein. Cancer Res. 1995; 55:3068–3072.

56. Roudier MP, True LD, Higano CS, Vesselle H, Ellis W, Lange P, Vessella RL. Phenotypic heterogeneity of end-stage prostate carcinoma metastatic to bone. Hum Pathol. 2003; 34:646–653.

57. Shah RB, Mehra R, Chinnaiyan AM, Shen R, Ghosh D, Zhou M, Macvicar GR, Varambally S, Harwood J, Bismar TA, Kim R, Rubin MA, Pienta KJ. Androgen-independent prostate cancer is a heterogeneous group of diseases: lessons from a rapid autopsy program. Cancer Res. 2004; 64:9209–9216.

58. Birtle AJ, Freeman A, Masters JR, Payne HA, Harland SJ. Tumour markers for managing men who present with metastatic prostate cancer and serum prostate-specific antigen levels of < 10 ng/mL. BJU Int. 2005; 96:303–307.

59. Davis JN, Wojno KJ, Daignault S, Hofer MD, Kuefer R, Rubin MA, Day ML. Elevated E2F1 inhibits transcription of the androgen receptor in metastatic hormone-resistant prostate cancer. Cancer Res. 2006; 66:11897–11906.

60. Mostaghel EA, Page ST, Lin DW, Fazil L, Coleman IM, True LD, Knudsen B, Hess Dl, Nelson CC, Matsumoto AM,

Bremner WJ, Gleave ME, Nelson PS. Intraprostatic androgens and androgen-regulated gene expression persist after testosterone suppression: therapeutic implications for castration-resistant prostate cancer. Cancer Res. 2007; 67:5033–5041.

61. Tamburrino L, Salvianti F, Marchiani S, Pinzani P, Nesi G, Serni S, Forti G, Baldi E. Androgen receptor (AR) expression in prostate cancer and progression of the tumor: Lessons from cell lines, animal models and human specimens. Steroids. 2012; 77:996–1001.

62. Ginestier C, Hur MH, Charafe-Jauffret E, Monville F, Dutcher J, Brown M, Jacquemier J, Viens P, Kleer CG, Liu S, Schott A, Hayes D, Birnbaum D, et al. ALDH1 is a marker of normal and malignant human mammary stem cells and a predictor of poor clinical outcome. Cell Stem Cell. 2007; 1:555–567.

63. Liu S, Cong Y, Wang D, Sun Y, Deng L, Liu Y, Martin-Trevino R, Shang L, McDermott SP, Landis MD, Hong S, Adams A, D'Angelo R, et al. Breast cancer stem cells transition between epithelial and mesenchymal states reflective of their normal counterparts. Stem Cell Reports. 2013; 2:78–91.

64. Dieter SM, Ball CR, Hoffmann CM, Nowrouzi A, Herbst F, Zavidij O, Abel U, Arens A, Weichert W, Brand K, Koch M, Weitz J, Schmidt M, et al. Distinct types of tumor-initiating cells form human colon cancer tumors and metastases. Cell Stem Cell. 2011; 9:357–365.

65. Hermann PC, Huber SL, Herrler T, Aicher A, Ellwart JW, Guba M, Bruns CJ, Heeschen C. Distinct populations of cancer stem cells determine tumor growth and metastatic activity in human pancreatic cancer. Cell Stem Cell. 2007; 1:313–323.

66. Sarry JE1, Murphy K, Perry R, Sanchez PV, Secreto A, Keefer C, Swider CR, Strzelecki AC, Cavelier C, Récher C, Mansat-De Mas V, Delabesse E, Danet-Desnoyers G, et al. Human acute myelogenous leukemia stem cells are rare and heterogeneous when assayed in NOD/SCID/IL2Rgammac-deficient mice. J Clin Invest. 2011; 121:384–395.

67. Chen R, Nishimura MC, Bumbaca SM, Kharbanda S, Forrest WF, Kasman IM, Greve JM, Soriano RH, Gilmour LL, Rivers CS, Modrusan Z, Nacu S, Guerrero S, et al. A hierarchy of self-renewing tumor-initiating cell types in glioblastoma. Cancer Cell. 2010; 17:362–375.

68. Liu AY, Roudier MP, True LD. Heterogeneity in primary and metastatic prostate cancer as defined by cell surface CD profile. Am J Pathol. 2004; 165:1543–1556.

69. Issacs JT, Coffey DS. Adaptation versus selection as the mechanism responsible for the relapse of prostatic cancer to androgen ablation therapy as studied in the Dunning R-3327-H adenocarcinoma. Cancer Res. 1981; 41:5070–5075.

70. Craft N, Chhor C, Tran C, Belldegrun A, DeKernion J, Witte ON, Said J, Reiter RE, Sawyers CL. Evidence for clonal outgrowth of androgen-independent prostate cancer cells from androgen-dependent tumors through a two-step process. Cancer Res. 2009; 59:5030–5036.

SUPPLEMENTARY FIGURES AND TABLES

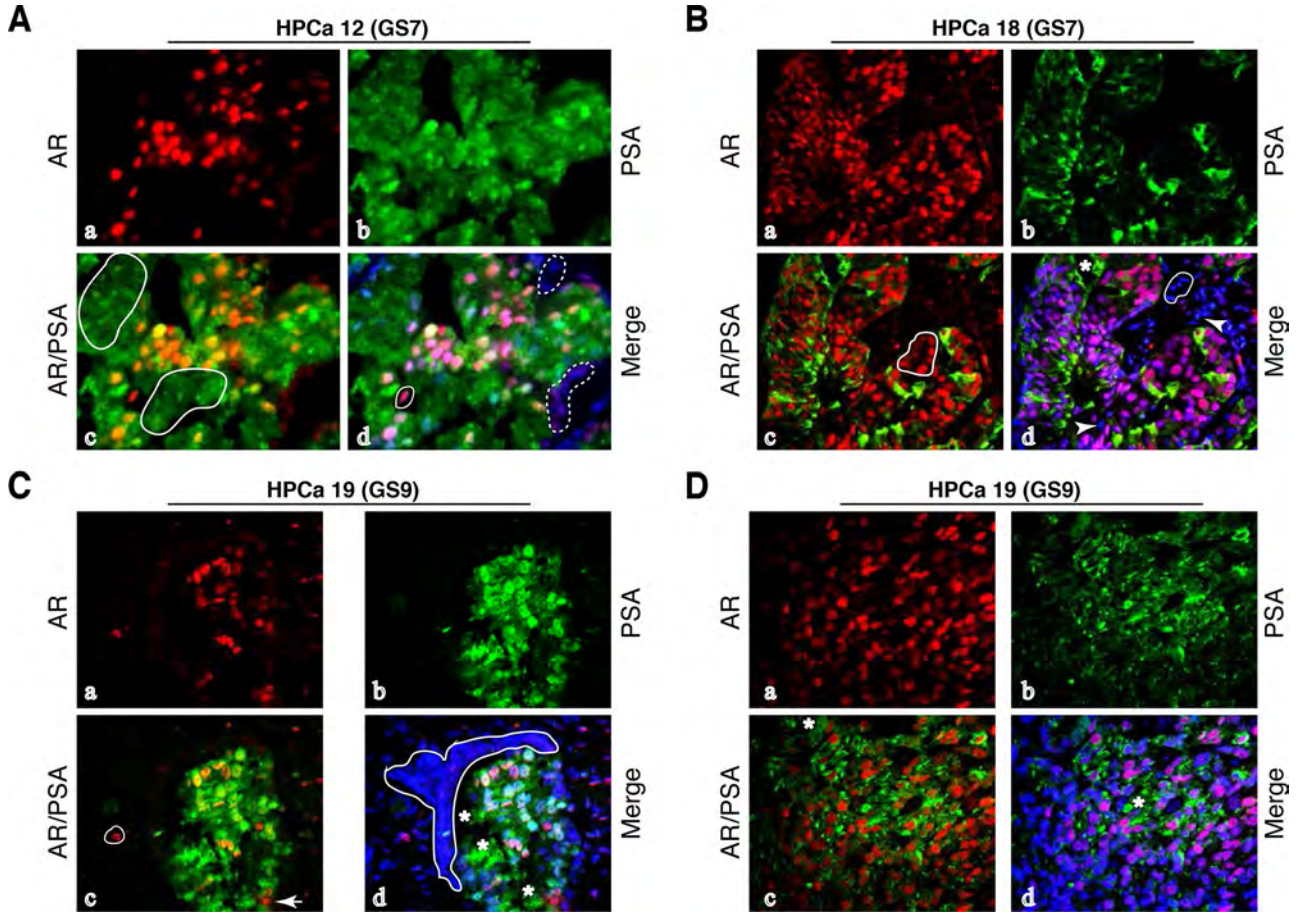

Supplementary Figure 1: Discordant PSA and AR protein expression and subtypes of PCa cells in untreated HPCa. A. Representative immunofluorescence images (×400) illustrating 4 subpopulations of PCa cells in HPCa 12. Although most cells are AR^+PSA^+ PCa cells marked by red nuclei and green cytoplasm, AR^-PSA^+ cells can be seen by green staining alone (panel c, white circled areas), AR^+PSA^- cells by red staining alone (panel d, one white circled area), and AR^-PSA^- cells by being negative or low for both red and green staining (panel d, dashed white circled areas). **B.** Representative immunofluorescence images (×400) illustrating 4 subpopulations of PCa cells in HPCa 18. AR^+PSA^- cells are identified by red staining alone (panel c, white circled area), AR^-PSA^+ cells by green staining alone (panel d, white asterisk), and AR^-PSA^- cells by being negative or low for both colors (panel d, white circled area and white arrowheads). **C–D.** Representative immunofluorescence images (×400) illustrating 4 subpopulations of PCa cells in HPCa 19. AR^+PSA^- cells are identified by red staining alone (Cc, white circled area and white arrow), AR^-PSA^+ cells by green staining alone (Cd and Dc-d, white asterisks), and AR^-PSA^- cells by being negative (or low staining) for both colors (Cd, white circled area).

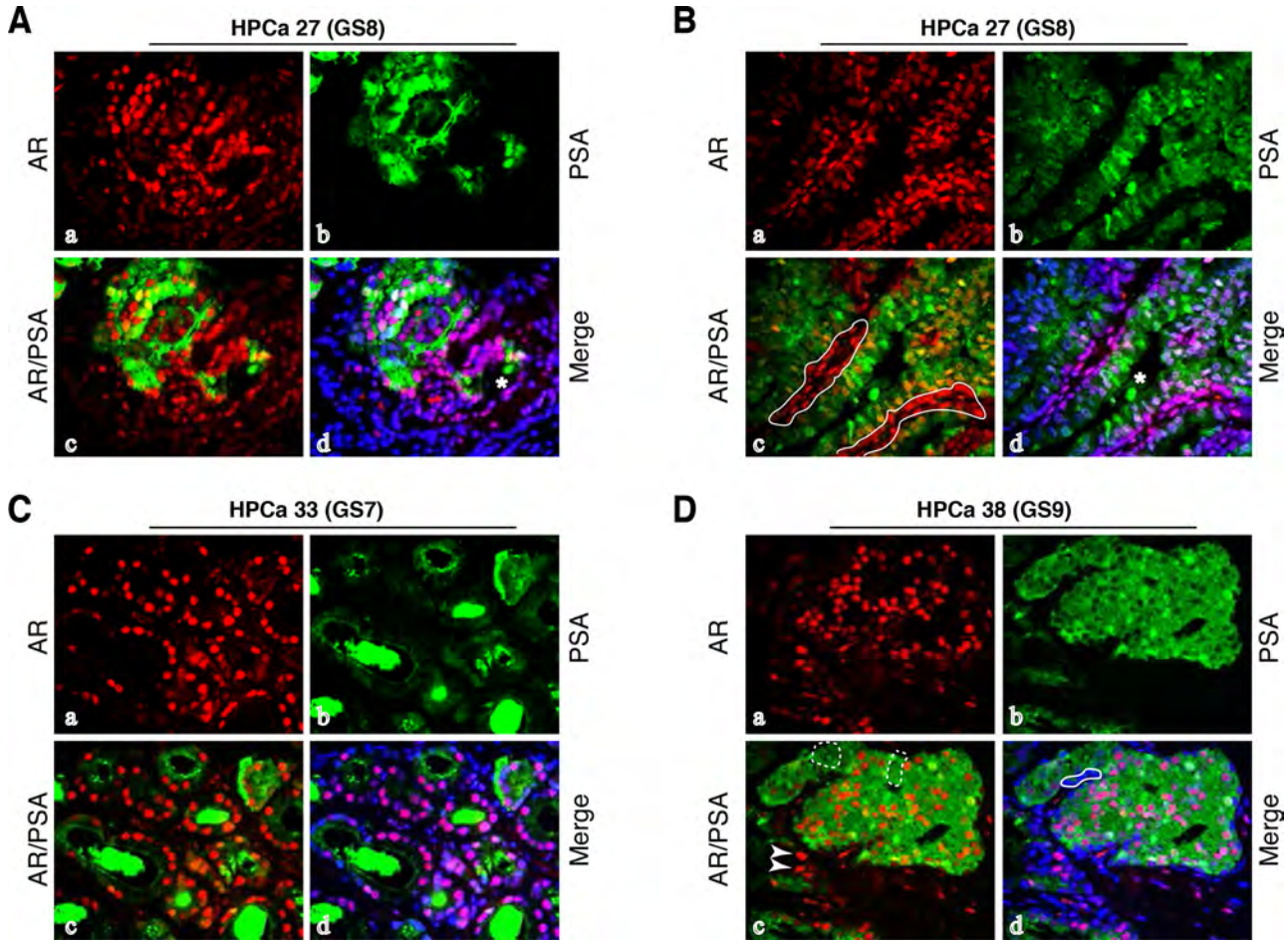

Supplementary Figure 2: Discordant PSA and AR protein expression and subtypes of PCa cells in untreated HPCa. A–B. Representative immunofluorescence images (×400) illustrating 4 subpopulations of PCa cells in HPCa 27. AR^+PSA^- cells are quite abundant in this sample (Ac, red alone cells; Bc, white circled area). Rare AR^-PSA^+ cells can be seen by green staining alone (Bd, white asterisk). AR^-PSA^- cells are negative or low for both red and green staining (Ad and Bd, cells positive for DAPI only). **C.** Representative immunofluorescence images (×400) of AR and PSA staining in HPCa 33. This Gleason 7 tumor manifests numerous small glands in which PSA^+ secretions can be observed in the lumen. There are many AR^+PSA^- cells (Cc, cells with red nuclei alone) and AR^-PSA^- cells (Cd, cells low or negative for both red and green signals). **D.** Representative immunofluorescence images (×400) illustrating 4 subpopulations of PCa cells in HPCa 38. AR^+PSA^+ cells are marked by red nuclei and green cytoplasm (panel c), AR^+PSA^- cells by red staining alone (panel c, white arrowheads), AR^-PSA^+ cells by green staining alone (panel c, white dashed circled cells), and AR^-PSA^- cells by being negative or low for both red and green staining (panel d, white circled area and many single DAPI-positive cells).

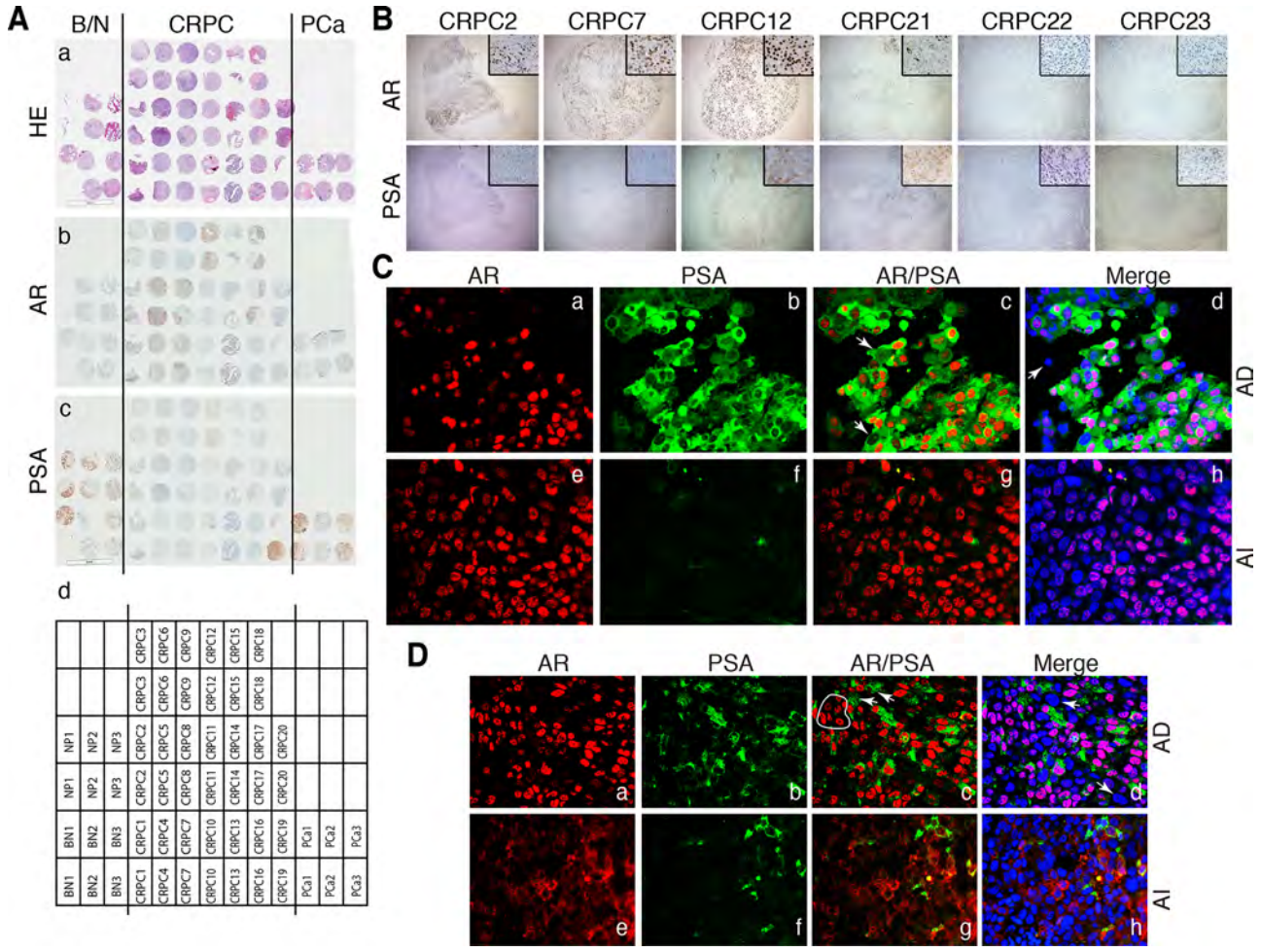

Supplementary Figure 3: Discordant PSA and AR protein expression, 4 subtypes of PCa cells, and increase of PSA$^{-/lo}$ PCa cells in CRPC. A. AR and protein expression in 20 CRPC patient samples on a TMA. Shown on top are HE (a) and AR (b) and PSA (c) IHC images of the TMA and below the TMA grid (d). The 20 CRPC samples are in the middle (demarcated by two vertical lines whereas several benign/normal prostate and PCa samples are shown on the left and right, respectively. All samples were cut in duplicate. NP, normal prostate (i.e., no cancer); BN, benign prostate from patients with PCa; PCa, hormone-naïve prostate cancer. CRPC1–13, PCa patients treated with castration (mostly bicalutamide) and eventually failed after months to years; CRPC14–17, patients failed both radiation and hormonal therapies; CRPC18, the patient failed radiation and cryotherapy; CRPC19, the patient with advanced PCa treated with Lupron for 2 weeks; CRPC20, the patient received 4 months of Lupron treatment plus 2 months of Casodex. **B.** IHC analysis of AR and PSA in the TMA samples. Shown are 7 CRPC samples illustrating prominent loss of PSA, heterogeneous expression of AR, and discordant AR and PSA expression (insets: 400×). CRPC21 – CRPC23 were 3 separate patient CRPC samples not included in the TMA. **C.** Double immunofluorescence staining of AR and PSA in AD vs. AI LNCaP xenograft tumors. Arrows indicate AR^{-}PSA^{+} (c) or AR^{-}PSA$^{-/lo}$ (d) cells. Note significantly increased PSA$^{-/lo}$ LNCaP cells in the AI tumor (f). Shown are representative confocal images (original magnification; ×400). **D.** Double immunofluorescence staining of AR and PSA in AD vs. AI LAPC4 xenograft tumors. In panel c, the white circle indicates several AR^{+}PSA$^{-/lo}$ cells and arrows indicate AR^{-}PSA^{+} cells. In panel d, arrows point to AR^{-}PSA$^{-/lo}$ cells. Note significantly increased PSA$^{-/lo}$ LAPC4 cells in the AI tumor (f). Shown are representative confocal images (original magnification; ×400).

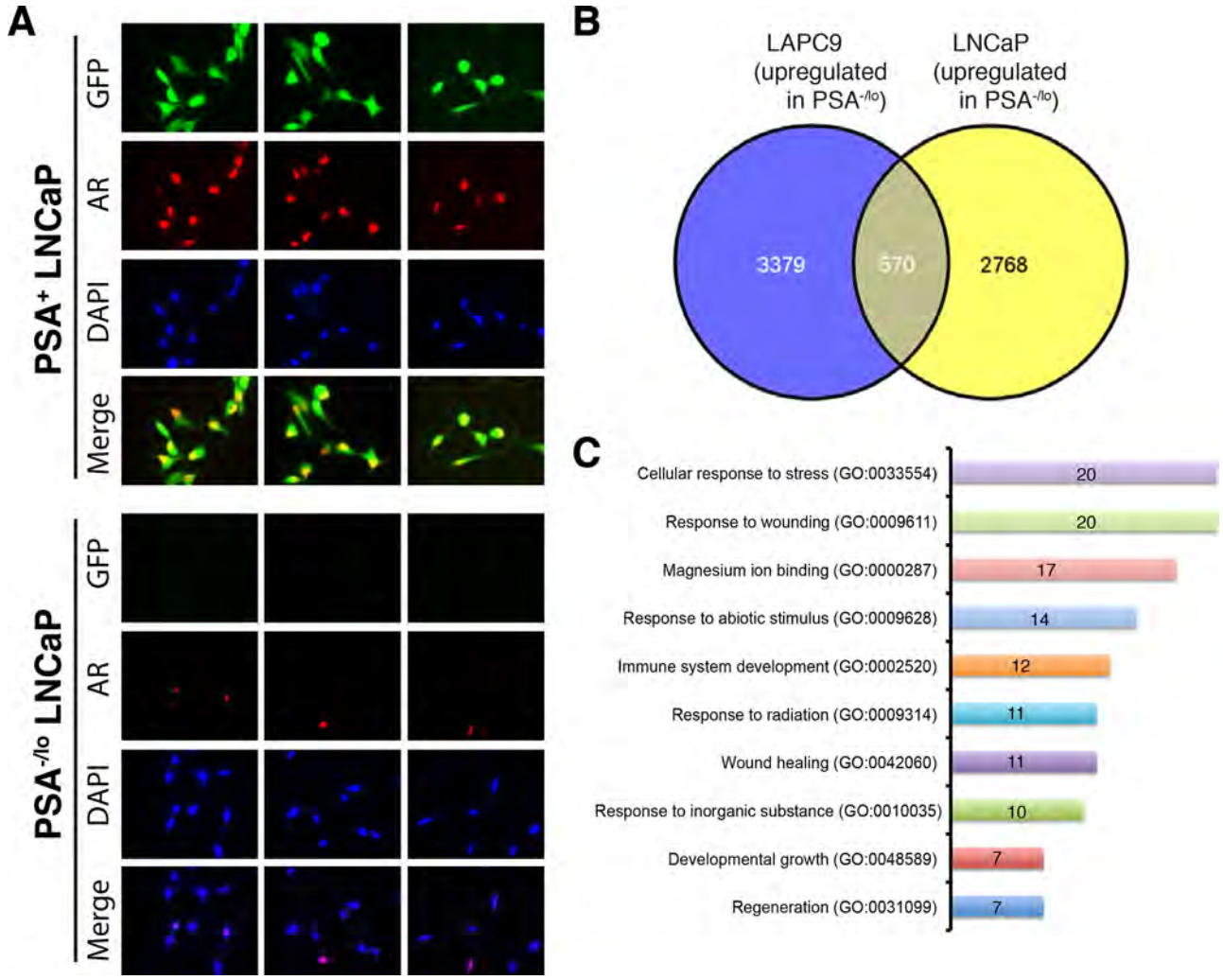

Supplementary Figure 4: PSA$^{-/lo}$ PCa cells are heterogeneous in AR expression and overexpress anti-stress genes. A. GFP^{+} (i.e., PSA^{+}) LNCaP cells express high levels of nuclear AR whereas GFP$^{-/lo}$ (PSA$^{-/lo}$) LNCaP cells are negative or weakly positive for nuclear AR. Shown are 3 representative fields (×400) of purified GFP^{+} (top) and GFP^{-} (bottom) LNCaP cells stained for AR and DAPI, representing 3 independent sorts. **B–C.** Commonly upregulated genes in PSA$^{-/lo}$ LAPC9 and LNCaP cells. Shown in A is Venn diagram presentation of commonly upregulated genes and in B is GO analysis performed using DAVID. The EASE score (a modified Fishcer's Exact test) cut off was set to stringent *p*-value of 0.005 and the top 10 GO categories appeared under GO term 'Biological Process' are presented in the graph. The GO terms and the GO term numbers are presented on the Y-axis and the gene counts are presented inside the bars. The genes for 'Cellular response to stress' are LPO, XRCC2, GEN1, SNCA, SMC5, BRCA2, LIG4, TP73, DCLRE1C, FANCD2, BCL2, GPX3, TPO, MAPK8, TLK1, TLK2, POLQ, MAP2K7, WDR33, and FGD4. The genes for 'Response to wounding' are CCL2, GATM, FUT10, IGF1, ABHD2, GPR68, TP73, PLAA, SLC11A1, F5, FCN3, SAA1, BCL2, IL1RAP, PDGFRA, SPRR3, SERPINB2, SOX15, BMPR1B, and PLAU. The genes for 'Response to abiotic stimulus' are KCNMA1, TG, PTPRC, CCL2, XRCC2, TGFBR1, BRCA2, LIG4, SNAI2, DCLRE1C, FANCD2, BCL2, MAPK8, and RHO. The genes for 'Immune system development' are PTPRC, HSPD1P6, SWAP70, TGFBR1, FUT10, BRCA2, HSPD1P1, LIG4, HSPD1P5, HSPD1P4, DCLRE1C, TAL1, SNRK, BCL2, ZAP70, and HSPD1. The genes for 'Response to radiation' are DCLRE1C, PTPRC, XRCC2, CCL2, FANCD2, BCL2, BRCA2, MAPK8, LIG4, SNAI2, and RHO. The genes for 'Wound healing' are SLC11A1, F5, GATM, SAA1, FUT10, PDGFRA, SPRR3, SERPINB2, SOX15, IGF1, and PLAU.

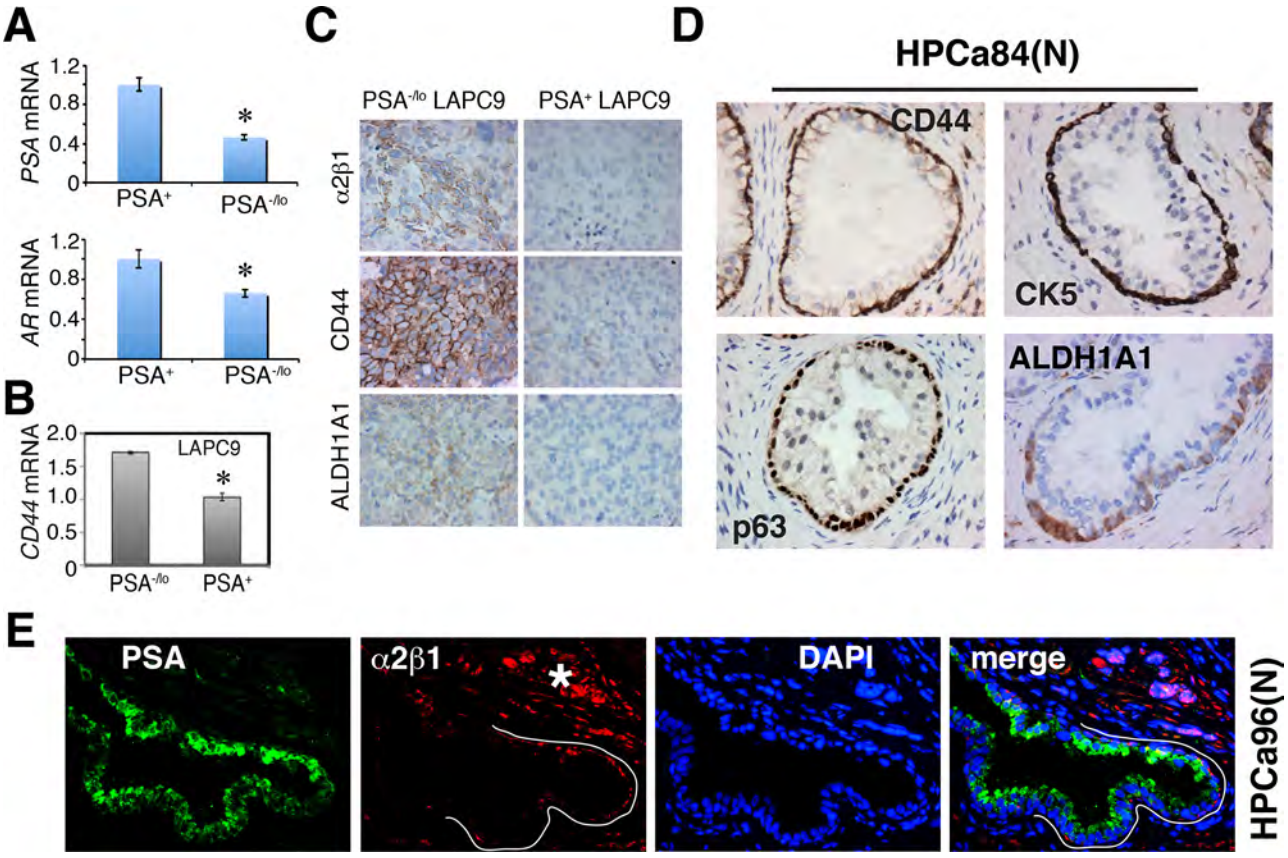

Supplementary Figure 5: Relationship between PSA$^{-/lo}$ PCa cells and other tumorigenic subsets in xenograft tumors and HPCa samples. A. PSA$^{-/lo}$ LAPC9 cells express lower levels of *PSA* (top) and *AR* (bottom) mRNAs than the corresponding PSA^{+} cells. The two populations of LAPC9 cells were freshly purified out from maintenance AD LAPC9 reporter tumors and used in qRT-PCR of *AR* and *PSA*. Shown are the qPCR results ($n = 3$ independent experiments). *$P < 0.001$. **B.** PSA$^{-/lo}$ LAPC9 cells express higher levels of *CD44* mRNAs than the corresponding PSA^{+} cells. Shown are the qPCR results ($n = 3$). *$P < 0.01$. **C.** PSA$^{-/lo}$ LAPC9 tumors serially passaged in intact male NOD/SCID mice have higher % of α2β1^{+}, CD44^{+}, and ALDH1A1^{+} cells compared to corresponding PSA^{+} LAPC9 cell-derived tumors. Shown are representative IHC images from the 3^{0} generation tumors. Original magnification, ×400. **D–E.** Marker expression in normal (benign) prostate tissues. Shown in D are basal expression of CK5 and p63 as well as CD44 and ALDH1A1 in benign prostatic glands in HPCa84(N). Shown in E are dual IF images in HPCa96(N) of PSA, which is expressed in the luminal layer, and α2β1, which is expressed in a fraction of basal cells (demarcated by white line; *indicates α2β1 expression in some stromal cells). Similar results were obtained in HPCa93(N) (not shown). Note that although CK5, p63, and CD44 are expressed in virtually all basal cells, ALDH1A1 and α2β1 are expressed in only a fraction of basal cells (all images: ×200).

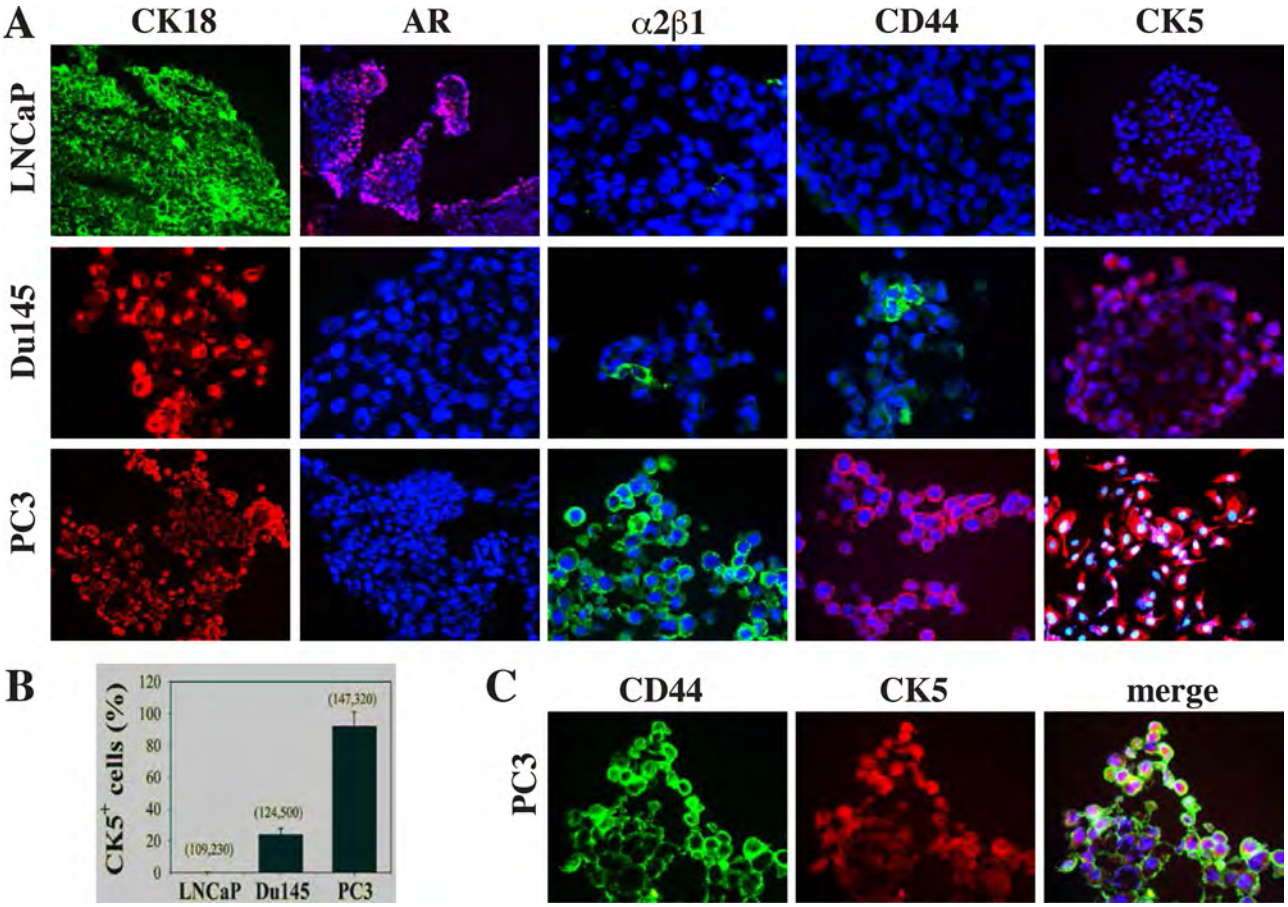

Supplementary Figure 6: Marker expression in 3 PCa cell lines. A. LNCaP, Du145, and PC3 cell spheres/spheroids on cryosections were used in immunostaining for the molecules indicated. Note that all three PCa cell lines expressed CK18 but only LNCaP cells stained positive for AR. **B.** The % of CK5+ cells was quantified in LNCaP, Du145 or PC3 spheres/spheroids. The total numbers of cells counted were indicated parentheses. **C.** In PC3 cell spheroids, CD44 staining overlapped with CK5 staining. Original magnifications: ×200.

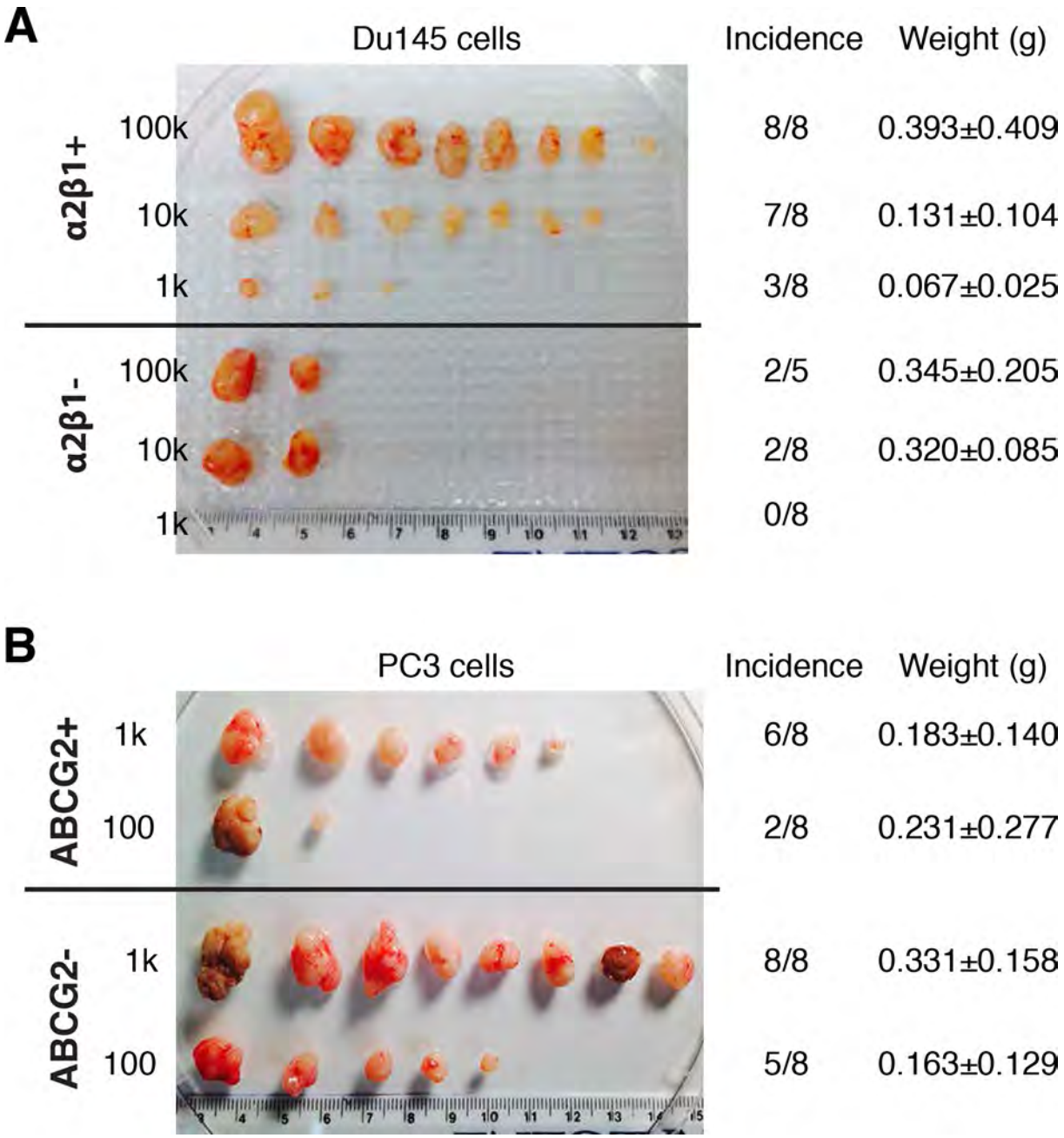

Supplementary Figure 7: LDA tumorigenic assays in subpopulations of Du145 (A) and PC3 (B) cells. (A) Integrin $\alpha2\beta1^+$ and $\alpha2\beta1^-$ Du145 cells were FACS-purified from log-phase cultures and implanted, at the indicated numbers, subcutaneously, in 50% Matrigel in female NOD/SCID mice. The experiment was terminated 74 d after implantation. (B) $ABCG2^+$ and $ABCG2^-$ PC3 cells were purified from cultures and implanted, at the indicated numbers, subcutaneously, in 50% Matrigel in female NOD/SCID mice. The experiment was terminated 57 d after implantation. Not shown were tumor images of the 10k injections, which were harvested 47 d after implantation. The 10k $ABCG2^+$ (incidence 5/5) and $ABCG2^-$ (incidence 7/8) PC3 tumors were 0.316 ± 0.191 and 0.240 ± 0.138 g, respectively. For both A and B, tumor incidence (also see Table 1) and mean tumor weight (no statistical significance) are indicated.

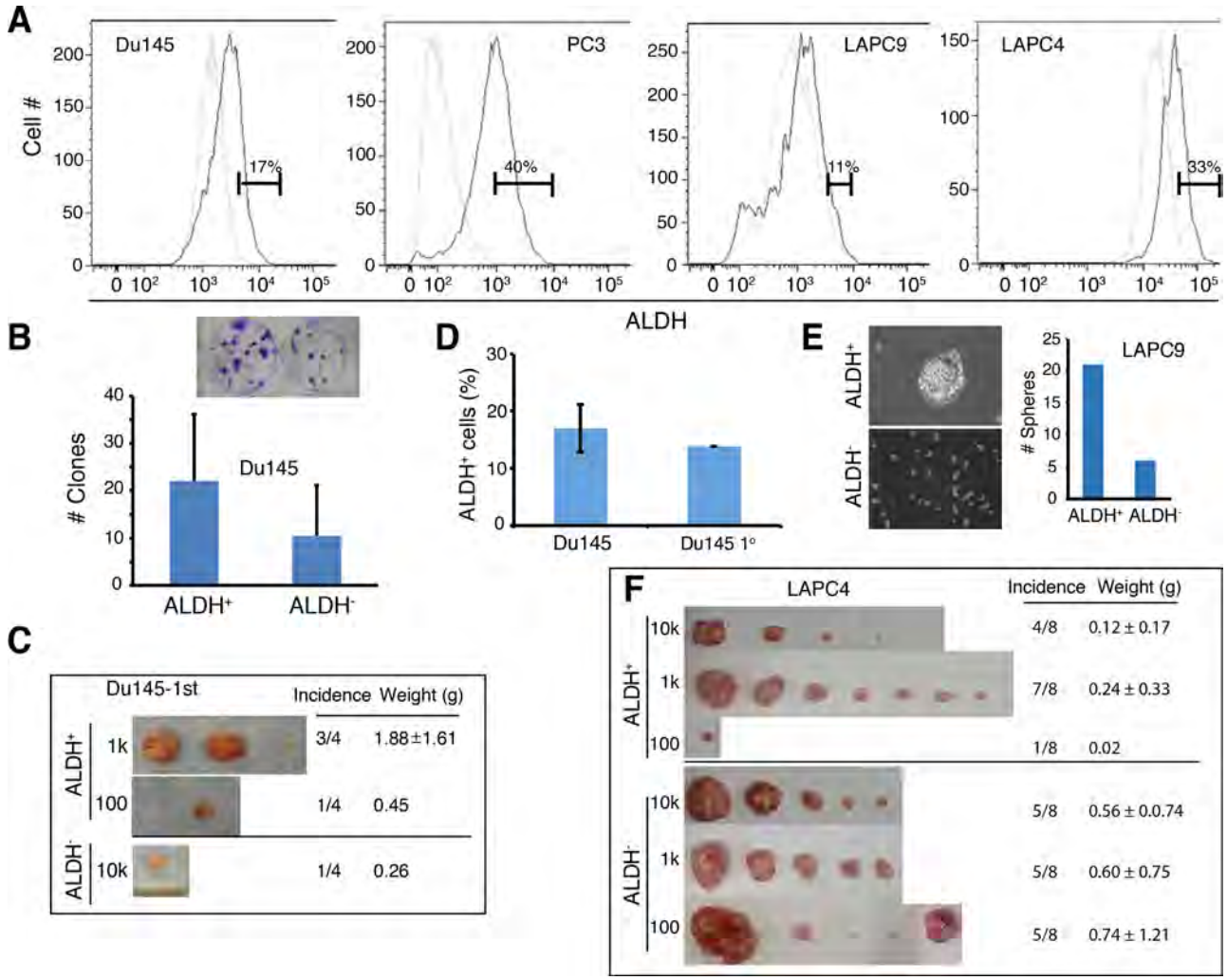

Supplementary Figure 8: The ALDH⁺ PCa cell subpopulations are enriched in tumor-initiating cells. A. Shown are the representative FACS profiles of ALDH activities in four PCa models assessed by the ALDHFLOUR assays. **B.** ALDH⁺ and ALDH⁻ cells were sorted from cultured Du145 cells and plated in 6-well dishes at clonal density (100 cell per well). 15 days after plating, holoclones were counted. Shown are the clone number in bar graph (mean ± S.D) and representative clone images (inset). **C.** Purified ALDH⁺ and ALDH⁻ Du145 cells were subcutaneously implanted in NOD/SCID mice at the indicated cell doses. Tumor images, incidence and weights (mean ± S.D) are shown. **D.** The percentage of ALDH⁺ Du145 cells in parental Du145 cell culture and 1° tumors derived from ALDH⁺ cells. **E.** ALDH⁺ and ALDH⁻ LAPC9 cells were purified and cultured in anchorage-independent conditions in IMDM-15% FBS. 24 d later, spheres were counted and photographed. Insets were representative images of spheres derived from ALDH⁺ and ALDH⁻ LAPC9 cells, respectively. **F.** Sorted ALDH⁺ and ALDH⁻ cells from LAPC4 xenograft tumors were subcutaneously injected in intact male mice. Shown are tumor weights (mean ± S.D) and incidence of tumors derived from indicated cell doses (also see Table 2).

A

Tumorigenicity of the orthotopically implanted LAPC9 cells

Cell type (number)[a]	Incidence[b]	Term. time (d)[c]	Weight (g)[d]
CD44+			
1,000	2/5 (40%)	65	0.1
10,000	5/9 (56%)*	65	1.2
CD44-			
1,000	0/8	90	
10,000	1/12 (8.3%)	76	0.05

[a]LAPC9 xenograft tumors were digested into single-cell suspension and used in sorting for CD44+ and CD44- cells. Either 1,000 or 10,000 cells were implanted in 50% Matrigel into the DP of the intact male NOD/SCID mice.
[b]Refers to tumors developed/total number of implants. The % incidence was indicated.
*P < 0.001 compared to the incidence of CD44- cells.
[c]Time (in days) from tumor implantation to termination (term.).
[d]The mean tumor weight in grams.

B

C

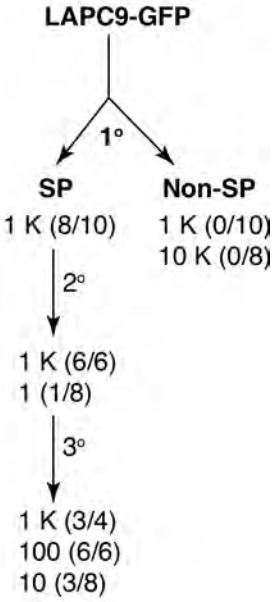

D

Supplementary Figure 9: Tumorigenic properties of prospectively purified CD44+ and SP LAPC9 cells. A. LDA transplantation assays in CD44+ and CD44– LAPC9 cells implanted in the DP of male NOD/SCID mice. Experimental details and outcome are indicated in the Table legend. This represents an independent experiment from what was shown in Table 2. **B.** CD44+ and CD44– LAPC9 cells were purified, resepctively, from the CD44+ and CD44– cell-derived 1° tumors (in A) and implanted in the DP of male NOD/SCID mice (1,000 cells/injection). The experiment was terminated 3 months after tumor cell injections. **C–D.** An independent tumor transplantation assay in SP and non-SP LAPC9 cells. The SP and non-SP cells were purified out from a LAPC9-GFP xenograft tumor and indicated numbers of cells were implanted subcutaneously in male NOD/SCID mice. The SP cells were subsequently purified out from regenerated tumors for 2° and 3° transplantations. Tumor incidence is indicated in parentheses. Shown in D is the image (inset, GFP) of the tumor derived from a single SP cell injection in 2° transplantations (C).

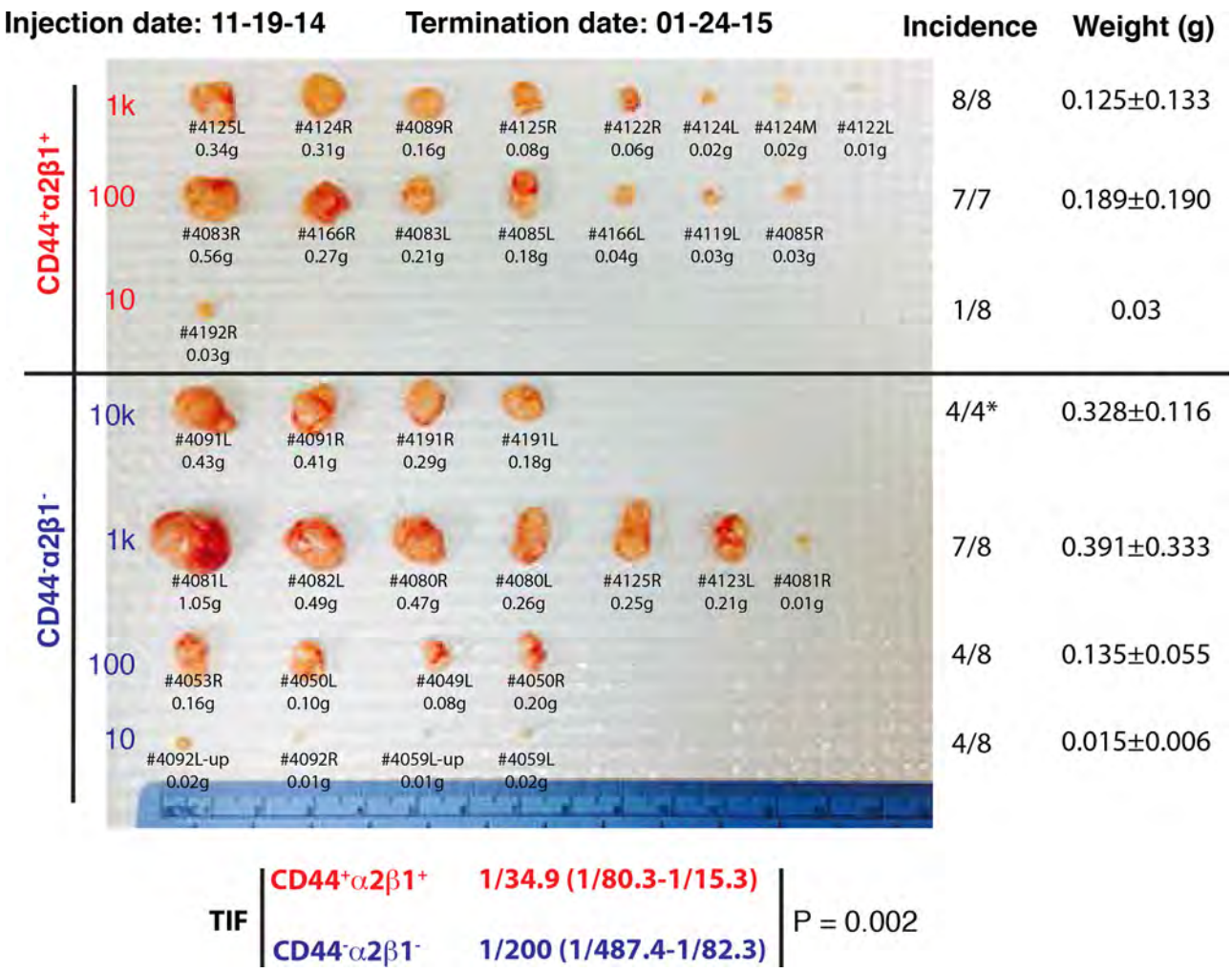

Supplementary Figure 10: CD44⁺α2β1⁺ LAPC4 cells are more tumorigenic than CD44⁻α2β1⁻ cells. CD44⁺α2β1⁺ and CD44⁻α2β1⁻ LAPC4 cells were FACS-purified from maintenance xenograft tumors and implanted, at the indicated numbers, subcutaneously, in 50% Matrigel in female NOD/SCID mice. The experiment was terminated 66 d after implantation. Not shown were tumor images of the 4 10k injections of CD44⁻α2β1⁻ LAPC4 cells, which were harvested one week earlier due to IACCUC regulation (lower panel, indicated by an asterisk). Shown on the right are tumor incidence and mean tumor weight. Shown below is the calculated TIF and *P* value (also see Table 2).

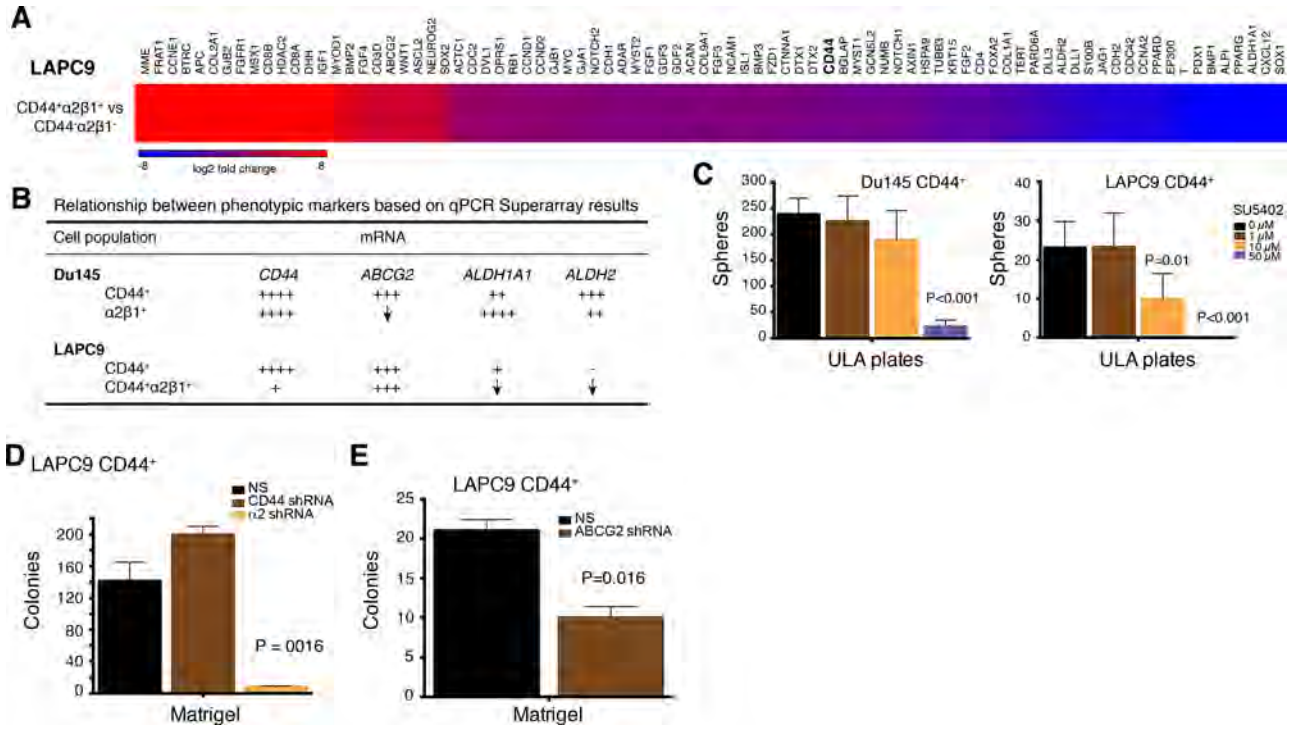

Supplementary Figure 11: Gene expression and functional studies in tumorigenic PCa cell populations. A. Expression of 84 stem cell-related genes in the CD44$^+$α2β1$^+$ LAPC9 cells. Relative expression levels were normalized to 5 internal controls (B2M, HPRT1, RPL13A, GAPDH and ACTB). Scale bars depict fold changes (in log 2 ratio), centered at 0. Interestingly, CD44 mRNA (highlighted in bold) was not among the highest expressed genes. **B.** Relative mRNA levels of CD44, ABCG2, ALDH1A1, and ALDH2 in the indicated Du145 and LAPC9 cell populations. ++++ to +, strongest to moderately increased; –, no significant enrichment in marker-positive cells;↓, decreased in marker positive population. **C.** The FGFR inhibitor SU5402 dose-dependently inhibited the sphere formation of CD44$^+$ PCa cells. FACS-purified Du145 and LAPC9 CD44$^+$ cells were plated in 6-well ULA plates (2,000 cells/well) and treated with SU5402 at 1, 10, and 50 μM. Spheres were enumerated 2 weeks after plating. *P* values were indicated where appropriate (Student's *t*-test). **D–E.** Knocking down integrin α2 and ABCG2 but not CD44 inhibited clonogenic activity of CD44$^+$ LAPC9 cells. FACS-purified LAPC9 CD44$^+$ cells were infected with non-silencing (NS) or 3 target silencing lentiviral vectors (MOI 20) and plated in Matrigel-coated 12-well plates (3,000 cells/well). Spheres were enumerated 2 weeks after plating. *P* values were indicated where appropriate (Student's *t*-test).

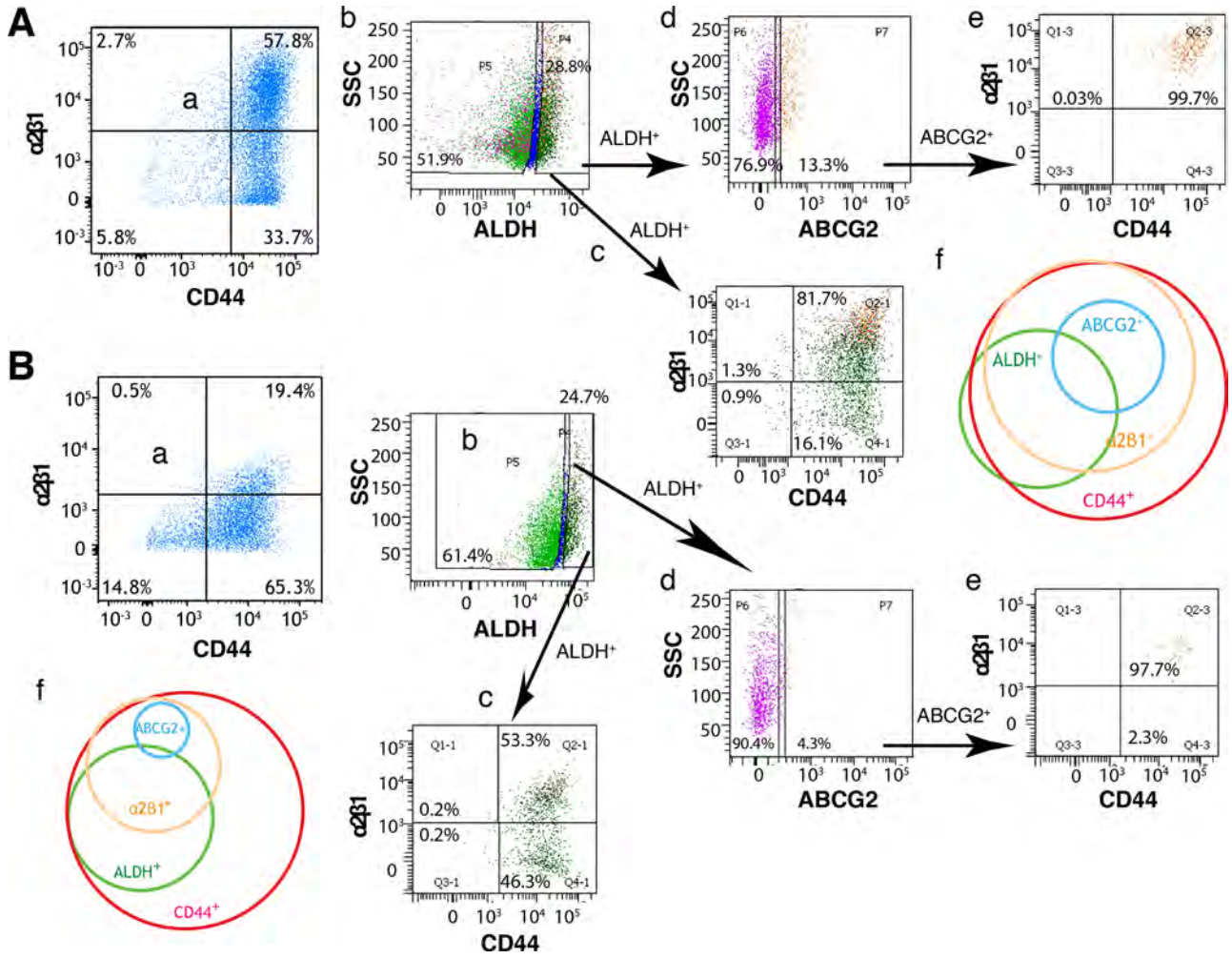

Supplementary Figure S12: Phenotypic relationship between different tumorigenic subpopulations of Du145 (A) and LAPC9 (B) cells. (A) Cultured Du145 cells were used in flow analysis of CD44 and integrin α2β1 expression, in which $CD44^+α2β^+$ cells constituted 57.8% of the total (a) whereas the $ALDH^+$ populations represented ~29% (b). Approximately 82% of the $ALDH^+$ population was $CD44^+α2β^+$ (c) whereas only ~13% of $ALDH^+$ cells were $ABCG2^+$ (d). ~98% (i.e., 81.7% + 16.1%) of $ALDH^+$ cells were $CD44^+$ (c) while virtually 100% of $ABCG2^+$ Du145 cells were harbored in the $CD44^+α2β^+$ cell population (e). A summary Venn diagram was presented in f. (B) LAPC9 cells were acutely purified from xenograft tumors and used in flow analysis of CD44 and integrin α2β1 expression, in which $CD44^+α2β^+$ cells constituted 19.4% of the total (a) whereas the $ALDH^+$ populations represented ~25% (b). Approximately 53% of the $ALDH^+$ population was $CD44^+α2β^+$ (c) whereas only ~4% of $ALDH^+$ cells were $ABCG2^+$ (d). Nearly 100% (i.e., 53.3% + 46.3% = 99.6%) of $ALDH^+$ cells were $CD44^+$ (c) while 98% $ABCG2^+$ Du145 cells were harbored in the $CD44^+α2β^+$ cell population (e). A summary Venn diagram was presented in f.

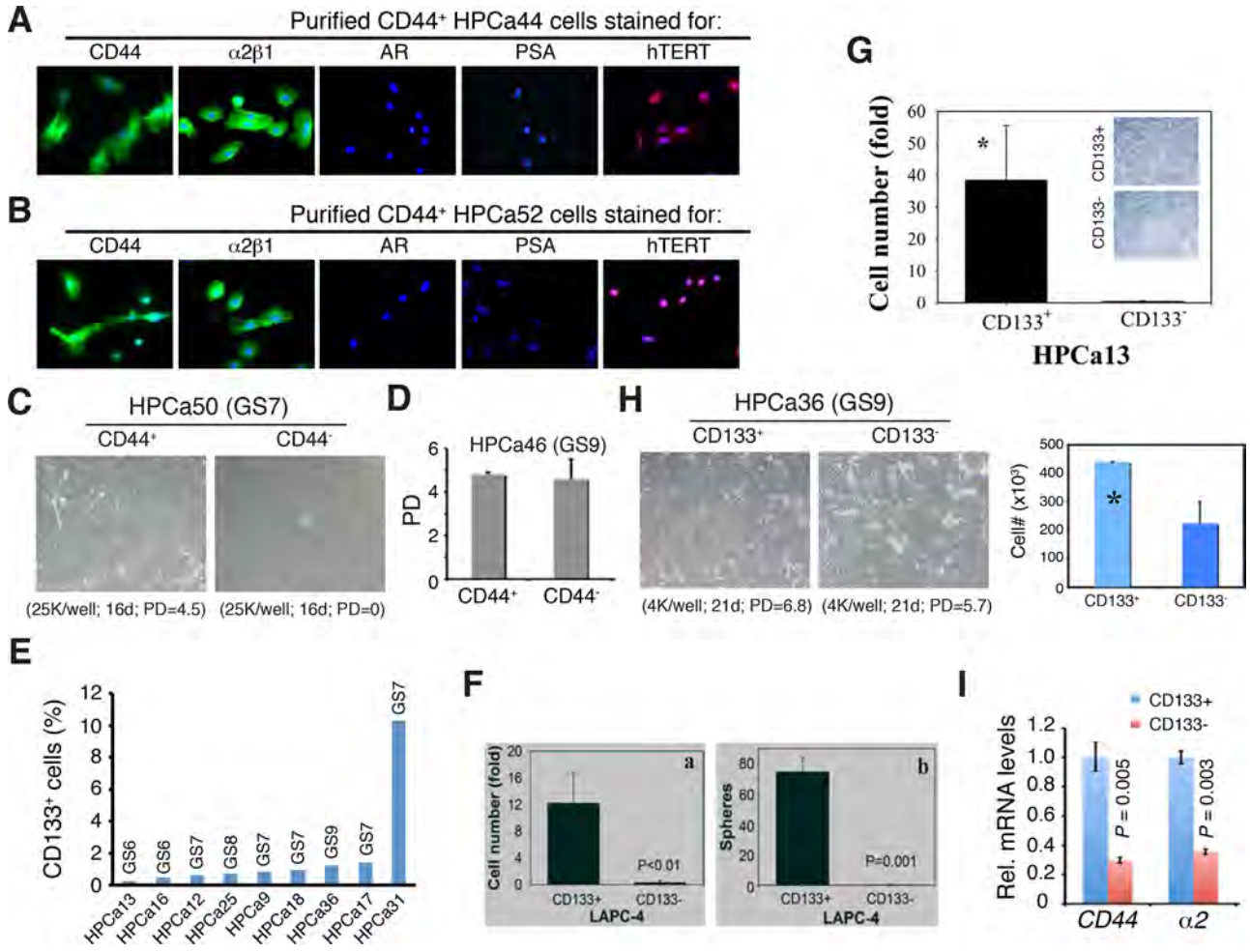

Supplementary Figure 13: *In vitro* studies on CD44⁺ and CD133⁺ HPCa cells. A–B. Highly FACS-purified primary CD44⁺ HPCa44 (A) and HPCa52 (B) cells were plated on collagen in serum-free PrEGM supplemented with a cocktail of mitogens (37, 38) overnight followed by IF labeling of the molecules indicated. Shown are representative images (original magnification: ×400) of the overlay of DAPI (for nucleus) and the indicated markers. Note that all CD44⁺ HPCa cells stained positive for CD44, α2β1, and hTERT but negative for AR and PSA. **C.** CD44⁺ HPCa50 cells possess higher survival advantages compared to the corresponding CD44⁻ cells. Purified CD44⁺ and CD44⁻ HPCa50 cells were plated in quadruplicate on collagen-coated 6-well dishes. Shown below are the cell numbers plated, time when surviving cells were enumerated, and the cumulative PDs. In this experiment, few CD44⁻ HPCa50 cells survived. **D.** CD44⁺ and CD44⁻ HPCa46 cells exhibit similar proliferative potential. Purified CD44⁺ and CD44⁻ HPCa46 cells were plated in triplicate on collagen-coated 6-well dishes (10,000 cells/well). Live cell numbers were determined 23 days after plating. Shown are the cumulative PDs (mean ± S.D). **E.** CD133 expression (%) in untreated HPCa samples. The combined Gleason score (GS) of patient tumors is indicated. **F.** The CD133⁺ LAPC4 cells possess higher proliferative and sphere-forming potentials than corresponding CD133⁻ cells. 15, 000 CD133⁺ or CD133⁻ LAPC4 cells freshly purified from xenograft tumors were plated in triplicate in 6-well plates coated with collagen (a) or a layer of agarose (b). Cell numbers (a) or spheres (b) were determined 3 weeks after plating. **G.** CD133⁺ (2, 000) and CD133⁻ (100, 000) HPCa13 cells were freshly purified out using MACS and plated, in quadruplicate, on collagen-coated dishes and cultured in 1% O2. Cell number (expressed as fold increase) was enumerated 3 weeks after plating. **P* < 0.001. Shown in the inset are representative microphotographs (original magnification: ×100). **H.** CD133⁺ and CD133⁻ HPCa36 cells were freshly purified out using MACS and plated, in quadruplicate, on a feeder layer of Swiss 3T3 cells in 12-well culture plates (4, 000 cells/well). Cell number was determined 3 weeks after plating and bars represent the mean ± S.D (right; **P* < 0.01). Shown on the left are representative microphotographs (original magnification: ×100) and the cumulative PDs. **I.** CD133⁺ HPCa40 cells also overexpress *CD44* and integrin *α2* mRNAs. Primary tumor HPCa40 (Gleason 7) was used to purify out Lin⁻CD133⁺ and Lin⁻CD133⁻ PCa cells, which were analyzed, by qPCR, for *CD44* and *α2* mRNAs. *P* values (Student *t*-test) are indicated.

Supplemental Table 1: *Oncomine* data sets analyzed in the current study.

Data	Year	Name	Source	Accession no.	# Genes	# Sample	Normal/Tumor	Metastasis (pri/metastasis)	Gleason Score (5/6/7/8/9/10)	Patient death/Survival	Recurrence (BCR free survival) (No/Yes, 1,3,5 year)	Horm Refrac (No/Yes)	Platform	Publication	Title
1	2009	Arredouani			19,574	21	8/13	NA	NA	NA	NA	NA	Human Gneome U133 Plus 2.0 Array	Clin Cancer Res 2009/09/15	Identification of the transcription factor single-minded homologue 2 as a potential biomarker and immunotherapy target in prostate cancer
2	2010	Barwick	GEO	GSE18655	487	139	NA/139	NA	2/36/90/5/6/0	NA	88/13, 51/23, 21/27	NA	Illumina DASL Human Cancer Panel	Br J Cancer 2010/02/02	Prostate cancer genes associated with TMPRSS2-ERG gene fusion and prognostic of biochemical recurrence in multiple cohorts
3	2005	Best2	GEO	GSE2443	12,624	20	NA	NA	0/0/3/5/0/0	2 year: 3/5	NA	(10/10)	Human Genome U133A Array	Clin Cancer Res 2005/10/01	Molecular alterations in primary prostate cancer after androgen ablation therapy
4	2005	Bittner	GEO	GSE2109	19,574	60	NA	59/1	NA	NA	NA	NA	Human Genome U133 Plus 2.0 Array	Not Published 2005/01/15	Expression Project for Oncology - Prostate Samples
5	2007	Chandran	GEO	GSE6752	14,738	31	NA	10/21	0/0/10/0/0/0	NA	NA	NA	CodeLink UniSet Human 20K I Bioarray	BMC Cancer 2007/04/12	Gene expression profiles of prostate cancer reveal involvement of multiple molecular pathways in the metastatic process
6	2004	Glinsky			12,624	79	NA/79	None:17,Focal:6, Invasive: 18, Established: 38	2/15/44/10/8/0	NA	NA, 53/26, 42/32 (include total followup time)	NA	Human Genome U133A Array	J Clin Invest 2004/03/01	Gene expression profiling predicts clinical outcome of prostate cancer
7	2012	Grasso	GEO	GSE35988	19,189	122	28/59	59/35	0/0/2/1/0/0 (2 neuroendocrine differntiation sample)	31/NA, 28/3, 18/12, (include followup time, and dead: 35)	NA	NA	Agilent Human Genome 44K	Nature 2012/05/20	The mutational landscape of lethal castration-resistant prostate cancer
8	2004	Holzbeierlein			8,603	54 (1 cell line)	4/40	40/9	0/0/2/4/1/0	41/NA, 33/1, 13/3	41/2, 33/4, 13/10	6/3	Human Genome U95A-Av2 Array	Am J Pathol 2004/01/01	Gene expression analysis of human prostate carcinoma during hormonal therapy identifies androgen-responsive genes and mechanisms of therapy resistance
9	2004	Lapointe	GEO	GSE3933	10,166	112	41/62	62/9	0/24/22/10/5/0	NA	14/3,NA,NA (at 27th month 22/7)	NA	Platform not pre-defined in Oncomine	Proc Natl Acad Sci U S A 2004/01/20	Gene expression profiling identifies clinically relevant subtypes of prostate cancer
10	2002	LaTulippe			8,603	35	3/23	23/9	0/2/14/2/5	NA	14/9	NA	Human Genome U95A-Av2 Array	Cancer Res 2002/08/01	Comprehensive gene expression analysis of prostate cancer reveals distinct transcriptional programs associated with metastatic disease
11	2006	Liu	EMBL-EBI	E-TABM-26	12,624	57	13/44	NA	0/13/16/10/0/0	NA	NA	NA	Human Genome U133A Array	Cancer Res 2006/04/15	Sex-determining region Y box 4 is a transforming oncogene in human prostate cancer cells
12	2001	Luo			5,064	25	9/16	NA	NA	NA	NA	NA	Platform not pre-defined in Oncomine	Cancer Res 2001/06/15	Human prostate cancer and benign prostatic hyperplasia: molecular dissection by gene expression profiling
13	2002	Luo2			15,302	30	15/15	NA	2/3/7/1/2/0	NA	NA	NA	Hu35KsubD Array, Hu35KsubC Array, Human Genome U95A-Av2 Array, Hu35KsubB Array, Hu35KsubA Array	Mol Carcinog 2002/01/01	Gene expression analysis of prostate cancers
14	2001	Magee			5,338	15	4/8	8/3	NA	NA	NA	NA	HumanGeneFL Array	Cancer Res 2001/08/01	Expression profiling reveals hepsin overexpression in prostate cancer.
15	2008	Nakagawa	GEO	GSE10645	487	596	NA	NA	4/79/290/69/145/9	594/2, 579/15, 522/55	581/13, 543/51, 476/116	NA	Illumina DASL Human Cancer Panel	PLoS ONE 2008/05/28	A tissue biomarker panel predicting systemic progression after PSA recurrence post-definitive prostate cancer therapy
16	2006	Nanni	GEO	GSE3868	12,624	26 pri cultures, 4 cell lines	4/23 (3 precusor)	NA	0/4/17/0/1/0	NA	17/5, 1/7, NA	NA	Human Genome U133A Array	Mol Cancer Res 2006/02/01	Epithelial-restricted gene profile of primary cultures from human prostate tumors: a molecular approach to predict clinical behavior of prostate cancer
17	2008	Setlur	GEO	GSE8402	6,084	363	NA	NA	0/110/153/41/54/0	357/6, 317/41, 277/86	NA	NA	Illumina DASL Transcriptionally Informative Gene Panel	J Natl Cancer Inst 2008/06/04	Estrogen-dependent signaling in a molecularly distinct subclass of aggressive prostate cancer
18	2002	Singh	Broad Institute		8,603	102	50/52	NA	4/15/29/2/2/0	NA	42/8	NA	Human Genome U95A-Av2 Array	Cancer Cell 2002/03/01	Gene expression correlates of clinical prostate cancer behavior
19	2007	Tamura	GEO	GSE6811	16,459	35	NA	23/12	NA	NA	NA	10/25	Platform not pre-defined in Oncomine	Cancer Res 2007/06/01	Molecular features of hormone-refractory prostate cancer cells by genome-wide gene expression profiles
20	2010	Taylor3	GEO	GSE21034	22,238	185 (6 cell lines)	29/131	131/19	0/41/74/8/7/0	131/NA, 110/1, 59/2 (131/19)	115/9, 86/21, 37/24	NA	Platform not pre-defined in Oncomine	Cancer Cell 2010/07/13	Integrative genomic profiling of human prostate cancer
21	2007	Tomlins	GEO	GSE6099	10,656	101	23/30 (precursor:17)	30/19	0/10/8/5/7/0	NA	NA	3/16	Platform not pre-defined in Oncomine	Nat Genet 2007/01/01	Integrative molecular concept modeling of prostate cancer progression
22	2006	True	GEO	GSE5132	3,432	31	NA	NA	0/4/21/1/5/0	NA	NA	NA	Platform not pre-defined in Oncomine	Proc Natl Acad Sci U S A 2006/07/18	A molecular correlate to the Gleason grading system for prostate adenocarcinoma
23	2003	Vanaja			17,779	40	8/27	27/5	0/12/0/0/15/0	NA	NA	NA	Human Genome U133A Array, Human Genome U133B Array	Cancer Res 2003/07/15	Transcriptional silencing of zinc finger protein 185 identified by expression profiling is associated with prostate cancer progression
24	2005	Varambally	GEO	GSE3325	19,574	19	6/7	7/6	NA	NA	NA	NA/6	Human Genome U133 Plus 2.0 Array	Cancer Cell 2005/11/01	Integrative genomic and proteomic analysis of prostate cancer reveals signatures of metastatic progression
25	2008	Wallace	GEO	GSE6956	12,603	89	20/69	NA	1/17/48/1/2/0	NA	NA	NA	Human Genome U133A 2.0 Array	Cancer Res 2008/02/01	Tumor immunobiological differences in prostate cancer between African-American and European-American men
26	2001	Welsh			8,603	34	9/25	NA	0/7/9/5/2/0	NA	NA	NA	Human Genome U95A-Av2 Array	Cancer Res 2001/08/15	Analysis of gene expression identifies candidate markers and pharmacological targets in prostate cancer
27	2004	Yu	GEO	GSE6919	8,603	112	23/65	65/24	3/15/27/7/12/0	60/NA, 34/2, 9/3	NA	NA	Human Genome U95A-Av2 Array	J Clin Oncol 2004/07/15	Gene expression alterations in prostate cancer predicting tumor aggression and preceding development of malignancy

Supplementary Table S1: *Oncomine* data sets analyzed in the current study

Supplementary Table S2: HPCa and HPCa(N) samples used in this study*

Patient	Age	Gleason	Stage	Marker(s) analyzed (%)$					Experiments
				CD133	ALDH	CD44	α2β1	CD44α2β1	
HPCa4	63	7 (4+3)	N/A			17.8			Marker quantification
HPCa6	68	7 (3+4)	T2a, N0, MX			4.0			Marker quantification
HPCa7	66	7 (4+3)	N/A			15.0			Marker quantification
HPCa8	56	6 (3+3)	T2c, NX, MX			12.4			Marker quantification
HPCa9	62	7 (4+3)	N/A	0.84					Marker quantification
HPCa10	71	6 (3+3)	T2a, NX, MX			3.3			Marker quantification
HPCa12	59	7 (4+3)	N/A	0.61					Marker quantification; AR/PSA IF
HPCa13	62	6 (3+3)	N/A	0.25					$CD133^{+/-}$ clonal assay
HPCa14	68	7 (4+3)	T3, N1, MX			5.63			Marker quantification: AR/PSA IF
HPCa16	58	6 (3+3)	pT3a, pN0, pMX	0.46					Marker quantification
HPCa17	60	7 (4+3)	T2c, N0, MX	1.4					Marker quantification
HPCa19	61	9 (4+5)	pT3b, NX, MX, G4						AR/PSA IF
HPCa18	68	7 (4+3)	N/A	0.94		19.4			Marker quantification; AR/PSA IF
HPCa25	58	8 (3+5)	pT2c, NX, MX, G4	0.73		7.7			Marker analysis
HPCa27	47	8 (4+4)	pT3a, pNX, pMX, G4, R1			4.8			Marker quantification; AR/PSA IF
HPCa31	63	7 (3+4)	N/A	10.3		71.4			Marker quantification; AR/PSA IF
HPCa33	59	7 (3+4)	pT2, pNX, pMX, G3, R1						AR/PSA IF

(*Continued*)

Patient	Age	Gleason	Stage	Marker(s) analyzed (%)[$]					Experiments
				CD133	ALDH	CD44	α2β1	CD44α2β1	
HPCa34	58	7 (4+3)	N/A			5.5			Marker quantification
HPCa36	65	9 (4+5)	pT3b, pR1, pN0, pMX	1.23					Marker quantification
HPCa37	59	9 (4+5)	pT3b, R1, pNX, pMX						AR/PSA IF
HPCa38	63	9 (4+5)	pT3b, RpNX, pMX						AR/PSA IF
HPCa39	63	7 (3+4)	pT3a, NX, MX, G3–4			56.5			Marker quantification
HPCa40	58	7 (3+4)	pT2a, pNX, pMX						qPCR CD44, Φ2, and CD133
HPCa41	49	9 (4+5)	pT2a, pNX, pMX			18.6			Marker quantification
HPCa42	54	9 (5+4)	T3b, NX, MX			20.3			Marker quantification
HPCa43	55	7 (4+3)	T3a, NX, MX			13.3			Marker quantification; clonal analysis
HPCa44	61	9 (5+4)	pT3b, R, pNX, pMX			30.5			Marker quantification; clonal analysis
HPCa45	70	9 (4+5)	pT2c, R, pNX, pMX			3.6			Marker quantification
HPCa46	51	9 (4+5)	T2c, NX, MX			19.6			Marker quantification; clonal analysis
HPCa47	56	7 (4+3)	pT2c, R, pNX, pMX			5.45			Marker quantification
HPCa48	59	7 (3+4)	T2c, NX, MX			1.53			Marker quantification
HPCa49	57	7 (4+3)	T3b, R1, NX, MX			2.65			Marker quantification
HPCa50	60	7 (4+3)	T3a, NX, MX			7.9			Marker quantification; clonal, & clonogenic
HPCa51	44	7 (4+3)	pT3a, pNX, pMX, G3			6.1			Marker quantification; clonogenic analysis
HPCa52	63	8 (4+4)	pT2a			3.2			Marker quantification
HPCa53	58	7 (4+3)	T3a, NX, MX						Clonal & clonogenic assays

(*Continued*)

Patient	Age	Gleason	Stage	Marker(s) analyzed (%)[$]					Experiments
				CD133	ALDH	CD44	α2β1	CD44α2β1	
HPCa54	61	8 (4+4)	pT3a, R1, pNX, pMX						Clonal & clonogenic assays
HPCa57	53	7 (3+4)	pT2c, NX, MX, G3, R1						Clonal & clonogenic assays
HPCa58	58	7 (3+4)	pT3a, NX, MX, G3, R1						Clonal & clonogenic assays
HPCa60	54	8 (3+5)	T2c, NX, MX			8.7			qPCR of AR/PSA/ CD44; Marker quantification[#]
HPCa61	56	6 (3+3)	T2c, NX, MX						qPCR of AR/PSA/ CD44
HPCa62	59	7 (4+3)	pT2c, pNX, pMX			2.4			qPCR of AR/PSA/ CD44; Marker quantification[#]
HPCa63	51	7 (4+3)	pT2c, pNX, pMX						Clonal & clonogenic assays
HPCa65	59	7 (4+3)	T3b, NX, MX			19.9			qPCR of AR/PSA/ CD44; Marker quantification[#]
HPCa66	58	6 (3+3)	pT2c, pNX, pMX			15.0			qPCR of AR/PSA/ CD44; Marker quantification[#]
HPCa68	64	6 (3+3)	T2c, NX, MX						Clonal & clonogenic assays
HPCa72	58	7 (3+4)	pT2a, pNX, pMX			10.2			qPCR of AR/PSA/ CD44; Marker quantification[#]
HPCa74	59	7 (3+4)	pT2c, NX, MX			16.2			qPCR of AR/PSA/ CD44; Marker quantification[#]
HPCa76	64	7 (4+3)	T3a, NX, MX			0.02			qPCR of AR/PSA/ CD44; Marker quantification[#]
HPCa77	46	6 (3+3)	T2c, NX, MX			14.2			Marker quantification[#]
HPCa78	64	7 (3+4)	pT2c, pNX, pMX			19.2			qPCR of AR/PSA/ CD44; Marker quantification[#]
HPCa79	67	7 (4+3)	pT3a, pNX, pMX, G3			8.2			Marker a quantification[#]
HPCa80	65	9 (4+5)	T2c, NX, MX			4.4			Marker quantification[#]
HPCa81	54	7 (3+4)	pT2c, pNX, pMX			20.9			Marker quantification[#]

(*Continued*)

Patient	Age	Gleason	Stage	Marker(s) analyzed (%)[$]					Experiments
				CD133	ALDH	CD44	α2β1	CD44α2β1	
HPCa83	69	7 (3+4)	T2a, NX, MX						AR/PSA IF
HPCa84 & HPCa84(N)	66	7 (4+3)	T3a, R1, N0, MX						Marker IHC
HPCa87	57	9 (4+5)	pT3b, pNX, pMX, G4, R1			UD			Marker quantification
HPCa89 & HPCa89(N)	55	9 (4+5)	pT3a, pN0, pMX			24			qPCR of AR/PSA/CD44; Marker quantification[#]
HPCa91	60	8 (3+5)	pT3a, NX, MX			UD			Marker quantification
HPCa93 & HPCa93(N)	58	7 (4+3)	pT2c, pNX, pMX			0.99			Marker quantification[#]
HPCa96 & HPCa96(N)	55	9 (5+4)	T3b, R1, N1, MX						Marker IF; α2β1 cell counting
HPCa98	64	8 (4+4)	pT3a			5.74			IF of PSA and α2β1; Marker quantification[#]
HPCa101[**]	71	9 (4+5)	pT3a, NX, MX		1.5	91.5	4.1	3.9	Marker quantification
HPCa102	55	6 (3+3)	pT2c, pNX, pMX			24.8			qPCR of AR/PSA/CD44; Marker quantification[#]
HPCa110 & HPCa110(N)	73	8 (4+4)	pT3, N0, MX						IF of PSA and CD44; α2β1 cell counting
HPCa124	65	9 (4+5)	pT2b, N0, cM0		7.2	81.4	50.4	49.7	Marker quantification
HPCa126	68	7 (3+4)	pT2c, pN0, pMX		4.4	UD	UD	UD	Marker quantification
HPCa128 & HPCa128(N)	61	7 (3+4)	T3b, N0, MX		3.6	2.4	8.3		UD IF of PSA & ALDH1A1; Marker quantification
HPCa134 & HPCa134(N)	65	7 (4+3)	pT2a, R1, pN0						Analysis of $ALDH^+CD44^+\alpha2\beta1^+$ cells

[*]HPCa samples were obtained from radical prostatectomy with patients' consent under IRB LAB04–0498. The # refers to de-identified patient numbers used in our lab.

HPCa(N) refers to normal (benign) tissues from the matching HPCa samples.

[$]The % marker-positive cells were determined by FACS, MACS, or immunofluorescence (IF) staining. IHC, immunohistochemistry (i.e., Marker quantification).

[#]Part of the information for these samples was presented in ref. 12.

[**]Analyzed in early xenograft tumors.

Supplementary Table S3: Marker expression and tumorigenic properties in 4 commonly used PCa cell lines

Cells	Markers (%)[a]							Clonogenicity[b] (%)	Tumorigenicity[c]	Metastasis[d]
	CD44	α2β1	CK5	Tel	CK18	AR	PSA			
LNCaP	–	–	–	–	+	+	+	0.5	+	+/-
Du145	28	5.5	22	+	+	–	–	0.9	++	++
PC3	99	100	90	+++	+	–	–	1.2	+++	+++
PPC-1	99	100	92	+++	+	–	–	1.9	+++	+++

[a]For CD44, α2β1, and CK5 staining, cells cultured on coverslips were used in immunofluorescent staining. The % of marker-positive cells was determined by randomly counting 600 – 1,000 cells. Telomerase (Tel) activity in these cells was determined as previously described (Bhatia et al., *J. Biol. Chem*. 283:27957–72, 2008) and presented as relative levels, i.e., from negative (–) to very strong (+++). For luminal cell markers (CK18, AR, and PSA), cells were qualitatively assessed in tumor cell spheres/spheroids as either positive (+) or negative (see Supplementary Figure 6).

[b]Clonogenicity was performed by plating 1,000 – 10,000 cells (depending on cell types) on a layer of solidified agarose gel and quantifying spheres that arose in 1–2 weeks (see Materials & Methods).

[c]Tumorigenicity was determined by injecting 100 – 1,000,000 cells in 50% Matrigel subcutaneously in male NOD/SCID mice and scoring tumor latency, incidence, and weight. +, ++, and +++ refer to increasing tumor development with lower numbers of cells implanted (see also Table 1).

[d]The metastatic potential of these cells was determined by implanting 100,000 or 1,000,000 GFP-labeled tumor cells in the dorsal prostate of male NOD/SCID mice and analyzing, 3–5 months after implantation (depending on cell types), the levels of GFP^+ cells that had metastasized to the lung, lymph nodes, pancreas, brain, and kidney. +/–, ++, and +++ refer to increasing levels of metastasis to these end organs. Note that the quantitative results for metastasis assays are to be presented elsewhere.

Supplementary Table S4: Different PCa models possess distinct tumorigenic subsets[*]

Cells	$ABCG2^+$	$CD44^+$	$α2β1^+$	$CD44^+α2β1^+$	SP^+	$ALDH^+$
Du145	+ (10×)	+ (30×)	+ (31×)	+ (2×)[#]	UD	+ (>60×)
PC3	–	N/A	N/A	N/A	UD	+ (4×)
LAPC9	–	+ (6–19×)	–	+ (>900×)	+ (>500×)	+ (~90×)
LAPC4	N/A	–	–	+ (5.7×)	UD	–

[*]Based on data in Tables 1 and 2. +, more tumorigenic compared to the corresponding marker-negative subpopulation; –, no significant difference between the marker-positive vs. marker-negative subpopulations. Numbers in parentheses indicate relative fold enrichment in tumor-initiating activity (TIF). N/A, not assayed (or not applicable as PC3 cells were nearly 100% positive for CD44 and α2β1); UD, undetectable; ALDH, Aldefluor assay.

[#]Did not reach statistical significance.

Supplementary Table S5: RT^2 Profiler™ PCR Array Human Stem Cell List of Genes*

Stem Cell Specific Markers: ***Cell Cycle Regulators:*** APC, AXIN1, CCNA2, CCND1, CCND2, CCNE1, CDC2, CDC42, EP300, FGF1, FGF2, FGF3, FGF4, MYC, NOTCH2, PARD6A, RB1. ***Chromosome and Chromatin Modulators:*** GCN5L2, HDAC2, MYST1, MYST2, RB1, TERT. ***Genes Regulating Symmetric/Asymmetric Cell Division:*** DHH, NOTCH1, NOTCH2, NUMB, PARD6A. ***Self-Renewal Markers:*** HSPA9B, MYST1, MYST2, NEUROG2, SOX1, SOX2. ***Cytokines and Growth Factors:*** BMP1, BMP2, BMP3, CXCL12, FGF1, FGF2, FGF3, FGF4, GDF2, GDF3, IGF1, JAG1. ***Genes Regulating Cell-Cell Communication:*** DHH, DLL1, GJA1, GJB1, GJB2, JAG1. ***Cell Adhesion Molecules:*** APC, BGLAP, CD4, CD44, CDH1, CDH2, COL9A1, CTNNA1, CXCL12, NCAM1. ***Metabolic Markers:*** ABCG2, ALDH1A1, ALDH2, FGFR1.
Stem Cell Differentiation Markers: ***Embryonic Cell Lineage Markers:*** ACTC, ASCL2, FOXA2, IPF1, ISL1, KRT15, MSX1, MYOD1, T. ***Hematopoietic Cell Lineage Markers:*** CD3D, CD4, CD8A, CD8B1, MME. ***Mesenchymal Cell Lineage Markers:*** AGC1, ALPI, BGLAP, COL1A1, COL2A1, COL9A1, PPARG. ***Neural Cell Lineage Markers:*** CD44, NCAM1, OPRS1, S100B, TUBB3.
Signaling Pathways Important for Stem Cell Maintenance: ***Notch Pathway:*** DLL1, DLL3, DTX1, DTX2, DVL1, EP300, GCN5L2, HDAC2, JAG1, NOTCH1, NOTCH2, NUMB. ***Wnt Pathway:*** ADAR, APC, AXIN1, BTRC, CCND1, FRAT1, FZD1, MYC, PPARD, WNT1.

*This stem cell gene expression qPCR panel was custom-made by the SuperArray Bioscience Corporation. The 84 genes are categorized into several different functional groups by GO terms.

MOLECULAR CARCINOGENESIS 54:679–687 (2015)

IN PERSPECTIVE

Regulation of NANOG in Cancer Cells

Shuai Gong,[1,2] Qiuhui Li,[1] Collene R. Jeter,[1] Qingxia Fan,[2] Dean G. Tang,[1,3]* and Bigang Liu[1]***

[1]*Department of Epigenetics and Molecular Carcinogenesis, University of Texas M.D Anderson Cancer Center, Science Park, Smithville, Texas*
[2]*The First Affiliated Hospital of Zhengzhou University, Zhengzhou, Henan, China*
[3]*Cancer Stem Cell Institute, Research Center for Translational Medicine, East Hospital, Tongji University School of Medicine, Shanghai, China*

As one of the key pluripotency transcription factors, NANOG plays a critical role in maintaining the self-renewal and pluripotency in normal embryonic stem cells. Recent data indicate that NANOG is expressed in a variety of cancers and its expression correlates with poor survival in cancer patients. Of interest, many studies suggest that NANOG enhances the defined characteristics of cancer stem cells and may thus function as an oncogene to promote carcinogenesis. Therefore, NANOG expression determines the cell fate not only in pluripotent cells but also in cancer cells. Although the regulation of NANOG in normal embryonic stem cells is reasonably well understood, the regulation of NANOG in cancer cells has only emerged recently. The current review provides a most updated summary on how NANOG expression is regulated during tumor development and progression.

Key words: NANOG; NANOGP8; cancer stem cells; tumor development

INTRODUCTION

Recent studies indicate that most human tumors harbor a population of cancer cells termed cancer stem cells (CSCs) that possess biological properties characteristic of normal stem cells, i.e., self-renewal and differentiation [1]. CSCs are thought to be immortal being able to persist in tumors and to contribute to relapse and metastasis [2,3]. As CSCs can potentially arise from oncogenic reprogramming, identification of stem cell-related and self-renewal molecules (transcription factors, cell surface proteins, stemness genes, and microRNAs) responsible for the manifestation of stem cell properties of somatic cancer cells is a critical question and can in turn lead to identification of novel therapeutic targets for cancer. Recently accumulated evidence suggests that NANOG is a crucial factor that can confer cancer cells certain CSC properties such as self-renewal, tumorigenicity, metastasis, and drug-resistance.

NANOG is a divergent homeobox domain protein first discovered in embryonic stem cells (ESCs) with canonical functions in the transcriptional regulation of self-renewal and pluripotency [4,5]. Together with SOX2 and OCT4, NANOG plays a key role in maintaining the properties of ESCs [6,7]. Through forming a transcriptional network, the three key factors generally function together to control the expression of a whole set of pluripotent-related genes and establish the pluripotency of ESCs [4,5]. NANOG is highly expressed in pluripotent cells such as ESCs, and EG (embryonic germ) and EC (embryonal carcinoma) cells, and its expression is downregulated upon differentiation [4]. Overexpression of Nanog[1] protein not only maintains the pluripotency of mouse ESCs in the absence of extrinsic factor, leukemia inhibitory factor (LIF) [4,8], but also promotes human ESC growth in feeder-free conditions [9]. Moreover, ectopic NANOG expression can improve reprogramming in a cell-division-rate-independent manner [10]. In contrast, downregulation of NANOG induces both mouse and human ESC differentiation [9,11]. Therefore, NANOG protein level determines the fate of pluripotent cells.

Although silenced in normal somatic cells, aberrant expression of NANOG has been reported in many types of human cancers, including carcinomas of the brain, breast, cervix, colon, gastric, head and neck, liver, lung, kidney, oral cavity, ovary, pancreas, prostate, and other organs [12–30]. Importantly, the expression levels of NANOG are often positively correlated with treatment resistance and poor survival of cancer patients. Various studies have shown that upregulation of NANOG expression enhances the tumorigenicity both in vivo and in vitro whereas

[1] In this paper, NANOG is used to refer to human protein whereas Nanog to mouse protein and Nanog protein/mRNA/gene in general.

Grant sponsor: NIH; Grant number: R01-CA155693; Grant sponsor: Department of Defense; Grant numbers: W81XWH-13-1-0352; W81XWH-14-1-0575; Grant sponsor: CPRIT; Grant number: RP120380; Grant sponsor: CPRIT; Grant number: RP120394

*Correspondence to: Department of Epigenetics and Molecular Carcinogenesis, the University of Texas M.D Anderson Cancer, Science Park, 1808 Park Road 1C, Smithville, TX 78957, USA.
**Correspondence to: Oncology Department, the First Affiliated Hospital, Zhengzhou University, Zhengzhou 450000, P.R. China.

Received 9 March 2015; Revised 19 April 2015; Accepted 1 May 2015
DOI 10.1002/mc.22340
Published online 27 May 2015 in Wiley Online Library (wileyonlinelibrary.com).

repression or ablation of NANOG inhibits tumor initiation. Thus, NANOG expression is linked to tumor progression, therapeutic resistance, relapse and metastasis. In this review, we focus our discussion on how NANOG expression could be regulated during various tumorigenic processes.

Regulation of NANOG During Tumor Progression

Human ESC NANOG arises from *NANOG1*, composed of four exons, three introns, and a 915 bp open reading frame (ORF), located on chromosome 12. As is common for genes expressed during embryogenesis, there exist numerous copies of *NANOG* scattered throughout the genome, including one tandem duplication (*NANOG2*, also called *NANOGP1*) and ten intronless retrotransposed paralogs, identified as *NANOGP2* to *NANOGP11* [31].

The majority of NANOG retrogene variants are considered pseudogenes, as these are degenerate copies with various defects such as deletions, frame shifts, premature stop codons, etc. Only *NANOGP8*, located on chromosome 15, has a complete ORF and can encode a protein nearly identical to that encoded by *NANOG1,* with the exception of two conserved amino acid substitutions (Ala16 to Glu, and Gln253 to His) [28,31,32]. To date, several pieces of evidence suggest that NANOGP8 exerts divergent biological functions in prostate cancer cells [28,33,34].

In ESCs, regulation of NANOG expression has been extensively investigated since NANOG was discovered, and many proteins have been reported to be capable of modulating the expression of NANOG. For example, TCF3 and p53 negatively regulate NANOG expression by binding to the promoter of *NANOG* whereas LIF and BMP signaling and their downstream effectors STAT3 and T may also be involved in NANOG regulation [35–37]. Among the NANOG-regulating proteins, SOX2 and OCT4 play a particularly important role via a composite Oct4/Sox2 motif localized ~180 bp upstream of the transcription start site of the *NANOG* promoter [38,39].

In contrast to our knowledge on NANOG regulation in ESCs, we have just begun to understand how NANOG might be regulated at the molecular level in cancer cells. Here, we discuss the evidence for regulation of NANOG expression in cancer cells by active STAT3, p53, HH signaling, microRNAs, hypoxia, and various post-translational modifications (Figure 1).

Regulation of NANOG by STAT3

In ESCs, STAT3 is the major effector of the LIF pathway that is required for the maintenance of ESC stemness. LIF-induced phosphorylation of STAT3 (pSTAT3, the active form) directly binds to the enhancer of the *Nanog* gene, hence upregulating the transcription of *Nanog* in mouse ES cells. Interestingly, E-Cadherin in mouse ES cells greatly promotes Nanog expression at both mRNA and protein levels possibly involving pSTAT3-induced upregulation of Nanog transcription [40].

Aberrant STAT3 signaling, i.e., the constitutively active STAT3 has been implicated in multiple tumor systems and tumorigenic processes. For example, in hepatocellular carcinoma (HCC), pSTAT3 has been shown to positively regulate NANOG expression. In a human HCC cell line HepG2, the Hepatitis C virus (HCV) core exhibited the ability to upregulate the expression of NANOG, leading to cell proliferation. In this cell model, HCV enhanced the activity of STAT3, and the pSTAT3 then directly bound the regulatory regions of *NANOG* to enhance the expression of NANOG [41] (Figure 1). In breast cancer cells, NANOG formed a complex with STAT3, which then translocated into the nucleus to regulate their common target genes [15].

Regulation of NANOG by p53 and Hedgehog Pathways

The transcription factor p53 represents one of the most important tumor suppressors due to its ability to induce cell apoptosis and senescence, promote DNA repair, inhibit epithelial to mesenchymal transition (EMT), and mediate many other processes [42–44]. Hedgehog (HH) and its downstream transcription factors Gli1, Gli2 (HH-GLI), are also important regulators that promote the self-renewal of ESCs and postnatal neuronal stem cells (NSCs) during early embryonic and nervous system development [45,46]. In mouse ESCs, p53 directly binds the promoter of *Nanog* and negatively regulates its transcription in response to DNA damage [36]. Thus, loss of p53 enhances the reprogramming efficiency leading to increased generation of induced pluripotent stem (iPS) cells. Two studies have shown that HH-GLI signaling pathway and p53 directly regulate the expression of NANOG in neural stem cells from brain tissues and brain tumors [12,13]. Po et al. detected high levels of NANOG protein in stem cells from cerebellum and medulloblastoma and identified that Gli1 and Gli2 interacted with the promoter region of *NANOG* and activated the transcription of *NANOG* gene [12]. They also demonstrated that the HH, in cooperation with loss of p53, positively modulated NANOG expression. Meanwhile, Zbinden et al. reported that NANOG, mainly NANOGP8, is highly expressed in the glioblastoma multiforme (GBM) and NANOG/P8 controlled the proliferation of GBM stem cells and contributed to the tumorigenicity of GBM [13]. They further demonstrated that GLI, and NANOG formed a positive loop by regulating each other, and the positive loop was suppressed by p53. These findings led the authors to hypothesize that the functional network of HH-GLI-NANOG-p53 plays a critical role in regulating glioma stem cells [13] (Figure 1).

Regulation of NANOG by MicroRNAs

MicroRNAs (miRNAs) are small, nonprotein-coding RNAs, roughly 19–24 nucleotides in length [47,48]. As

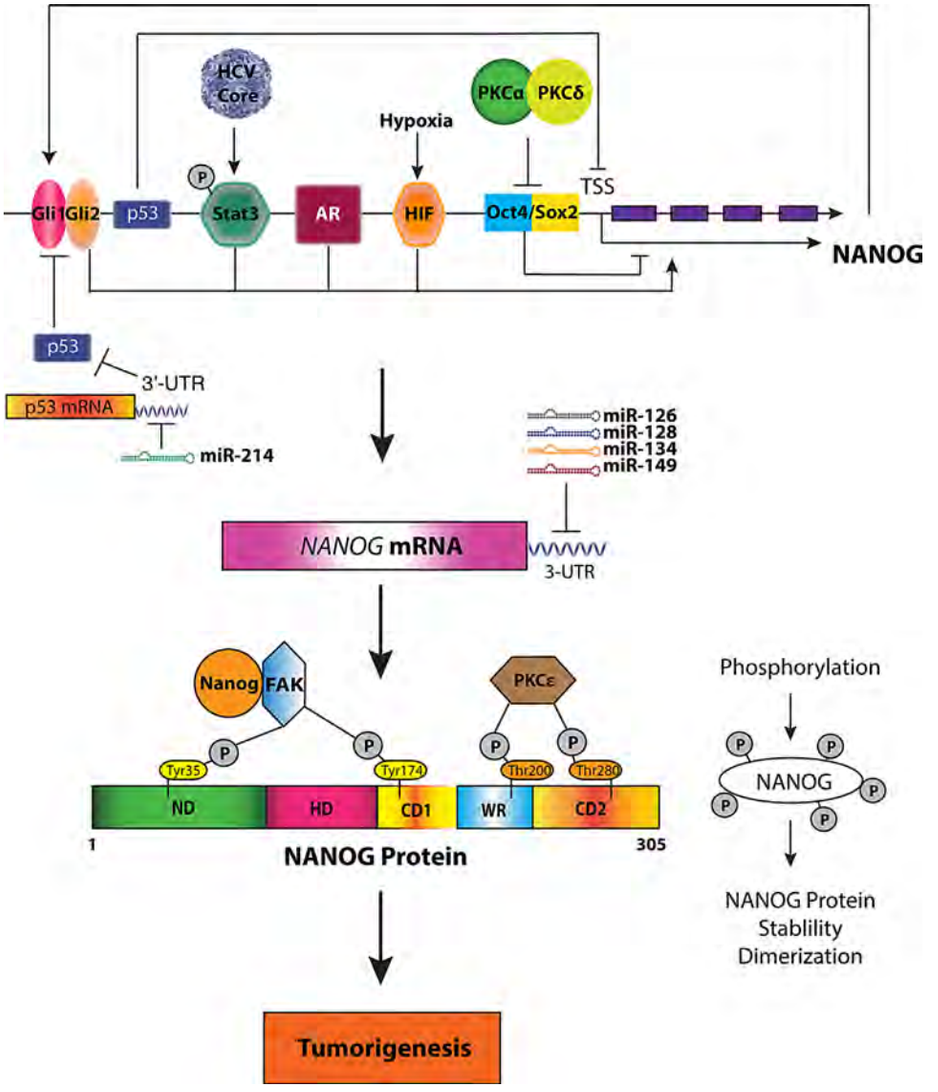

Figure 1. Regulation of NANOG expression in cancer cells. Presented are several reported scenarios whether NANOG expression is regulated at the transcriptional, mRNA, and protein levels. *At the transcriptional level*, AR (androgen receptor) binds the promoter of *Nanog* and enhances its expression. Hypoxia increases the expression of Nanog through HIF binding the promoter of Nanog. HCV core increases the activity of STAT3 and improves the binding of pSTAT3 to the regulatory region of Nanog to induce its expression. PKCα and PKCδ suppress the binding of OCT4-SOX composite to the promoter of *Nanog*, and therefore inhibit Nanog transcription. In mouse ES cells, p53 directly binds to the Nanog gene promoter to repress its expression. In human GBM stem cells, NANOG and GLI transcription factors form a positive feedback loop that positively regulate the transcription of each other and is suppressed by p53. *At the mRNA level*, most miRNAs (miR-126, -128, -134, -149) directly bind to the complementary sites in the 3′-untranlated region (3′-UTR) of the Nanog gene, and induce the translational repression or transcript degradation. However, miR-214 enhances the Nanog expression through mediating the degradation of p53. This mechanism of regulation may be applicable to both NANOG1 and NANOGP8. *At the protein level*, PKCε enhances the activity of NANOG by phosphorylating NANOG protein at Thr 200 and Thr 280. NANOG also forms complex with FAK, which, in turn, phosphorylates NANOG at Tyr 35 and Tyr 174, and hence improves its activity. ND, N-terminal domain; HD, homeodomain; CD1, C1-terminal domain; WR, tryptophan-rich domain; CD2, C2-terminal domain.

endogenous regulators of gene expression, miRNAs induce translational repression or transcript degradation by binding to the complementary sites in the 3′-untranlated region (3′-UTR) of their target genes, thereby playing a crucial role in diverse physiologic processes such as proliferation, differentiation, apoptosis, and stem cell maintenance [49–51]. Dysregulation in miRNA expression or functions is involved in various human cancers, indicating that miRNAs have an important impact on the tumorigenesis. For example, our group has reported that microRNA-34a (miR-34a) acts as a tumor suppressor to restrict clonogenecity, sphere formation, tumor growth and metastasis of prostate CSCs by directly repressing the expression of CD44 [52]. Newly accumulated evidence suggests that miRNAs also

target NANOG directly or indirectly to modulate tumorigenic processes.

miR-134

miR-134 is a brain-enriched microRNA essential for vertebrate central nervous system development [53,54]. miR-134 expression is dramatically reduced in glioma tissues compared with normal brain tissues and the reduction of miR-134 is strongly associated with aggressive progression and poor prognosis in gliomas, indicating that miR-134 serves as a tumor- suppressive miRNA in brain tumors [55]. The regulation of Nanog expression by miR-134 was first reported in mouse ESCs [53]. Recently, Niu et al. provided direct evidence to support miR-134 functioning as a tumor suppressor in human gliomas by targeting NANOG [56]. They found that the miR-134 level was not only significantly lower in clinical glioma samples and glioblastoma cell line U87 compared to normal brain tissues, but was also greatly reduced in grade III and IV gliomas compared to grade I and II tumors. miR-134 promoted apoptosis, impaired the invasiveness and migration capability, and inhibited proliferation of U87 cells. Importantly, overexpression of miR-134 in U87 cells directly targeted the NANOG gene to reduce its mRNA and protein levels [56].

miR-128

miR-128 is also a brain-enriched microRNA with developmental-specific expression patterns, mainly in mature, differentiated neurons rather than in astrocytes [57]. miR-128 has been observed to be downregulated in many tumors including glioblastoma, medulloblastoma [58,59], breast cancer [60], prostate cancer [61], and ovarian cancer [62], suggesting that miR-128 is also a tumor-suppressive miRNA. Recently, our group reported that overexpression of miR-128 inhibited prostate cancer cell proliferation, invasion, and clonogenic and sphere-formation in vitro, and suppressed tumor regeneration in vivo [63]. We also showed that the tumor-suppressive functions of miR-128 were related to its ability to directly target several "stemness" genes including NANOG and BMI-1 [63].

miR-126 and miR-149

It was recently reported that NANOG, SOX2, and OCT4 in prostate cancer cell lines were regulated by miR-126 and miR-149. With quantitative RT-PCR, the authors observed that inhibition of miR-126 or/miR-149 by their inhibitors significantly elevated the mRNA levels of NANOG, SOX2, and OCT4 [64].

miR-214

miR-214 is considered an oncogenic miRNA based on the observations that not only is its aberrant expression detected in multiple human cancers [65–67] but also elevated miR-214 levels are positively associated with chemoresistance and metastasis [66,67]. Studying the functions of miR-214 in ovarian cancer cells, Xu et al. provided an example of how miRNAs could indirectly regulate NANOG expression [65]. They found that enforced miR-214 expression led to enhanced NANOG expression and characteristics of ovarian CSCs (OCSCs). In contrast, miR-214 knockdown decreased NANOG expression and OCSC properties. Mechanistic studies showed that miR-214 directly interacted with the 3′-UTR of p53 to repress p53, which, in turn, led to increased NANOG expression. Elevation of NANOG expression by miR-214 was p53-dependent. These results together indicate that miR-214 regulates NANOG expression via targeting p53 [65] (Figure 1).

Regulation of NANOG by Hypoxia

Hypoxia, defined as oxygen deprivation, is a common feature of the solid tumor microenvironment and often occurs in a pathophysiological condition where the consumption of oxygen exceeds the blood supply, leading to local tumor regions with very low level of oxygen. Hypoxia often exists in the inner part of solid tumors, creating an environment beneficial to the growth of undifferentiated tumor cells [33]. Therefore, hypoxia is considered as a critical component of the CSC niche and plays an important role in the maintenance of CSC behavior and properties, including self-renewal, differentiation, invasion, metastasis, therapeutic resistance, and genetic instability. The response to hypoxia by tumor cells is mainly mediated by the family of hypoxia-inducible factor (HIF) transcription factors.

Recent evidence shows that hypoxia promotes the expression of ESC markers such as NANOG, OCT4, SOX2, KLF4, and cMYC in several tumor types. For example, Ruohola-Baker' group used RT-PCR strategy to investigate the gene expression signature of 11 different cancer cell lines under hypoxic conditions (2% O_2). The cell lines included prostate, brain, kidney, cervix, lung, colon, liver, and breast tumors. They discovered that hypoxia upregulated the expression of reprogramming inducing genes: NANOG, OCT4, SOX2, KLF4, cMYC, and the miR-302 cluster, and verified that the genes unregulated in cancer cell lines were HIF-dependent. By employing immunohistochemical staining, they further observed a strong correlation between NANOG-, OCT4-, and HIF-positive region in primary prostate tumor samples and the significantly higher expression of NANOG and OCT4 in high-grade prostate cancer [68].

Similarly, Wu et al. reported that hypoxia treatment of laryngeal cancer cell lines significantly expanded G0/G1 stage (a fundamental feature of stem cells) and increased the $CD133^+$ CSC subpopulation [69]. They also found that hypoxia increased the mRNA levels of stem cell genes *NANOG*, *OCT4*, and *SOX2*, as well as their protein levels [69]. Consistent with the results in laryngeal cancer cells, another group independently

reported that hypoxia exhibited similar effects on extending the G0/G1 stage and increasing the $CD44^+$ and $ABCG2^+$ cell populations in prostate cancer cells lines, PC3 and Du145 [33]. Upon hypoxia treatment (1% O_2), the expression of NANOG, OCT4, HIF-1α, and HIF-2α was greatly elevated at both mRNA and protein levels. Moreover, up-regulated *NANOG* mRNA expression by hypoxia was predominately derived from retrogene NANOGP8 locus [33]. Hypoxia has also been shown to selectively enhance the expression of NANOG in human non-small cell lung carcinoma cells, leading to resistance to CTL-mediated lysis [70].

Taken together, the above findings indicate that hypoxia, via HIF, induces the expression of NANOG (Figure 1) and other stem cell makers (OCT4, SOX2, MYC, etc.) and support the notion that hypoxia promotes cancer progression via, at least partly, regulating the CSC properties.

Regulation of NANOG by Post-Translational Modifications

Post-translational modifications (PTMs) occur on nearly all proteins, particularly on transcription factors, and represent a powerful approach to regulate the stability and functions of proteins. PTMs can function as an "on-off switch" to control signaling cascades and play the critical roles in regulating multiple cellular functions such as transcriptional activity, subcellular localization, protein folding, and protein stability, etc. In general, PTMs include amino acid modifications (phosphorylation, acetylation, methylation, amidation, formylation, etc) and group attachment (e.g., ubiquitination, sumoylation, and neddylation).

As one of the master regulators in ESCs, NANOG is subject to multiple types of PTMs and the modifications confer NANOG with diverse functions. Because NANOG protein harbors numerous serine (Ser), threonine (Thr), and tyrosine (Tyr) residues, it is natural to hypothesize that NANOG might be modified by phosphorylation (Figure 1). Indeed, in mouse ESCs, Nanog is phosphorylated at Ser52, Ser65, Ser71, and Thr-287 by an unidentified kinase. This phosphorylation facilitates the binding between Nanog and the prolyl isomerase Pin1, and hence improves the stability of Nanog by preventing Nanog degradation from ubiquitin-mediated degradation [71]. In support, by developing a multiplexed assay for kinase specificity (MAKS), Brumbaugh et al. reported that NANOG contains 11 phosphorylation sites including Ser52, Ser65, Ser71, and that ERK2 directly phosphorylates NANOG at Ser52 in vitro [72]. However, work from Dong's group indicated that phosphorylation of Nanog in mouse ESCs at Ser52, Ser71, and Ser78 (not Ser65), by ERK1 rather than ERK2, inhibited NANOG transactivation, induced cell differentiation, and reduced Nanog stability through proteomic degradation [73]. In fact, inhibition of ERK1 activity promoted Nanog transactivation and increased the protein levels. Their findings suggest that the Nanog protein level is modulated through ERK1 phosphorylation, and ERK1 signaling negatively regulates Nanog activity in maintenance of ESC pluripotency [73].

In human head and neck squamous cell carcinoma (HNSCC) cells, Pan's group found that NANOG was phosphorylated by protein kinase Cε (PKCε) at multiple sites and the phosphorylation at Thr200 and Thr280 enhanced NANOG activity, promoted NANOG protein stability, increased NANOG homodimerization, and regulated Bmi1 activity by binding the promoter of BMI1, and thereby induced tumorigenesis [74]. Accordingly, forced expression of phosphorylation-insensitive T200A or T280A mutant NANOG impaired its capacity to promote cell proliferation, colony formation, invasion, migration and the CSC expansion. Their results illustrate that phosphorylation of NANOG at certain sites is required for sustaining NANOG stability, dimerization, and regulating BMI1 and thus promoting tumorigenic properties in HNSCC cells [74]. Unexpectedly, another group presented opposite results and conclusions for effects of PKC on NANOG [75]. The authors investigated the relationship between PKC activity and NANOG expression in several human cancer cell lines including nasopharyngeal carcinoma NPC-076, hepatocellular carcinoma (HepG2 and Hep3B), bladder carcinoma (HT1376 and T24), colorectal cancer (SW620), and embryonal carcinoma cells (NT2/D1 and NCCIT). They observed that either inhibition or knockdown PKC, particularly PKCα and PKCδ, dramatically promoted NANOG expression, and PKC inhibitors enhanced *NANOG* promoter activity, whereas activation of PKC by phorbol-12-myristate-13-acetate (PMA) suppressed NANOG and its target genes expression [75]. The induction of NANOG expression by PKC inhibitors required Octamer–Sox composite element. The reasons behind the discrepancy of the differential PKC effects on NANOG expression in the two studies [74,75] need further investigation. Another study reported that NANOG not only promoted the activity and expression of focal adhesion kinase (FAK) by binding the promoter region of *FAK,* but also interacted with FAK protein, which, in turn, phosphorylated NANOG at Tyr 35 and Tyr174 in a dose dependent manner [76]. The phosphorylation of NANOG by FAK significantly promoted cell invasion of HEK293 and human colon cancer cells SW480 and SW620 [76].

Besides phosphorylation (Figure 1), NANOG stability in ESCs is also affected by ubiquitination through its PEST motif [77]. Additionally, NANOG expression is negatively regulated by sumoylation in pluripotent cells [78]. Whether similar modifications in NANOG exist in cancer cells remains unclear.

CONCLUSIONS AND PERSPECTIVES

There is no doubt that many other molecules may also have the capacity to regulate NANOG expression.

For example, BMI1, a transcriptional repressor belonging to the Polycomb group of proteins, has been shown to significantly enhance NANOG expression in breast cancer cells [79]. In prostate cancer cells, androgen receptor (AR) has been reported to directly bind to the *NANOG* promoter and hence upregulate NANOG expression at both mRNA and protein level [80].

Regarding the regulation of NANOG in cancer cells, most current studies focus on the transcription, mainly based on the regulation of *NANOG1* gene. The most popular mode of regulation is that the effectors (e.g., p53, p-STAT3, HIF) directly bind to the promoter region of *NANOG1* and consequently modulates NANOG expression (Figure 1). However, there is strong evidence that *NANOG* mRNA transcripts in a variety of cancer cell lines and tumor samples are predominantly derived from the NANOGP8 locus, whereas NANOG1 is highly expressed only in pluripotent cells. Therefore, several questions and caveats are associated with many of these studies. First, human *NANOG1* and *NANOGP8* genes are located on chromosomes 12 and 15, respectively, and the two genes possess different promoter regions. Theoretically, the regulatory mechanisms for their expression in cancer cells should be distinct. If the majority of *NANOG* mRNA species are derived from the retrogene NANOGP8 locus, how could the mechanisms that engage the 5′-regulatory sequences of *NANOG1* operate to regulate NANOGP8 expression? In fact, only very few papers presented some evidence relating to the regulation of NANOGP8 in cancer cells (Figure 2). In GBM CSCs, Zbinden et al. have demonstrated that NANOGP8 and GLi1 positively regulate each other and form a protein complex, which is antagonized by p53; consequently, NANOGP8, Gli1, and p53 form a functional network to modulate GBM CSCs [13] (Figure 2]. Ma et al. have observed that hypoxia enhances the expression of NANOGP8 but not NANOG1 in prostate cancer cells maintained under hypoxic conditions [33], presumably via HIF1-mediated transactivation (Figure 2). However, both papers did not provide the detailed molecular mechanisms as to how the *NANOGP8* retrogene might be regulated in the two types of cancer cells. Through TRANSFAC analyses of the NANOGP8 promoter, we have found several putative NANOGP8 promoter-binding factors include SP1, MYC (c-MYC), TCF, and ETS (Jeter et al., unpublished data), suggesting that these factors might be involved in regulating NANOGP8 expression in cancer cells. Clearly, more detailed and extensive investigations on how NANOGP8 expression in somatic cancer cells are needed.

Second, because microRNAs function mainly through binding to the complementary sequences in the 3′-UTR of their target transcripts, and because 3′-UTR's of NANOG1 and NANOGP8 are nearly identical, it is reasonable to speculate that those microRNAs that function as either tumor suppressive or oncogenic to target *NANOG1* transcripts should

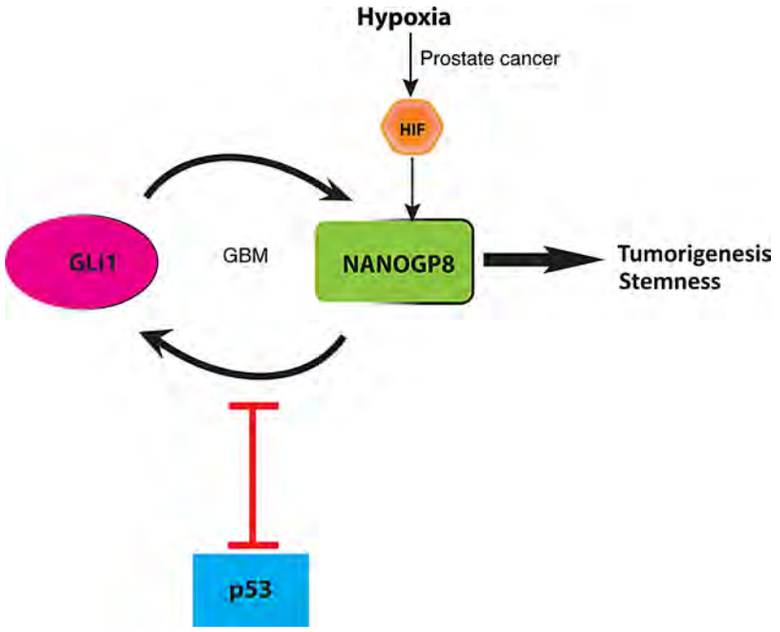

Figure 2. Examples of NANOGP8 regulation in cancer cells. This figure presents the so far reported examples of how NANOGP8 could be potentially regulated in cancer cells. In prostate cancer cells, hypoxia increases NANOGP8 mRNA through HIF. On the other hand, in GBM cells, NANOGP8 forms a positive feedback loop with Gli1, which is antagonized by p53. See Text for details.

have similar impacts on the expression of NANOGP8. **Third**, as the two conserved amino acid differences between NANOG1 protein and NANOGP8 protein occur at the residue 16 (Ala to Glu) and residue 253 (Gln to His), and the two amino acid changes do not involve Ser, Thr, Tyr, and Lys (i.e., potential phosphorylation, ubiquitination and sumolyation sites), it is tempting to speculate that signaling pathways that result in PTMs on NANOG1 should exert similar effects on NANOGP8.

NANOG expression has been reported to be elevated in a variety of cancers, and NANOG expression levels seem to positively correlate with the malignancy and patient survival, implicating NANOG as an oncogenic factor in cancer development. Because NANOG is not expressed in most normal adult tissues, NANOG and its related signaling pathways might represent novel targets for therapeutic development. Thus, understanding the regulation of NANOG during cancer progression will be of significance in developing new strategies to battle against cancer.

ACKNOWLEDGEMENTS

Work related to NANOG in the Tang lab was supported, in part, by grants from NIH R01-CA155693 (DGT), Department of Defense W81XWH-13-1-0352 and W81XWH-14-1-0575 (DGT), and CPRIT RP120380 (DGT) and CPRIT RP120394 (CJ). S. Gong was a graduate student jointly trained by Zhengzhou University (Henan, China) and the University of Texas M.D Anderson Cancer Center and supported by the China Scholar Council.

REFERENCES

1. Visvader JE, Lindeman GJ. Cancer stem cells in solid tumours: Accumulating evidence and unresolved questions. Nat Rev Cancer 2008;8:755–768.
2. Zhang S, Balch C, Chan MW, et al. Identification and characterization of ovarian cancer-initiating cells from primary human tumors. Cancer Res 2008;68:4311–4320.
3. Alvero AB, Chen R, Fu HH, et al. Molecular phenotyping of human ovarian cancer stem cells unravels the mechanisms for repair and chemoresistance. Cell Cycle 2009;8:158–166.
4. Chambers I, Colby D, Robertson M, et al. Functional expression cloning of Nanog, a pluripotency sustaining factor in embryonic stem cells. Cell 2003;113:643–655.
5. Mitsui K, Tokuzawa Y, Itoh H, et al. The homeoprotein Nanog is required for maintenance of pluripotency in mouse epiblast and ES cells. Cell 2003;113:631–642.
6. Boiani M, Scholer HR. Regulatory networks in embryo-derived pluripotent stem cells. Nat Rev Mol Cell Biol 2005;6:872–884.
7. Nichols J, Zevnik B, Anastassiadis K, et al. Formation of pluripotent stem cells in the mammalian embryo depends on the POU transcription factor Oct4. Cell 1998;95:379–391.
8. Pei D. Regulation of pluripotency and reprogramming by transcription factors. J Biol Chem 2009;284:3365–3369.
9. Darr H, Mayshar Y, Benvenisty N. Overexpression of NANOG in human ES cells enables feeder-free growth while inducing primitive ectoderm features. Development 2006;133:1193–1201.
10. Hanna J, Saha K, Pando B, et al. Direct cell reprogramming is a stochastic process amenable to acceleration. Nature 2009;462:595–601.
11. Hyslop L, Stojkovic M, Armstrong L, et al. Downregulation of NANOG induces differentiation of human embryonic stem cells to extraembryonic lineages. Stem Cells 2005;23:1035–1043.
12. Po A, Ferretti E, Miele E, et al. Hedgehog controls neural stem cells through p53-independent regulation of Nanog. EMBO J 2010;29:2646–2658.
13. Zbinden M, Duquet A, Lorente-Trigos A, et al. NANOG regulates glioma stem cells and is essential in vivo acting in a cross-functional network with GLI1 and p53. EMBO J 2010;29:2659–2674.
14. Nagata T, Shimada Y, Sekine S, et al. Prognostic significance of NANOG and KLF4 for breast cancer. Breast Cancer 2014;21:96–101.
15. Bourguignon LY, Peyrollier K, Xia W, Gilad E. Hyaluronan-CD44 interaction activates stem cell marker Nanog, Stat-3-mediated MDR1 gene expression, and ankyrin-regulated multidrug efflux in breast and ovarian tumor cells. J Biol Chem 2008;283:17635–17651.
16. Ye F, Zhou C, Cheng Q, Shen J, Chen H. Stem-cell-abundant proteins Nanog, Nucleostemin and Musashi1 are highly expressed in malignant cervical epithelial cells. BMC Cancer 2008;8:108.
17. Lin T, Ding YQ, Li JM. Overexpression of Nanog protein is associated with poor prognosis in gastric adenocarcinoma. Med Oncol 2012;29:878–885.
18. Meng HM, Zheng P, Wang XY, et al. Overexpression of nanog predicts tumor progression and poor prognosis in colorectal cancer. Cancer Biol Ther 2010;9:295–302.
19. Zhang J, Espinoza LA, Kinders RJ, et al. NANOG modulates stemness in human colorectal cancer. Oncogene 2013;32:4397–4405.
20. Yu CC, Chen YW, Chiou GY, et al. MicroRNA let-7a represses chemoresistance and tumourigenicity in head and neck cancer via stem-like properties ablation. Oral Oncol 2011;47:202–210.
21. Shan J, Shen J, Liu L, et al. Nanog regulates self-renewal of cancer stem cells through the insulin-like growth factor pathway in human hepatocellular carcinoma. Hepatol 2012;56:1004–1014.
22. Chiou SH, Wang ML, Chou YT, et al. Coexpression of Oct4 and Nanog enhances malignancy in lung adenocarcinoma by inducing cancer stem cell-like properties and epithelial-mesenchymal transdifferentiation. Cancer Res 2010;70:10433–10444.
23. Li XQ, Yang XL, Zhang G, et al. Nuclear beta-catenin accumulation is associated with increased expression of Nanog protein and predicts poor prognosis of non-small cell lung cancer. J Transl Med 2013;11:114.
24. Bussolati B, Bruno S, Grange C, Ferrando U, Camussi G. Identification of a tumor-initiating stem cell population in human renal carcinomas. FASEB J 2008;22:3696–3705.
25. Chiou SH, Yu CC, Huang CY, et al. Positive correlations of Oct-4 and Nanog in oral cancer stem-like cells and high-grade oral squamous cell carcinoma. Clin Cancer Res 2008;14:4085–4095.
26. Lee M, Nam EJ, Kim SW, Kim S, Kim JH, Kim YT. Prognostic impact of the cancer stem cell-related marker NANOG in ovarian serous carcinoma. Int J Gynecol Cancer 2012;22:1489–1496.
27. Wen J, Park JY, Park KH, et al. Oct4 and Nanog expression is associated with early stages of pancreatic carcinogenesis. Pancreas 2010;39:622–626.
28. Jeter CR, Badeaux M, Choy G, et al. Functional evidence that the self-renewal gene NANOG regulates human tumor development. Stem Cells 2009;27:993–1005.
29. Jeter CR, Liu B, Liu X, et al. NANOG promotes cancer stem cell characteristics and prostate cancer resistance to androgen deprivation. Oncogene 2011;30:3833–3845.
30. Hart AH, Hartley L, Parker K, et al. The pluripotency homeobox gene NANOG is expressed in human germ cell tumors. Cancer 2005;104:2092–2098.

31. Booth HA, Holland PW. Eleven daughters of NANOG. Genomics 2004;84:229–238.
32. Zhang J, Wang X, Li M, et al. NANOGP8 is a retrogene expressed in cancers. FEBS J 2006;273:1723–1730.
33. Ma Y, Liang D, Liu J, et al. Prostate cancer cell lines under hypoxia exhibit greater stem-like properties. PLoS ONE 2011;6:e29170.
34. Zhang K, Fowler M, Glass J, Yin H. Activated 5'flanking region of NANOGP8 in a self-renewal environment is associated with increased sphere formation and tumor growth of prostate cancer cells. Prostate 2014;74:381–394.
35. Pereira L, Yi F, Merrill BJ. Repression of Nanog gene transcription by Tcf3 limits embryonic stem cell self-renewal. Mol Cell Biol 2006;26:7479–7491.
36. Lin T, Chao C, Saito S, et al. p53 induces differentiation of mouse embryonic stem cells by suppressing Nanog expression. Nat Cell Biol 2005;7:165–171.
37. Suzuki A, Raya A, Kawakami Y, et al. Nanog binds to Smad1 and blocks bone morphogenetic protein-induced differentiation of embryonic stem cells. Proc Natl Acad Sci USA 2006;103:10294–10299.
38. Rodda DJ, Chew JL, Lim LH, et al. Transcriptional regulation of nanog by OCT4 and SOX2. J Biol Chem 2005, 280:24731–24737.
39. Kuroda T, Tada M, Kubota H, et al. Octamer and Sox elements are required for transcriptional cis regulation of Nanog gene expression. Mol Cell Biol 2005;25:2475–2485.
40. Hawkins K, Mohamet L, Ritson S, Merry CL, Ward CM. E-cadherin and, in its absence, N-cadherin promotes Nanog expression in mouse embryonic stem cells via STAT3 phosphorylation. Stem Cells 2012;30:1842–1851.
41. Zhou JJ, Chen RF, Deng XG, et al. Hepatitis C virus core protein regulates NANOG expression via the stat3 pathway. FEBS Lett 2014;588:566–573.
42. Vogelstein B, Lane D, Levine AJ. Surfing the p53 network. Nature 2000;408:307–310.
43. Oren M. Decision making by p53: Life, death and cancer. Cell Death Differ 2003;10:431–442.
44. Goh AM, Coffill CR, Lane DP. The role of mutant p53 in human cancer. J Pathol 2011;223:116–126.
45. Clement V, Sanchez P, de Tribolet N, Radovanovic I, Ruiz i Altaba A. HEDGEHOG-GLI1 signaling regulates human glioma growth, cancer stem cell self-renewal, and tumorigenicity. Curr Biol 2007;17:165–172.
46. Stecca B, Ruiz i Altaba A. A GLI1-p53 inhibitory loop controls neural stem cell and tumour cell numbers. EMBO J 2009;28:663–676.
47. Bagga S, Bracht J, Hunter S, et al. Regulation by let-7 and lin-4 miRNAs results in target mRNA degradation. Cell 2005, 122:553–563.
48. Makeyev EV, Maniatis T. Multilevel regulation of gene expression by microRNAs. Science 2008;319:1789–1790.
49. Sirotkin AV, Laukova M, Ovcharenko D, Brenaut P, Mlyncek M. Identification of microRNAs controlling human ovarian cell proliferation and apoptosis. J Cell Physiol 2010;223:49–56.
50. Lee YS, Kim HK, Chung S, Kim KS, Dutta A. Depletion of human micro-RNA miR-125b reveals that it is critical for the proliferation of differentiated cells but not for the down-regulation of putative targets during differentiation. J Biol Chem 2005;280:16635–16641.
51. Hatfield SD, Shcherbata HR, Fischer KA, Nakahara K, Carthew RW, Ruohola-Baker H. Stem cell division is regulated by the microRNA pathway. Nature 2005;435:974–978.
52. Liu C, Kelnar K, Liu B, et al. The microRNA miR-34a inhibits prostate cancer stem cells and metastasis by directly repressing CD44. Nat Med 2011;17:211–215.
53. Tay YM, Tam WL, Ang YS, et al. MicroRNA-134 modulates the differentiation of mouse embryonic stem cells, where it causes post-transcriptional attenuation of Nanog and LRH1. Stem Cells 2008;26:17–29.
54. Bicker S, Khudayberdiev S, Weiss K, Zocher K, Baumeister S, Schratt G. The DEAH-box helicase DHX36 mediates dendritic localization of the neuronal precursor-microRNA-134. Genes Dev 2013;27:991–996.
55. Zhong J, Li B. Reduced expression of microRNA-134 correlates with malignancy and poor prognosis in human glioma. J Clin Neurosci 2015;22:583–587.
56. Niu CS, Yang Y, Cheng CD. MiR-134 regulates the proliferation and invasion of glioblastoma cells by reducing Nanog expression. Int J Oncol 2013;42:1533–1540.
57. Smirnova L, Grafe A, Seiler A, Schumacher S, Nitsch R, Wulczyn FG. Regulation of miRNA expression during neural cell specification. Eur J Neurosci 2005;21:1469–1477.
58. Venkataraman S, Alimova I, Fan R, Harris P, Foreman N, Vibhakar R. MicroRNA 128a increases intracellular ROS level by targeting Bmi-1 and inhibits medulloblastoma cancer cell growth by promoting senescence. PLoS ONE 2010;5:e10748.
59. Ciafre SA, Galardi S, Mangiola A, et al. Extensive modulation of a set of microRNAs in primary glioblastoma. Biochem Biophys Res Commun 2005;334:1351–1358.
60. Masri S, Liu Z, Phung S, Wang E, Yuan YC, Chen S. The role of microRNA-128a in regulating TGFbeta signaling in letrozole-resistant breast cancer cells. Breast Cancer Res Treat 2010;124:89–99.
61. Khan AP, Poisson LM, Bhat VB, et al. Quantitative proteomic profiling of prostate cancer reveals a role for miR-128 in prostate cancer. Mol Cell Proteomics 2010;9:298–312.
62. Woo HH, Laszlo CF, Greco S, Chambers SK. Regulation of colony stimulating factor-1 expression and ovarian cancer cell behavior in vitro by miR-128 and miR-152. Mol Cancer 2012;11:58.
63. Jin M, Zhang T, Liu C, et al. miRNA-128 suppresses prostate cancer by inhibiting BMI-1 to inhibit tumor-initiating cells. Cancer Res 2014;74:4183–4195.
64. Fujii T, Shimada K, Tatsumi Y, Fujimoto K, Konishi N. Syndecan-1 responsive microRNA-126 and 149 regulate cell proliferation in prostate cancer. Biochem Biophys Res Commun 2015;456:183–189.
65. Xu CX, Xu M, Tan L, et al. MicroRNA miR-214 regulates ovarian cancer cell stemness by targeting p53/Nanog. J Biol Chem 2012;287:34970–34978.
66. Penna E, Orso F, Cimino D, et al. microRNA-214 contributes to melanoma tumour progression through suppression of TFAP2C. EMBO J 2011;30:1990–2007.
67. Yang H, Kong W, He L, et al. MicroRNA expression profiling in human ovarian cancer: miR-214 induces cell survival and cisplatin resistance by targeting PTEN. Cancer Res 2008;68:425–433.
68. Mathieu J, Zhang Z, Zhou W, et al. HIF induces human embryonic stem cell markers in cancer cells. Cancer Res 2011;71:4640–4652.
69. Wu CP, Du HD, Gong HL, et al. Hypoxia promotes stem-like properties of laryngeal cancer cell lines by increasing the CD133+ stem cell fraction. Int J Oncol 2014;44:1652–1660.
70. Hasmim M, Noman MZ, Lauriol J, et al. Hypoxia-dependent inhibition of tumor cell susceptibility to CTL-mediated lysis involves NANOG induction in target cells. J Immunol 2011;187:4031–4039.
71. Moretto-Zita M, Jin H, Shen Z, Zhao T, Briggs SP, Xu Y. Phosphorylation stabilizes Nanog by promoting its interaction with Pin1. Proc Natl Acad Sci USA 2010;107:13312–13317.
72. Brumbaugh J, Russell JD, Yu P, Westphall MS, Coon JJ, Thomson JA. NANOG is multiply phosphorylated and directly modified by ERK2 and CDK1 in vitro. Stem Cell Reports 2014;2:18–25.
73. Kim SH, Kim MO, Cho YY, et al. ERK1 phosphorylates Nanog to regulate protein stability and stem cell self-renewal. Stem Cell Res 2014;13:1–11.
74. Xie X, Piao L, Cavey GS, et al. Phosphorylation of Nanog is essential to regulate Bmi1 and promote tumorigenesis. Oncogene 2014;33:2040–2052.

75. Chu WK, Dai PM, Li HL, Pao CC, Chen JK. Nanog expression is negatively regulated by protein kinase C activities in human cancer cell lines. Carcinogenesis 2013;34:1497–1509.
76. Ho B, Olson G, Figel S, Gelman I, Cance WG, Golubovskaya VM. Nanog increases focal adhesion kinase (FAK) promoter activity and expression and directly binds to FAK protein to be phosphorylated. J Biol Chem 2012;287:18656–18673.
77. Ramakrishna S, Suresh B, Lim KH, et al. PEST motif sequence regulating human NANOG for proteasomal degradation. Stem Cells Dev 2011;20:1511–1519.
78. Wu Y, Guo Z, Wu H, et al. SUMOylation represses Nanog expression via modulating transcription factors Oct4 and Sox2. PLoS ONE 2012;7:e39606.
79. Paranjape AN, Balaji SA, Mandal T, et al. Bmi1 regulates self-renewal and epithelial to mesenchymal transition in breast cancer cells through Nanog. BMC Cancer 2014;14:785.
80. Kregel S, Szmulewitz RZ, Griend DJ. The pluripotency factor Nanog is directly upregulated by the androgen receptor in prostate cancer cells. The Prostate 2014;74:1530–1543.

Androgen receptor and prostate cancer stem cells: biological mechanisms and clinical implications

Qu Deng[1,2] and **Dean G Tang**[1,2,3]

[1]Department of Epigenetics and Molecular Carcinogenesis, University of Texas MD Anderson Cancer Center, Science Park, Park Road 1C, Smithville, Texas 78957, USA
[2]Program in Molecular Carcinogenesis, University of Texas Graduate School of Biomedical Sciences, Houston, Texas, USA
[3]Cancer Stem Cell Institute, Research Center for Translational Medicine, Shanghai East Hospital, Tongji University School of Medicine, Shanghai 200120, China

Correspondence should be addressed to D G Tang
Email
dtang@mdanderson.org

Abstract

Prostate cancer (PCa) contains phenotypically and functionally distinct cells, and this cellular heterogeneity poses clinical challenges as the distinct cell types likely respond differently to various therapies. Clonal evolution, driven by genetic instability, and intraclonal cancer cell diversification, driven by cancer stem cells (CSCs), together create tumor cell heterogeneity. In this review, we first discuss PCa stem cells (PCSCs) and heterogeneity of androgen receptor (AR) expression in primary, metastatic, and treatment-failed PCa. Based on literature reports and our own studies, we hypothesize that, whereas PCSCs in primary and untreated tumors and models are mainly AR^-, PCSCs in CRPCs could be either AR^+ or $AR^{-/lo}$. We illustrate the potential mechanisms AR^+ and AR^- PCSCs may employ to propagate PCa at the population level, mediate therapy resistance, and metastasize. As a result, targeting AR alone may not achieve long-lasting therapeutic efficacy. Elucidating the roles of AR and PCSCs should provide important clues to designing novel personalized combinatorial therapeutic protocols targeting both AR^+ and AR^- PCa cells.

Key Words
- androgen receptor
- prostate cancer
- cancer stem cells
- prostate cancer stem cells
- castration-resistant prostate cancer

Endocrine-Related Cancer (2015) **22**, T209–T220

Cancer stem cells and tumor heterogeneity

Tumors contain genetically heterogeneous cellular clones, which constantly evolve during disease progression and clinical treatment. Clonal evolution, driven by genetic instability of cancer cells, generates cellular heterogeneity and promotes tumor progression. For instance, genome-wide DNA sequencing of three individual prostate tumors revealed the existence of three or more clones within each cancer (Cooper *et al*. 2015). Even morphologically normal regions could possess as many as ten genetic mutations (Cooper *et al*. 2015). In untreated primary prostate cancer (PCa), genetic alterations such as TMPRSS2-ERG fusion and PTEN deletion within tumor clones could activate critical signaling pathways such as ERG and PI3K, thus driving clonal evolution (Berger *et al*. 2011, Haffner *et al*. 2015). In a longitudinal tracking of a castration-resistant PCa (CRPC) patient with nine prostate tumor foci at the initial presentation, it was found that during the 17 years of tumor progression, only the tumor clones with *PTEN*, *P53*, and *SPOP* mutations gained additional genetic alterations and gave rise to lethal metastatic tumors. Surprisingly, the lethal clone (defined by the presence of the same *PTEN*, *P53*, and *SPOP* mutations) in this patient was found to arise from a morphologically low-grade (Gleason 3) tumor focus rather than the predominant Gleason 4 tumor foci (Haffner *et al*. 2013). Whole-genome

http://erc.endocrinology-journals.org
DOI: 10.1530/ERC-15-0217

This paper forms part of a thematic review section on Stem Cells and Cancer. The guest editor for this section was Dean Tang, The University of Texas MD Anderson Cancer Center, Smithville, TX, USA. Dean Tang was not involved in the handling of this paper, on which he is listed as an author.

exome sequencing in 50 lethal and heavily pretreated metastatic CRPCs also confirmed the monoclonal origin of lethal CRPC (Grasso *et al*. 2012). These examples highlight the importance of genetically driven clonal evolution in driving PCa progression.

On the other hand, there is also strong evidence that tumor cells within a genetically identical clone possess different tumorigenic ability and, in most cases, are organized in a hierarchical manner (reviewed in Tang (2012), Kreso & Dick (2014) and Yang *et al*. (2014)). Sitting at the apex of this tumorigenic hierarchy is the small subset of stem-like cancer cells, or cancer stem cells (CSCs) that possess high self-renewal and differentiation ability. In other words, CSCs sustain an established tumor clone through unlimited self-renewal and maintain intraclonal heterogeneity through generating both tumorigenic and less or non-tumorigenic cancer cells. Similar to normal hematopoietic stem cells (HSCs), which are among the best understood adult stem cells, the best characterized CSCs are CSCs in leukemia or leukemic stem cells (LSCs; Kreso & Dick 2014). Like HSCs, LSCs are undifferentiated, lacking the expression of lineage differentiation markers. Subsequent studies have led to the identification of CSCs in multiple human solid tumors, and a common phenotypic feature of these CSCs seems to be the lack of differentiation markers and regulators (Tang 2012, Kreso & Dick 2014, Yang *et al*. 2014).

In a strict sense, CSCs in human tumors are defined as a population of cancer cells that, when prospectively purified out from patient tumors, xenografts, and even long-term cultures, can regenerate and also indefinitely propagate human tumors in immunodeficient mice. In reality, the CSC properties of a candidate population of human tumor cells are best assessed by performing limiting dilution tumor-regeneration assays combined with serial tumor transplantations and cell biological (e.g., clonal in 2D, clonogenic in 3D, sphere formation, single-cell division, differentiation, etc.) as well as molecular (e.g., RNA-Seq and ChIP-Seq) characterizations (reviewed in Rycaj & Tang (2015)). The tumor cell population that can initiate or regenerate tumors at low cell doses is considered to be tumor-initiating or tumor-regenerating cells, and the tumor cell population that can propagate human xenograft tumors long-term is called tumor-propagating cells (Rycaj & Tang 2015). Unfortunately, many of the reported CSC populations do not fully satisfy this strict definition. For example, some studies only utilized cell lines to perform *in vitro* assays without tumor experiments, whereas some others only performed tumor experiments without further carrying out serial transplantations. Such shortcomings have created a lot of confusions in the field and led many to even disbelieve the presence of CSCs. Recent lineage tracing studies in genetically driven mouse model tumors (i.e., glioblastoma and intestinal and skin tumors) have provided definitive evidence for CSCs (Rycaj & Tang 2015).

PCa stem cells

The CSC model helps explain the generation of tumor cell heterogeneity from the viewpoint of stem cell maturation and differentiation. PCa is well known to be a highly heterogeneous malignancy with each tumor harboring many tumor clones (Haffner *et al*. 2013, Cooper *et al*. 2015). Therefore, it is not surprising that many PCa stem cell (PCSC) populations have been reported (reviewed in Chen *et al*. (2013) and Rybak *et al*. (2015)). PCSCs are defined, more or less, using a spectrum of *in vitro* and *in vivo* assays used to define other CSCs (see above). *In vitro*, PCSCs preferentially express stem cell and CSC-associated molecules and self-renewal genes (e.g., Bmi1, Stat3, Nanog, Sox2, Oct4) and possess high clonal and clonogenic capacities, and *in vivo*, PCSCs possess higher tumor-initiating and serial tumor-propagating activities than non-PCSCs in immunodeficient mice (Chen *et al*. 2013, Kroon *et al*. 2013, Rybak *et al*. 2015). Three papers, published in 2005, simultaneously provided the earliest proof-of-principle evidence for PCSCs: the side population (SP) in the LAPC9 human xenografts was enriched in tumor-initiating cells (Patrawala *et al*. 2005); ABCG2, a surface pump protein normally involved in cellular detoxification, mediated efflux of androgen in putative PCSCs (Huss *et al*. 2005); and the $CD44^+$ $\alpha2\beta1^+CD133^+$ PCa cells from patient prostate tumors possessed high clonogenic survivability in methylcellulose (Collins *et al*. 2005).

Since 2012 our lab has been employing and developing a variety of experimental strategies to elucidate the cellulose basis and molecular regulation of PCa cell heterogeneity and to link PCa cell heterogeneity to therapy resistance and tumor relapse. In virtually all of our PCSC studies, we have performed tumor regeneration and, in many cases, serial tumor transplantation assays. Using the SP analysis, we provided the very first piece of evidence that the SP in certain PCa xenograft models is enriched in tumor-regenerating and tumor-propagating cells and thus satisfies the strict definition of CSCs (Patrawala *et al*. 2005). Using cell surface markers, our systematic studies have provided convincing evidence that the CD44 high-expressing (i.e., $CD44^+$) PCa cell

http://erc.endocrinology-journals.org
DOI: 10.1530/ERC-15-0217

Published by Bioscientifica Ltd.

population in most, though not all, PCa models we have studied is significantly enriched in PCSCs with enhanced tumor-regenerating, tumor-propagating, and metastatic capacities (Patrawala *et al.* 2006, 2007, Liu *et al.* 2011, 2015). Using holoclone assays, we have shown that the PCa cell holoclones, like stem cell-enriched primary keratinocyte holoclones, possess long-term tumor-propagating CSC properties (Li *et al.* 2008*a*). Using lentiviral-mediated lineage tracing, we have recently demonstrated that the phenotypically undifferentiated PCa cell population that lacks the expression of prostate-specific antigen (PSA; i.e., $PSA^{-/lo}$) harbors self-renewing long-term tumor-propagating PCSCs, which express stem cell gene expression and epigenetic profiles, can undergo authentic asymmetric cell division, and are intrinsically refractory to castration treatments (Qin *et al.* 2012, Liu *et al.* 2015).

Similar to the heterogeneity of CSC populations in other tumor systems (Tang 2012), the PCSC pool is heterogeneous containing CSC subsets with distinct tumor-regenerating and tumor-propagating capabilities (Liu *et al.* 2015), potentially explaining many different PCSC populations reported by others (e.g., Collins *et al.* 2005, Miki *et al.* 2007, Dubrovska *et al.* 2009, Rajasekhar *et al.* 2011, Domingo-Domenech *et al.* 2012). Also similar to the undifferentiated nature of LSCs and other CSCs (Tang 2012), a common phenotypic trait of the reported PCSC populations is the lack of expression of differentiation regulators and markers such as androgen receptor (AR) (see below), PSA (Qin *et al.* 2012), and MHC molecules (Domingo-Domenech *et al.* 2012).

One of the major unresolved questions related to PCSCs is whether any subpopulation of PCa cells acutely purified from primary patient tumors or CRPCs truly possesses hardcore CSC properties such as regenerating tumors at the single-cell level and enabling serial tumor transplantations. Although patient tumor or early patient-derived xenograft (PDX) cells have been demonstrated in many experimental settings to possess at least certain CSC properties (especially *in vitro*), this question has dodged a direct answer mainly due to our current technical difficulty in reconstituting human PCa development in immunodeficient mice (Chen *et al.* 2013).

AR heterogeneity in PCa

AR is a master regulator of normal prostate differentiation and development. The human *AR* gene, located on chromosome Xq11-12, encodes a protein with four functional domains: the NH2-terminal domain (NTD), the DNA-binding domain (DBD), the hinge domain, and the ligand-binding domain (LBD) (Fig. 1). The prostate is one of the main organs that express AR, and the AR protein is expressed in the luminal cell layer of the prostatic glands. AR signaling critically regulates development, differentiation, and maintenance of the prostate as documented in both human and animal studies.

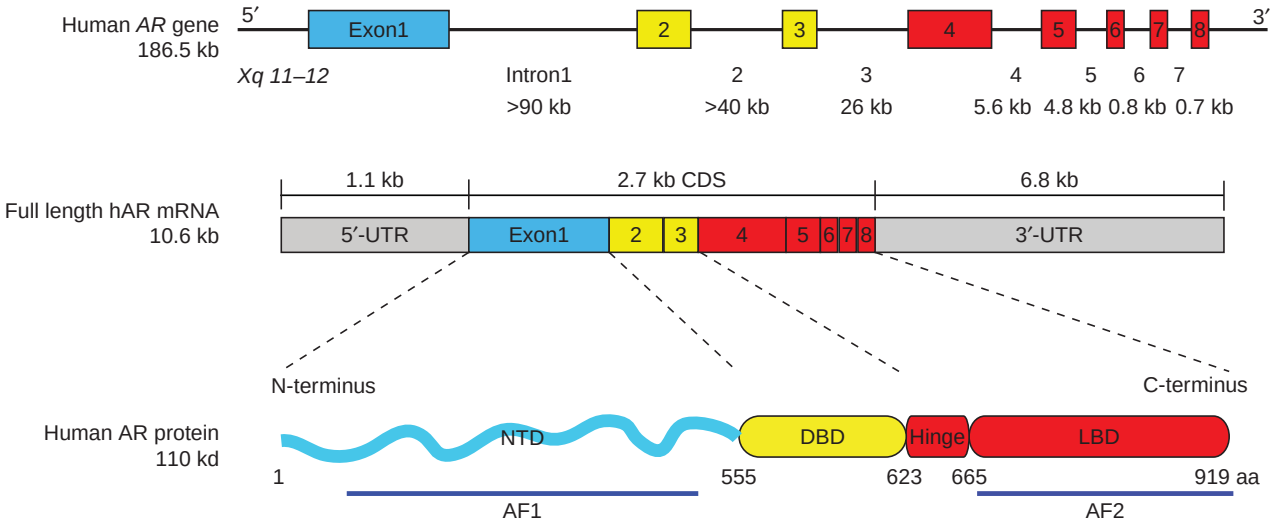

Figure 1

Genomic organization of the *AR* gene and overall domain structure of the androgen receptor (AR) protein. The *AR* gene is mapped to the long arm of the X chromosome and spans about 186.5 kb. It contains eight exons interrupted by introns of various lengths (indicated below). The mRNA of the *AR* gene is 10.6 kb with exon 1 coding for the NH2-terminal domain (NTD), exons 2 and 3 for the DNA-binding domain (DBD), and exons 4–8 for the hinge and ligand-binding domain (LBD). The full length AR protein contains 919 amino acids consisting of a very flexible NTD and a constant DBD, hinge domain, and LBD. The constitutively active AF1 domain is located in the NTD, and the LBD consists of the AF2 domain.

http://erc.endocrinology-journals.org
DOI: 10.1530/ERC-15-0217

Published by Bioscientifica Ltd.

Somatic mutations of the *AR* gene lead to the malfunction of AR and androgen insensitivity syndrome in humans in which 46 XY individuals present female phenotype and the prostate is absent (Quigley *et al*. 1995). The *AR* NTD knockout male mice all have small immature testes and lack secondary reproductive organs (Kerkhofs *et al*. 2009).

Simanainen *et al*. (2007) established an *AR* exon 3 knockout mouse model and observed underdeveloped prostates in the male mice with delayed structural and functional differentiation of the prostate epithelium. There was also increased proliferation in the *AR* deficient epithelium (Simanainen *et al*. 2007). In another prostate-specific AR knockout mouse model, Wu *et al*. (2007) also reported increased proliferation and less differentiation of the epithelium. These genetic studies suggest that AR promotes prostate differentiation and suppresses epithelium proliferation in the mature prostate; in this way, AR signaling maintains the homeostasis and relative dormancy of mature prostate epithelium. Consistent with this pro-differentiation role of AR, the prostate epithelial-specific *AR* knockout promoted transgenic adenocarcinoma mouse prostate (TRAMP) tumor development, providing genetic evidence for a tumor-suppressive function of AR (Niu *et al*. 2008).

Somewhat paradoxically, however, AR expression is frequently overexpressed in PCa and, in fact, AR is thought to be required for prostate tumorigenesis and, hence, targeting AR and AR signaling has long been a therapeutic strategy. Androgen-deprivation therapy (ADT) aims to block androgen synthesis (e.g., abiraterone) or AR functions (e.g., bicalutamide, enzalutamide). Nevertheless, AR expression has been observed to be heterogeneous in primary and, in particular, treatment-failed patient tumors. Ruizeveld de Winter *et al*. (1990) examined AR by immunohistochemistry (IHC) staining in 26 primary PCas and found that 7 cases presented a considerable heterogeneity in AR expression and the proportion of AR-expressing cells was decreased in the more aggressive tumors. Similar AR IHC staining by Masai *et al*. (1990) showed that AR expression correlated inversely with grade. Also, Chodak *et al*. (1992) analyzed AR expression in 57 untreated PCas and observed that AR content was significantly higher in differentiated tumors compared to that of poorly differentiated tumors. Our own studies revealed AR^- PCa cells to be present in all nine primary PCa samples we examined representing approximately 5–30% of the total (Liu *et al*. 2015). Overall, these and many other studies suggest that, although AR^- cells may not be dominant in treatment naïve tumors, all primary prostate tumors nevertheless harbor both AR^+ and AR^- cells or clones (Fig. 2, bottom; Liu *et al*. 2015).

AR heterogeneity in hormone-refractory PCa has been observed since the early 1990s. van der Kwast *et al*. (1991) examined AR expression in CRPC and found that in 13 of 17 tumors, over 80% of the tumor cells were AR^+. However, three tumors showed a considerable heterogeneity in AR expression, and in one sample nearly all tumor cells appeared $AR^{-/lo}$. Sadi *et al*. (1991) observed similar AR heterogeneity in needle biopsy specimens of 17 patients with stage D PCa. Ruizeveld de Winter *et al*. (1994) examined AR expression in locally progressive CRPC and found that less differentiated PCa cells tended toward diminished AR expression. Computer quantification of nuclear AR levels in PCa patient samples showed that the AR concentration per cell was significantly more heterogeneous in poor responders (Sadi & Barrack 1993). Our own IHC staining of AR on a tissue microarray of CRPC samples revealed highly heterogeneous AR expression patterns across individuals: there were AR^+ as well as AR^- CRPC cores, and within one single CRPC, there were regions that were AR^+, AR^-, or a mixture of both populations (Liu *et al*. 2015).

AR expression varies in metastases as well. Shah *et al*. (2004) investigated AR expression by IHC in the metastatic lesions of 30 CRPC patients who underwent warm autopsy and observed wide variations in AR expression between tumor samples. Specifically, 31% (83 of 265) of the metastatic samples had $<50\%$ AR^+ cells and 41.5% (100 of 265) metastases had $<10\%$ AR^+ cells. Five patient metastases had $<1\%$ AR^+cells (Shah *et al*. 2004). Similarly, Davis *et al*. (2006) reported that both AR^+ cells and AR staining intensity decreased in metastatic CRPC cells compared with benign tissues or untreated PCa. Of note, two commonly used PCa cell lines, Du145 and PC3, which were derived from brain and bone metastasis, respectively, and possess high tumorigenic and metastatic capacities, lack AR expression. ARCaP cells, derived from the ascites fluid of a disseminated CRPC, express little AR (Zhau *et al*. 1996). Bone metastases MDA PCa 118a/118b also completely lack AR (and PSA) expression (Li *et al*. 2008*b*).

Similar AR heterogeneity has also been observed in prostatic-specific transgenic mouse models. In a ARR_2Pb driven c-Myc (i.e., Hi-Myc) model (Ellwood-Yen *et al*. 2003), the residual tumors 5 months post-castration expressed low and heterogeneous levels of cytoplasmic AR compared to the intact mice. These castration-resistant Hi-Myc tumor cells were also quiescent as shown by negative Ki67 staining (Ellwood-Yen *et al*. 2003). In a prostate-specific *Pten*-deleted mouse prostate, although

http://erc.endocrinology-journals.org
DOI: 10.1530/ERC-15-0217

Published by Bioscientifica Ltd.

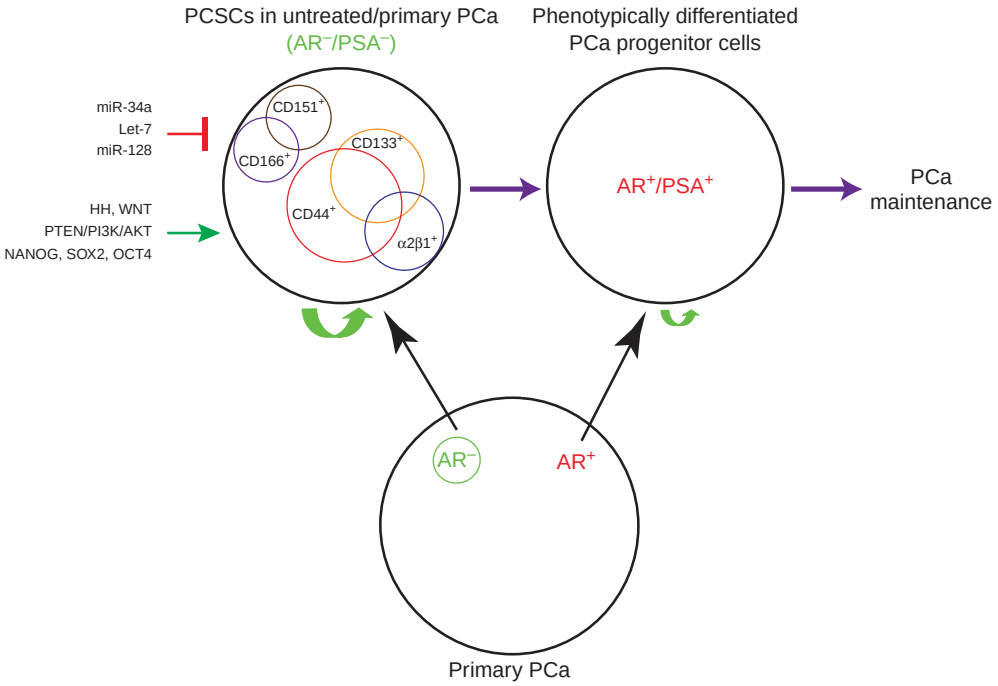

Figure 2

Prostate cancer stem cells (PCSCs) in untreated/primary prostate cancer (PCa). Primary PCa contains androgen receptor (AR)$^+$ PCa cells as the majority and AR$^-$ PCa cells being the minority (below). Depicted on top (left) are several representative PCSC populations reported in primary PCa and untreated prostate tumor models, which are mostly AR$^-$ and PSA$^-$ but have the capacity to differentiate into more mature AR$^+$/PSA$^+$ PCa cells (right). The PSA$^{-/lo}$ PCSC population has unlimited self-renewal potential (indicated by a large green arrow), whereas differentiated AR$^+$/PSA$^+$ PCa progenitors cells have more limited self-renewal activity (indicated by a small green arrow) (Qin *et al.* 2012, Liu *et al.* 2015). The PCSCs can be positively regulated through HH (Hedgehog), WNT, and PTEN signaling pathways, as well as by transcription factors such as NANOG, SOX2, and OCT4. On the other hand, several miRNAs including miR-34a, let-7, and miR-128 have been reported to negatively regulate PCSCs.

most tumor cells expressed AR after 10 weeks' castration, the expression level was weaker and more diffuse compared to the hormonally intact prostate (Wang *et al.* 2003).

AR heterogeneity in CRPCs has a genetic basis. A recent sequencing study of 150 metastatic PCa and CRPCs suggests that genetic alterations of AR (mutations, amplifications) (approximately 63% patients) become enriched in CRPCs compared to those in untreated tumors (Robinson *et al.* 2015). In addition to mutations in *AR* itself, alterations of members in the AR signaling pathway were also observed in metastatic CRPCs, including FOXA1 and NCOR1/2, among others. Similarly, by comparing 50 lethal CRPCs and 11 primary cancers, Grasso *et al.* (2012) identified mutations in FOXA1 and MLL2 in CRPCs that likely change the AR signaling in treatment-failed tumors.

PCSCs in primary and untreated PCa: AR negativity and signaling mechanisms

The preceding discussions highlight the presence of AR$^-$ PCa cells in untreated PCa (Liu *et al.* 2015). This is an important point as the AR$^-$ PCa cells are expected to not respond well to AR-targeting therapies. This point would be consistent with reports that androgen-independent PCa cells preexist in primary tumors, which may become selected during ADT (Issacs & Coffey 1981, Fiñoes *et al.* 2013, Liu *et al.* 2015). Interestingly, in many reported PCSC populations in untreated PCa models or primary tumors, AR expression is often low or undetectable (Fig. 2). For example, the CD44$^+$α2β1$^+$CD133$^+$ cells purified from seven human tumor samples (Collins *et al.* 2005), the ABCG2$^+$ putative PCSCs (Huss *et al.* 2005), and the CD44$^+$ cells in several PCa xenografts (Patrawala *et al.* 2006) were all AR$^-$. In fact, the AR$^-$CD44$^+$ PCSCs were shown to be able to differentiate, at the clonal level, into AR$^+$CD44$^-$ cells (Patrawala *et al.* 2006). Gu *et al.* (2007) also showed that the human prostate epithelial cells immortalized by overexpressing hTERT (HPET cells)-expressed stem cell molecules, such as CD44 and Nanog, could regenerate three prostate epithelial cell types and were AR negative. Miki *et al.* (2007) showed mutually exclusive expression patterns of CD133 and AR by IHC

http://erc.endocrinology-journals.org
DOI: 10.1530/ERC-15-0217

Published by Bioscientifica Ltd.

staining in 16 clinical specimens. Rajasekhar *et al*. (2011) reported both AR and PSA negativity in the TRA-1-60$^+$CD151$^+$and CD166$^+$ PCSC population, which possessed high tumorigenic ability and could generate differentiated AR$^+$ and PSA$^+$ tumors *in vivo*. The docetaxel-resistant PCSCs that lacked the expression of MHC molecules were also negative for AR and PSA (Domingo-Domenech *et al*. 2012). Likewise, the PSA$^{-/lo}$ PCSC population was enriched in AR$^-$ PCa cells (Qin *et al*. 2012, Liu *et al*. 2015). These and many other studies (reviewed in Liu *et al*. 2015) suggest that PCSCs in primary and untreated tumors seem to be generally AR$^-$; in other words, AR$^-$ (and PSA$^-$) cells are highly enriched in primary and/or untreated PCSC populations (Fig. 2). Vice versa, loss of AR expression has been shown to promote PCSC generation through SATA3 signaling (Schroeder *et al*. 2014). It remains to be seen whether the AR$^+$ and AR$^-$ PCa cells in untreated/primary PCa possess distinct self-renewal, tumor-propagating properties, and drug sensitivities as these two populations of PCa cells have not been prospectively separated, purified out, and compared for their biological properties.

PCSCs in untreated PCa remain AR$^-$ presumably because these cells are simply less differentiated. Alternatively, molecules such as ABCG2 are preferentially expressed in PCSCs (Huss *et al*. 2005), which mediates the efflux of androgens leading to the degradation of ligand-less AR in PCSCs. We have shown that at least some of the PCSCs (e.g., SP, CD44$^+$, ABCG2$^+$, and PSA$^{-/lo}$) have been able to self-renew based on serial tumor-transplantation assays and asymmetric cell divisions using clonal and time-lapse analyses (Patrawala *et al*. 2005, 2006, Qin *et al*. 2012, Liu *et al*. 2015). A fraction of PSA$^{-/lo}$ PCa cells can undergo authentic asymmetric cell division regenerating a PSA$^{-/lo}$ daughter cell as well as a differentiated PSA$^+$ cell, which subsequently undergoes rapid proliferation (Qin *et al*. 2012, Liu *et al*. 2015). Self-renewal is a shared property for both normal stem cells and CSCs, and, not surprisingly, many molecules and pathways that regulate self-renewal in normal stem cells have been reported to operate in PCSCs (Fig. 2). For example, we have shown that NANOG is preferentially expressed in several PCSC populations and its expression is important for CSC properties as its knockdown severely impairs tumor regeneration (Jeter *et al*. 2009). In contrast, inducible expression of NANOG alone is sufficient to reprogram bulk cancer cells into stem-like cancer cells with enhanced tumor-regenerating and tumor-propagating activities (Jeter *et al*. 2011). Our results suggest that certain pluripotency molecules may also be functionally important for PCSC self-renewal and other properties. In support, several other studies have similarly implicated OCT4 and SOX2 in conferring on PCSC activities (Linn *et al*. 2010, Kregel *et al*. 2013). Interestingly, reciprocal relationships between AR and NANOG, OCT4, and SOX2 have been noted in these studies.

Hedgehog (HH) and WNT signaling often act together and play important roles in regulating self-renewal. The importance of WNT/β-catenin signaling is illustrated by the observations that treatment of LNCaP and C4-2 cells with WNT-3a increased their sphere formation rate and size, with increased nuclear β-catenin accumulation (Bisson & Prowse 2009). Although AR antagonist bicalutamide reduced the sphere size, the sphere formation rate did not change, thus suggesting a role of WNT signaling in PCSC self-renewal independently from AR (Bisson & Prowse 2009). Bmi1 acts downstream of HH and has been shown to be necessary for self-renewal of several populations of normal stem cells as well as CSCs (Lessard & Sauvageau 2003, Park *et al*. 2003). Lukacs *et al*. (2010) investigated the effects of Bmi1 loss in the presence of overactivated Wnt signaling on murine prostate stem cells (PSCs) and demonstrated that Bmi1 expression was required for the Wnt pathway to modulate self-renewal in the PSCs. In addition, several other signaling molecules and pathways may also be involved in regulating PCSCs. For example, the PTEN/PI3K/AKT pathway has been reported to be essential for PCSC proliferation independent of AR status (Dubrovska *et al*. 2009).

The E-twenty-six (Ets)-related gene (ERG), which is essential to maintain adult HSC self-renewal during stress-induced hematopoiesis (Loughran *et al*. 2008, Ng *et al*. 2011), is deregulated in most PCa through the most common genetic event TMPRSS2-ERG fusion (Tomlins *et al*. 2005, Mosquera *et al*. 2009). TMPRSS2-ERG expression is associated with a relative increase in clonogenic PCa cells (Casey *et al*. 2012). Interestingly, although the expression of the TMPRSS2-ERG fusion gene is expected to occur in AR$^+$ PCa cells due to the TMPRESS2 regulation by AR, recent evidence suggests that the TMPRSS2-ERG fusion protein may also be expressed in the AR$^-$ PCSCs. Polson *et al*. (2013) demonstrated that in CD133$^+$α2β1$^+$primary tumor cells with stem cell properties, TMPRSS2-ERG and AR expression was not necessarily concordant. While most of the marker-positive cells were AR negative, they expressed ERG at both RNA and protein levels, which may help maintain the PCSC properties such as self-renewal in the marker positive cells (Polson *et al*. 2013).

http://erc.endocrinology-journals.org
DOI: 10.1530/ERC-15-0217

Published by Bioscientifica Ltd.

Taken together, the above discussions indicate that many well-known signaling molecules and pathways can regulate and confer the CSC properties in AR^- PCSCs (Chen *et al*. 2013, Rybak *et al*. 2015). These molecules and pathways represent obvious therapeutic targets, and therapeutics targeting these PCSC-specific signaling nodes could, in principle, be utilized in conjunction with the ADT regimens.

PCSCs in CRPC might be AR^+ or AR^-

It is well appreciated that AR heterogeneity becomes more pronounced in CRPCs than in the primary tumors (Liu *et al*. 2015) and activation of alternative AR signaling in PCa cells may promote PCa cell proliferation under androgen-deprived environment (Wang *et al*. 2009*a*). What is the cell of origin of CRPCs? AR^+ or AR^- PCa cells? As early as 1981, Isaacs and Coffey (1981), working on the Dunning R3327H rat prostatic adenocarcinoma model, proposed that castration selected for androgen-insensitive cells that preexisted in the untreated tumors. Craft *et al*. (1999), working on the LAPC9 xenograft model, also provided histological evidence for the outgrowth of the androgen-independent clones in the later stages of CRPC development. Fiñones *et al*. (2013) demonstrated androgen-independent PCa cells in untreated early-stage prostate adenocarcinomas. These androgen-independent and androgen-insensitive PCa cells may not necessarily be AR^-, because PCa cells that overexpress AR and splice variants that lack the LBD may also be insensitive or refractory to androgen ablation. Our recent work provided direct evidence of AR^- PCa cells in primary patient tumors (Liu *et al*. 2015). As many PCSCs have been shown to be AR^- and resistant to castration and other therapeutics (Qin *et al*. 2012, Chen *et al*. 2013, Liu *et al*. 2015, Rybak *et al*. 2015), it is reasonable to postulate that the AR^- PCa cells that preexist in untreated tumors could be favored as 'initiators' or the cells of origin of CRPCs (Fig. 3). These AR^- PCa cells could be expanded on the ADT-induced elimination of AR^+ cells as well as due to the de-differentiation from AR^+ PCa cells (Fig. 3), much like therapy- or microenvironment-induced de-differentiation of non-CSCs in other tumor systems (Tang 2012, Kreso & Dick 2014). As a result, the AR^- PCa cells in CRPCs may function as the CSCs for the AR^- CRPC clones (Fig. 3). The best example is the $PSA^{-/lo}$ PCSC population, which has been evinced to possess significant tumor-regenerating and tumor-propagating activities in fully castrated male mice (Qin *et al*. 2012). Germann *et al*. (2012) showed that PCa cells expressing stem cell markers such as ALDH1A1 and NANOG became enriched in the BM18 castration model, and the castration-resistant stem-like PCa cells had a luminal progenitor phenotype but were negative for AR. Jiao *et al*. (2012) identified a $CD166^+$ cell population in both human and mouse CRPCs, which was enriched in basal stem/progenitor cells that were $CK5^+/p63^+/CK8^+/AR^-/TROP2^{hi}$ and displayed enhanced sphere formation and tissue regeneration abilities. Also, studies on NANOG (Jeter *et al*. 2009, 2011) and SOX2 (Kregel *et al*. 2013) show that PCa cells expressing these molecules are castration resistant and express relatively low levels of AR. These observations raise the possibility that the AR^- PCSCs may gain growth advantages in an androgen-deficient environment, leading to distinct AR^- clones in CRPC (Fig. 3).

On the other hand, most CRPCs clearly have AR^+ cells and clones (Liu *et al*. 2015). Although these AR^+ cells in CRPCs can potentially be derived from the differentiation of AR^- PCa cells (Fig. 2), it is very likely that at least some AR^+ PCa cells can survive androgen deprivation and function as the cells of origin as well as CSCs for CRPCs (Fig. 3). This is not very difficult to understand because the AR^+ PCa cells in most untreated primary tumors constitute the bulk cell population (Fig. 2). It is conceivable that due to their abundance, some of these AR^+ PCa cells, under the selective pressure from androgen deprivation, may selectively gain genetic alterations such as the *AR* gene amplification and TMPRSS2-ERG fusion, resulting in the expansion of AR^+ clones (Fig. 3, right). In the resultant AR^+ PCa cell clones, AR may likely be still functioning to regulate both conventional as well as new AR target genes (Wang *et al*. 2009*a*). The regulation of conventional AR targets can be achieved through intratumoral androgen synthesis. Alternatively, AR signaling in the AR^+ CRPC clones may be executed through ligand-independent AR splice variants and/or AR crosstalks with activated receptors such as the epidermal growth factor receptor (EGFR). In fact, there is evidence that certain AR^+ cell populations are refractory to castration and can function as the cell of origin for PCa in mouse models. Wang *et al*. (2009*b*) showed that castration-resistant Nkx3.1-expressing cells (CARNs) that expressed luminal markers including AR represented a rare population of androgen-resistant cells in the murine prostate that could function as the cells of origin for PCa caused by *Pten* deletion.

Interestingly, expressing wild-type AR at physiological levels in AR^- PC3 cells induced growth inhibition (Litvinov *et al*. 2006), whereas knocking down AR in AR-expressing metastatic PCa cells like LNCaP and its

http://erc.endocrinology-journals.org
DOI: 10.1530/ERC-15-0217

Published by Bioscientifica Ltd.

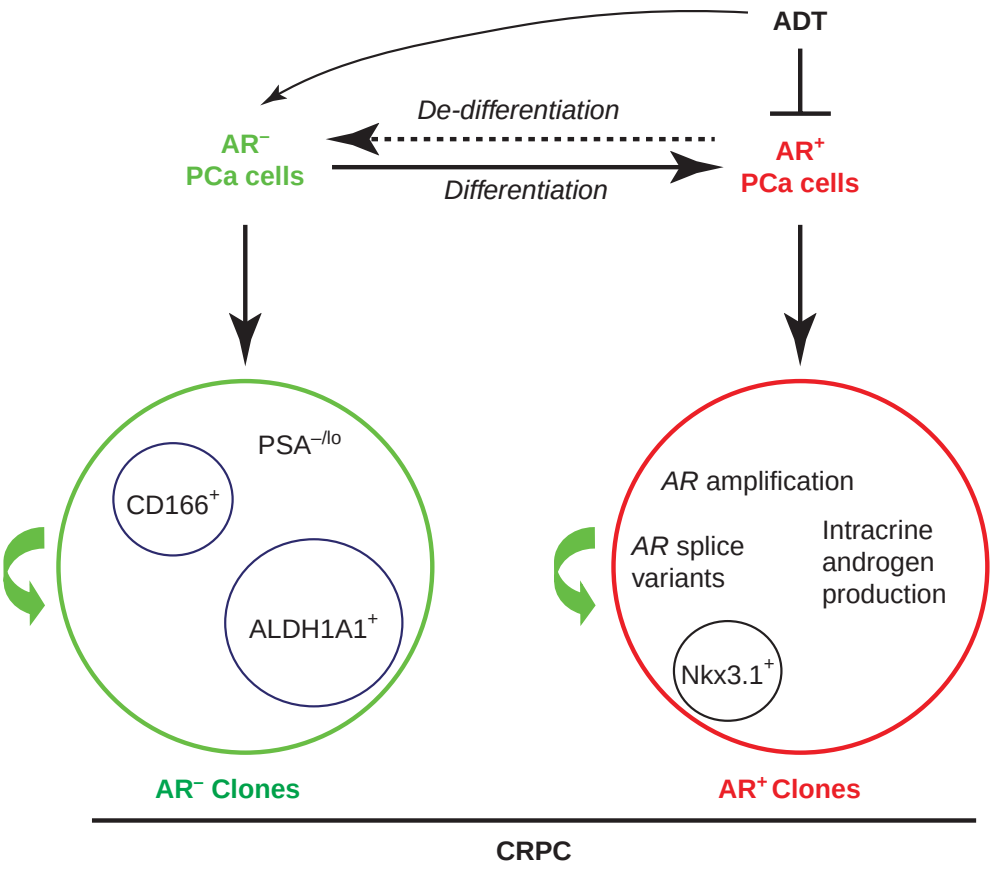

Figure 3

Hypothetical PCSCs in CRPC. Androgen-deprivation therapy (ADT) selectively targets androgen receptor (AR)$^+$ prostate cancer (PCa) cells and has been shown to enrich AR$^-$ PCa cells, which may result from preferential elimination by ADT of AR$^+$ cells as well as de-differentiation of AR$^+$PCa cells to AR$^-$cells (top). Clinical castration-resistant PCas (CRPCs) contain distinct AR$^+$ and AR$^-$ clones, both of which might contain their own CSCs. In AR$^+$clones, PCSCs could have *AR* amplification or ligand-independent AR signaling pathways to support the self-renewal in an androgen-deprived environment. Several potential cancer stem cell (CSC) subpopulations in AR$^-$ and AR$^+$ PCa cell clones are indicated.

derivative C4-2 resulted in growth inhibition and apoptotic cell death and compromised tumor development (Cheng *et al.* 2006, Snoek, *et al.* 2009). The contrasting roles of AR in AR$^-$ vs AR$^+$ PCa cell lines imply differential involvement of AR in AR$^+$ and AR$^-$ PCSCs in CRPCs. Regardless, the phenotype of PCSCs in CRPCs may well be context dependent, and both AR$^+$ and AR$^-$ clones, which possess their own intraclonal CSCs, likely coexist in hormone-refractory tumors (Fig. 3). The development of critical experimental tools that can allow the prospective separation of AR$^+$ and AR$^-$ CRPC cells is needed to clarify the precise functions of AR$^+$ vs AR$^-$ PCSCs in CRPC.

AR and PCSCs in PCa metastasis

Metastasis is common in CRPC patients. The acquisition of invasive properties through epithelial-mesenchymal transition (EMT), a normal development process, is crucial for the evolution of metastatic populations (Tam & Weinberg 2013, Puisieux *et al.* 2014). There is accumulating evidence supporting the fact that ADT may induce an EMT in PCa cells (Jennbacken *et al.* 2010, Tanaka *et al.* 2010, Sun *et al.* 2012, 2014, Wu *et al.* 2012, Jacob *et al.* 2014), and EMT is well known to promote CSC traits. Studies by Tanaka *et al.* (2010) and Jennbacken *et al.* (2010) showed that N-cadherin was upregulated in castration-resistant LNCaP, LAPC4, and LAPC9 xenograft models. Sun *et al.* (2012) interrogated EMT marker expression in mouse and human CRPC samples and observed overall higher levels of mesenchymal markers in CRPC compared to non-castrated samples. They proposed a negative feedback loop model between ZEB1 and AR to explain the ADT-induced EMT. To some extent, AR signaling may be involved in the EMT switching in PCa cells. The study on AR and ZEB2 suggests that AR may function differently between AR$^+$ and AR$^-$ cell lines (Jacob *et al.* 2014).

http://erc.endocrinology-journals.org
DOI: 10.1530/ERC-15-0217

Published by Bioscientifica Ltd.

Specifically, ZEB2 expression positively correlate with AR expression in LNCaP cells, but the opposite is true in PC3 and DU145 cells. In addition, the AR splice variants AR3 and ARv567es were shown to promote EMT in PCa cells (Wu *et al*. 2012, Sun *et al*. 2014).

CSCs not only play an important role in tumor initiation and treatment resistance but also seem to be involved in distant metastases. Tanaka *et al*. (2010) have shown that the castration-resistant, N-cadherin positive PCa cells are enriched in stem cell markers including CD44 and NANOG. *Vice versa*, $Lin^-CD44^+CD133^+Sca\text{-}1^+CD117^+$ mouse PSCs express higher levels of mesenchymal markers N-cadherin and vimentin compared to the non-stem cells (Sun *et al*. 2012). On the other hand, EMT may also suppress the stemness in PCa cells (Celia-Terrassa *et al*. 2012). This is not entirely surprising because mesenchymal-epithelial transition (MET) is equally important and required for metastatic colonization. Research on the role of MET in PCa metastasis is very limited.

Clinical implications and perspectives

Studies about the potential prognostic role of AR in PCa are controversial, and most evidence suggests that AR is not prognostic in PCa (Ford *et al*. 2003, Fleischmann *et al*. 2011, Minner *et al*. 2011, Tamburrino *et al*. 2012, Lu-Yao *et al*. 2014). Minner *et al*. (2011) examined the AR expression in more than 2800 treatment-naïve PCa patient samples and observed no significant correlation between the AR expression level and the risk of biochemical recurrence. Studies by Fleischmann *et al*. (2011) of 382 lymph node metastases showed that AR is not prognostic in node positive PCa although higher AR does correlate with a larger size of metastases. Despite significant improvements in the efficiency of the ADT to block AR signaling, up to now, there is also no clear correlation between androgen signaling ablation and patient prognosis. A study by Ford *et al*. (2003) in 24 CRPC patients showed that 33% of patients have AR amplification and the patients with AR gene amplification had a recurrence 5 months earlier than those without amplification; however, no statistically significant survival disadvantage was observed in the AR amplified patients. More recently, Lu-Yao *et al*. (2014) performed a median 110 months follow-up study of a cohort consisting of 66 717 PCa patients who underwent primary ADT or conservative management and found that primary ADT was not associated with improved long-term overall or disease-specific patient survival. Furthermore, the AR heterogeneity in PCa indicates that targeting AR signaling alone may be of a limited role in preventing disease recurrence in the long term.

PCSCs may represent the driving force of tumor progression and metastases. A number of studies have shown that the expression of stem-cell markers has prognostic significance in PCa, as well as other cancer types (Kakarala & Wicha 2008, Li, *et al*. 2010). Studies on $PSA^{-/lo}$ PCSCs suggest that intratumoral PSA expression is inversely correlated with the tumor Gleason score and patient survival (Qin *et al*. 2012). Multiple studies have shown that the AR^- tumor cells are enriched in PCSC populations, implicating a pivotal role of PCSCs in ADT resistance. Hence, targeting PCSCs specifically in an adjuvant setting might be helpful in preventing CRPC. Preclinical studies in PCSCs targeting have provided promising results. For instance, we have demonstrated that microRNA-34a (miR-34a) potently inhibits the PCa progression and metastasis via directly targeting CD44 (Liu *et al*. 2011). We have also reported several other microRNAs including let7b and miR-128 in suppressing PCSC self-renewal and tumor progression (Liu & Tang 2011, Liu *et al*. 2012, Jin *et al*. 2014). At the same time, direct inhibition of WNT, PTEN/PI3K/AKT, and others cell-signaling pathways has shown tumor suppressive effects via lowering PCSCs population (e.g., Dubrovska *et al*. 2010, Rybak *et al*. 2015).

Understanding and elucidating the roles of and the interrelationship between AR heterogeneity and PCSCs could offer fresh insight on designing novel therapeutics to target lethal CRPC and metastasis. Recent evidence suggests that in untreated tumors, PCSCs seem to be largely AR^-,whereas in CRPCs, PCSCs may be either AR^+ or AR^-. In other words, both AR^+ and AR^- PCa cell clones coexist in most CRPCs (Fig. 3). In principle, PCSCs, whether AR^+or AR^-, are endowed with the fundamental trait of stemness, which is regulated by unique cohorts of genes, epigenetic landscape, and environmental factors (Kreso & Dick 2014). It is high time for us to develop novel therapeutics that target the stemness of PCSCs, which, when used in conjunction with ADT, should help prevent tumor recurrence.

Declaration of interest

The authors declare that there is no conflict of interest that could be perceived as prejudicing the impartiality of this review.

Funding

Work in the authors' lab was supported, in part, by grants from NIH (NCI R01-CA155693), DOD (W81XWH-13-1-0352 and W81XWH-14-1-0575), CPRIT (RP120380), and MDACC Center for Cancer Epigenetics (D G Tang).

http://erc.endocrinology-journals.org
DOI: 10.1530/ERC-15-0217

Published by Bioscientifica Ltd.

Author contribution statement
Q Deng and D G Tang conceptualized the paper; Q Deng wrote the draft; D G Tang finalized the manuscript.

Acknowledgements
We thank other members of the Tang lab for helpful discussions. We apologize to the colleagues whose work was not cited due to space constraint.

References

Berger MF, Lawrence MS, Demichelis F, Drier Y, Cibulskis K, Sivachenko AY, Sboner A, Esgueva R, Pflueger D, Sougnez C *et al.* 2011 The genomic complexity of primary human prostate cancer. *Nature* **470** 214–220. (doi:10.1038/nature09744)

Bisson I & Prowse DM 2009 WNT signaling regulates self-renewal and differentiation of prostate cancer cells with stem cell characteristics. *Cell Research* **19** 683–697. (doi:10.1038/cr.2009.43)

Casey OM, Fang L, Hynes PG, Abou-Kheir WG, Martin PL, Tillman HS, Petrovics G, Awwad HO, Ward Y, Lake R *et al.* 2012 TMPRSS2- driven ERG expression *in vivo* increases self-renewal and maintains expression in a castration resistant subpopulation. *PLoS ONE* **7** e41668. (doi:10.1371/journal.pone.0041668)

Celia-Terrassa T, Meca-Cortes O, Mateo F, de Paz AM, Rubio N, Arnal-Estape A, Ell BJ, Bermudo R, Diaz A, Guerra-Rebollo M *et al.* 2012 Epithelial-mesenchymal transition can suppress major attributes of human epithelial tumor-initiating cells. *Journal of Clinical Investigation* **122** 1849–1868. (doi:10.1172/JCI59218)

Chen X, Rycaj K, Liu X & Tang DG 2013 New insights into prostate cancer stem cells. *Cell Cycle* **12** 579–586. (doi:10.4161/cc.23721)

Cheng H, Snoek R, Ghaidi F, Cox ME & Rennie PS 2006 Short hairpin RNA knockdown of the androgen receptor attenuates ligand-independent activation and delays tumor progression. *Cancer Research* **66** 10613–10620. (doi:10.1158/0008-5472.CAN-06-0028)

Chodak GW, Kranc DM, Puy LA, Takeda H, Johnson K & Chang C 1992 Nuclear localization of androgen receptor in heterogeneous samples of normal, hyperplastic and neoplastic human prostate. *Journal of Urology* **147** 798–803.

Collins AT, Berry PA, Hyde C, Stower MJ & Maitland NJ 2005 Prospective identification of tumorigenic prostate cancer stem cells. *Cancer Research* **65** 10946–10951. (doi:10.1158/0008-5472.CAN-05-2018)

Cooper CS, Eeles R, Wedge DC, Van Loo P, Gundem G, Alexandrov LB, Kremeyer B, Butler A, Lynch AG, Camacho N *et al.* 2015 Analysis of the genetic phylogeny of multifocal prostate cancer identifies multiple independent clonal expansions in neoplastic and morphologically normal prostate tissue. *Nature Genetics* **47** 367–372. (doi:10.1038/ng.3221)

Craft N, Chhor C, Tran C, Belldegrun A, DeKernion J, Witte ON, Said J, Reiter RE & Sawyers CL 1999 Evidence for clonal outgrowth of androgen-independent prostate cancer cells from androgen-dependent tumors through a two-step process. *Cancer Research* **59** 5030–5036.

Davis JN, Wojno KJ, Daignault S, Hofer MD, Kuefer R, Rubin MA & Day ML 2006 Elevated E2F1 inhibits transcription of the androgen receptor in metastatic hormone-resistant prostate cancer. *Cancer Research* **66** 11897–11906. (doi:10.1158/0008-5472.CAN-06-2497)

Domingo-Domenech J, Vidal SJ, Rodriguez-Bravo V, Castillo-Martin M, Quinn SA, Rodriguez-Barrueco R, Bonal DM, Charytonowicz E, Gladoun N, de la Iglesia-Vicente J *et al.* 2012 Suppression of acquired docetaxel resistance in prostate cancer through depletion of notch- and hedgehog-dependent tumor-initiating cells. *Cancer Cell* **22** 373–388. (doi:10.1016/j.ccr.2012.07.016)

Dubrovska A, Kim S, Salamone RJ, Walker JR, Maira SM, Garcia-Echeverria C, Schultz PG & Reddy VA 2009 The role of PTEN/Akt/PI3K signaling in the maintenance and viability of prostate cancer stem-like cell populations. *PNAS* **106** 268–273. (doi:10.1073/pnas.0810956106)

Dubrovska A, Elliott J, Salamone RJ, Kim S, Aimone LJ, Walker JR, Watson J, Sauveur-Michel M, Garcia-Echeverria C, Cho CY *et al.* 2010 Combination therapy targeting both tumor-initiating and differentiated cell populations in prostate carcinoma. *Clinical Cancer Research* **16** 5692–5702. (doi:10.1158/1078-0432.CCR-10-1601)

Ellwood-Yen K, Graeber TG, Wongvipat J, Iruela-Arispe ML, Zhang J, Matusik R, Thomas GV & Sawyers CL 2003 Myc-driven murine prostate cancer shares molecular features with human prostate tumors. *Cancer Cell* **4** 223–238. (doi:10.1016/S1535-6108(03)00197-1)

Fiñones RR, Yeargin J, Lee M, Kaur AP, Cheng C, Sun P, Wu C, Nguyen C, Wang-Rodriguez J, Meyer AN *et al.* 2013 Early human prostate adenocarcinomas harbor androgen-independent cancer cells. *PLoS ONE* **8** e74438. (doi:10.1371/journal.pone.0074438)

Fleischmann A, Rocha C, Schobinger S, Seiler R, Wiese B & Thalmann GN 2011 Androgen receptors are differentially expressed in Gleason patterns of prostate cancer and down-regulated in matched lymph node metastases. *Prostate* **71** 453–460. (doi:10.1002/pros.21259)

Ford OH III, Gregory CW, Kim D, Smitherman AB & Mohler JL 2003 Androgen receptor gene amplification and protein expression in recurrent prostate cancer. *Journal of Urology* **170** 1817–1821. (doi:10.1097/01.ju.0000091873.09677.f4)

Germann M, Wetterwald A, Guzman-Ramirez N, van der Pluijm G, Culig Z, Cecchini MG, Williams ED & Thalmann GN 2012 Stem-like cells with luminal progenitor phenotype survive castration in human prostate cancer. *Stem Cells* **30** 1076–1086. (doi:10.1002/stem.1087)

Grasso CS, Wu YM, Robinson DR, Cao X, Dhanasekaran SM, Khan AP, Quist MJ, Jing X, Lonigro RJ, Brenner JC *et al.* 2012 The mutational landscape of lethal castration-resistant prostate cancer. *Nature* **487** 239–243. (doi:10.1038/nature11125)

Gu G, Yuan J, Wills M & Kasper S 2007 Prostate cancer cells with stem cell characteristics reconstitute the original human tumor *in vivo*. *Cancer Research* **67** 4807–4815. (doi:10.1158/0008-5472.CAN-06-4608)

Haffner MC, Mosbruger T, Esopi DM, Fedor H, Heaphy CM, Walker DA, Adejola N, Gurel M, Hicks J, Meeker AK *et al.* 2013 Tracking the clonal origin of lethal prostate cancer. *Journal of Clinical Investigation* **123** 4918–4922. (doi:10.1172/JCI70354)

Haffner MC, De Marzo AM, Yegnasubramanian S, Epstein JI & Carter HB 2015 Diagnostic challenges of clonal heterogeneity in prostate cancer. *Journal of clinical oncology* **33** e38–e40. (doi:10.1200/JCO.2013.50.3540)

Huss WJ, Gray DR, Greenberg NM, Mohler JL & Smith GJ 2005 Breast cancer resistance protein-mediated efflux of androgen in putative benign and malignant prostate stem cells. *Cancer Research* **65** 6640–6650. (doi:10.1158/0008-5472.CAN-04-2548)

Isaacs JT & Coffey DS 1981 Adaptation versus selection as the mechanism responsible for the relapse of prostatic cancer to androgen ablation therapy as studied in the Dunning R-3327-H adenocarcinoma. *Cancer Research* **41** 5070–5075.

Jacob S, Nayak S, Fernandes G, Barai RS, Menon S, Chaudhari UK, Kholkute SD & Sachdeva G 2014 Androgen receptor as a regulator of ZEB2 expression and its implications in epithelial-to-mesenchymal transition in prostate cancer. *Endocrine-Related Cancer* **21** 473–486. (doi:10.1530/ERC-13-0514)

Jennbacken K, Tesan T, Wang W, Gustavsson H, Damber JE & Welen K 2010 N-cadherin increases after androgen deprivation and is associated with metastasis in prostate cancer. *Endocrine-Related Cancer* **17** 469–479. (doi:10.1677/ERC-10-0015)

Jeter CR, Badeaux M, Choy G, Chandra D, Patrawala L, Liu C, Calhoun-Davis T, Zaehres H, Daley GQ & Tang DG 2009 Functional evidence that the self-renewal gene NANOG regulates human tumor development. *Stem Cells* **27** 993–1005. (doi:10.1002/stem.29)

Jeter CR, Liu B, Liu X, Chen X, Liu C, Calhoun-Davis T, Repass J, Zaehres H, Shen JJ & Tang DG 2011 NANOG promotes cancer stem cell

Published by Bioscientifica Ltd.

characteristics and prostate cancer resistance to androgen deprivation. *Oncogene* **30** 3833–3845. (doi:10.1038/onc.2011.114)

Jiao J, Hindoyan A, Wang S, Tran LM, Goldstein AS, Lawson D, Chen D, Li Y, Guo C, Zhang B *et al.* 2012 Identification of CD166 as a surface marker for enriching prostate stem/progenitor and cancer initiating cells. *PLoS ONE* **7** e42564. (doi:10.1371/journal.pone.0042564)

Jin M, Zhang T, Liu C, Badeaux MA, Liu B, Liu R, Jeter C, Chen X, Vlassov AV & Tang DG 2014 miRNA-128 suppresses prostate cancer by inhibiting BMI-1 to inhibit tumor-initiating cells. *Cancer Research* **74** 4183–4195. (doi:10.1158/0008-5472.CAN-14-0404)

Kakarala M & Wicha MS 2008 Implications of the cancer stem-cell hypothesis for breast cancer prevention and therapy. *Journal of clinical oncology* **26** 2813–2820. (doi:10.1200/JCO.2008.16.3931)

Kerkhofs S, Denayer S, Haelens A & Claessens F 2009 Androgen receptor knockout and knock-in mouse models. *Journal of molecular endocrinology* **42** 11–17. (doi:10.1677/JME-08-0122)

Kregel S, Kiriluk KJ, Rosen AM, Cai Y, Reyes EE, Otto KB, Tom W, Paner GP, Szmulewitz RZ & VanderGriend DJ 2013 Sox2 is an androgen receptor-repressed gene that promotes castration-resistant prostate cancer. *PLoS ONE* **8** e53701. (doi:10.1371/journal.pone.0053701)

Kreso A & Dick JE 2014 Evolution of the cancer stem cell model. *Cell Stem Cell* **14** 275–291. (doi:10.1016/j.stem.2014.02.006)

Kroon P, Berry PA, Stower MJ, Rodrigues G, Mann VM, Simms M, Bhasin D, Chettiar S, Li C, Li PK *et al.* 2013 JAK-STAT blockade inhibits tumor initiation and clonogenic recovery of prostate cancer stem-like cells. *Cancer Research* **73** 5288–5298. (doi:10.1158/0008-5472.CAN-13-0874)

van der Kwast TH, Schalken J, Ruizeveld de Winter JA, van Vroonhoven CC, Mulder E, Boersma W & Trapman J 1991 Androgen receptors in endocrine-therapy-resistant human prostate cancer. *International Journal of Cancer* **48** 189–193. (doi:10.1002/ijc.2910480206)

Lessard J & Sauvageau G 2003 Bmi-1 determines the proliferative capacity of normal and leukaemic stem cells. *Nature* **423** 255–260. (doi:10.1038/nature01572)

Li HW, Chen X, Calhoun-Davis T, Claypool K & Tang DG 2008*a* PC3 human prostate carcinoma cell holoclones contain self-renewing tumor-initiating cells. *Cancer Research* **68** 1820–1825. (doi:10.1158/0008-5472.CAN-07-5878)

Li ZG, Mathew P, Yang J, Starbuck MW, Zurita AJ, Liu J, Sikes C, Multani AS, Efstathiou E, Lopez A *et al.* 2008*b* Androgen receptor-negative human prostate cancer cells induce osteogenesis in mice through FGF9-mediated mechanisms. *Journal of Clinical Investigation* **118** 2697–2710. (doi:10.1172/JCI33637C1)

Li T, Su Y, Mei Y, Leng Q, Leng B, Liu Z, Stass SA & Jiang F 2010 ALDH1A1 is a marker for malignant prostate stem cells and predictor of prostate cancer patients' outcome. *Laboratory Investigation* **90** 234–244. (doi:10.1038/labinvest.2009.127)

Linn DE, Yang X, Sun F, Xie Y, Chen H, Jiang R, Chen H, Chumsri S, Burger AM & Qiu Y 2010 A role for OCT4 in tumor initiation of drug-resistant prostate cancer cells. *Genes & Cancer* **1** 908–916. (doi:10.1177/1947601910388271)

Litvinov IV, Antony L, Dalrymple SL, Becker R, Cheng L & Isaacs JT 2006 PC3, but not DU145, human prostate cancer cells retain the coregulators required for tumor suppressor ability of androgen receptor. *Prostate* **66** 1329–1338. (doi:10.1002/pros.20483)

Liu C & Tang DG 2011 MicroRNA regulation of cancer stem cells. *Cancer Research* **71** 5950–5954. (doi:10.1158/0008-5472.CAN-11-1035)

Liu C, Kelnar K, Liu B, Chen X, Calhoun-Davis T, Li H, Patrawala L, Yan H, Jeter C, Honorio S *et al.* 2011 The microRNA miR-34a inhibits prostate cancer stem cells and metastasis by directly repressing CD44. *Nature Medicine* **17** 211–215. (doi:10.1038/nm.2284)

Liu C, Kelnar K, Vlassov AV, Brown D, Wang J & Tang DG 2012 Distinct microRNA expression profiles in prostate cancer stem/progenitor cells and tumor-suppressive functions of let-7. *Cancer Research* **72** 3393–3404. (doi:10.1158/0008-5472.CAN-11-3864)

Liu X, Chen X, Chen X, Rycaj K, Chao HP, Deng Q, Jeter C, Liu C, Honorio S & Li H 2015 Systematic dissection of phenotypic, functional, and tumorigenic heterogeneity of human prostate cancer cells. *Oncotarget* [in press].

Loughran SJ, Kruse EA, Hacking DF, de Graaf CA, Hyland CD, Willson TA, Henley KJ, Ellis S, Voss AK, Metcalf D *et al.* 2008 The transcription factor Erg is essential for definitive hematopoiesis and the function of adult hematopoietic stem cells. *Nature Immunology* **9** 810–819. (doi:10.1038/ni.1617)

Lukacs RU, Memarzadeh S, Wu H & Witte ON 2010 Bmi-1 is a crucial regulator of prostate stem cell self-renewal and malignant transformation. *Cell Stem Cell* **7** 682–693. (doi:10.1016/j.stem.2010.11.013)

Lu-Yao GL, Albertsen PC, Moore DF, Shih W, Lin Y, DiPaola RS & Yao SL 2014 Fifteen-year survival outcomes following primary androgen-deprivation therapy for localized prostate cancer. *JAMA Internal Medicine* **174** 1460–1467. (doi:10.1001/jamainternmed.2014.3028)

Masai M, Sumiya H, Akimoto S, Yatani R, Chang CS, Liao SS & Shimazaki J 1990 Immunohistochemical study of androgen receptor in benign hyperplastic and cancerous human prostates. *Prostate* **17** 293–300. (doi:10.1002/pros.2990170405)

Miki J, Furusato B, Li H, Gu Y, Takahashi H, Egawa S, Sesterhenn IA, McLeod DG, Srivastava S & Rhim JS 2007 Identification of putative stem cell markers, CD133 and CXCR4, in hTERT-immortalized primary nonmalignant and malignant tumor-derived human prostate epithelial cell lines and in prostate cancer specimens. *Cancer Research* **67** 3153–3161. (doi:10.1158/0008-5472.CAN-06-4429)

Minner S, Enodien M, Sirma H, Luebke AM, Krohn A, Mayer PS, Simon R, Tennstedt P, Muller J, Scholz L *et al.* 2011 ERG status is unrelated to PSA recurrence in radically operated prostate cancer in the absence of antihormonal therapy. *Clinical Cancer Research* **17** 5878–5888. (doi:10.1158/1078-0432.CCR-11-1251)

Mosquera JM, Mehra R, Regan MM, Perner S, Genega EM, Bueti G, Shah RB, Gaston S, Tomlins SA, Wei JT *et al.* 2009 Prevalence of TMPRSS2-ERG fusion prostate cancer among men undergoing prostate biopsy in the United States. *Clinical Cancer Research* **15** 4706–4711. (doi:10.1158/1078-0432.CCR-08-2927)

Ng AP, Loughran SJ, Metcalf D, Hyland CD, de Graaf CA, Hu Y, Smyth GK, Hilton DJ, Kile BT & Alexander WS 2011 Erg is required for self-renewal of hematopoietic stem cells during stress hematopoiesis in mice. *Blood* **118** 2454–2461. (doi:10.1182/blood-2011-03-344739)

Niu Y, Altuwaijri S, Yeh S, Lai KP, Yu S, Chuang KH, Huang SP, Lardy H & Chang C 2008 Targeting the stromal androgen receptor in primary prostate tumors at earlier stages. *PNAS* **105** 12188–12193. (doi:10.1073/pnas.0804701105)

Park IK, Qian D, Kiel M, Becker MW, Pihalja M, Weissman IL, Morrison SJ & Clarke MF 2003 Bmi-1 is required for maintenance of adult self-renewing haematopoietic stem cells. *Nature* **423** 302–305. (doi:10.1038/nature01587)

Patrawala L, Calhoun T, Schneider-Broussard R, Zhou J, Claypool K & Tang DG 2005 Side population is enriched in tumorigenic, stem-like cancer cells, whereas ABCG2+ and ABCG2- cancer cells are similarly tumorigenic. *Cancer Research* **65** 6207–6219. (doi:10.1158/0008-5472.CAN-05-0592)

Patrawala L, Calhoun T, Schneider-Broussard R, Li H, Bhatia B, Tang S, Reilly JG, Chandra D, Zhou J, Claypool K *et al.* 2006 Highly purified CD44+ prostate cancer cells from xenograft human tumors are enriched in tumorigenic and metastatic progenitor cells. *Oncogene* **25** 1696–1708. (doi:10.1038/sj.onc.1209327)

Patrawala L, Calhoun-Davis T, Schneider-Broussard R & Tang DG 2007 Hierarchical organization of prostate cancer cells in xenograft tumors: the CD44+α2β1+ cell population is enriched in tumor-initiating cells. *Cancer Research* **67** 6796–6805. (doi:10.1158/0008-5472.CAN-07-0490)

Polson ES, Lewis JL, Celik H, Mann VM, Stower MJ, Simms MS, Rodrigues G, Collins AT & Maitland NJ 2013 Monoallelic expression of TMPRSS2/ERG in prostate cancer stem cells. *Nature Communications* **4** 1623. (doi:10.1038/ncomms2627)

Published by Bioscientifica Ltd.

Puisieux A, Brabletz T & Caramel J 2014 Oncogenic roles of EMT-inducing transcription factors. *Nature Cell Biology* **16** 488–494. (doi:10.1038/ncb2976)

Qin J, Liu X, Laffin B, Chen X, Choy G, Jeter CR, Calhoun-Davis T, Li H, Palapattu GS, Pang S *et al.* 2012 The PSA-/lo prostate cancer cell population harbors self-renewing long-term tumor-propagating cells that resist castration. *Cell Stem Cell* **10** 556–569. (doi:10.1016/j.stem.2012.03.009)

Quigley CA, De Bellis A, Marschke KB, el-Awady MK, Wilson EM & French FS 1995 Androgen receptor defects: historical, clinical, and molecular perspectives. *Endocrine Reviews* **16** 271–321. (doi:10.1210/edrv-16-3-271)

Rajasekhar VK, Studer L, Gerald W, Socci ND & Scher HI 2011 Tumour-initiating stem-like cells in human prostate cancer exhibit increased NF-kappaB signalling. *Nature Communications* **2** 162. (doi:10.1038/ncomms1159)

Robinson D, Van Allen EM, Wu YM, Schultz N, Lonigro RJ, Mosquera JM, Montgomery B, Taplin ME, Pritchard CC, Attard G *et al.* 2015 Integrative clinical genomics of advanced prostate cancer. *Cell* **161** 1215–1228. (doi:10.1016/j.cell.2015.05.001)

Ruizeveld de Winter JA, Trapman J, Brinkmann AO, Boersma WJ, Mulder E, Schroeder FH, Claassen E & van der Kwast TH 1990 Androgen receptor heterogeneity in human prostatic carcinomas visualized by immunohistochemistry. *Journal of Pathology* **160** 329–332. (doi:10.1002/path.1711600409)

Ruizeveld de Winter JA, Janssen PJ, Sleddens HM, Verleun-Mooijman MC, Trapman J, Brinkmann AO, Santerse AB, Schroder FH & van der Kwast TH 1994 Androgen receptor status in localized and locally progressive hormone refractory human prostate cancer. *American Journal of Pathology* **144** 735–746.

Rybak AP, Bristow RG & Kapoor A 2015 Prostate cancer stem cells: deciphering the origins and pathways involved in prostate tumorigenesis and aggression. *Oncotarget* **6** 1900–1919.

Rycaj K & Tang DG 2015 Cell-of-origin of cancer versus cancer stem cells: Assays and interpretations. *Cancer Research* [in press]. (doi:10.1158/0008-5472.CAN-15-0798)

Sadi MV & Barrack ER 1993 Image analysis of androgen receptor immunostaining in metastatic prostate cancer. Heterogeneity as a predictor of response to hormonal therapy. *Cancer* **71** 2574–2580. (doi:10.1002/1097-0142(19930415)71:8<2574::AID-CNCR2820710823>3.0.CO;2-1)

Sadi MV, Walsh PC & Barrack ER 1991 Immunohistochemical study of androgen receptors in metastatic prostate cancer. Comparison of receptor content and response to hormonal therapy. *Cancer* **67** 3057–3064. (doi:10.1002/1097-0142(19910615)67:12<3057::AID-CNCR2820671221>3.0.CO;2-S)

Schroeder A, Herrmann A, Cherryholmes G, Kowolik C, Buettner R, Pal S, Yu H, Müller-Newen G & Jove R 2014 Loss of androgen receptor expression promotes a stem-like cell phenotype in prostate cancer through STAT3 signaling. *Cancer Research* **74** 1227–1237. (doi:10.1158/0008-5472.CAN-13-0594)

Shah RB, Mehra R, Chinnaiyan AM, Shen R, Ghosh D, Zhou M, Macvicar GR, Varambally S, Harwood J, Bismar TA *et al.* 2004 Androgen-independent prostate cancer is a heterogeneous group of diseases: lessons from a rapid autopsy program. *Cancer Research* **64** 9209–9216. (doi:10.1158/0008-5472.CAN-04-2442)

Simanainen U, Allan CM, Lim P, McPherson S, Jimenez M, Zajac JD, Davey RA & Handelsman DJ 2007 Disruption of prostate epithelial androgen receptor impedes prostate lobe-specific growth and function. *Endocrinology* **148** 2264–2272. (doi:10.1210/en.2006-1223)

Snoek R, Cheng H, Margiotti K, Wafa LA, Wong CA, Wong EC, Fazli L, Nelson CC, Gleave ME & Rennie PS 2009 *In vivo* knockdown of the androgen receptor results in growth inhibition and regression of well-established, castration-resistant prostate tumors. *Clinical Cancer Research* **15** 39–47. (doi:10.1158/1078-0432.CCR-08-1726)

Sun Y, Wang BE, Leong KG, Yue P, Li L, Jhunjhunwala S, Chen D, Seo K, Modrusan Z, Gao WQ *et al.* 2012 Androgen deprivation causes epithelial-mesenchymal transition in the prostate: implications for androgen-deprivation therapy. *Cancer Research* **72** 527–536. (doi:10.1158/0008-5472.CAN-11-3004)

Sun F, Chen HG, Li W, Yang X, Wang X, Jiang R, Guo Z, Chen H, Huang J, Borowsky AD *et al.* 2014 Androgen receptor splice variant AR3 promotes prostate cancer via modulating expression of autocrine/paracrine factors. *Journal of Biological Chemistry* **289** 1529–1539. (doi:10.1074/jbc.M113.492140)

Tam WL & Weinberg RA 2013 The epigenetics of epithelial-mesenchymal plasticity in cancer. *Nature Medicine* **19** 1438–1449. (doi:10.1038/nm.3336)

Tamburrino L, Salvianti F, Marchiani S, Pinzani P, Nesi G, Serni S, Forti G & Baldi E 2012 Androgen receptor (AR) expression in prostate cancer and progression of the tumor: lessons from cell lines, animal models and human specimens. *Steroids* **77** 996–1001. (doi:10.1016/j.steroids.2012.01.008)

Tanaka H, Kono E, Tran CP, Miyazaki H, Yamashiro J, Shimomura T, Fazli L, Wada R, Huang J, Vessella RL *et al.* 2010 Monoclonal antibody targeting of N-cadherin inhibits prostate cancer growth, metastasis and castration resistance. *Nature Medicine* **16** 1414–1420. (doi:10.1038/nm.2236)

Tang DG 2012 Understanding cancer stem cell heterogeneity and plasticity. *Cell Research* **22** 457–472. (doi:10.1038/cr.2012.13)

Tomlins SA, Rhodes DR, Perner S, Dhanasekaran SM, Mehra R, Sun XW, Varambally S, Cao X, Tchinda J, Kuefer R *et al.* 2005 Recurrent fusion of TMPRSS2 and ETS transcription factor genes in prostate cancer. *Science* **310** 644–648. (doi:10.1126/science.1117679)

Wang S, Gao J, Lei Q, Rozengurt N, Pritchard C, Jiao J, Thomas GV, Li G, Roy-Burman P, Nelson PS *et al.* 2003 Prostate-specific deletion of the murine Pten tumor suppressor gene leads to metastatic prostate cancer. *Cancer Cell* **4** 209–221. (doi:10.1016/S1535-6108(03)00215-0)

Wang Q, Li W, Zhang Y, Yuan X, Xu K, Yu J, Chen Z, Beroukhim R, Wang H, Lupien M *et al.* 2009*a* Androgen receptor regulates a distinct transcription program in androgen-independent prostate cancer. *Cell* **138** 245–256. (doi:10.1016/j.cell.2009.04.056)

Wang X, Kruithof-deJulio M, Economides KD, Walker D, Yu H, Halili MV, Hu YP, Price SM, Abate-Shen C & Shen MM 2009*b* A luminal epithelial stem cell that is a cell of origin for prostate cancer. *Nature* **461** 495–500. (doi:10.1038/nature08361)

Wu CT, Altuwaijri S, Ricke WA, Huang SP, Yeh S, Zhang C, Niu Y, Tsai MY & Chang C 2007 Increased prostate cell proliferation and loss of cell differentiation in mice lacking prostate epithelial androgen receptor. *PNAS* **104** 12679–12684. (doi:10.1073/pnas.0704940104)

Wu K, Gore C, Yang L, Fazli L, Gleave M, Pong RC, Xiao G, Zhang L, Yun EJ, Tseng SF *et al.* 2012 Slug, a unique androgen-regulated transcription factor, coordinates androgen receptor to facilitate castration resistance in prostate cancer. *Molecular Endocrinology* **26** 1496–1507. (doi:10.1210/me.2011-1360)

Yang T, Rycaj K, Liu ZM & Tang DG 2014 Cancer stem cells: constantly evolving and functionally heterogeneous therapeutic targets. *Cancer Research* **74** 2922–2927. (doi:10.1158/0008-5472.CAN-14-0266)

Zhau HY, Chang SM, Chen BQ, Wang Y, Zhang H, Kao C, Sang QA, Pathak SJ & Chung LW 1996 Androgen-repressed phenotype in human prostate cancer. *PNAS* **93** 15152–15157. (doi:10.1073/pnas.93.26.15152)

Received in final form 13 August 2015
Accepted 18 August 2015
Made available online as an Accepted Preprint
18 August 2015

Published by Bioscientifica Ltd.

Seminars in Cancer Biology 35 (2015) 191–199

Contents lists available at ScienceDirect

Seminars in Cancer Biology

journal homepage: www.elsevier.com/locate/semcancer

Review

Cancer stem cells and cell size: A causal link?

Qiuhui Li[a,1], Kiera Rycaj[a,1], Xin Chen[a,*], Dean G. Tang[a,b,*]

[a] Department of Epigenetics and Molecular Carcinogenesis, University of Texas M.D. Anderson Cancer Center, Science Park, Smithville, TX 78957, USA
[b] Cancer Stem Cell Institute, Research Center for Translational Medicine, East Hospital, Tongji University School of Medicine, Shanghai 200120, China

ARTICLE INFO

Article history:
Received 30 June 2015
Accepted 8 July 2015
Available online 1 August 2015

Keywords:
Stem cells
Cancer
Cancer stem cells
Cell size

ABSTRACT

The majority of normal animal cells are 10–20 μm in diameter. Many signaling mechanisms, notably PI3K/Akt/mTOR, Myc, and Hippo pathways, tightly control and coordinate cell growth, cell size, cell division, and cell number during homeostasis. These regulatory mechanisms are frequently deregulated during tumorigenesis resulting in wide variations in cell sizes and increased proliferation in cancer cells. Here, we first review the evidence that primitive stem cells in adult tissues are quiescent and generally smaller than their differentiated progeny, suggesting a correlation between small cell sizes with the stemness. Conversely, increased cell size positively correlates with differentiation phenotypes. We then discuss cancer stem cells (CSCs) and present some evidence that correlates cell sizes with CSC activity. Overall, a causal link between CSCs and cell size is relatively weak and remains to be rigorously assessed. In the future, optimizing methods for isolating cells based on size should help elucidate the connection between cancer cell size and CSC characteristics.

1. Stem cells and cell size

In multicellular organisms, homeostatic control mechanisms are regulated so that internal conditions ensuring cell number and size remain stable and relatively constant (reviewed in [1]). These control mechanisms are an integration of extracellular nutritional environments and multiple cell-specific growth, mitogenic, and survival signals that coalesce to create a balanced homeostatic state in terms of rates of synthesis and degradation of macromolecules, and thus cell size. The majority of animal cells are 10–20 μm in diameter and rarely vary more than 2-fold outside of this range suggesting that the mechanism for cell size regulation is highly conserved [2]. Nonetheless, the mechanisms that control cell size and the relationship between cell growth (cell mass increase over time), cell division, and cell lifespan remain poorly understood.

A correlation between size and lifespan was first observed in yeast [3] and similar observations have also been made in mammalian cells. For example, as yeast cells approach quiescence, proliferation slows but cell growth continues, and thus cells increase in size with age. Mammalian cells in vivo also steadily increase in size with age. In a recent study, a genetic link between cell size, growth rate and lifespan has been reported in yeast cells [4]. Authors show that mutations that increase cell size concomitantly increase growth rate and decrease life span. Thus, small cell mutants age slowly and are long-lived while large cells grow, divide and age dramatically faster in comparison. Specifically, intracellular RNA and protein contents increase with age, even though the synthesis of macromolecules decreases, and these elevations contribute to the increase in the cell size, numbers of inclusion bodies, and other cellular components [5].

Cell growth and proliferation are distinct processes that both require extensive instructive signals. It is unclear what types of mechanisms coordinate cellular growth and the cell cycle in metazoan cells. It has been suggested that commitment to proliferation is dependent upon the attainment of a minimum "critical cell size" [6,7]. In support, large cells tend to divide faster than small cells [8]. One group found that both the expression and the activity of G1-phase cyclins are modulated by growth rate and cell size in yeast, suggesting that the proliferative capacity correlates with cell size and cell growth rates, such that the largest cells begin to proliferate five times faster than the smallest cells [9]. Other experiments in mammalian cells support the conclusion that cell size correlates closely with the proliferative potential of cells [10–12]. Another group examined cell size distributions in lymphoblasts and showed that growth rate is size-dependent throughout the cell cycle. Alternatively, authors concluded that cell division probability varies independently with cell size and age, indicating that

* Corresponding author at: Department of Epigenetics and Molecular Carcinogenesis, University of Texas M.D. Anderson Cancer Center, Science Park, Smithville, TX 78957, USA.
E-mail addresses: xchen7@mdanderson.org (X. Chen), dtang@mdanderson.org (D.G. Tang).
[1] These authors contributed equally to this work.

http://dx.doi.org/10.1016/j.semcancer.2015.07.002
1044-579X/

mammalian cells have an intrinsic mechanism for cell size maintenance [13].

Mammalian adult stem cells are rare, long-living cells with the inherent traits of both indefinite self-renewal and multilineage differentiation capabilities [14]. Thus, stem cells normally divide asymmetrically into a new stem cell and a committed progenitor, the latter of which has limited self-renewing ability and can give rise to progeny that are more restricted in their differentiating potential and finally to functionally mature cells. Between the two, primitive stem cells are generally smaller than differentiated cells. Stem cells are also generally detected in a predominantly quiescent state, a reversible arrest in proliferation as determined by an integration of diverse antimitogenic signals. The proliferative and quiescent states have vastly different metabolic needs, the former requiring tremendous metabolic energy in order to synthesize DNA, protein, and lipids. Indeed, quiescent cells are widely reported to exhibit reduced nucleotide synthesis, as well as reduced metabolic activity and cell size. As expected, most studies that look at cell size have described stem cells to be much smaller in size than the more committed and highly proliferative cells. For example, in murine bone marrow (BM), hematopoietic stem cells (HSCs) are small measuring between 4 and 5 μm [15,16]. Another group described human BM HSCs ($Lin^-CD34^+c\text{-}Kit^+$) to be small at ~6 μm [17]. Neuroblasts (neural stem cells) and myoblasts are notably smaller than their differentiated daughter cells, i.e., neurons and skeletal muscle cells, respectively. The presence of heterogeneous $CD34^+CD45^-$ nonhematopoietic tissue-committed, putative stem cells that measure 5–7 μm has also been described [18]. Finally, small pluripotent epiblastic-like cells of 8–10 μm from the rat skeletal muscle [19], very small embryonic-like (VSEL) stem cells of 3 μm from the bone marrow [20], very small stem cell-like cells (2–4 μm) that express embryonic markers such as SSEA-4, Oct-4, Nanog, Sox-2, and c-kit in the human ovarian surface epithelium [21] have been reported. Whether these latter, small-sized, putative stem cells truly possess stem cell properties (i.e., self-renewal and multi-lineage differentiation) has not been rigorously examined and remains somewhat controversial.

Identification of different sized subpopulations has been largely based on regular light or electron microscopy [15–18], fluorescence-activated cell sorting (FACS) [22], size-sieving methods [23], centrifugal elutriation, and long-term culture under specific conditions [24] (Fig. 1). These methods have been instrumental in producing evidence that cell size is related to cell cycle [25], cell proliferation [26–28], and differentiation [29,30]. For example, the differentiation marker involucrin has been reported to correlate with increasing cell size and terminal differentiation in human epidermal cultures [31]. In studies utilizing human epidermal keratinocytes, the smallest cells sorted by centrifugal elutriation expressed the highest levels of basal cell markers (p63 and basonuclin) and possessed the greatest clonogenicity in culture [26,28,30]. Vice versa, the proliferative potential of human fibroblasts and keratinocytes was shown to be inversely dependent on cell size [26,27].

When utilizing FACS, cells of different sizes can be separated based on forward scatter (FSC), which is an indirect measurement of size, versus light scatter (LSC), which is a measurement of the cell's granularity (Fig. 1A). Alternatively, a mixture of synthetic beads of predefined sizes can be employed in FACS to fractionate subpopulations of cells of varying sizes (Fig. 1C and D). In one study, human corneal epithelial cells were sorted by FACS based on FSC [32]. Four fractions (A–D) of cells ranging in size from 10 to 16, 17 to 23, 24 to 30, and >31 μm in diameter, respectively, were isolated. Cell size was shown to positively correlate with the expression of the differentiation markers keratin (K) 3, K12, and involucrin and inversely with the levels of stem cell–associated markers ΔNp63 and ABCG2 and with colony-forming efficiency and growth capacity. Cells with the smallest size contained the greatest number of BrdU label-retaining slow-cycling cells, displayed the highest percentage of cells immunopositive to p63 and ABCG2 and negative to K3 and involucrin, expressed the highest levels of ΔNp63 and ABCG2 mRNA and the lowest levels of K3, K12, and involucrin, and possessed the highest colony-forming efficiency and growth capacity [32].

As discussed above, when keratinocytes undergo terminal differentiation, both in vivo and in culture, they increase progressively in cellular size [31,33]. In studying the p53/MDM2 regulatory loop in human epidermal differentiation, one group found that induction of MDM2 and downregulation of p53 characterized the transition from proliferation to differentiation in primary human keratinocytes. These changes correlated with an increase in cell size and an irreversible commitment to terminal differentiation [29]. The same group also found that upon differentiation, keratinocytes continued DNA replication after cell division was suppressed [34]. As a consequence of this phenomenon, referred to as endoreplication, cell growth results not in proliferation, but rather in an increased cellular size and polyploidy.

Size has also been interrogated in mesenchymal cells. In order to obtain homogeneous subpopulations of stem cells from human umbilical cord matrix, one group applied the counterflow centrifugal elutriation to separate cells with distinct characteristics with respect to size, morphology and proliferative activity [35]. In another study, both FACS and the elutriation method were used to identify a phenotypically distinct population of mesenchymal stem/progenitor cells (MSPCs) within human BM [36]. The MSPC activity resided within a population of rare, small $CD45^-CD73^+CD90^+CD105^+$ cells that lacked CD44. These rare MSPCs, which were between 5 and 12 μm in diameter, expanded rapidly in culture and demonstrated tri-lineage mesenchymal differentiation potential into osteoblasts, chondrocytes, and adipocytes [36]. Other studies utilizing normal human peripheral blood cells and hematopoietic progenitor cells have also uncovered a correlation between cell volume with stem cell marker expression, allowing for the identification of small stem cells [37].

Rapidly self-renewing mesenchymal stem cells (MSCs) of ~7 μm [22,39] or even smaller VSEL stem cells [20,38] have been described in the BM. Size-sieving based approach using smaller pores, for example, 3 μm, has also been employed to isolate very small BM MSCs with proliferation and self-renewal capacities that lack markers of osteoblastic differentiation and can serve as progenitors for all mesenchymal cell lineages, including osseous, adipose, and cartilaginous tissues [23]. In another study, equine umbilical cords were processed and cells separated into larger and smaller sieved populations using multi-dishes with 8-μm pore transwell inserts [40]. Cells from both populations (i.e., >8-μm and <8-μm) expressed MSC and pluripotency markers and were able to differentiate into mesodermic and ectodermic lineages. After sieving, both large intervascular and small perivascular cells were rapidly replicating cells. However, sieved cells (i.e., <8-μm) had more proliferative potential than un-sieved cells. Interestingly, Katsube et al. measured the proliferation and cellular thickness of human MSCs by atomic force microscopy and found that the MSCs with high proliferative activity were small and those with low proliferative activity were flat and large [41]. The MSCs with medium proliferative activity were of intermediate size.

The VESL stem cells described above [20,38] have the phenotype of $CXCR4^+Sca\text{-}1^+CD45^-Lin^-$ in murine BM and are highly enriched at the mRNA and protein levels for markers in embryonic pluripotent stem cells. A transmission electron microscopy study showed that these cells were extremely small (2–4 μm) and had the ability to differentiate into cells from all three germ cell layers in vitro [42]. The same group later isolated a similar population of $CXCR4^+AC133^+CD34^+Lin^-CD45^-$ mononuclear cells

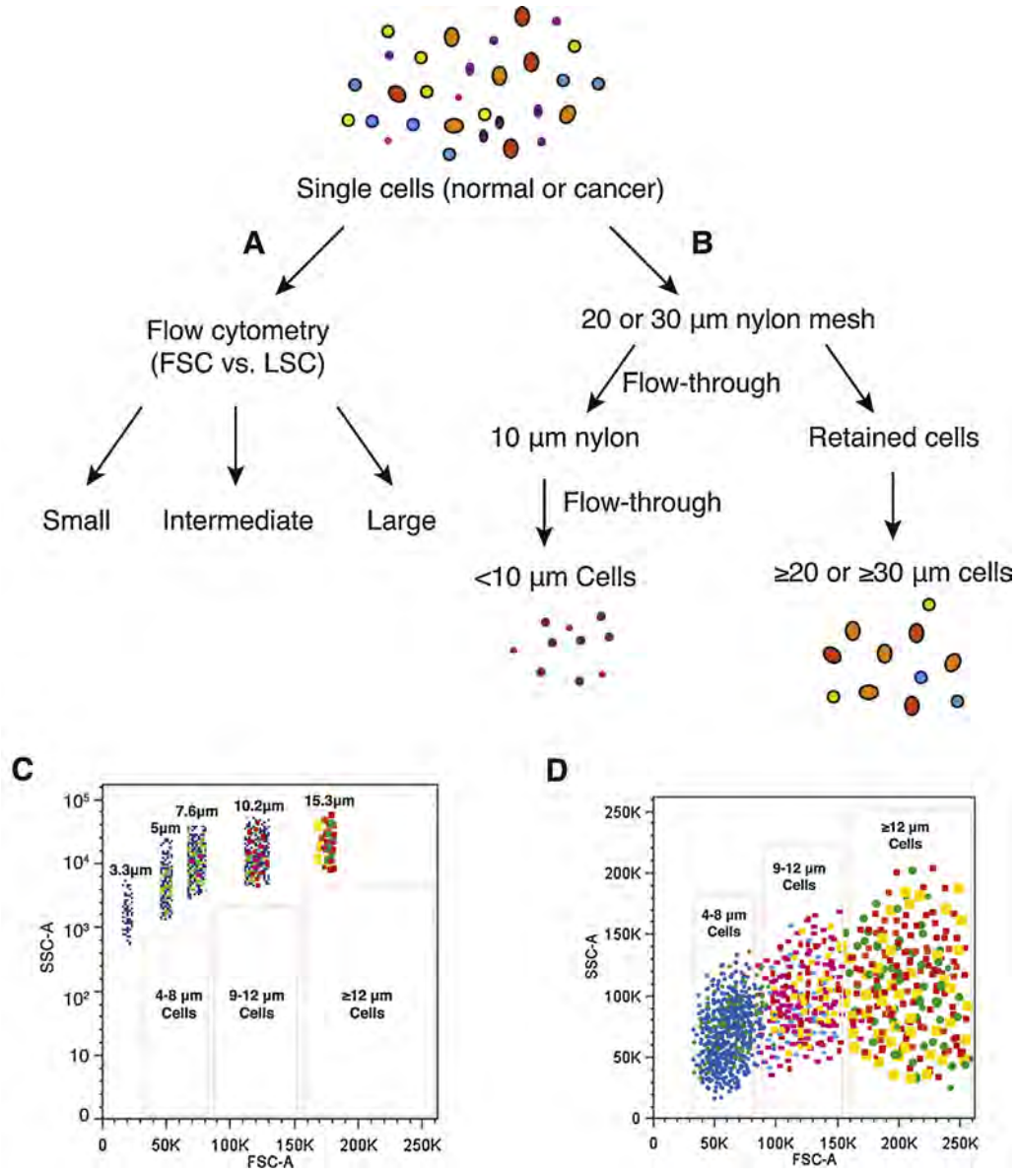

Fig. 1. Schematic illustration of strategies to enrich cell populations with varying sizes. (A) Single cells from normal or cancerous cultures or tissues can be separated into (relatively) small, intermediate and large cell populations based on the forward scatter (FSC) intensity value in flow cytometry (i.e., FSC-based FACS). (B) Size-sieving approach using nylon mesh filtration. Single cells are separated into small cells (<10 μm) and large cells (≥20 or 30 μm) using 20 or 30 μm nylon mesh. (C and D) Cell populations with different sizes can be more precisely purified via a beads-sizing method by FACS (i.e., beads sizing-based FACS).

Source: Modified from Figure 1-A of Ref. [32].

from human cord blood (CB), which were very small (3–5 μm) and expressed embryonic transcription factors Oct-4 and Nanog [43]. The authors showed that murine VSELs could differentiate into the hematopoietic lineage after coculture over OP9 stromal cells [44]. Nevertheless, these observations on VSELs have recently become controversial because studies from an independent group found no evidence for VSELs in murine BM, no molecular signatures associated with pluripotency in any mouse BM cells smaller than 7 μm across [45]. In addition, the small cells did not form spheres in vitro and differentiate into blood cells [45].

In contrast to the above studies that correlate small cell size with adult stem cell properties, a recent study reported an opposite correlation in mouse mammary stem cells (MaSCs) [46]. In addition to the $CD24^{+}CD29^{hi}CD49f^{hi}Sca1^{-}$ marker profile, adult MaSCs can be defined by the property of size. Based on FACS FSC, cells with a low FSC (approximately <10 μM) lacked outgrowth potential and failed to reconstitute the mammary gland when transplanted into the cleared fat pads of syngeneic mice. In contrast, cells >10 μM in size had increased outgrowth potential as compared with Lin^{-} control cells. Limiting dilution transplantation assays indicated that the repopulating ability of $Lin^{-}CD24^{-}CD29^{hi}$ cells that were >10 μM in size was significantly increased as compared with cells marked by CD24 and CD29 alone [46].

2. Cancer stem cells

Cancer is characterized by the excessive and uncontrolled expansion of abnormal, malignant cells that display morphological, proliferative, and functional heterogeneity. Morphological heterogeneity is further manifested in tumor cells of variegating size, shape, thickness, nucleus/cytoplasm ratio, etc. In order to explain this tumor cell heterogeneity, two models have been proposed, one being the cancer stem cell (CSC) concept [47,48]. This model postulates that, akin to growth of normal proliferative tissues, growth

of tumors or expansion of a tumor clone is driven by a population of cells endowed with both self-renewal and differentiation capabilities [48]. CSCs, as with normal stem cells, are long-lasting and have self-renewal capabilities. Both human cancers (or tumor clones) and regenerating normal tissues are organized in a hierarchical manner according to stages of differentiation and proliferative potential with stem cells as the common denominator. However, this does not necessarily imply that CSCs are always derived from normal stem cells. Stem cells are often the target of genetic events that are necessary or sufficient for malignant transformation; however, restricted progenitors, due to their cycling feature, oftentimes represent the preferred transformation targets [47]. Even differentiated cells can undergo oncogenic reprogramming and de-differentiation and be transformed [47]. Both normal stem cells and CSCs share the ability to self renew and produce differentiated progeny, and thus parallels can be found between signaling pathways that regulate these attributes. A CSC is set apart from a normal stem cell in that it has acquired the capacity for indefinite proliferation through accumulated genetic mutations and epigenetic alterations. In this case, when signaling pathways that regulate normal stem cell self-renewal are dysregulated, tumorigenesis occurs. Multiple approaches have been employed to identify, enrich, purify, and characterize CSCs in different tumor systems [47].

3. Cancer stem cells and cell size

Tumors generally contain multiple clones, in which differentially sized tumor cells can be easily observed. It seems reasonable to speculate, a priori, that a certain population of cells in tumors with certain sizes might be endowed with particular characteristics to promote survival and longevity. In other words, can cell size be used as a determinant of CSCs vs. non-CSCs? Very few studies by far have been conducted to prospectively address this interesting question. A group recently generated a liver-derived progenitor cell (LDPC) line, RA1, by overexpressing the simian virus 40 (SV40) large T antigen (TAg) in primary LDPCs [49]. Interestingly, following transformation, LDPCs decreased in size significantly and the propagating cells measured 1 μm in diameter compared with the 10 μm size of the parental LDPCs. These small

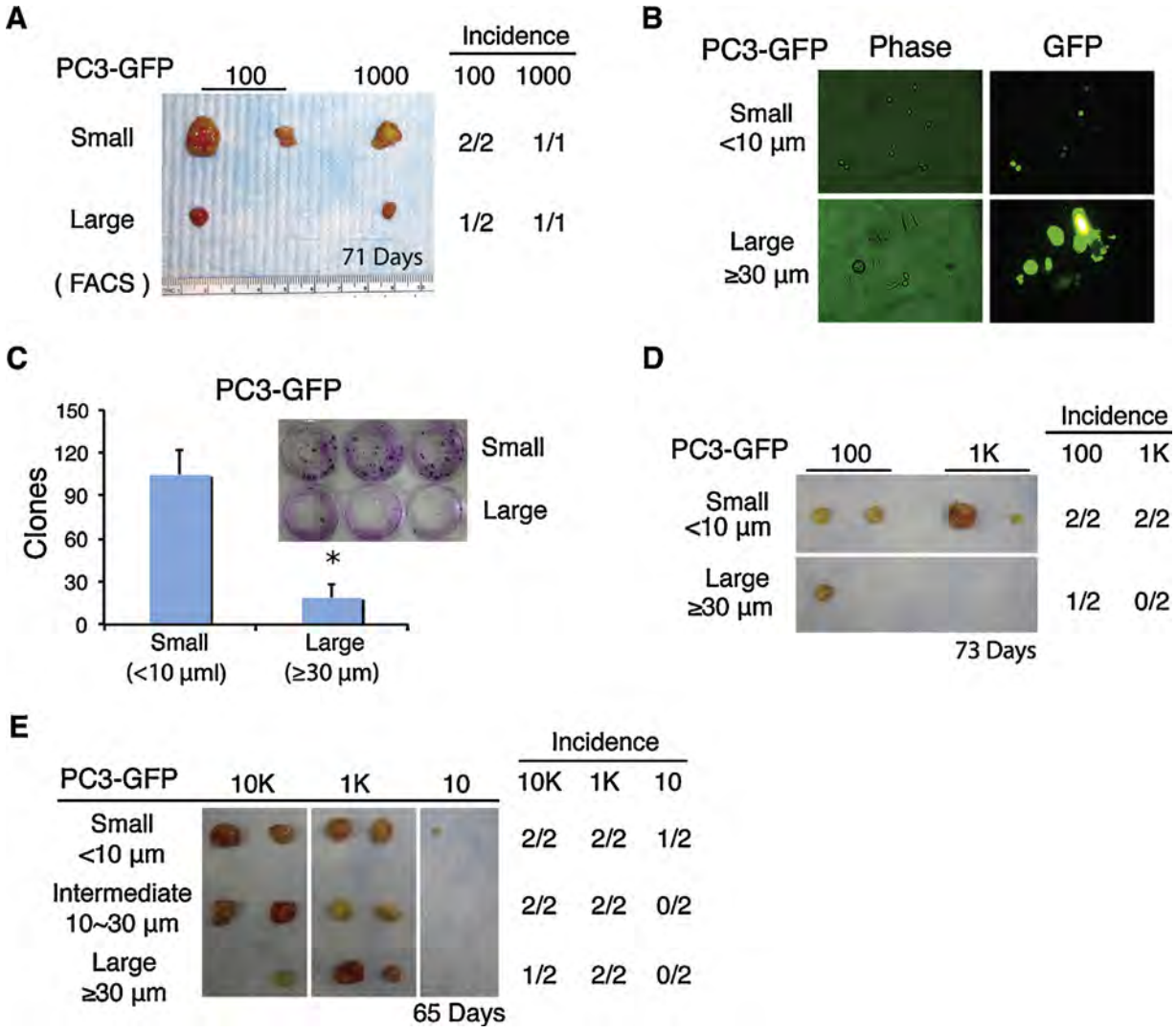

Fig. 2. Small PC3 cells tend to be more clonal and tumorigenic than the isogenic large cells. (A) FSC-based FACS-purified small PC3-GFP cells exhibited a trend of increasing tumorigenicity than isogenic large cells. (B–E) PC3 cells were separated by size-sieving using nylon mesh into three (small, intermediate, and large) sizes and then used in various in vitro and in vivo assays. (B) Morphologic validation and GFP checking of small (<10 μm) and corresponding large (≥30 μm) cells. (C) Clonal assays. PC3-GFP cells of two different sizes were plated in 6-well plates (300 cells per well). Clones were counted 14 days after plating. Presented are the mean ± SD from triplicate wells (*$P < 0.05$). (D–E) Two independent tumor experiments. PC3-GFP cells were separated by nylon mesh into the 3 sizes indicated and subcutaneously injected into NOD/SCID female mice at different cell doses. Presented are tumor images, tumor incidence, and the time (days; bottom) when tumors were harvested.

cells multiplied continuously and, after passage 36, they started to increase in size and reached a maximum size of 10–12 μm by passage 42. The authors speculated [49] that forced cell cycle entry by TAg might have been the trigger for the "reprogramming" of cells causing a change in their cell size, possibly via the process of 'de-differentiation', a feature observed in other stem cells and CSCs. To date, RA1 cells are the smallest mammalian cells to be reported in the literature.

Bortolomai et al. investigated cancer stem/tumor initiating cell characteristics in the human epidermoid carcinoma cell line, A431, via growth as non-adherent spheres in specific media and ALDH enzymatic activity [50]. Spheres manifested increased stem-cell like properties including holoclone formation, high ALDH activity (the ALDH-positive fraction increased from 46% in adherent cultures to 65% in spheres), and a transient induction of stem cell markers such as Nanog, Nestin and Oct4. When compared to parental cells, spheres were greatly enriched in a podoplanin-positive subpopulation characterized by small cell sizes and the ability to propagate tumors in nude mice at a lower cell dose [50].

In contrast, Srivastava et al. interrogated the DAOY medulloblastoma cell line with respect to the relationship between cell size and stem-like potential and observed opposing results [51]. They purified SP/non-SP DAOY cells, which were also sorted separately for viability, cell size, cell cycle status, and proliferative capacity evaluation. The SP, non-SP, $CD133^+$, and $CD133^-$ fractions were all capable of reconstituting the original parental DAOY population. However, SP cells, which have been shown to enrich for CSCs in many tumor systems [47], differed from the non-SP cells with respect to increased cell size, decreased S-phase, and slightly decreased proliferative capacity. Another example of stem-like cancer cells with increased cell size is polyploid giant cancer cells (PGCCs) that are frequently found in human solid tumors. These cells are large atypical cancer cells with multiple copies of DNAs and have been recently been studied in human ovarian cancer cell lines and primary ovarian cancer [52]. Of interest, these PGCCs are highly resistant to oxygen deprivation, express normal and CSC markers, divide asymmetrically and cycle slowly, and, surprisingly, can differentiate into adipose, cartilage and bone cells. A

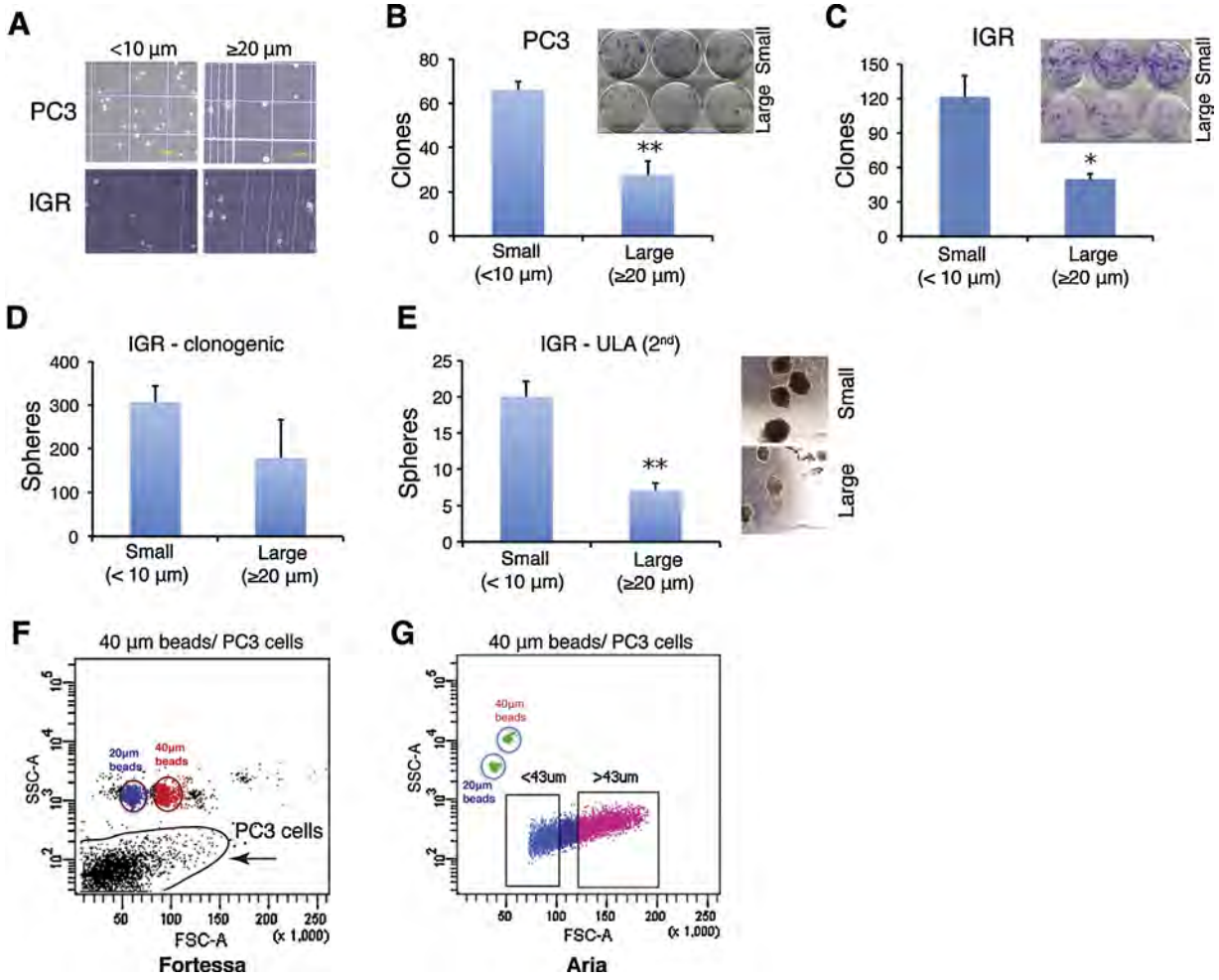

Fig. 3. Small prostate cancer cells (<10 μm) are more clonal and clonogenic than isogenic large cells (≥20 μm) in both PC3 (A and B) and IGR-CaP1 (IGR; C–E) cell lines. (A) Morphologic validation of different cell sizes separated by nylon mesh. (B) Clonal assay in PC3 cells. PC3 cells were sorted into small (<10 μm) and large (≥20 μm) sized populations by nylon mesh, and plated in 6-well plates (300 cells per well). Clones were counted 14 days after plating. Presented are the mean ± SD from triplicate wells (**$P < 0.01$). Shown in the inset is the Giemsa-stained image. (C) Clonal assay in IGR-CaP1 cells. Sorted small and large IGR-CaP1 cells were plated in 6-well plates (200 cells per well) and clones were enumerated 14 days after plating. Presented are the mean ± SD from triplicate wells (*$P < 0.05$). (D) Clonogenic assay in IGRCaP1 cells. Small and large IGR cells were mixed with Matrigel and plated in 12-well plates (1000 cells/well) and colonies were counted in 2 weeks. The large cells showed reduced colony-forming activity in comparison to small cells although this difference was not statistically significant. (E) Secondary (2°) sphere formation assays in IGR-CaP1 cells. Nylon mesh-separated cells were plated in 6-well ultra-low attachment (ULA) plates (1000 cells per well), and cultured in serum-free medium for 2 weeks. 1° spheres were harvested, digested into single-cell suspension, re-sorted into small cell (<10 μm) and large cells (≥20 μm) by nylon mesh and plated into the ULA plates (1000 cells per well) for 2° sphere formation assays. Spheres were counted after 2 weeks (*$P < 0.05$). (F and G) Ongoing trials of beads sizing based FACS protocol in PC3 cells. Different FACS machines exhibited distinct sorting profiles.

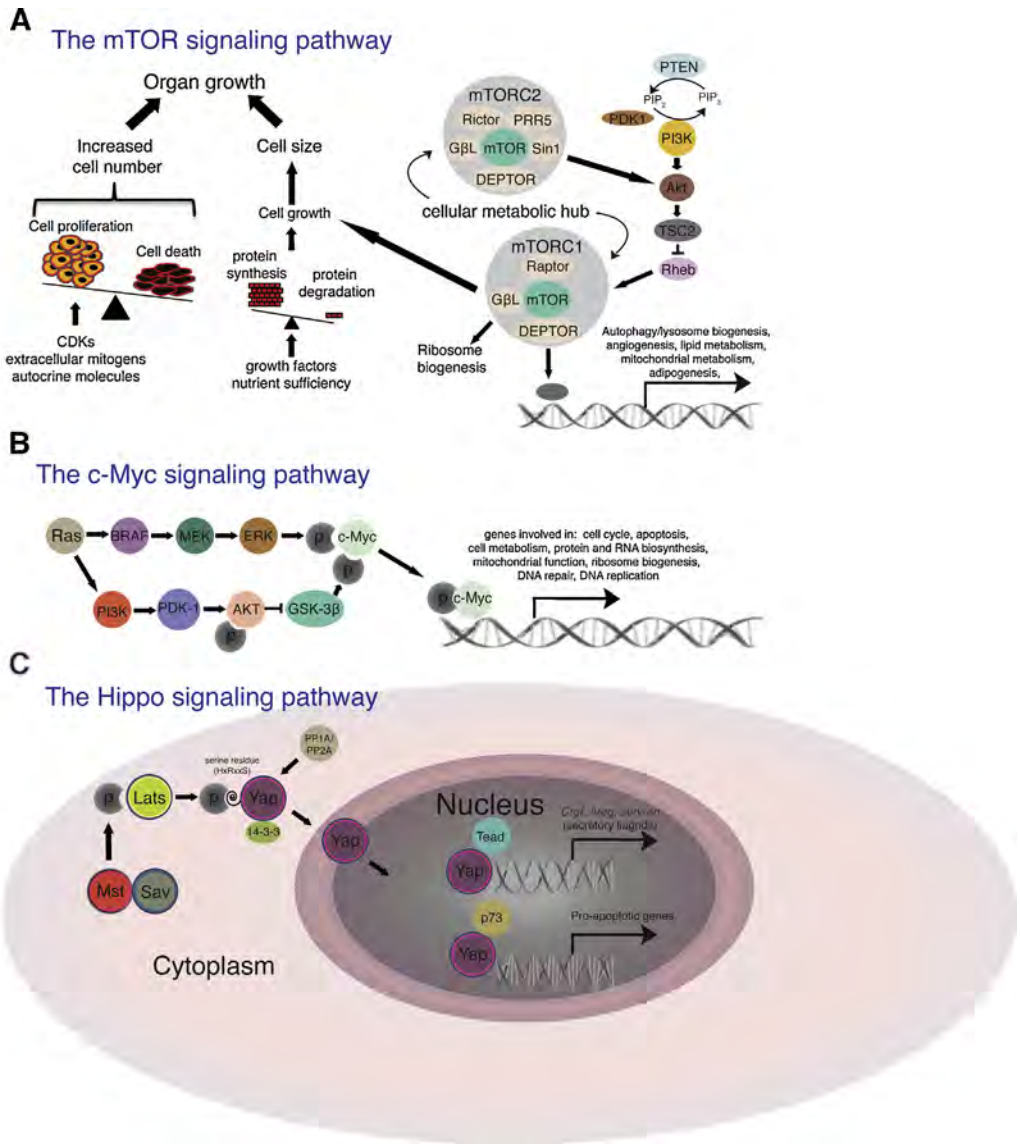

Fig. 4. Three major signaling pathways that regulate cell size in normal cells. (A) The PI3K/AKT/mTOR pathway. An increase in cell number and cell size both can lead to organ growth. Cell number is dependent on the intricate balance between cell proliferation, which is controlled by extracellular mitogens and inhibitory molecules, and cell death, which is initiated in response to developmental cues or lack of survival factors. Cell size is dependent on cell growth, which is controlled by a balance between protein synthesis and protein degradation based on extracellular growth factors and nutrient sufficiency. Central to the regulation of cell growth is the mTOR pathway. The core components of the mTOR pathway are shown. (B) The c-Myc pathway. The Ras/PI3K/ERK pathway induces c-Myc. Myc mainly functions as a transcription factor to regulate target genes including those involved in cell cycle, apoptosis, cell metabolism and protein and RNA biosynthesis. Myc is also frequently upregulated in cancer cells due to genomic amplification (not shown). (C) The Hippo pathway. The pathway is thought to sense cell density and to regulate gene expression for control of organ size. The key downstream effector of the mammalian Hippo pathway is the Yes-associated protein (YAP), which function as a transcription co-activator. Mst is a mammalian homolog of Drosophila Hippo and encodes a kinase that phosphorylates Lats with cooperation from Sav. Phosphorylated Lats then exerts kinase activity on YAP. Phosphorylated YAP is then trapped in the cytoplasm by a 14-3-3 protein, until de-phosphorylation by a phosphatase such as PP1A allows translocation to the nucleus, thereby facilitating transcriptional regulation.

single PGCC can form cancer cell spheroids in vitro and generate tumors in immunodeficient mice, which manifest a mesenchymal phenotype with increased expression of CSC markers CD44 and CD133 and become more resistant to treatment with cisplatin [52].

Our laboratory, in the past 10 years, has been meticulously dissecting prostate cancer cell heterogeneity. Using cell surface markers, SP, holoclone and sphere formation, as well as tumor transplantation and serial transplantation assays, we have provided strong evidence for the presence of CSCs in long-term cultured prostate cancer cell lines and xenografts as well as in primary patient tumors [53–61]. We have recently made attempts to determine a correlation between CSCs and cell size in the most aggressive, fully undifferentiated prostate cancer cells PC3. PC3 cells completely lack differentiation markers such as androgen receptor (AR) and prostate-specific antigen (PSA). Virtually 100% of PC3 cells express commonly used CSC surface markers such as CD44 and integrin $\alpha 2\beta 1$; consequently, these markers would not differentiate between tumorigenic CSCs vs. non-CSCs. We have shown that PC3 holoclones harbor long-term self-renewing tumor-propagating cells [57].

To address whether cell size is able to provide tumorigenic stratification in PC3 cells, we first utilized FSC-based FACS sorting (Figure 1A) to fractionate PC3 into, relatively, large and small sized populations and then implanted 100 and 1,000 cells, respectively, subcutaneously, in NOD/SCID mice. This experiment revealed a tendency of small cells being more tumorigenic manifested by more and larger tumors regenerated (Figure 2A). We then employed

size-sieving approach by using nylon mesh of different pore sizes (Figure 1B) to separate PC3 cells into two cell populations varying in the cell sizes, i.e., small (< 10 μm) and large (≧ 20 or 30 μm) (Figure 2B-E; Figure 3A-B) followed by clonal (i.e., 2D) and clonogenic (i.e., 3D) assays as well as in vivo tumor regeneration. In two independent experiments, small PC3 cells demonstrated higher clonal capacity than large PC3 cells (Figure 2C; Figure 3B). Importantly, two separate tumor experiments again revealed the trend of small PC3 cells being more tumorigenic (Figure 2D-E). Similar studies in another AR^-/PSA^- prostate cancer cell line IGR also revealed that small IGR cells displayed higher clonal (Figure 3C) and clonogenic (Figure 3D-E) capacities than corresponding large cells.

The above studies suggest that in two undifferentiated prostate cancer cell models, small-sized cells possess higher CSC-associated properties (i.e., higher clonal, clonogenic, and tumorigenic capacities). Serial tumor transplantations are needed to verify the true CSC traits in small prostate cancer cells. Current experimental strategies in fractionating cancer cells into different sizes have obvious pros and cons. Nylon mesh-based size sieving represents a cheap and facile method that is gentle on cells leading to high viability; but purity is a concern and precise cell sizes cannot be determined. FACS produces populations with higher purity; however, the high speed at which cells are sorted leads to low cell viability. Also, the use of forward angle light scatter is not an accurate measure of cell size as light scatter is influenced by a number of factors. Finally, although FACS with beads sizing has been used to fractionate normal cells into cell populations of different sizes [32,46], our preliminary studies in PC3 cells, which vary widely in sizes in culture, demonstrate that this approach might not be readily applicable to cultured human cancer cells as two flow cytometers give completely different flow profiles (Figure 3F-G).

4. Perspectives

Significant progress has been made in the identification of three key and inter-connected regulatory pathways, i.e., mTOR, Myc, and Hippo, that control normal cell growth, and this has given us clues as to how cell size is controlled in homeostasis and how cancer cells might have abnormal cell size control mechanisms (Figure 4). The PI3K/AKT/mTOR signaling pathway is a major regulator of cell growth and thus a key determinant of cell size [62]. Critical inputs regulating this pathway include growth factors, amino acids, stress, energy status, and oxygen. The activated pathway promotes protein synthesis, lipogenesis, and energy metabolism, activities that directly relate to cell size (Figure 4A). Many of the components of the PI3K signaling pathway, which is upstream of both mTOR complexes, are mutated in human caners. Additionally, the loss of p53 promotes mTOR complex activation. Another major regulator is Myc, a transcription factor that increases cell growth and cell size in multiple tissues and organisms (Figure 4B). Myc is frequently over expressed as a consequence of genomic amplification and heightened growth or mitogenic signaling from, e.g., Ras activation (Figure 4B). Endoreplication and cell enlargement is stimulated in keratinocytes by continuous activation of c-Myc [34]. Continuous activity of c-Myc also results in increased cellular size and loss of the cell cycle control in other cell types when mitosis is impaired [63–66]. When c-Myc is knocked out in the epidermis, there is a loss of the proliferative compartment and premature differentiation. The keratinocyte cells size, growth and endoreplication are all reduced and the stem cell amplification is compromised [66]. The Hippo pathway controls tissue/organ size via regulating cell number and cell size [67] (Figure 4C). YAP, the main downstream target of this pathway promotes organ growth via activation of mTOR. PTEN, an upstream regulator of mTOR, is a critical mediator of YAP regulation. Therefore, YAP is the functional link between the mTOR and HIPPO pathways that regulates cell size, tissue growth and hyperplasia [68]. Both Myc and YAP are frequently overexpressed in human cancers.

Other factors have also been found that regulate cell size. One example is the transcription factor myostatin, a negative regulator of skeletal muscle size that inhibits muscle cell differentiation. Myostatin inhibits activation of the Akt/mTOR/p70S6 protein synthesis pathway, which mediates both differentiation in myoblasts and hypertrophy in myotubes [69]. Ion channel activity has been shown to simultaneously affect cell cycle and cell volume in the S phase of the cell cycle in embryonic stem cells [70]. Also, the Erg channel is critical in controlling cell volume during cell cycle in embryonic stem cells. In support of this, cell death following Erg inhibition is a consequence of the inability to regulate cell volume [71]. The Notch pathway has been studied in relationship to cell size. Recently, type II neural stem cells in Drosophila are used for studying CSC-initiated tumorigenesis [72]. These cells, marked by a transcriptional target of Notch involved in their self-renewal and the absence of a differentiation-promoting transcription factor, give rise to immature progenitors that are small in size. Notch signaling is required for the maintenance of these normal stem cells although the specific mechanisms are unclear. When Notch signaling is inhibited, these neural stem cells exhibit reduced cell growth and cell size [72]. Finally, ectopic expression of the p21 cyclin-dependent kinase inhibitor has been shown to induce hypertrophy, increase cell size and reduce the replicative lifespan of cells [73].

Cell size is a reflection of the balance between anabolic and catabolic processes that are initiated by various signaling pathways (Figure 4). Cell size thus can dynamically change based on the total net input of these signals. Clear correlations between cell size and particular phenotypes such as stem cell features have been discovered in normal cell lineages. Limited reports and our preliminary studies also suggest that small cancer cells appear to be more tumorigenic and possess more CSC properties. However, whether a relationship truly exists between cell sizes and all CSCs is less clear, may likely be tumor cell type-dependent, and requires more thorough investigations. This is due in part to the various cell fractionation methods that may favor certain cell sizes over others or that are simply not technically adept. Recent advances in computer science, micro fabrication, and micro fluidic devices have spurred the rapid development of precision mass-quantifying approaches, allowing more precise quantification in cell size. Future studies should aim to further relate cell size (a phenotype) to functional properties such as stemness based on a combination of next-generation techniques.

Conflict of interest

None.

Acknowledgements

Work in the authors' lab was supported, in part, by grants from NIH (NCI R01-CA155693), DOD (W81XWH-13-1-0352 and W81XWH-14-1-0575), CPRIT (RP120380), and MDACC Center for Cancer Epigenetics (all to D.G.T). X. Chen was supported, in part, by a DOD postdoc fellowship PC141581. We apologize to the colleagues whose work was not cited due to space constraint.

References

[1] Lloyd AC. The regulation of cell size. Cell 2013;154:1194–205.
[2] Conlon I, Raff M. Size control in animal development. Cell 1999;96:235–44.

[3] Mortimer RK, Johnston JR. Life span of individual yeast cells. Nature 1959;183:1751–2.
[4] Yang J, Dungrawala H, Hua H, Manukyan A, Abraham L, Lane W, et al. Cell size and growth rate are major determinants of replicative lifespan. Cell Cycle 2011;10:144–55.
[5] Phipps SM, Berletch JB, Andrews LG, Tollefsbol TO. Aging cell culture: methods and observations. Methods Mol Biol 2007;371:9–19.
[6] Coelho CM, Leevers SJ. Do growth and cell division rates determine cell size in multicellular organisms? J Cell Sci 2000;113(Pt 17):2927–34.
[7] Stocker H, Hafen E. Genetic control of cell size. Curr Opin Genet Dev 2000;10:529–35.
[8] Hunt AM. The Cell Cycle. Oxford: University Press; 1993.
[9] Zhang J, Del Aguila R, Schneider C, Schneider BL. The importance of being big. J Invest Dermatol 2005;10:131–41.
[10] Son S, Tzur A, Weng Y, Jorgensen P, Kim J, Kirschner MW, et al. Direct observation of mammalian cell growth and size regulation. Nat Methods 2012;9:910–2.
[11] Rouzaire-Dubois B, Malo M, Milandri JB, Dubois JM. Cell size-proliferation relationship in rat glioma cells. Glia 2004;45:249–57.
[12] Dolznig H, Grebien F, Sauer T, Beug H, Mullner EW. Evidence for a size-sensing mechanism in animal cells. Nat Cell Biol 2004;6:899–905.
[13] Tzur A, Kafri R, LeBleu VS, Lahav G, Kirschner MW. Cell growth and size homeostasis in proliferating animal cells. Science 2009;325:167–71.
[14] Weissman IL. Stem cells: units of development, units of regeneration, and units in evolution. Cell 2000;100:157–68.
[15] Matsuoka T, Tavassoli M. Electron microscopic identification of hemopoietic progenitor cells by exploiting their sugar-recognizing receptors using a newly developed minibead technique. Exp Hematol 1989;17:326–9.
[16] Radley JM, Ellis S, Palatsides M, Williams B, Bertoncello I. Ultrastructure of primitive hematopoietic stem cells isolated using probes of functional status. Exp Hematol 1999;27:365–9.
[17] Berardi AC, Wang A, Levine JD, Lopez P, Scadden DT. Functional isolation and characterization of human hematopoietic stem cells. Science 1995;267:104–8.
[18] Vacanti MP, Roy A, Cortiella J, Bonassar L, Vacanti CA. Identification and initial characterization of spore-like cells in adult mammals. J Cell Biochem 2001;80:455–60.
[19] Young HE, Duplaa C, Yost MJ, Henson NL, Floyd JA, Detmer K, et al. Clonogenic analysis reveals reserve stem cells in postnatal mammals. II. Pluripotent epiblastic-like stem cells. Anat Rec A 2004;277:178–203.
[20] Zuba-Surma EK, Kucia M, Abdel-Latif A, Dawn B, Hall B, Singh R, et al. Morphological characterization of very small embryonic-like stem cells (VSELs) by ImageStream system analysis. J Cell Mol Med 2008;12:292–303.
[21] Virant-Klun I, Zech N, Rozman P, Vogler A, Cvjeticanin B, Klemenc P, et al. Putative stem cells with an embryonic character isolated from the ovarian surface epithelium of women with no naturally present follicles and oocytes. Differentiation 2008;76:843–56.
[22] Smith JR, Pochampally R, Perry A, Hsu SC, Prockop DJ. Isolation of a highly clonogenic and multipotential subfraction of adult stem cells from bone marrow stroma. Stem Cells 2004;22:823–31.
[23] Hung SC, Chen NJ, Hsieh SL, Li H, Ma HL, Lo WH. Isolation and characterization of size-sieved stem cells from human bone marrow. Stem Cells 2002;20:249–58.
[24] D'Ippolito G, Howard GA, Roos BA, Schiller PC. Sustained stromal stem cell self-renewal and osteoblastic differentiation during aging. Rejuvenation Res 2006;9:10–9.
[25] Gao FB, Raff M. Cell size control and a cell-intrinsic maturation program in proliferating oligodendrocyte precursor cells. J Cell Biol 1997;138:1367–77.
[26] Barrandon Y, Green H. Cell size as a determinant of the clone-forming ability of human keratinocytes. Proc Natl Acad Sci U S A 1985;82:5390–4.
[27] Angello JC, Pendergrass WR, Norwood TH, Prothero J. Proliferative potential of human fibroblasts: an inverse dependence on cell size. J Cell Physiol 1987;132:125–30.
[28] Parsa R, Yang A, McKeon F, Green H. Association of p63 with proliferative potential in normal and neoplastic human keratinocytes. J Invest Dermatol 1999;113:1099–105.
[29] Dazard JE, Piette J, Basset-Seguin N, Blanchard JM, Gandarillas A. Switch from p53 to MDM2 as differentiating human keratinocytes lose their proliferative potential and increase in cellular size. Oncogene 2000;19:3693–705.
[30] Tseng H, Green H. Association of basonuclin with ability of keratinocytes to multiply and with absence of terminal differentiation. J Cell Biol 1994;126:495–506.
[31] Watt FM, Green H. Involucrin synthesis is correlated with cell size in human epidermal cultures. J Cell Biol 1981;90:738–42.
[32] De Paiva CS, Pflugfelder SC, Li DQ. Cell size correlates with phenotype and proliferative capacity in human corneal epithelial cells. Stem Cells 2006;24:368–75.
[33] Banks-Schlegel S, Green H. Involucrin synthesis and tissue assembly by keratinocytes in natural and cultured human epithelia. J Cell Biol 1981;90:732–7.
[34] Gandarillas A, Davies D, Blanchard JM. Normal and c-Myc-promoted human keratinocyte differentiation both occur via a novel cell cycle involving cellular growth and endoreplication. Oncogene 2000;19:3278–89.
[35] Majore I, Moretti P, Hass R, Kasper C. Identification of subpopulations in mesenchymal stem cell-like cultures from human umbilical cord. Cell Commun Signal 2009;7:6.
[36] Hall SR, Jiang Y, Leary E, Yavanian G, Eminli S, O'Neill DW, et al. Identification and isolation of small CD44-negative mesenchymal stem/progenitor cells from human bone marrow using elutriation and polychromatic flow cytometry. Stem Cells Tranl Med 2013;2:567–78.
[37] Sharma S, Cabana R, Shariatmadar S, Krishan A. Cellular volume and marker expression in human peripheral blood apheresis stem cells. Cytometry A 2008;73:160–7.
[38] Ratajczak MZ, Zuba-Surma EK, Wysoczynski M, Wan W, Ratajczak J, Wojakowski W, et al. Hunt for pluripotent stem cell – regenerative medicine search for almighty cell. J Autoimmun 2008;30:151–62.
[39] Colter DC, Class R, DiGirolamo CM, Prockop DJ. Rapid expansion of recycling stem cells in cultures of plastic-adherent cells from human bone marrow. Proc Natl Acad Sci U S A 2000;97:3213–8.
[40] Corradetti B, Lange-Consiglio A, Barucca M, Cremonesi F, Bizzaro D. Size-sieved subpopulations of mesenchymal stem cells from intervascular and perivascular equine umbilical cord matrix. Cell Prolif 2011;44:330–42.
[41] Katsube Y, Hirose M, Nakamura C, Ohgushi H. Correlation between proliferative activity and cellular thickness of human mesenchymal stem cells. Biochem Biophys Res Commun 2008;368:256–60.
[42] Kucia M, Reca R, Campbell FR, Zuba-Surma E, Majka M, Ratajczak J, et al. A population of very small embryonic-like (VSEL) CXCR4(+)SSEA-1(+)Oct-4+ stem cells identified in adult bone marrow. Leukemia 2006;20:857–69.
[43] Kucia M, Halasa M, Wysoczynski M, Baskiewicz-Masiuk M, Moldenhawer S, Zuba-Surma E, et al. Morphological and molecular characterization of novel population of CXCR4+ SSEA-4+ Oct-4+ very small embryonic-like cells purified from human cord blood: preliminary report. Leukemia 2007;21:297–303.
[44] Ratajczak J, Wysoczynski M, Zuba-Surma E, Wan W, Kucia M, Yoder MC, et al. Adult murine bone marrow-derived very small embryonic-like stem cells differentiate into the hematopoietic lineage after coculture over OP9 stromal cells. Exp Hematol 2011;39:225–37.
[45] Miyanishi M, Mori Y, Seita J, Chen JY, Karten S, Chan CK, et al. Do pluripotent stem cells exist in adult mice as very small embryonic stem cells? Stem Cell Rep 2013;1:198–208.
[46] Machado HL, Kittrell FS, Edwards D, White AN, Atkinson RL, Rosen JM, et al. Separation by cell size enriches for mammary stem cell repopulation activity. Stem Cell Transl Med 2013;2:199–203.
[47] Tang DG. Understanding cancer stem cell heterogeneity and plasticity. Cell Res 2012;22:457–72.
[48] Kreso A, Dick JE. Evolution of the cancer stem cell model. Cell Stem Cell 2014;14:275–91.
[49] Aravalli RN, Behnan Sahin M, Cressman EN, Steer CJ. Establishment and characterization of a unique 1 microm diameter liver-derived progenitor cell line. Biochem Biophys Res Commun 2010;391:56–62.
[50] Bortolomai I, Canevari S, Facetti I, De Cecco L, Castellano G, Zacchetti A, et al. Tumor initiating cells: development and critical characterization of a model derived from the A431 carcinoma cell line forming spheres in suspension. Cell Cycle 2010;9:1194–206.
[51] Srivastava VK, Nalbantoglu J. Flow cytometric characterization of the DAOY medulloblastoma cell line for the cancer stem-like phenotype. Cytometry A 2008;73:940–8.
[52] Zhang S, Mercado-Uribe I, Xing Z, Sun B, Kuang J, Liu J. Generation of cancer stem-like cells through the formation of polyploid giant cancer cells. Oncogene 2014;33:116–28.
[53] Patrawala L, et al. Side population (SP) is enriched in tumorigenic, stem-like cancer cells whereas ABCG2^{+} and ABCG2^{-} cancer cells are similarly tumorigenic. Cancer Res 2005;65:6207–19.
[54] Patrawala L, et al. Highly purified CD44^{+} prostate cancer cells from xenograft human tumors are enriched in tumorigenic and metastatic progenitor cells. Oncogene 2006;25:1696–708.
[55] Patrawala L, Calhoun-Davis T, Schneider-Broussard R, Tang DG. Hierarchical organization of prostate cancer cells in xenograft tumors: The CD44$^{+}\alpha2\beta1^{+}$ cell population is enriched in tumor-initiating cells. Cancer Res 2007;67:6796–805.
[56] Tang DG, et al. Prostate cancer stem/progenitor cells: identification, characterization, and implications. Mol Carcinog 2007;46:1–14.
[57] Li HW, Chen X, Calhoun-Davis T, Claypool K, Tang DG. PC3 Human prostate carcinoma cell holoclones contain self-renewing tumor-initiating cells. Cancer Res 2008;68:1820–5.
[58] Li HW, et al. Methodologies in assaying prostate cancer stem cells. Methods Mol Biol 2009;569:85–138.
[59] Liu C, et al. The microRNA miR-34a inhibits prostate cancer stem cells and metastasis by directly repressing CD44. Nat Med 2011;17:211–5.
[60] Qin J, et al. The PSA$^{-/lo}$ prostate cancer cell population harbors self-renewing long-term tumor-propagating cells that resist castration. Cell Stem Cell 2012;10:556–69.
[61] Jeter CR, Yang T, Wang J, Chao H, Tang DG. Nanog in cancer stem cells and tumor development: an update and outstanding questions. Stem Cells 2015;33(8):2381–90.
[62] Laplante M. Sabatini DM. mTOR signaling in growth control and disease. Cell 2012;149:274–93.
[63] Li Q, Dang CV. c-Myc overexpression uncouples DNA replication from mitosis. Mol Cell Biol 1999;19:5339–51.
[64] Johnston LA, Prober DA, Edgar BA, Eisenman RN, Gallant P. Drosophila myc regulates cellular growth during development. Cell 1999;98:779–90.
[65] Iritani BM, Eisenman RN. c-Myc enhances protein synthesis and cell size during B lymphocyte development. Proc Natl Acad Sci U S A 1999;96:13180–5.

[66] Zanet J, Pibre S, Jacquet C, Ramirez A, de Alboran IM, Gandarillas A. Endogenous Myc controls mammalian epidermal cell size, hyperproliferation, endoreplication and stem cell amplification. J Cell Sci 2005;118:1693–704.
[67] Tumaneng K, Russell RC, Guan KL. Organ size control by Hippo and TOR pathways. Curr Biol 2012;22:R368–79.
[68] Tumaneng K, Schlegelmilch K, Russell RC, Yimlamai D, Basnet H, Mahadevan N, et al. YAP mediates crosstalk between the Hippo and PI(3)K-TOR pathways by suppressing PTEN via miR-29. Nat Cell Biol 2012;14:1322–9.
[69] Trendelenburg AU, Meyer A, Rohner D, Boyle J, Hatakeyama S, Glass DJ. Myostatin reduces Akt/TORC1/p70S6K signaling, inhibiting myoblast differentiation and myotube size. Am J Physiol 2009;296C:1258–70.
[70] Andang M, Hjerling-Leffler J, Moliner A, Lundgren TK, Castelo-Branco G, Nanou E, et al. Histone H2AX-dependent GABA(A) receptor regulation of stem cell proliferation. Nature 2008;451:460–4.
[71] Abdelhady S, Kitambi SS, Lundin V, Aufschnaiter R, Sekyrova P, Sinha I, et al. Erg channel is critical in controlling cell volume during cell cycle in embryonic stem cells. PLOS ONE 2013;8:e72409.
[72] Song Y, Lu B. Regulation of cell growth by Notch signaling and its differential requirement in normal vs. tumor-forming stem cells in Drosophila. Genes Dev 2011;25:2644–58.
[73] Demidenko ZN, Blagosklonny MV. Growth stimulation leads to cellular senescence when the cell cycle is blocked. Cell Cycle 2008;7:3355–61.

STEM CELLS®

CANCER STEM CELLS

Concise Review: NANOG in Cancer Stem Cells and Tumor Development: An Update and Outstanding Questions

COLLENE R. JETER,[a] TAO YANG,[b] JUNCHEN WANG,[b] HSUEH-PING CHAO,[a] DEAN G. TANG[a,b]

Key Words. NANOG • Cancer stem cells • Tumor development • Self-renewal

[a]Department of Epigenetics and Molecular Carcinogenesis, The University of Texas M.D. Anderson Cancer Center, Science Park, Smithville, Texas, USA; [b]Cancer Stem Cell Institute, Research Center for Translational Medicine, Shanghai East Hospital, Tongji University School of Medicine, Shanghai, People's Republic of China

Correspondence: Collene R. Jeter, Ph.D, Department of Epigenetics and Molecular Carcinogenesis, The University of Texas M.D. Anderson Cancer Center, Science Park, Park Road 1C, Smithville, Texas 78957, USA. Telephone: 512-237-6491; Fax: 512-237-2475; e-mail: cjeter@mdanderson.org; or Dean G. Tang, Ph.D, Department of Epigenetics and Molecular Carcinogenesis, The University of Texas M.D. Anderson Cancer Center, Science Park, Park Road 1C, Smithville, Texas 78957, USA. Telephone: 512-237-9575; Fax: 512-237-2475; e-mail: dtang@mdanderson.org

Received January 15, 2015; accepted for publication March 8, 2015; first published online in STEM CELLS *EXPRESS* March 26, 2015. Available online without subscription through the open access option.

1066-5099/2015/$30.00/0

http://dx.doi.org/10.1002/stem.2007

ABSTRACT

The homeobox domain transcription factor NANOG, a key regulator of embryonic development and cellular reprogramming, has been reported to be broadly expressed in human cancers. Functional studies have provided strong evidence that NANOG possesses protumorigenic attributes. In addition to promoting self-renewal and long-term proliferative potential of stem-like cancer cells, NANOG-mediated oncogenic reprogramming may underlie clinical manifestations of malignant disease. In this review, we examine the molecular origin, expression, biological activities, and mechanisms of action of NANOG in various malignancies. We also consider clinical implications such as correlations between NANOG expression and cancer prognosis and/or response to therapy. We surmise that NANOG potentiates the molecular circuitry of tumorigenesis, and thus may represent a novel therapeutic target or biomarker for the diagnosis, prognosis, and treatment outcome of cancer. Finally, we present critical pending questions relating NANOG to cancer stem cells and tumor development. STEM CELLS *2015;33:2381–2390*

INTRODUCTION

The master transcription factor NANOG confers self-renewal and ground state pluripotency to embryonic and reprogrammed cells. NANOG regulates embryonic stem cell (ESC) pluripotency and cell-fate specification through complex interactions with a myriad of factors, including OCT4, SOX2, and KLF4 [1]. Cellular reprogramming of somatic cells to induced pluripotent stem (iPS) cells via the forced expression of ESC self-renewal factors, including NANOG, has unveiled the potency of aberrant expression of developmental programs [2–4]. Unlike engineered reprogramming for the purposes of regenerative medicine, uncontrolled and spontaneous acquisition of stem cell programs has profound pathophysiological implications, particularly in regards to cancer.

Oncogenic transformation mirrors cellular reprogramming. The acquisition of developmental programs has been shown to correlate with tumorigenic cells that possess unlimited self-renewal (i.e., cancer stem cells; CSCs). For example, SOX2 has been detected in squamous cell carcinoma and nonsmall cell lung cancer and SOX2 levels correlate with CSC attributes in glioblastoma [5], breast cancer [6], and Ewing's sarcoma [7]. NANOG, the focus of this review, has been broadly detected in primary human tumors of diverse origin, including those arising in the brain, breast, esophagus, colon, ovary, and prostate, among others.

Functional studies have provided compelling evidence that NANOG plays a vital role in malignant disease, correlating with cell proliferation and various malevolent properties such as clonogenic growth, tumorigenicity, invasiveness, and therapeutic resistance. Among the earliest work, ectopic expression of mouse and human NANOG in NIH3T3 cells, respectively, promoted entry into S-phase and foci formation in soft agar [8, 9]. Furthermore, $Rb1^{-/-}$ mouse fibroblasts cultured under sphere-forming conditions upregulated *Nanog* mRNA concurrently with reprogramming to a CSC phenotype, including the acquisition of a cytotoxic-drug effluxing side population, increased expression of stem cell (and CSC) markers (e.g., CD44 and CD133), and tumor-initiating cell capabilities upon transplantation [10]. Overexpression of NANOG in immortalized but benign HEK-293 cells promoted malignant transformation, accompanied by enhanced proliferation, anchorage-independent growth in soft agar, and, importantly, tumor formation in athymic nude mice [11]. Taken together, these findings provide evidence that NANOG possesses oncogenic potential.

Despite this evidence, however, NANOG's role in cancer is somewhat enigmatic, as NANOG does not appear to function as a

classic oncogene. For example, unlike transgenic mouse models in which Oct4 overexpression caused dysplastic and aggressive tumor-like growths in a remarkably short time frame in the skin and intestinal epithelia [12], Nanog overexpression in two similar doxycycline-inducible transgenic mouse models induced only modest hyperplastic outgrowths in the intestinal and colonic epithelium [13] and stratified epithelium of the forestomach and esophagus [14]. In a parallel study, we reported human NANOG overexpression in the K14-compartment in transgenic mice to be insufficient to elicit tumor development, despite signs of skin and lingual hyperplasia in early life [15]. In another transgenic mouse model overexpressing murine Nanog in adult mammary tissues, Nanog alone was also found to be insufficient to elicit tumor formation, even after prolonged expression [16]. However, when coexpressed with Wnt-1, Nanog enhanced mammary tumorigenesis and metastasis [16]. Consequently, NANOG seems to function as a cooperating or potentiating protumorigenic molecule in the appropriate context.

NANOG Origins in Cancer: Biochemical and Regulatory Implications

Elucidating the origins of *NANOG* transcripts in human cells has been confounded by the presence of multiple and, in some cases, highly similar paralogs, as a consequence of retrotransposition [17]. Recently, the location and genomic organization of all human *NANOG* loci have been clarified, including the evolutionary source of *NANOG* (referred to as *NANOG1*) with classic intron/exon structure and located on chromosome 12, a tandem duplication referred to as *NANOG2* (aka *NANOGP1*), and nine other intronless retrogene derivatives [18, 19]. *NANOGP8*, located on chromosome 15, is the only retrogene with an intact open reading frame (Fig. 1A), with the remainder considered pseudogenes as they harbor indels (resulting in frame shifts) and/or deleterious truncations [15, 20].

It is currently unknown to what degree the three full-length NANOG protein variants potentially encoded by *NANOG1*, *NANOG2*, and *NANOGP8* loci possess unique biochemical activities or biological properties. Although *NANOG2* mRNA is quite distinct from that derived from either of the other two loci due to alternative 5′ exon usage (encoding a shorter NANOG2 protein with an alternative N terminus), NANOG1 and NANOGP8 only differ by a single conserved amino acid (aa), with both encoding proteins of 305 aa and NANOGP8 harboring a Q253H substitution in the C-terminal transactivation domain (Fig. 1A). At this moment, there are only a few reliable strategies to distinguish between the two mRNA species (Fig. 1A, 1B). One strategy relies on direct sequencing of the open reading frame to detect the 759G>C that results in the Q253H aa change in NANOGP8 (Fig. 1A). Of note, a 22-bp deletion in the 3′-UTR is polymorphic in *NANOG1* and monomorphic in *NANOGP8*, and thus should not be used as a definitive feature to distinguish between transcripts [21]. Another distinguishing strategy takes advantage of the synonymous 144G>A in *NANOGP8*, a nucleotide change detectable by virtue of RFLP (restriction fragment length polymorphism) due to the introduction of an AlwNI cut site (Fig. 1A). Subsequent gel electrophoresis banding patterns of digested PCR products implicate NANOG origins, such that *NANOG1* gives rise to undigestible fragments and *NANOGP8* is subject to AlwNI fragmentation (as illustrated in Fig. 1B; refer to [22]). Finally, there is a stretch of ~18 bp sequence at the 5′-untranslated region (5′-UTR) following the transcription start site that is unique to *NANOG1* or *NANOGP8* mRNA, which can theoretically be exploited to distinguish between the two transcripts (Fig. 1).

Using these strategies, the primary source of NANOG in cancer has been reported by numerous groups to be the retrotransposed locus *NANOGP8* [21–27]. This preferential expression may be due to the fact that the *NANOG1* locus is transcriptionally silenced during cell-fate specification early in embryogenesis. Nevertheless, *NANOG1* has been reported to be the origin of NANOG in certain cancer types, such as hepatocellular carcinoma [28] and some colorectal cancers [23]. It should be born in mind that as a retrogene derivative, *NANOGP8* possesses distinct promoter elements relative to *NANOG1*. For example, TRANSFAC analyses of the *NANOGP8* promoter in silico fail to identify OCT4/SOX2 elements present in the promoter of *NANOG1* (Fig. 1C, Jeter et al., unpublished observations). Thus, as a consequence of *cis*-element differences, trans factors regulating *NANOG* mRNA transcriptional activation or repression in cancer cells will vary depending on the locus-of-origin for *NANOG* expression and the cellular context.

Structurally, NANOG1 protein has an N-terminal "interference" domain, a homeodomain essential for DNA binding, and a C-terminal transactivation domain with a tryptophan-rich region involved in NANOG dimerization (Fig. 1D). Of note, enforced expression of the murine Nanog1 dimer, but not the monomer, has been found to functionally replace wild-type Nanog to sustain cytokine-independent self-renewal of mouse ESCs [29]. Although both NANOG1 and NANOGP8 have been demonstrated to have similar reprogramming capabilities [30] (and thus may have overlapping roles in promoting malignant disease), some biochemical distinctions between the two proteins have been reported [31]. It will be very interesting to determine both the shared and potentially distinct biological functions between NANOG1 and NANOGP8.

NANOG as a Regulator of Proliferation and Chromatin Remodeling in ESCs

The balance between self-renewal and differentiation in dividing stem (and progenitor) cells is fundamental to development, tissue homeostasis, and tumorigenesis. Both mouse and human ESCs proliferate rapidly, largely by virtue of an abbreviated G1 phase in the pluripotent state [32, 33]. Considering that NANOG1 overexpression increases cell proliferation and shortens the G1-S transition in human ESCs, NANOG appears to function as a vital transcription factor regulating cell-cycle progression in ESCs [34]. Chromatin immunoprecipitation combined with reporter-based transfection assays have demonstrated that NANOG1 can bind to the regulatory regions of *CDK6* and *CDC25A* genes, thereby positively regulating their transcription. The effects of NANOG1 overexpression on S-phase entry could be mitigated by the siRNA-mediated downregulation of *CDK6* or *CDC25A* transcripts (and resultant proteins) alone, suggesting that CDK6 and CDC25A

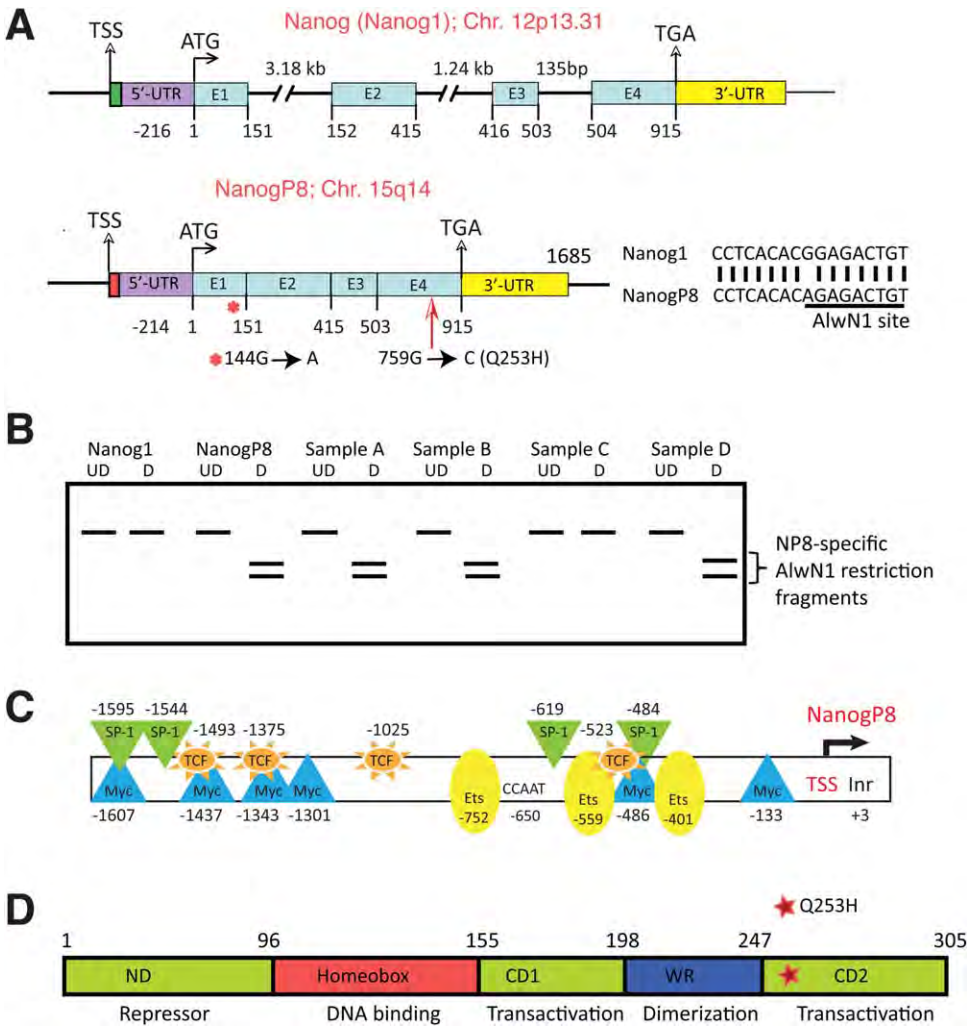

Figure 1. Genomic architecture and functional domains of NANOG. **(A):** *NANOG1* has a classic intron/exon structure with four exons (E), whereas *NANOGP8* is a retrotransposed gene and thus lacks introns. Both genes possess a 915-bp open reading frame, nearly identical between the two loci except for the 144 G>A transition often used to discriminate between *NANOG1* and *NANOGP8* mRNA species (see **B**, below), and the 759 G>C giving rise to the single conserved aa change (Q253H). The 5′-UTRs (untranslated regions) and 3′-UTRs are also highly conserved, except for the first ~18-bp, which are unique to each gene (marked by a green and red rectangle) and could theoretically be exploited to differentiate between the *NANOG1* versus *NANOGP8* mRNA species. (B): The 144 G>A transition can be used for DNA fingerprinting, giving unique AlwN1 digestion fragments for *NANOGP8* (NP8). The sequences in this region can be used to design RT-PCR primers flanking the AlwN1 cut site, and then digested (D) versus undigested (UD) PCR products separated by gel electrophoresis (shown is a representation of anticipated fragments) should reveal unique digestion fragments for each NANOG variant, corresponding to the locus of origin. **(C):** The proximal promoter (2 kb upstream of TSS) of *NANOGP8* was analyzed using the Transcription Element Search System online tool to identify candidate transcription factor binding sites based on TRANSFAC motifs. The nucleotide positions for the indicated motifs are shown relative to the TSS. Four putative *NANOGP8* promoter-binding factors include SP1, MYC (c-MYC), TCF, and ETS. **(D):** NANOG protein has an N-terminal "interference" domain to which corepressors may bind (ND), homeodomain important for DNA binding, and a C-terminal transactivation domain containing two subdomains (CD1 and CD2) and a tryptophan-rich (WR) domain involved in dimerization and activation. The asterisk indicates the conserved aa change (Q253H) in NANOGP8. Abbreviation: TSS, transcriptional start site.

are downstream cell cycle effectors of NANOG1 during the G1 to S transition in human ESCs [34].

Using fluorescent, ubiquitin-sensitive cell cycle reporters, human ESCs were recently shown to be particularly susceptible to differentiation in G1, such that altering the cell cycle of ESCs facilitates changes in cell specification [35]. Although these data convincingly demonstrate that differentiation and the cell cycle are intimately linked in ESCs, whether a dividing ESC remains pluripotent or gives rise to differentiated progeny is dictated at the molecular level. In addition to the regulatory activities of master transcription factors, cell state transitions during embryogenesis are governed by the epigenetic landscape in a given cell. Thus, the interplay of pluripotency-maintaining transcription factors together with chromatin modifiers collaboratively represses differentiation and maintains the primitive and renewing stem cell state. Endogenous murine Nanog1 and Oct-4 protein complexes have been found to interact with each other and associate with proteins from multiple transcriptional repression complexes, including the NuRD, Sin3A, and Pml complexes [36, 37]. Although immunoprecipitation failed to detect Mbd3 among the components of the nuclear remodeling and

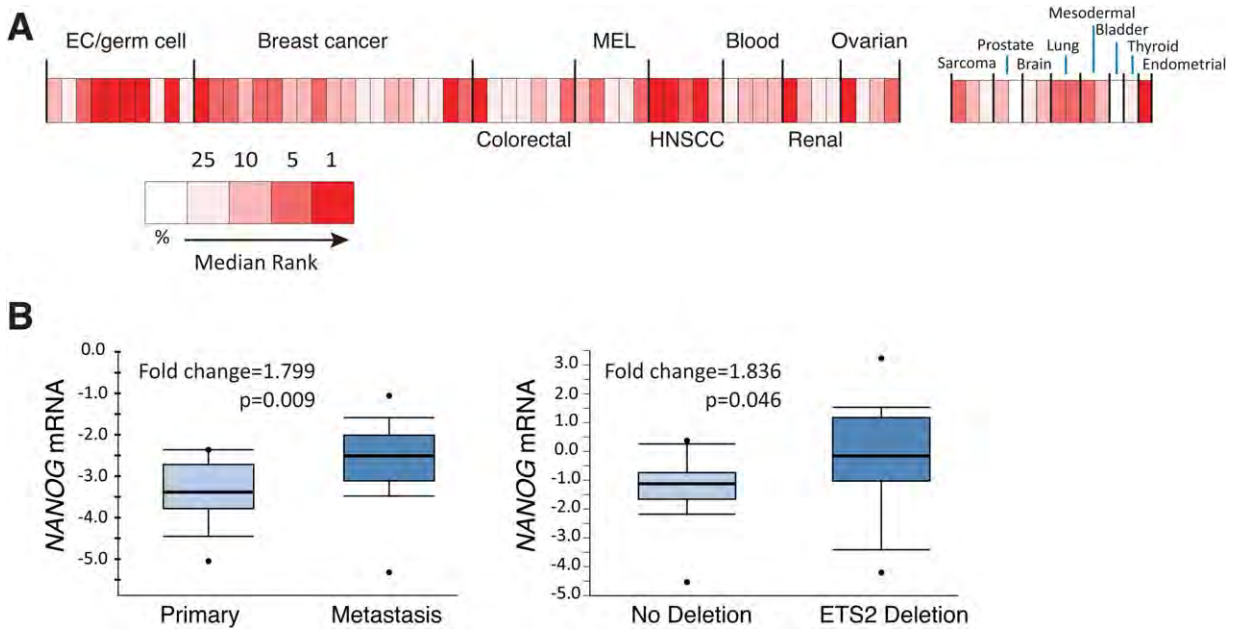

Figure 2. *Oncomine* analysis of *NANOG* transcripts in malignant diseases. **(A):** *Oncomine* analysis of *NANOG* mRNA expression in malignant diseases, filtered according to a threshold of $>1.5\times$ upregulated and $p < .05$. The heat map indicates the median gene rank for expression in the indicated dataset/tissue type (scale shown below), where white indicates that NANOG was not among the top 25%. Datasets (72 in total; Supporting Information Table S1) were clustered by tissue type into the indicated categories, with expression in EC/germ cell tumors (positive control) placed at the front and the remaining tissues presented according to the relative frequency of datasets with a positive correlation. **(B):** Box plot presentation of two prostate cancer datasets (from A, above). Gene expression was normalized using total intensity, median centered, and log(2) transformed to give equal weight to expression values relative to the median for analysis. The box plot on the left and right is based on the *Chandran* (*Prostate*, *BMC Cancer*, *2007*) and *Grasso* (*Prostate*, *Nature*, *2012*) datasets (Supporting Information Table S1), respectively. Abbreviations: EC, embryonal carcinoma; HNSCC, head and neck squamous cell carcinoma; MEL, melanoma.

histone deacetylase complex (e.g., Mta1, Mta2, Hdac1, etc.) pulled down with Nanog1 in murine ESCs [37], overexpression of Mbd3—the essential scaffold of the NuRD complex—has been found to augment Nanog-mediated reprogramming of mouse embryonic fibroblasts (MEFs) [36]. Nevertheless, even in Mbd3$^{-/-}$ mouse ESCs, Nanog1 and Oct-4 can communicate with distinct repression complexes (termed Nanog and Oct4-associated deacetylase [NODE]) to control gene transcription and ESC differentiation [37]. In human ESCs, NANOG co-occupies and represses developmental genes in concert with lysine-specific demethylase 1, a component of NuRD and the transcriptional repression complex coREST [38]. The NANOG/OCT4/SOX2 interactome is also thought to encompass members of the Polycomb group (PcG) family of transcriptional repressors and SetDB1 (reviewed in [39]). In addition to this myriad of chromatin remodeling complexes associated with transcriptional repression, NANOG has also been found to associate with transcriptional activators such as components of the SWItch/Sucrose NonFermentable (SWI/SNF) nucleosome remodeling complex and Wdr5 of the trithorax group [37, 40]. In mesenchymal stem cells (MSCs), NANOG and OCT4 transactivate expression of the DNA methyltransferase DNMT1, which subsequently downregulates the cyclin-dependent kinase inhibitors p16 and p21 and represses differentiation genes to maintain the self-renewal of MSCs [41]. Furthermore, more recent research has shown that members of the genomic methylation regulatory ten-eleven translocation (TET) family, specifically the methylcytosine hydroxylases TET1 and TET2, are recruited by Nanog1 to activate the expression of pluripotency genes and fulfill somatic cell reprogramming [42, 43].

Conceptual Overview of the Protumorigenic Effects of NANOG

Oncomine analysis reveals that *NANOG* mRNA is elevated in many types of cancer relative to matched benign tissues (Fig. 2A). Also, as we shall describe below, immunohistochemistry (IHC) shows that NANOG protein is heterogeneously expressed in both the nucleus and cytoplasm in a wide variety of primary human patient tumors. The presence of NANOG in neoplastic cells suggests a functional role for this molecule in tumor development or disease progression. However, given NANOG's apparent lack of direct oncogenic activity in transgenic animal models [13–16], how does this pluripotency factor execute its protumorigenic properties? Compelling evidence suggests that NANOG may foster CSC traits by imbuing subsets of cancer cells with self-renewal potential, thereby bolstering the immortality of the entire tumor population. FIRST, NANOG mRNA and protein are enriched in many CSC populations such as the CD44$^+$ breast [44], prostate [25], and oral squamous [45] cancer cells, CD133$^+$ prostate [25], brain [46, 47], and ovarian [48] cancer cells, and CD24$^+$ hepatocellular carcinoma cells [28], among others. Of clinical relevance, elevated NANOG expression has been frequently associated with worse clinical outcome in numerous epithelial malignancies (see below). SECOND, enforced NANOG expression increases the frequency of CSCs such as CD133$^+$ and AldeFLUOR$^+$ breast cancer cells [49]. THIRD, in contrast, RNAi-mediated *NANOG* knockdown leads to attenuated CSC properties such as sphere formation and clonogenic efficiency in breast and prostate cancer cells [25].

A positive correlation between NANOG levels and proliferation has been frequently reported in cancer cells. Although it is currently unknown whether this phenomenon is directly associated with cell fate (as in ESCs), increased proliferation is a hallmark of neoplastic disease. NANOG knockdown in human gastric cancer cells reduced the proliferative, invasive, and migratory capacity of cancer cells, associated with increased apoptosis and cell cycle arrest at the S phase [50]. Similar scenarios have been reported in response to NANOG inhibition in a variety of other cell types, such as glioblastoma [51] and breast [52] and prostate [25] carcinoma cells. Interestingly, NANOG knockdown in breast cancer cells appeared to modulate cell cycle progression by inducing G_0/G_1 arrest correlating with decreased levels of the cell cycle regulatory protein cyclin D1 [52].

Molecular oncogenesis can be thought of as a process of spontaneous cellular reprogramming. Unlike engineered reprogramming to generate iPS cells, deregulated and abnormal expression of NANOG (and/or other stem cell-related factors) could foster "oncogenic reprogramming" facilitating dynamic acquisition of states enhancing the adaptability of tumor cells to the gauntlet of challenges neoplastic cells face during tumor development and disease progression. Biologically plastic, renewing tumor cells may be intrinsically resistant to anticancer therapeutics and enriched upon experimental and clinical treatments. Thus, NANOG-expressing cancer cells have been observed to mediate therapy resistance, tumor recurrence, and distant metastasis. For example, NANOG has been observed to promote chemoresistance, increased cell migration, and epithelial mesenchymal transition (EMT) [49, 53, 54], a reversibly acquired cell state associated with metastasis. Microarray and quantitative real-time PCR analysis showed a parallel, elevated expression of *NANOG* and *OCT4* in lung adenocarcinoma. Double knockdown of NANOG and OCT4 suppressed the expression of *Slug*, a key EMT regulatory transcription factor, reversed the EMT process, and blocked the tumorigenic and metastatic ability, thereby greatly improving the mean survival time of lung carcinoma cell-transplanted immune-compromised mice [53]. IHC analysis demonstrated the presence of NANOG, OCT4, and Slug in high-grade lung adenocarcinoma, with triple positivity potentially indicating a worse prognostic outcome, and providing rationale to therapeutically manipulate NANOG/OCT4 signaling to control EMT, repress tumor-initiating ability, and inhibit metastatic spread [53].

Another crucial hurdle in the gauntlet cancer cells face is immunity. NANOG expressing cancer cells purportedly possess enhanced capabilities to evade the immune system. Hypoxia-induced NANOG in nonsmall cell lung cancer protects against cytotoxic T lymphocyte-mediated tumor cell killing, possibly via a mechanism involving the signal transducer and activator of transcription 3 (STAT-3) [55]. Vaccine-induced evolution and immune evasion of TC-1 human papillomavirus cervical cancer cells has also been shown to depend upon NANOG expression, as NANOG knockdown rendered xenograft tumors susceptible to immune surveillance in vivo [56]. Mechanistically, NANOG induced CSC phenotypes and immune evasion through T-cell leukemia/lymphoma 1A/Akt (Tcl1a/Akt) in human cervical cancer, a signaling axis potentially conserved in a variety of other cancer types [57]. Furthermore, NANOG expression levels correlate with stage and prognosis of cervical cancer in patients, suggesting that NANOG may foster the development and progression of cervical cancer by facilitating immune evasion capabilities among CSCs [57].

NANOG Expression and Function in Somatic Human Cancers

Here, we shall briefly describe clinical and xenograft studies implicating NANOG in the development of a variety of human malignancies and organized according to the tissue of origin. Although amplification of the short arm of chromosome 12 encoding NANOG is a "hotspot" for oncogenic transformation and considered pathognomonic in male germ cell tumors (for a review, see [58]), our focus here is on somatic human cancers.

Prostate Cancer

The protumorigenic functions of NANOG in prostate cancer (PCa) have been clarified by functional studies [25, 49, 59]. Working on PCa cell lines, xenografts, and primary tumor specimens, we first demonstrated that NANOG short-hairpin RNA (shRNA) inhibited PCa sphere formation, clonal growth, and tumor development [25]. A gain-of-function strategy was then used in which tetracycline-inducible PCa cell lines with NANOGP8 overexpression were established to further investigate the functions and mechanisms of NANOG in prostate tumorigenesis, and we found that NANOG induction phenotypically and functionally reprogrammed PCa cells and led to the emergence of castration-resistant PCa [49]. Substantiating these findings, NANOGP8 induction has been observed in some PCa cell and xenograft models [49, 60, 61]. In contrast, knocking down NANOG in undifferentiated, $PSA^{-/lo}$ CSCs inhibited xenograft tumor regeneration [62]. These findings suggest that NANOG might be a key regulatory factor mediating castration resistance and may therefore represent a critical, clinically relevant target for treatment of lethal, late-stage PCa. In support of this suggestion and of potential interest, *NANOG* mRNA is elevated in some PCa metastases (Fig. 2B, left) and in PCa harboring ETS2 deletion (Fig. 2; right).

NANOG protein is heterogeneously expressed as a gradient in PCa cells and enriched in $CD44^+$ and $CD44^+CD133^+$ cells (compared to marker-negative cells) and in primary tumor samples (compared to long-term cultured cells [25]). Interestingly, NANOG appeared to inversely correlate with expression of androgen receptor [25], suggesting a possible mechanism by which NANOG may promote castration resistance. Castration-tolerant PCa repopulating cells from early passage xenografts have also been reported to express NANOG, which appeared to largely localize to the cytoplasm [63]. NANOG protein was induced by hypoxia and positively correlated with hypoxia-inducible factor 1 α in primary prostate tumors [64]. These findings were corroborated by independent observations of hypoxia-mediated upregulation of *NANOGP8* mRNA in Du145 and PC3 PCa cells [65].

Hepatocellular Carcinoma

Hepatocellular carcinoma (HCC) exhibits cellular heterogeneity and stemness-related genes are preferentially expressed in NANOG-positive CSCs [66, 67]. However, it remains unclear whether or how these CSCs contribute to HCC initiation and

progression. Using a chemoresistant HCC xenograft model, CD24 was shown to mark relatively quiescent NANOG-expressing tumor cells with serial sphere- and tumor-forming capabilities, metastatic potential, and the capacity to differentiate in vitro [28]. That NANOG was epistatic to CD24 and critical for the tumorigenicity of these cells was demonstrated by the ability of NANOG overexpression to rescue tumor development in CD24 knockdown cells and to enhance serial sphere formation [28].

In primary tumor specimens, increased expression of NANOG was found to correlate with a worse clinical outcome in HCC [67]. Using a NANOG promoter reporter system, a small fraction of liver cancer cells exhibiting enhanced self-renewal, clonogenicity, and tumor initiation were isolated [66]. These $NANOG^+$ CSCs were invasive, metastatic, and resistant to therapeutic agents (e.g., sorafenib and cisplatin). Furthermore, NANOG knockdown reduced self-renewal, accompanied with decreased expression of stemness-related genes and increased expression of mature hepatocyte-specific genes [66]. In a separate study, a significant correlation was noted between NANOG expression and the expression of NODAL, P-SMAD3, and SNAIL [54]. The coexpression of NANOG and P-SMAD3 may be a potential predictor of poor prognosis for HCC patients. Additionally, HCC cells in the tumor edge areas displayed higher NANOG expression than cells in the tumor center, which might suggest an important role for NANOG in HCC invasion and metastasis [54]. Finally, in tissue microarray analyses of two cohorts of HCC patients ($n = 323$) the coexpression of stemness markers NANOG and OCT4 in HCC concurred with aggressive tumor behaviors and predicted worse clinical outcome [67].

Leukemia

Transcripts of the retrogene derivative *NANOG2* were reported in mixed lymphocytic leukemia, suggesting that *NANOG2* could be involved in regulating leukemic stem cell functions [68]. More recently, Cao et al. used a sequencing-based method encompassing the crucial distinguishing 759G>C transition to demonstrate that *NANOGP8* is the predominant source of NANOG in acute T-cell lymphoblastic leukemia (T-ALL), including primary patient samples [69]. RNAi-mediated NANOG attenuation in T-ALL cells was associated with loss of proliferation, reduced self-renewal, and increased apoptosis via blocking cell cycle progression through p53 signaling [69].

Glioblastoma Multiforme

Glioblastoma multiforme (GBM) is a highly invasive and incurable brain tumor [70, 71]. In GBM, an important signaling pathway implicated in tumor growth, CSC expansion, and specific expression of ESC-like stemness signature is the Hedgehog-GLI (HH-GLI), which appears to exert its function through direct regulation of NANOGP8 [46]. Using a loss-of-function approach, NANOGP8 was shown to be a HH-GLI mediator essential for GBM formation and sustenance as well as the survival and expansion of CD133-positive GBM CSCs [46, 70]. It is noteworthy that three GLI-*cis* elements are present upstream of *NANOG1* and two in *NANOGP8* regulatory regions, and functional analysis has revealed that NANOG is regulated by GLI, and vice versa, forming a positive feedback loop that is negatively regulated by p53 [46]. Analysis of tissue microarrays of 80 low-grade (WHO Grade II) and 98 high-grade human gliomas (WHO grades III and IV) revealed higher protein levels of NANOG, KLF4, OCT4, and SOX2 in high-grade gliomas, as compared to low-grade ones [72]. NANOG was subsequently identified as an independent prognostic factor in the subgroups of low-grade astrocytoma, high-grade astrocytoma and glioblastomas [72].

Colorectal Cancers

Both NANOGP8 and NANOG1 have been implicated in colorectal cancer (CRC) [22, 23]. In clinical CRC samples, the NANOG protein is expressed only in a small fraction of cancer cells; however, single *NANOG1*-positive CRC cells isolated via promoter-tracking constructs could form spheres similar to embryoid bodies derived from ESCs [23]. *NANOG1* expression appeared to be regulated by c-Jun and β-catenin/TCF4 as c-Jun could bind to the *NANOG1* promoter via the octamer M1 DNA element [23]. Interestingly, AlwN1 DNA fingerprinting (Fig. 1A, 1B) revealed that *NANOGP8* transcripts were detected in all CRC specimens tested, unlike *NANOG1* mRNA species, which were detected in only some CRC samples [23]. Using the same RFLP strategy with AlwN1 digestion, *NANOGP8* mRNA was detected in CRC liver metastases and NANOGP8 functionally promoted the clonogenic potential and tumorigenic capacity of CRC cells [22].

IHC analysis in 175 CRC samples demonstrated that high levels of NANOG protein strongly correlated with poor prognosis, lymph node metastasis, and Dukes classification [73]. NANOG protein was higher in CD133-positive CRC cells and overall 72 of the 360 cases (20%) positively expressed NANOG protein [74]. Univariate and Spearman correlation analyses associated *NANOGP8* expression with histological grade, lymph node metastasis, tumor-nodes-metastasis (TNM) stage, and liver metastasis [74]. Consequently, NANOGP8 might be considered a significant biomarker for postoperative liver metastasis of CRC patients.

Lung Cancer

In a study of 163 lung cancer patients, the expression levels of NANOG protein in lung cancer tissues were upregulated compared to the normal lung tissues and positively correlated with clinical stages [64]. Furthermore, NANOG overexpression predicted a worse prognosis for lung cancer patients [75]. In another study [65], *NANOGP8* mRNA was detected in 84.8% (39 out of 46) of lung cancer samples and was found to be expressed at high levels even in the early clinical stages, suggesting that *NANOGP8* mRNA detection could represent a new tool to help diagnose lung cancer irrespective of the clinical stage.

Breast Cancer

In a study comprising 100 breast cancer patients, patients with strong NANOG expression had significantly lower disease-free and overall survival rates than those with weak NANOG expression [76]. As discussed above, NANOG expression has been frequently correlated with CSC marker expression, functional properties, and therapy resistance in breast cancer cells. For example, NANOG knockdown in MCF-7 cells inhibited tumor growth, sphere formation, and drug resistance

[25] and blocked cell cycle progression, colony formation, and migration [52]. NANOG-mediated chemoresistance in MCF-7 cells apparently occurred via complex formation with STAT-3 downstream of hyaluronan-induced CD44 activation, resulting in the expression of the multidrug transporter MDR1 (ABCB1) [44]. Protein kinase Cε has also been proposed to be an intermediate in NANOG-mediated drug resistance in breast cancer cells by direct phosphorylation of NANOG leading to increased miR-21 levels and upregulation of antiapoptotic proteins including inhibitor of apoptosis proteins (IAPs) and drug resistance mediators such as MDR1 [77]. Regardless of the underlying mechanisms, there exists solid evidence linking NANOG to breast cancer chemotherapy resistance.

Pancreatic Cancer

In a tissue microarray analysis of 43 human pancreatic cancer, IHC for NANOG and OCT4 followed by Kaplan-Meier analysis revealed that high NANOG (and OCT4) expression predicted a worse prognosis and inversely correlated with patient survival [78]. Double knockdown of *NANOG* and *OCT4* significantly reduced proliferation, migration, invasion, chemoresistance, and tumor regeneration capacity of Panc-1 cells [68]. In a separate study of a small cohort of pancreatic ductal adenocarcinoma (PDAC) patient samples, NANOG was found to be coexpressed with the adult stem cell marker leucine-rich repeat-containing G-protein coupled receptor 5, which might mark the cell-of-origin for PDAC [79].

Ovarian Cancer

Ovarian cancer (OC) is the most lethal in all gynecological malignancies. *NANOG* mRNA and NANOG protein were enriched in OC cells with sphere-forming, tumor regeneration, and chemodrug resistance properties [80]. IHC examination of a large cohort of OC patients revealed increased nuclear NANOG protein in OC specimens (compared with benign tissues) correlating with pathological grade and tumor stage [81]. More recently, NANOG expression was shown to be significantly associated with risk of high-grade cancer development, severe histological subtypes, chemotherapeutic resistance, and poor overall and disease-free survival [82]. shRNA-mediated NANOG depletion impeded OC cell proliferation, migration, and invasion associated with an increase in mRNA expression of *E-cadherin*, *caveolin-1*, *FOXO1*, *FOXO3a*, *FOXJ1*, and *FOXB1*, whereas NANOG overexpression enhanced OC cell migration and invasion [82]. Of note, microRNAs may also be involved in *NANOG* posttranscriptional regulation, as miR-214 has been shown to regulate ovarian cancer stem cell (OCSC) properties by targeting the p53/NANOG axis [48]. Specifically, miR-214 levels showed a positive relationship with the frequency of OCSCs and NANOG protein such that the sphere-forming potential and the percentage of $ALDH1^+$ OCSC population were enhanced by enforced expression of miR-214 and attenuated by inhibition of miR-214 in a p53 wild-type background. Furthermore, p53 was directly repressed by miR-214 whereas miR-214 regulation of NANOG appeared to occur indirectly through p53 as forced p53 expression abrogated miR-214-induced NANOG [48]. p53 is known to be a negative regulator of *NANOG1* transcription in ESCs, suggesting that *NANOG1* might be a primary locus-of-origin for NANOG in OC cells. Regardless, these data demonstrate a critical role for miR-214 in modulating OCSC properties by regulating the p53-Nanog axis and suggest that both miR-214 and NANOG could represent therapeutic targets for OC [48].

Conclusions, Perspectives, and Outstanding Questions

Numerous investigations so far have causally linked NANOG to and also shed light on the role of NANOG in tumorigenesis, with implications in cancer prognosis and anticancer therapeutics. Since multiple oncogenic signal transduction pathways appear to modulate chemoresistance, EMT, metastasis, and other CSC properties through NANOG, this powerful reprogramming and stem cell-associated factor may represent a crucial molecular nexus underlying malignant disease. These findings demonstrate that NANOG is a protumorigenic factor that may serve in the clinic as a biomarker for cancer diagnosis, prognosis, and predictor of anticancer therapeutic efficacy. Furthermore, NANOG itself may represent a therapeutic target as its elimination is predicted to ablate CSC self-renewal and root out the cause of tumor recurrence and metastasis.

Nevertheless, there are also many critical outstanding questions about the involvement and mechanisms of NANOG in tumorigenic processes. Answers to these questions will facilitate the design of novel cancer therapeutics targeting NANOG. (a) Why is NANOG, unlike OCT4, nontumorigenic or only weakly tumorigenic by itself in transgenic animal models [12–16]? In what contexts does it function as a potentiating or cooperating oncogene? What cooperating oncogenic pathways does NANOG converge with in order to elicit transformation? The observations that NANOG, when coexpressed with Wnt-1, enhanced mammary tumorigenesis and metastasis [16] support the notion that the oncogenic functions of NANOG require synergistic cooperation with other genes/pathways. This caveat also appears to apply to SOX2, which has been found to induce the transformation of squamous basal stem cells of the esophagus and forestomach, only when coexpressed with activated STAT-3 [83]. It is also conceivable that other classic brakes to transformation, such as the tumor suppressor p53 may play a role in restricting the oncogenic properties of NANOG. In support, p53 negatively regulates a reciprocal loop between GLI1 and NANOG (NANOGP8) in glioblastoma [46] and represses NANOG (NANOG1) expression in ovarian cancer cells, a p53-NANOG regulatory axis antagonized by the oncogenic microRNA miR-214 [48]. Thus, p53 may impinge upon NANOG-mediated oncogenic reprogramming in preneoplastic or cancerous cells and further analysis of correlations between NANOG expression and p53 mutation remain outstanding. (b) Are there distinct biochemical differences between NANOG1 and NANOGP8 in the context of regulating tumor development? In more advanced disease stages, could NANOGP8 expression preferentially potentiate metastatic propensity or resistance to conventional therapy? As discussed earlier, somatic cancer cells seem to predominantly express the retrogene *NANOG8* rather than ESC-specific *NANOG1*. In fact, there is evidence that cancer cells shut down NANOG1 expression [25]. Then what is the advantage of expressing NANOGP8? Although NANOGP8

and NANOG1 seem to be equipotent in reprograming normal [30] and cancer [49] cells, preferential expression of NANOGP8 in cancer cells argues for at least some distinct mechanisms or biological properties of this protein. At a global level, context-dependent NANOG-induced malignant phenotypes may also be dictated by the presence of NANOG-interacting proteins, such as other transcription factors that could function to decode chromatin occupancy, or given the epigenome reprogramming proclivities of *NANOG1*, chromatin-remodeling factors. To date, the majority of mechanistic studies have been based on studies in vitro. A systems biology approach will ultimately be needed to permit deeper understanding of the temporal and intensity dynamics of NANOG-associated regulatory networks in somatic cancer cells. Practically, as most commercial antibodies are raised against NANOG1 protein and thus do not distinguish between NANOG1 versus NANOGP8 [31], some potentially NANOGP8-unique functions will only be uncovered when high-quality NANOGP8-specific antibodies become available. (c) Along this line of discussion, how is *NANOGP8* transcriptionally (and post-transcriptionally) regulated in somatic cancer cells? This is obviously an interesting question as *NANOGP8*, being a retrogene, is regulated differently than *NANOG1* (Fig. 1C). Elucidating the upstream regulators will also help develop therapeutics to target NANOG, which appears to function as an essential self-renewing molecule that fuels tumor maintenance, metastatic spread, and drug resistance.

Acknowledgments

The work in the authors' lab was supported, in part, by grants from NIH R01-CA155693 (D.G.T.), Department of Defense W81XWH-13-1-0352 and W81XWH-14-1-0575 (D.G.T.), CPRIT RP120380 (D.G.T.) and CPRIT RP120394 (C.R.J.), and the National Natural Science Foundation of China Grant No. 81372750 (T.Y.) and Grant No. 81372512 (J.W.).

Author Contributions

C.R.J. and T.Y. contributed equally to this work. T.Y.: wrote the early drafts of the paper; C.R.J.: edited early drafts and made significant re-writing on the manuscript; C.R.J.: participated in generating both Figure 1 and Figure 2; J.W.: had significant discussions with DGT and also participated in some final stages of writing; H.P.C.: was involved in generating Figure 2; D.G.T.: was responsible for final editing, writing, and approval of all figures and Text.

Disclosure of Potential Conflicts of Interest

The authors disclose no potential conflicts of interest.

References

1 Torres-Padilla ME, Chambers I. Transcription factor heterogeneity in pluripotent stem cells: A stochastic advantage. Development 2014;141:2173–2181.

2 Yu J, Vodyanik MA, Smuga-Otto K et al. Induced pluripotent stem cell lines derived from human somatic cells. Science 2007;318:1917–1920.

3 Park IH, Zhao R, West JA et al. Reprogramming of human somatic cells to pluripotency with defined factors. Nature 2008;451:141–146.

4 Takahashi K, Yamanaka S. Induction of pluripotent stem cells from mouse embryonic and adult fibroblast cultures by defined factors. Cell 2006;126:663–676.

5 Gangemi RM, Griffero F, Marubbi D et al. SOX2 silencing in glioblastoma tumor-initiating cells causes stop of proliferation and loss of tumorigenicity. Stem Cells 2009;27:40–48.

6 Leis O, Eguiara A, Lopez-Arribillaga E et al. Sox2 expression in breast tumours and activation in breast cancer stem cells. Oncogene 2012;31:1354–1365.

7 Riggi N, Suva ML, De Vito C et al. EWS-FLI-1 modulates miRNA145 and SOX2 expression to initiate mesenchymal stem cell reprogramming toward Ewing sarcoma cancer stem cells. Genes Dev 2010;24:916–932.

8 Zhang J, Wang X, Chen B et al. Expression of Nanog gene promotes NIH3T3 cell proliferation. Biochem Biophys Res Commun 2005;338:1098–1102.

9 Piestun D, Kochupurakkal BS, Jacob-Hirsch J et al. Nanog transforms NIH3T3 cells and targets cell-type restricted genes. Biochem Biophys Res Commun 2006;343:279–285.

10 Liu Y, Clem B, Zuba-Surma EK et al. Mouse fibroblasts lacking RB1 function form spheres and undergo reprogramming to a cancer stem cell phenotype. Cell Stem Cell 2009;4:336–347.

11 Lin YL, Han ZB, Xiong FY et al. Malignant transformation of 293 cells induced by ectopic expression of human Nanog. Mol Cell Biochem 2011;351:109–116.

12 Hochedlinger K, Yamada Y, Beard C et al. Ectopic expression of Oct-4 blocks progenitor-cell differentiation and causes dysplasia in epithelial tissues. Cell 2005;121:465–477.

13 Fischedick G, Wu G, Adachi K et al. Nanog induces hyperplasia without initiating tumors. Stem Cell Res 2014;13:300–315.

14 Piazzolla D, Palla AR, Pantoja C et al. Lineage-restricted function of the pluripotency factor NANOG in stratified epithelia. Nat Commun 2014;5:4226.

15 Badeaux MA, Jeter CR, Gong S et al. In vivo functional studies of tumor-specific retrogene NanogP8 in transgenic animals. Cell Cycle 2013;12:2395–2408.

16 Lu X, Mazur SJ, Lin T et al. The pluripotency factor nanog promotes breast cancer tumorigenesis and metastasis. Oncogene 2014;33:2655–2664.

17 Scerbo P, Markov GV, Vivien C et al. On the origin and evolutionary history of NANOG. PLoS One 2014;9:e85104.

18 Booth HA, Holland PW. Eleven daughters of NANOG. Genomics 2004;84:229–238.

19 Hart AH, Hartley L, Ibrahim M et al. Identification, cloning and expression analysis of the pluripotency promoting Nanog genes in mouse and human. Dev Dyn 2004;230:187–198.

20 Ambady S, Malcuit C, Kashpur O et al. Expression of NANOG and NANOGP8 in a variety of undifferentiated and differentiated human cells. Int J Dev Biol 2010;54:1743–1754.

21 Fairbanks DJ, Fairbanks AD, Ogden TH et al. NANOGP8: Evolution of a human-specific retro-oncogene. G3 (Bethesda) 2012;2:1447–1457.

22 Zhang J, Espinoza LA, Kinders RJ et al. NANOG modulates stemness in human colorectal cancer. Oncogene 2013;32:4397–4405.

23 Ibrahim EE, Babaei-Jadidi R, Saadeddin A et al. Embryonic NANOG activity defines colorectal cancer stem cells and modulates through AP1- and TCF-dependent mechanisms. Stem Cells 2012;30:2076–2087.

24 Ishiguro T, Sato A, Ohata H et al. Differential expression of nanog1 and nanogp8 in colon cancer cells. Biochem Biophys Res Commun 2012;418:199–204.

25 Jeter CR, Badeaux M, Choy G et al. Functional evidence that the self-renewal gene NANOG regulates human tumor development. Stem Cells 2009;27:993–1005.

26 Uchino K, Hirano G, Hirahashi M et al. Human Nanog pseudogene8 promotes the proliferation of gastrointestinal cancer cells. Exp Cell Res 2012;318:1799–1807.

27 Zhang J, Wang X, Li M et al. NANOGP8 is a retrogene expressed in cancers. FEBS J 2006;273:1723–1730.

28 Lee TK, Castilho A, Cheung VC et al. CD24(+) liver tumor-initiating cells drive self-renewal and tumor initiation through STAT3-mediated NANOG regulation. Cell Stem Cell 2011;9:50–63.

29 Wang J, Levasseur DN, Orkin SH. Requirement of Nanog dimerization for stem cell self-renewal and pluripotency. Proc Natl Acad Sci USA 2008;105:6326–6331.
30 Palla AR, Piazzolla D, Abad M et al. Reprogramming activity of NANOGP8, a NANOG family member widely expressed in cancer. Oncogene 2014;33:2513–2519.
31 Liu B, Badeaux MD, Choy G et al. Nanog1 in NTERA-2 and recombinant NanogP8 from somatic cancer cells adopt multiple protein conformations and migrate at multiple M.W species. PLoS One 2014;9: e90615.
32 Coronado D, Godet M, Bourillot PY et al. A short G1 phase is an intrinsic determinant of naive embryonic stem cell pluripotency. Stem Cell Res 2013;10:118–131.
33 Neganova I, Zhang X, Atkinson S et al. Expression and functional analysis of G1 to S regulatory components reveals an important role for CDK2 in cell cycle regulation in human embryonic stem cells. Oncogene 2009;28:20–30.
34 Zhang X, Neganova I, Przyborski S et al. A role for NANOG in G1 to S transition in human embryonic stem cells through direct binding of CDK6 and CDC25A. J Cell Biol 2009;184:67–82.
35 Pauklin S, Vallier L. The cell-cycle state of stem cells determines cell fate propensity. Cell 2013;155:135–147.
36 dos Santos RL, Tosti L, Radzisheuskaya A et al. MBD3/NuRD facilitates induction of pluripotency in a context-dependent manner. Cell Stem Cell 2014;15:102–110.
37 Liang J, Wan M, Zhang Y et al. Nanog and Oct4 associate with unique transcriptional repression complexes in embryonic stem cells. Nat Cell Biol 2008;10:731–739.
38 Adamo A, Sese B, Boue S et al. LSD1 regulates the balance between self-renewal and differentiation in human embryonic stem cells. Nat Cell Biol 2011;13:652–659.
39 Newman JJ, Young RA. Connecting transcriptional control to chromosome structure and human disease. Cold Spring Harb Symp Quant Biol 2010;75:227–235.
40 Ang YS, Tsai SY, Lee DF et al. Wdr5 mediates self-renewal and reprogramming via the embryonic stem cell core transcriptional network. Cell 2011;145:183–197.
41 Tsai CC, Su PF, Huang YF et al. Oct4 and Nanog directly regulate Dnmt1 to maintain self-renewal and undifferentiated state in mesenchymal stem cells. Mol Cell 2012;47: 169–182.
42 Costa Y, Ding J, Theunissen TW et al. NANOG-dependent function of TET1 and TET2 in establishment of pluripotency. Nature 2013;495:370–374.
43 Lee K, Hamm J, Whitworth K et al. Dynamics of TET family expression in porcine preimplantation embryos is related to zygotic genome activation and required for the maintenance of NANOG. Dev Biol 2014;386: 86–95.
44 Bourguignon LY, Peyrollier K, Xia W et al. Hyaluronan-CD44 interaction activates stem cell marker Nanog, Stat-3-mediated MDR1 gene expression, and ankyrin-regulated multidrug efflux in breast and ovarian tumor cells. J Biol Chem 2008;283:17635–17651.
45 Bourguignon LY, Earle C, Wong G et al. Stem cell marker (Nanog) and Stat-3 signaling promote MicroRNA-21 expression and chemoresistance in hyaluronan/CD44-activated head and neck squamous cell carcinoma cells. Oncogene 2012;31:149–160.
46 Zbinden M, Duquet A, Lorente-Trigos A et al. NANOG regulates glioma stem cells and is essential in vivo acting in a cross-functional network with GLI1 and p53. EMBO J 2010;29:2659–2674.
47 Niu CS, Li DX, Liu YH et al. Expression of NANOG in human gliomas and its relationship with undifferentiated glioma cells. Oncol Rep 2011;26:593–601.
48 Xu CX, Xu M, Tan L et al. MicroRNA miR-214 regulates ovarian cancer cell stemness by targeting p53/Nanog. J Biol Chem 2012;287:34970–34978.
49 Jeter CR, Liu B, Liu X et al. NANOG promotes cancer stem cell characteristics and prostate cancer resistance to androgen deprivation. Oncogene 2011;30:3833–3845.
50 Ji W, Jiang Z. Effect of shRNA-mediated inhibition of Nanog gene expression on the behavior of human gastric cancer cells. Oncol Lett 2013;6:367–374.
51 Sato A, Okada M, Shibuya K et al. Resveratrol promotes proteasome-dependent degradation of Nanog via p53 activation and induces differentiation of glioma stem cells. Stem Cell Res 2013;11:601–610.
52 Han J, Zhang F, Yu M et al. RNA interference-mediated silencing of NANOG reduces cell proliferation and induces G0/G1 cell cycle arrest in breast cancer cells. Cancer Lett 2012;321:80–88.
53 Chiou SH, Wang ML, Chou YT et al. Coexpression of Oct4 and Nanog enhances malignancy in lung adenocarcinoma by inducing cancer stem cell-like properties and epithelial-mesenchymal transdifferentiation. Cancer Res 2010;70:10433–10444.
54 Sun C, Sun L, Jiang K et al. NANOG promotes liver cancer cell invasion by inducing epithelial-mesenchymal transition through NODAL/SMAD3 signaling pathway. Int J Biochem Cell Biol 2013;45:1099–1108.
55 Hasmim M, Noman MZ, Lauriol J et al. Hypoxia-dependent inhibition of tumor cell susceptibility to CTL-mediated lysis involves NANOG induction in target cells. J Immunol 2011;187:4031–4039.
56 Noh KH, Lee YH, Jeon JH et al. Cancer vaccination drives Nanog-dependent evolution of tumor cells toward an immune-resistant and stem-like phenotype. Cancer Res 2012;72:1717–1727.
57 Noh KH, Kim BW, Song KH et al. Nanog signaling in cancer promotes stem-like phenotype and immune evasion. J Clin Invest 2012;122:4077–4093.
58 Hoei-Hansen CE. Application of stem cell markers in search for neoplastic germ cells in dysgenetic gonads, extragonadal tumours, and in semen of infertile men. Cancer Treat Rev 2008;34:348–367.
59 Zhang K, Fowler M, Glass J et al. Activated 5′ flanking region of NANOGP8 in a self-renewal environment is associated with increased sphere formation and tumor growth of prostate cancer cells. Prostate 2014;74:381–394.
60 Germann M, Wetterwald A, Guzman-Ramirez N et al. Stem-like cells with luminal progenitor phenotype survive castration in human prostate cancer. Stem Cells 2012;30: 1076–1086.
61 Seiler D, Zheng J, Liu G et al. Enrichment of putative prostate cancer stem cells after androgen deprivation: Upregulation of pluripotency transactivators concurs with resistance to androgen deprivation in LNCaP cell lines. Prostate 2013;73:1378–1390.
62 Qin J, Liu X, Laffin B et al. The PSA(-/lo) prostate cancer cell population harbors self-renewing long-term tumor-propagating cells that resist castration. Cell Stem Cell 2012;10: 556–569.
63 Toivanen R, Frydenberg M, Murphy D et al. A preclinical xenograft model identifies castration-tolerant cancer-repopulating cells in localized prostate tumors. Sci Transl Med 2013;5:187ra171.
64 Mathieu J, Zhang Z, Zhou W et al. HIF induces human embryonic stem cell markers in cancer cells. Cancer Res 2011;71:4640–4652.
65 Ma Y, Liang D, Liu J et al. Prostate cancer cell lines under hypoxia exhibit greater stem-like properties. PLoS One 2011;6: e29170.
66 Shan J, Shen J, Liu L et al. Nanog regulates self-renewal of cancer stem cells through the insulin-like growth factor pathway in human hepatocellular carcinoma. Hepatology 2012;56:1004–1014.
67 Yin X, Li YW, Zhang BH et al. Coexpression of stemness factors oct4 and nanog predict liver resection. Ann Surg Oncol 2012;19: 2877–2887.
68 Eberle I, Pless B, Braun M et al. Transcriptional properties of human NANOG1 and NANOG2 in acute leukemic cells. Nucleic Acids Res 2010;38:5384–5395.
69 Cao J, Li L, Chen C et al. RNA interference-mediated silencing of NANOG leads to reduced proliferation and self-renewal, cell cycle arrest and apoptosis in T-cell acute lymphoblastic leukemia cells via the p53 signaling pathway. Leuk Res 2013;37: 1170–1177.
70 Higgins DM, Wang R, Milligan B et al. Brain tumor stem cell multipotency correlates with nanog expression and extent of passaging in human glioblastoma xenografts. Oncotarget 2013;4:792–801.
71 Moon JH, Kwon S, Jun EK et al. Nanog-induced dedifferentiation of p53-deficient mouse astrocytes into brain cancer stem-like cells. Biochem Biophys Res Commun 2011; 412:175–181.
72 Elsir T, Edqvist PH, Carlson J et al. A study of embryonic stem cell-related proteins in human astrocytomas: Identification of Nanog as a predictor of survival. Int J Cancer 2014;134:1123–1131.
73 Meng HM, Zheng P, Wang XY et al. Over-expression of Nanog predicts tumor progression and poor prognosis in colorectal cancer. Cancer Biol Ther 2010;9:295–302.
74 Xu F, Dai C, Zhang R et al. Nanog: A potential biomarker for liver metastasis of colorectal cancer. Dig Dis Sci 2012;57:2340–2346.

75 Du Y, Ma C, Wang Z et al. Nanog, a novel prognostic marker for lung cancer. Surg Oncol 2013;22:224–229.

76 Nagata T, Shimada Y, Sekine S et al. Prognostic significance of NANOG and KLF4 for breast cancer. Breast Cancer 2014;21:96–101.

77 Bourguignon LY, Spevak CC, Wong G et al. Hyaluronan-CD44 interaction with protein kinase C(epsilon) promotes oncogenic signaling by the stem cell marker Nanog and the Production of microRNA-21, leading to down-regulation of the tumor suppressor protein PDCD4, anti-apoptosis, and chemotherapy resistance in breast tumor cells. J Biol Chem 2009;284:26533–26546.

78 Lu Y, Zhu H, Shan H et al. Knockdown of Oct4 and Nanog expression inhibits the stemness of pancreatic cancer cells. Cancer Lett 2013;340:113–123.

79 Amsterdam A, Raanan C, Schreiber L et al. LGR5 and Nanog identify stem cell signature of pancreas beta cells which initiate pancreatic cancer. Biochem Biophys Res Commun 2013;433:157–162.

80 Zhang S, Balch C, Chan MW et al. Identification and characterization of ovarian cancer-initiating cells from primary human tumors. Cancer Res 2008;68:4311–4320.

81 Pan Y, Jiao J, Zhou C et al. Nanog is highly expressed in ovarian serous cystadenocarcinoma and correlated with clinical stage and pathological grade. Pathobiology 2010; 77:283–288.

82 Siu MK, Wong ES, Kong DS et al. Stem cell transcription factor NANOG controls cell migration and invasion via dysregulation of E-cadherin and FoxJ1 and contributes to adverse clinical outcome in ovarian cancers. Oncogene 2013;32:3500–3509.

83 Liu K, Jiang M, Lu Y et al. Sox2 cooperates with inflammation-mediated Stat3 activation in the malignant transformation of foregut basal progenitor cells. Cell Stem Cell 2013;12:304–315.

See www.StemCells.com for supporting information available online.